NASA TECHNICAL NOTE

NASA TN D-5581

c. 1

NASA TN D-5581

GENERALIZED HOT-GAS INGESTION INVESTIGATION OF LARGE-SCALE JET VTOL FIGHTER-TYPE MODELS

by H. Clyde McLemore, Charles C. Smith, Jr., and Patricia G. Hemeter

Langley Research Center
Langley Station, Hampton, Va.

NATIONAL AERONAUTICS AND SPACE ADMINISTRATION • WASHINGTON, D. C. • JANUARY 1970

1. Report No. NASA TN D-5581	2. Government Accession No.	3. Recipient's Catalog No.
4. Title and Subtitle GENERALIZED HOT-GAS INGESTION INVESTIGATION OF LARGE-SCALE JET VTOL FIGHTER-TYPE MODELS		5. Report Date January 1970 6. Performing Organization Code
7. Author(s) H. Clyde McLemore, Charles C. Smith, Jr., and Patricia G. Hemeter		8. Performing Organization Report No. L-6805 10. Work Unit No. 721-03-11-01-23
9. Performing Organization Name and Address NASA Langley Research Center Hampton, Va. 23365		11. Contract or Grant No. 13. Type of Report and Period Covered Technical Note
12. Sponsoring Agency Name and Address National Aeronautics and Space Administration Washington, D.C. 20546		14. Sponsoring Agency Code

15. Supplementary Notes

16. Abstract

An investigation has been conducted in the Langley full-scale tunnel on large-scale jet VTOL fighter-type aircraft configurations to study the problem of hot-gas ingestion. The investigation is an extension of an earlier investigation and involves additional test configurations and more sophisticated instrumentation. The investigation includes tests of configurations with several exhaust-nozzle arrangements, inlet positions, and wing positions and sizes for a range of nozzle heights from about 1 to 5 effective nozzle diameters above the ground. The tests were conducted for a range of forward speeds from zero to about 35 knots and for side winds from about 8 to 12 knots.

17. Key Words Suggested by Author(s) VTOL fighter models Hot-gas ingestion	18. Distribution Statement Unclassified – Unlimited		
19. Security Classif. (of this report) Unclassified	20. Security Classif. (of this page) Unclassified	21. No. of Pages 152	22. Price* $3.00

*For sale by the Clearinghouse for Federal Scientific and Technical Information
Springfield, Virginia 22151

GENERALIZED HOT-GAS INGESTION INVESTIGATION OF LARGE-SCALE JET VTOL FIGHTER-TYPE MODELS

By H. Clyde McLemore, Charles C. Smith, Jr.,
and Patricia G. Hemeter
Langley Research Center

SUMMARY

An investigation to study the problem of hot-gas ingestion has been conducted in the Langley full-scale tunnel on large-scale jet VTOL fighter-type aircraft configurations. The investigation included several nozzle and inlet arrangements, wing sizes, and wing locations for a range of forward and side-wind conditions. The exhaust-gas source was a turbojet engine which normally operates at a nozzle pressure ratio of about 1.8 and a nozzle temperature of 1200° F (649° C), but in many of the tests the engine did not achieve this pressure ratio because of the hot-gas ingestion.

The ingestion of hot engine-exhaust gases into the inlets was found to be very dependent upon the aircraft configuration and upon the windspeed. The only arrangement of engine-exhaust nozzles that did not result in relatively high hot-gas ingestion was the in-line arrangement. The in-line arrangement of nozzles resulted in virtually no hot-gas ingestion, whereas the rectangular arrangement of nozzles resulted in an inlet-air temperature rise above ambient of 100° F to 200° F (55.5° C to 111° C) for many test conditions. The ingestion of hot exhaust gases was greatest at windspeeds from zero to about 20 knots, and there was virtually no ingestion at windspeeds greater than about 30 knots except for the configuration with the single-nozzle arrangement which still had a considerable amount of ingestion at the highest test speed of about 37 knots. Top inlets were, in general, less subject to hot-gas ingestion than side inlets, and the low-wing position and increased wing size were found to reduce the ingestion of some configurations. Deflecting the exhaust gases 25° rearward with vectoring nozzles generally eliminated the ingestion of hot exhaust gases.

INTRODUCTION

There is, at the present time, an increasing interest in the problems associated with jet VTOL aircraft. Hot-gas ingestion is one serious problem for jet VTOL aircraft because a thrust loss occurs as a result of the elevated temperature of the engine-inlet air or an uneven inlet temperature distribution across the engine face.

There has been a considerable amount of research into the problem of hot-gas ingestion during the past few years (refs. 1 to 14). The problem has not been solved, however, nor have the significant parameters involved and their effects been defined very well because of the large number of, and the interaction between, configurations and operating condition variables. For these same reasons, the hot-gas ingestion problem area has not been amenable to analytical treatment but has relied heavily on experimental work. The present investigation is a continuation of such experimental work to provide information for improving the understanding of the effects of the factors involved with a view toward improving prediction capability in this area and improving the capability to design and operate aircraft so as to minimize hot-gas ingestion. In the present investigation, the study of large-scale jet VTOL fighter-type configurations reported in reference 1 is extended to include additional configurations. The investigation was conducted in the Langley full-scale tunnel with four engine-exhaust arrangements for test variables of model height above the ground, wing size and vertical location, engine-inlet position, and windspeed and direction. Since the present investigation is an extension of that reported in reference 1, the results of both investigations are discussed and summarized in the present paper to present an overall picture.

SYMBOLS

The units for the physical quantities defined in this paper are given both in the U.S. Customary Units and in the International System of Units (SI).

D_e effective nozzle diameter (diameter of a circle whose area is equal to the sum of the areas of the individual nozzles), feet (meters)

h nozzle height above ground, feet (meters)

S_J total jet nozzle area, $feet^2$ ($meters^2$)

S_W wing area, $feet^2$ ($meters^2$)

ΔT inlet-air temperature rise (final inlet-air temperature minus initial ambient temperature), ^oF (^oC)

V windspeed, knots

X,Y model axes

ψ model heading (azimuth), degrees (positive, nose right)

Abbreviations:

N.D. denotes that no data are available

N.I. denotes that no ingestion occurred

MODEL AND APPARATUS

The model used in the present investigation was the same one that was used in the investigation of reference 1 except that additional inlet and exhaust-nozzle arrangements were employed. This model was approximately a 1/3-scale jet VTOL fighter configuration. The principal dimensions of the model are given in figure 1. Not all of the many configurations investigated are presented in figure 1, but each inlet, exhaust-nozzle, and wing arrangement is shown.

The model was powered by a turbojet engine (GE-YJ85-7), mounted horizontally in the fuselage, which could be fitted with various inlet and exhaust-nozzle arrangements to simulate several different jet VTOL configurations. The inlet and exhaust-nozzle arrangements are shown schematically in figure 2. The exhaust-nozzle area of the engine was 118 in^2 (761 cm^2) exclusive of the turning vanes. Each of the four nozzles in the multiple-nozzle arrangements was designed to have one-fourth of this total nozzle area, or 29.5 in^2 (190 cm^2).

The inlet and exhaust-nozzle arrangements were designed to simulate airplane configurations with inlets directly above the exhaust nozzles (lift engines mounted vertically) or configurations with normal forward-facing side inlets and deflected engine-exhaust nozzles for VTOL operation.

The model is shown mounted for tests in the Langley full-scale tunnel in figure 3. The model was supported by three 2-inch-diameter (5.08-cm) pipes to minimize obstruction of the exhaust flow. The pipes were restrained from bending by steel guy wires of 3/8-inch (0.95-cm) diameter.

The model was constructed almost entirely of stainless steel. The inlets to the engine had 1.00-inch-radius (2.54-cm) lips. (See figs. 4 and 5.) Each inlet was equipped with a rake of chromel-alumel thermocouple probes (location in inlets shown in fig. 5) which were constructed (as shown in fig. 5(c)) of 36-gage, welded, bare-bead wire which was in turn welded across 0.125-inch-diameter (0.318-cm), swaged, 24-gage wire. This type of construction utilizing the 0.005-inch-diameter (0.0127-cm), 36-gage probes was used to give a much faster temperature response rate (on the order of 0.2 second to reach actual temperature after a step input) than that of the probes of reference 1 (response rate on the order of 1.0 second). The airflow rate through the various inlets

was not determined during the present investigation; however, during the tests of reference 1, inlet total- and static-pressure probes permanently installed in the inlet rakes were used to determine that the flow was generally uniform in all inlets of a given configuration.

The exhaust nozzles were equipped so that they could be remotely controlled to direct the exhaust flow 25° rearward (measured from the vertical) or straight downward. The nozzles had vanes (as shown in figs. 6 to 9) to assure full turning of the exhaust stream. The nozzles were equipped with total-pressure probes and bare-bead thermocouples for setting the engine operating conditions.

The size of the model was, in general, dictated by the size of the engine. The engine exhaust-nozzle area was 118 in^2 (761 cm^2), or about one-ninth the nozzle area of a 25 000-pound (111 200-newton) jet VTOL fighter.

The two wings used on the model were triangular in shape and were flat plates 2 inches (5.08 cm) thick with rounded leading edges and beveled trailing edges. The wing sizes were such that the ratios of wing area to jet nozzle area were 43 and 85, with the smaller wing being representative of that of current VTOL fighter designs. The wings could be mounted in either a high or low position on the fuselage or could be removed entirely. For the wing-off configuration a 2-inch (5.08-cm) steel bar replaced the wing and was used as the rear-position fuselage support (see fig. 3(b)).

All the temperature and pressure data were recorded in the form of time histories by using oscillograph recorders.

TESTS AND TECHNIQUES

The tests were conducted in the Langley full-scale tunnel with the ground represented by a 42-foot-wide by 52-foot-long (12.8-meter by 15.8-meter) ground board. The edge of the ground board was approximately 21 exhaust-nozzle diameters to the side and about 19 diameters forward of model center reference, which is located 165.60 inches (420.62 cm) from the model nose. The model configurations investigated are described in table I. Nozzle heights for the lower surface nozzle arrangements were 1.17, 3.00, and 5.00 effective nozzle diameters. The effective diameter is 12.00 inches (30.48 cm). The side-nozzle-arrangement tests were conducted at the same model heights as were the tests for the lower surface nozzle arrangements; thus, the side nozzles were at a greater height above the ground than the nozzles in the other arrangements. The actual nozzle heights for the side nozzles were 2.22, 4.05, and 6.05 effective nozzle diameters. The tests were conducted for azimuth angles (ψ) of 0°, 45°, and 90°. For an azimuth angle of 0°, windspeeds of 0, 5.92, 11.85, 17.78, 23.70, 29.63, and 35.55 knots were

investigated, and at azimuth angles of 45° and 90° the windspeeds were 5.92 and 11.85 knots. All tests were conducted with the model at zero angle of attack.

The test procedure was as follows: (1) bring the wind-tunnel airspeed up to the desired test value, (2) start the engine and bring the speed up to idle power (70 percent) with the nozzles deflected 25° rearward, (3) increase engine speed to 80 percent of maximum and turn oscillograph recorders on (tests of ref. 1 showed no ingestion prior to 80 percent), (4) deflect nozzles to 0° (straight down), (5) pause 3 to 4 seconds to simulate time for final pilot checks before take-off, (6) bring engine as rapidly as possible to maximum speed, (7) run for 6 to 8 seconds at this condition, and (8) shut down. Even though ingestion in general did not occur with the nozzles deflected rearward 25°, during a few tests the engine stalled before maximum speed was attained. When this stall occurred, the test was repeated with the engine brought to maximum allowable speed (tailpipe temperature limit) before the nozzles were deflected downward.

Because of the short duration of each of the tests and the very large volume of the wind tunnel, the ambient temperature of the tunnel rarely increased more than 10° F (6° C) during a test, and from the time of downward deflection of the nozzles (time zero for the time histories) to the end of the test the ambient-temperature rise was estimated to be no more than 2° F (1° C). The inlet-air temperature rise was in general considered to be the increase in inlet-air temperature from the time of downward nozzle deflection to the time when stabilized inlet-air temperature conditions were reached some 10 to 12 seconds later. For the conditions in which ingestion occurred before downward nozzle deflection, the temperature rise was considered to be the increase in temperature above the initial ambient temperature condition.

Because of the question of whether the same test results would be obtained with the high-response thermocouples of the present investigation as were obtained with the low-response thermocouples of reference 1, some tests of reference 1 were repeated during the present investigation. The repeat tests were in general conducted for the model height indicated in reference 1 to result in maximum inlet-air temperature rise. For instance, the top-inlet repeat tests were for a nozzle height (h/D_e) of 3.00 and the side-inlet repeat tests were conducted at h/D_e of 1.17.

RESULTS AND DISCUSSION

The data presented herein should be viewed in the light of the general discussions of the mechanism of hot-gas ingestion presented in references 1 to 14. These papers indicate for still-air conditions that only small rises in the inlet-air temperature result from recirculation of hot exhaust gases by convection or from recirculation of the far-field flow, but a very high inlet-air temperature rise can result from the flow of exhaust gas up around the fuselage for some multiple-nozzle configurations. These reference

papers show that, near the ground, multiple-exhaust-nozzle arrangements can result in a jet efflux which tends to form a fountain of exhaust gas flowing upward between the main jet streams. This fountain of hot exhaust gas spreads outward along the bottom of the aircraft, upward around the fuselage, and directly into the inlets with very little time for cooling by mixing with the surrounding air. It should be noted that the aforementioned flow characteristics are greatly altered in the presence of surface winds (see ref. 1). With surface winds the far-field hot gases are blown back toward the inlet and are ingested. The surface winds also alter the fountain flow and thereby result in increased or decreased ingestion, depending upon the wind velocity and/or the nozzle and inlet configuration.

In addition to the characteristics of flow fields just mentioned, it must be realized that all these flow fields resulting from exhaust, winds, and configuration are very unsteady and do not result in well-defined steady-state test results. Because of these unsteady flow conditions, the ingestion of symmetrically located inlets for nominally symmetrical conditions may be quite different for some high-ingestion configurations. The important point to note in such cases is not that the temperature levels of symmetrical inlets are different, but rather the general level of inlet-air temperature rise. In general, for current turbojet engines, an average inlet-air temperature rise of about 30° F (16° C) would result in an engine thrust loss on the order of 10 percent; therefore, for the practical case, the inlet-air temperature rise should be kept down to this general level, and the very high ingestion of some configurations only serves to indicate configurations and operating conditions that should be avoided.

Presentation of Data

The data are presented in figures 10 to 39 as follows:

General Considerations

As stated previously, the thermocouples of the present investigation were much more responsive than those used in the investigation of reference 1. It was believed that more meaningful results would be obtained by use of the high-response thermocouples – results that would be of more use to the engine manufacturer who is interested in the frequency of the temperature variations as well as the overall level of temperature. Also, it has been suggested by some researchers that the overall level of inlet-air temperature may be misrepresented by low-response thermocouples. A comparison of the time-temperature histories obtained from the current investigation and from reference 1 are shown in figures 10 and 11 for configurations which are prone to hot-gas ingestion. The particular conditions of nozzle height and windspeed of figures 10 and 11 were selected because the average inlet-air temperature rise was maximum for these conditions. It can be seen from these data that either the high-response or the low-response thermocouples would provide adequate temperature information provided the average value of temperature was the desired information. As originally expected, however, the low-response thermocouples do not show the very rapid initial temperature rise when such rapid rise occurs, and they do not show rapid temperature fluctuations which are known to sometimes cause engine compressor stall (see refs. 1 and 2).

The data of figures 10 and 11 illustrate a limitation of the test data, which will be applicable to the other time-temperature histories presented herein, in that the nozzle pressure is very low for the ingestion-prone configurations. This low pressure is, of course, the result of reduced engine performance caused by the elevated inlet-air temperatures. Basically, the engine could not reach its normal maximum pressure after it had started ingesting hot gas. This low-pressure condition for cases in which high ingestion occurs is unfortunate from a research standpoint because the ingestion characteristics for a normal nozzle pressure ratio (on the order of 1.8 to 1.9) are not illustrated. The data, however, reflect the conditions that would exist for an actual operational vehicle

since a turbojet engine is used to provide the inlet and exhaust flow of the present investigation.

Another point that should be made relative to the fact that the tests were run in a wind tunnel is that the presence of the tunnel and test-chamber walls and the size limits of the ground board are not believed to have any significant effect on the results as compared with what they would have been in free air. Special tests and analyses were made in reference 1 to determine whether there was any such effect, and comparable results were obtained in both outdoor and tunnel tests. The forward lip of the ground board was about 19 effective nozzle diameters ahead of the model, with a boundary-layer thickness at the model of about 3.5 inches (0.0889 meter) at a windspeed of 11.85 knots or about 0.3 nozzle diameters. This boundary-layer thickness at the model might have some significance at the instant the nozzles are deflected downward and the exhaust flow starts forward along the ground board. Once the forward flow is established and reaches nearly to the forward edge of the ground board, however, boundary-layer thickness near the model probably has no significance for the present tests.

Time-Temperature Histories

All the inlet-air temperature rise data presented in the subject report were obtained from time-temperature history information similar to that presented in figures 12 to 15. The time-temperature histories are not presented for all test conditions, however, since it is believed that the great number of figures would tend to obscure rather than clarify the issue. The sample time-temperature histories are presented to illustrate the basic differences in ingestion caused by utilizing top or side inlets with and without a wing installed. These data from the rectangular-nozzle-arrangement configuration were selected for presentation because they represent the worst condition investigated from an ingestion standpoint and they show very well the great problem existing for the aircraft and engine designers – that is, the extreme temperature environment of high temperature values, of very rapid changes in the inlet-air temperature at a given probe location, and of large variation in temperature across the face of the inlets. For the high-ingestion test condition (low forward or lateral speed) maximum inlet-air temperature rises ΔT on the order of 300° F (167° C) were experienced and for this condition there were differences in temperature across the face of the engine inlet of as much as 200° F (111° C). It should also be noted that the inlet-air temperature rise occurred within 1 second after downward nozzle deflection and thus the hot gases could not be avoided by rapid vertical take-off.

For some of the tests, complete time-temperature histories could not be obtained because of engine compressor stall and flame-out before the desired operating condition was reached. For such tests the procedure was altered, and the time-temperature histories presented are for repeat tests in which the engine was brought to full speed before

downward nozzle deflection (see fig. 12(f)). It is not clear just why the engine stalled under some of the test conditions; however, it is known that the particular model of engine used for the present tests (the Y- or prototype model) was very sensitive to inlet airflow and/or temperature environment. The engine sometimes stalled for relatively low inlet-air temperature conditions, so inlet-air temperature rise is certainly not the sole cause of engine stall. Small perturbations of inlet pressures could not be measured for the present investigation because the long inlet-pressure tubes required would damp any rapid pressure changes. It is not known, therefore, whether inlet-pressure perturbations contributed to engine stall.

It should be noted that very few engine stalls occurred with the top-inlet configurations. To some extent, this fact can be attributed to the lower inlet temperatures of the top-inlet configurations as compared with the temperatures of the side-inlet configurations, but the lower number of stalls probably results primarily from the relatively long inlet ducting of the top-inlet configurations. The long ducting would allow for more mixing of the inlet air and probably more uniformly distributed temperatures and pressures at the face of the engine. This surmise is substantiated by the fact that tests reported in reference 2, which had engines standing upright in the fuselage with the actual engine inlet at the top of the fuselage, resulted in many engine stalls when the average inlet-air temperature rise was relatively small. In any case, the fact that this particular engine stalled is not the important point of the investigation. The important point is that very rapid inlet-air temperature changes can occur and must be eliminated in the design of the aircraft or accommodated by the design of the engine.

Variation of Average Inlet-Air Temperature Rise With Windspeed

The average inlet-air temperature rise data presented in figures 16 to 39 were obtained from time-temperature history information similar to that presented in figures 12 to 15. The average temperature of each probe was obtained and then arithmetically averaged for each inlet. The basic data on average inlet-air temperature rise are presented in figures 16 to 37 and are summarized in figures 38 and 39. These figures include data from the present series of tests and also some data from reference 1 to provide a complete presentation of all the configurations tested. The data are not discussed in great detail; rather, the principal characteristics are pointed out for each exhaust-nozzle and inlet arrangement.

Repeatability of test results.- Although the present series of tests was intended to extend the knowledge of causes and effects of hot-gas ingestion by testing additional generalized configurations, a few tests were conducted for the same configurations and test conditions of reference 1. These tests were made to provide a continuity of test results, to provide an indication of the repeatability of test results for this type of investigation,

and to provide information on the effects of thermocouple response characteristics such as that previously discussed. One problem now being investigated by NASA is that of scaling hot-gas ingestion results – that is, determining whether small-scale results can be scaled to give large-scale characteristics. One of the problems associated with scaling is the question of whether test results of a given model are repeatable. It could be that unstable exhaust flow characteristics would preclude repeating test results and therefore determination of scale effects would be very questionable.

The repeatability of the test results of reference 1 is shown in figures 16 to 19. The data for the top-inlet configurations (figs. 17 and 19) repeated very well in the present investigation, but the data for the side-inlet configurations (figs. 16 and 18) did not repeat well. The shape of the curves, though, was fairly well repeated for the side-inlet, rectangular nozzle arrangement and the gross magnitude of the inlet-air temperature rise was similar (see fig. 16). For the side-inlet, in-line nozzle arrangement, however, the correlation was not even this favorable (see fig. 18); thus, the test conditions have been examined and the literature has been searched to discover possible causes of the large discrepancies. It is known that the two front nozzles of the in-line arrangement in the current tests were inadvertently directed slightly rearward (2^{o} as noted from nozzle flow surveys) and it appears that the tests of reference 1 were conducted with the nozzle flow vertical. No detailed flow surveys were made for the tests of reference 1, but the flow impingement patterns on the floor beneath the model indicated that the exhaust flow was vertical. Data of references 6 and 7 show the ingestion to be very much a function of the angle of emission of the exhaust jets, particularly the in-plane angles of forward- and aft-mounted engines. Directing the exhaust flow only a degree or two rearward was shown to cause the exhaust flow to follow the direction of the deflection angle and reduce the ingestion of a forward-mounted engine. It is assumed, therefore, that differences in the ingestion pattern of the in-line configuration of figure 18 were a result of the small rearward nozzle deflection angle for the present tests.

The nozzle-flow alinements for all the present test configurations were as follows:

Nozzle arrangement	Alinement of flow in –			
	Nozzle 1	Nozzle 2	Nozzle 3	Nozzle 4
Rectangular	1^{o} aft; 0^{o} laterally	2^{o} aft	3^{o} aft	2^{o} aft
In-line	2^{o} aft; 0^{o} laterally	2^{o} aft	1^{o} forward	0^{o}
Side	2^{o} aft; 0^{o} laterally	0^{o}	----------	2^{o} forward; 4^{o} right
Single	1.5^{o} aft; 0^{o} laterally			

Although the hot-gas ingestion characteristics were not as repeatable as desired from reference 1 to the present investigation, the characteristics were found to repeat fairly well within each investigation. The small-scale tests of reference 5 and other large-scale tests of reference 7 have shown similar results. It is concluded, therefore, that hot-gas ingestion characteristics of a particular test vehicle are repeatable as to general character and level but not in detail.

Rectangular nozzle arrangement.- The average inlet-air temperature rise as a function of windspeed for the rectangular nozzle arrangement with side and top inlets is shown in figures 20 to 23. These data show the effects of nozzle height, wing size and location, and model heading. All the data show the same general pattern of high inlet-air temperature rise at low speeds with wind from any of the test directions, and little or no ingestion ($\Delta T \approx 0^{o}$) for forward speeds greater than about 30 knots.

Side inlets: For the side-inlet, rectangular nozzle arrangement, very high values of inlet-air temperature rise were experienced for zero and very low forward speeds when the model was near the ground. The inlet-air temperature rise was about 200^{o} F (111^{o} C) at the lowest test height, $h/D_e = 1.17$, but decreased very rapidly with increasing height (e.g., see results for inlet 1 in fig. 20).

After an initial increase in inlet-air temperature rise with increasing headwind to about 10 to 15 knots, the inlet-air temperature rise decreased very rapidly with further increases in the speed and ceased to be a problem ($\Delta T \approx 0^{o}$) for speeds on the order of 40 to 50 knots. Smoke flow studies showed that the hot exhaust was blown back beneath the model at these higher forward speeds.

The ingestion problem for side-wind conditions ($\psi = 45^{o}$ and $\psi = 90^{o}$), in the speed range investigated (0 to 12 knots), was about the same as that experienced for headwind conditions ($\psi = 0^{o}$).

Placing the wing low on the fuselage is seen to greatly reduce the hot-gas ingestion for the lowest test height ($h/D_e = 1.17$) for side-wind conditions, but very little effect of wing location is noted for headwinds. The high wing has very little effect on the ingestion characteristics for any of the wind conditions, and about the same results were obtained with or without a high wing installed (see fig. 21).

Top inlets: For the top-inlet, rectangular nozzle arrangement (with $S_W/S_J = 43$), the maximum average inlet-air temperature rise was about 100^{o} F (55.5^{o} C) and occurred at the intermediate test height ($h/D_e = 3.00$). (For example, see results for inlet 1 in fig. 22.) This temperature rise was about one-half that for the side-inlet arrangement.

The variation of inlet-air temperature rise with windspeed was similar to that for the side-inlet arrangement; that is, ingestion was quite high for zero and low speeds, but

decreased to zero by the time speeds on the order of 30 to 40 knots were reached. Ingestion was also about the same for either headwind or side-wind conditions.

For the nozzle height for maximum ingestion ($h/D_e = 3.00$), placing the wing in a low position greatly attenuated the ingestion. Also, the effect of wing size on the ingestion was very pronounced (see fig. 23). Without a wing installed, the maximum average inlet-air temperature rise was on the order of 200° F (111° C), whereas, with the largest wing tested $\left(S_W/S_J = 85\right)$, the maximum average ingestion values were usually on the order of 20° F to 30° F (11° C to 17° C). Wing size and placement are seen, therefore, to be very important from the standpoint of reducing the ingestion problem of the top-inlet, rectangular-nozzle-arrangement (lift-engine) configuration. The wing shields the inlets from the vertically rising hot-gas fountain of the rectangularly spaced nozzles.

Side nozzle arrangement.- The side nozzle arrangement was tested only with side inlets (similar to the arrangement of the Hawker Siddeley P.1127 presently being flight-tested at the Langley Research Center), since it was believed to be impractical to have top-inlet, side nozzle arrangements.

The variation of average inlet-air temperature rise as a function of windspeed, nozzle height, and wing size is shown in figures 24 and 25. The fact that the values of height noted in these figures are different from those on all the other figures was the result of the nozzles being on the side, rather than the bottom, of the fuselage. The bottom of the fuselage was at the same heights as for the tests of the other configurations.

The maximum average inlet-air temperature rise was somewhat lower than that of the rectangular arrangement – about 120° F (67° C) as compared with 200° F (111° C).

The same general variation of ingestion with windspeed is seen for the side nozzle arrangement as for the rectangular nozzle arrangement in that maximum ingestion usually occurred at low speeds (with either headwinds or side winds) followed by a rapid decrease in ingestion for further increases in speed. The ingestion was zero at about 30 knots.

The effect of wing size was quite small as might be expected, since the wing was above both the nozzles and the inlets.

Even though the inlet-air temperature rises were lower than for the rectangular nozzle arrangement, they were much too high and would cause a severe operational problem. The Hawker Siddeley P.1127 airplane, however, operates consistently in the VTOL mode with this same inlet and exit arrangement. In the P.1127, the front exhaust nozzles handle the relatively cold flow from the fan, and this cold flow from the front nozzles prevents the hot flow from the rear nozzles from going forward where it could be ingested into the inlets. Unpublished data show, however, that inlet-air temperature rise for the airplane P.1127 is the same as that for the present model in terms of percent of the

temperature of the front nozzles (10 percent in each case). For still-air conditions the P.1127 has an average inlet-air temperature rise of about 13° F (7° C) for a front-nozzle temperature of about 126° F (70° C) above ambient, whereas the present configuration has average ingestion of about 120° F (67° C) for a nozzle temperature of about 1134° F (630° C) above ambient.

In-line nozzle arrangement.- The average inlet-air temperature rise as a function of windspeed for the in-line nozzle arrangement with side and top inlets is shown in figures 26 to 31.

Side inlets: The ingestion is very low for the side-inlet, in-line nozzle configuration except for the lowest test height. Even at the lowest test height, however, the ingestion is significantly lower than for the other configurations, the maximum values of ΔT being about 60° F (33° C).

As with the other configurations, the ingestion initially increases with low speeds for both headwinds and side winds and then drops to zero for headwinds of about 30 knots.

There is no significant effect of wing size or vertical location on the ingestion characteristics of this configuration.

Top inlets: The top-inlet, in-line nozzle configuration has markedly lower ingestion than any of the other test configurations, the maximum values of ΔT being about 10° F (6° C) in headwinds and 40° F (22° C) in side winds.

There are no significant effects of nozzle height or of wing size or location on the ingestion characteristics of this configuration.

Single-nozzle arrangement.- The single-nozzle arrangement was tested in order to provide basic data to aid in the analysis and evaluation of the other, more practical, configurations. It is expected that exhaust flows that are spaced closely enough to coalesce before striking the ground will behave in more or less the same manner as a single exhaust. The important characteristic of the single nozzle is that it is symmetrical and it does not produce a fountain effect; therefore, any recirculation effect is caused by recirculation of the far-field flow. The flow characteristics are also fairly well known from investigations such as references 8 and 9, which include both theoretical and experimental results.

The average inlet-air temperature rise as a function of windspeed for the single-nozzle arrangement with side and top inlets is shown in figures 32 to 37.

Side inlets: The side-inlet, single-nozzle configuration had very little ingestion for zero windspeeds since there was no fountain of hot gases and most of the hot gases were blown far away from the model. There was a marked increase in ingestion with increasing headwind, however, and maximum ingestion occurred at much higher speeds (on the order

of 30 knots) than for the other configurations. The reason for this difference is probably that the single jet does not mix and slow down as fast as the others and therefore greater headwinds are required to turn the hot gases back toward the inlets. The maximum average inlet-air temperature rises, however, are about the same as for the other high-ingestion configurations.

Side winds show little effect on the ingestion but this characteristic is probably the result of the low side-wind speeds. Actually, because of the symmetry of the exhaust flow from the single nozzle, winds from any direction should result in somewhat similar ingestion characteristics.

There is a marked effect of nozzle height on the ingestion characteristics. Ingestion is greatly reduced as nozzle height is increased. There is also a large effect of wing height. Apparently the low wing aids in directing the hot gases away from the model. (See figs. 32 and 33.)

For the high wing position, wing size has no significant effect on the ingestion characteristics. (See fig. 34.)

Top inlet: The ingestion was low for all the top-inlet, single-nozzle configurations. Varying windspeed, raising or lowering the wing, or even taking the wing off had very little effect. (See figs. 35 to 37.) In general, it appears that hot-gas ingestion would not be a serious problem for the top-inlet, single-nozzle configuration.

CONCLUSIONS

Results of hot-gas ingestion tests conducted in the Langley full-scale tunnel on large-scale VTOL fighter-type aircraft configurations have indicated the following conclusions, which are virtually the same conclusions drawn in NASA TN D-4609 but which are now more completely documented:

1. Hot-gas ingestion is very configuration-dependent, the nozzle arrangement, inlet position, and wing location being important variables.

   (a) The rectangular nozzle arrangements and the side-inlet single-nozzle arrangement had the highest inlet-air temperature rises (on the order of 200° F (111° C)).

   (b) An in-line nozzle arrangement resulted in virtually no hot-gas ingestion except in side winds.

   (c) Side inlets generally resulted in higher inlet-air temperature rises than top inlets.

2. Winds have a large effect on the magnitude of the inlet-air temperatures.

(a) Except for the single-nozzle arrangement, maximum ingestion occurred at windspeeds from zero to about 20 knots. Maximum ingestion occurred at about 30 knots for the single-nozzle arrangement.

(b) With headwinds greater than about 30 knots, hot-gas ingestion was virtually eliminated except for the single-nozzle arrangement.

3. Deflecting the exhaust gases rearward 25° with vectoring nozzles generally eliminated the ingestion of hot exhaust gases.

4. The use of very sensitive inlet thermocouples was found to be unnecessary for determining the general level of inlet-air temperatures, but there are rapid fluctuations of temperature which could be measured only with high-response thermocouples.

5. Although various investigations have produced much information of a general nature which can be used as design guidelines, the solution of hot-gas ingestion problems is still in an exploratory stage; thus, at present, tests should be conducted on each configuration at each operating condition that is expected to be encountered.

Langley Research Center,
National Aeronautics and Space Administration,
Langley Station, Hampton, Va., September 12, 1969.

REFERENCES

1. McLemore, H. Clyde; and Smith, Charles C., Jr.: Hot-Gas Ingestion Investigation of Large-Scale Jet VTOL Fighter-Type Models. NASA TN D-4609, 1968.

2. Tolhurst, William H., Jr.; and Kelly, Mark W.: Characteristics of Two Large-Scale Jet-Lift Propulsion Systems. Conference on V/STOL and STOL Aircraft, NASA SP-116, 1966, pp. 205-228.

3. Kemp, E. D. G.: Studies of Exhaust Gas Recirculation for VTOL Aircraft. AIAA Paper No. 67-439, July 1967.

4. Harris, A. E.; Marbert, J. A.; and Tatom, J. W.: VTOL Transport Exhaust Gas Ingestion Model Tests. Proceedings of the Seventh Annual National Conference on Environmental Effects on Aircraft and Propulsion Systems, Nav. Air Propulsion Test Center and Inst. Environ. Sci., Sept. 1967, pp. 145-166.

5. Ryan, Patrick E.; Heim, Richard J.; and Cosgrove, Wayne J.: A Generalized Experimental Investigation of Hot Gas Recirculation and Ingestion for Jet VTOL Aircraft. NASA CR-1147, 1968.

6. Hall, Gordon R.; and Rogers, Kenneth H.: Recirculation Effects Produced by a Pair of Heated Jets Impinging on a Ground Plane. NASA CR-1307, 1969.

7. Hall, Gordon R.: Recirculation and Ingestion Characteristics of a Large-Scale VTOL Lift Engine Pod. NASA CR-72410, 1968.

8. Cox, M.; and Abbott, W. A.: Studies of the Flow Fields Created by Single Vertical Jets Directed Downwards Upon a Horizontal Surface. N.G.T.E. Mem. No. M.390, Min. Aviation (Brit.), Oct. 1964.

9. Abbott, W. A.: Studies of Flow Fields Created by Vertical and Inclined Jets When Stationary or Moving Over a Horizontal Surface. C.P. No. 911, Brit. A.R.C., 1967.

10. Lavi, Rahim; Hall, Gordon R.; and Stark, Wilbur W.: Full-Scale Ground Proximity Investigation of a VTOL Fighter Model Aircraft. NASA CR-1098, 1968.

11. Gittner, U.; Hoffert F.; and Lotz, M.: Interaction Between Airframe-Powerplant Integration and Hot Gas Ingestion for Jet-Lift V/STOL Transport Aircraft. Presented to AGARD 31st Flight Mechanics Panel Meeting on Integration of Propulsion System in Airframe (Friedrichshafen, Germany), Sept. 13-15, 1967.

12. Ryan, Patrick E.; and Cosgrove, Wayne J.: Empirically Determined Wind and Scale Effects on Hot Gas Recirculation Characteristics of Jet V/STOL Aircraft. NASA CR-1445, 1969.

13. Kirk, Jerry V.; and Barrack, Jerry P.: Reingestion Characteristics and Inlet Flow Distortion of V/STOL Lift Engine Fighter Configurations. AIAA Paper No. 68-78, Jan. 1968.

14. Barrack, Jerry P.; and Kirk, Jerry V.: Low-Speed Characteristics of High-Performance Lift-Engine V/STOL Aircraft. [Preprint] 680644, Soc. Automot. Eng., Oct. 1968.

TABLE I.- DESCRIPTION OF CONFIGURATIONS

Nozzle arrangement	Wing position	Inlet position	Wing size, S_W/S_J
Rectangular	High	Top	43; 85
		Side	43; 85
	Off	Top	
		Side	
In-line	High	Top	43; 85
		Side	43; 85
	Off	Top	
		Side	
Side	High	Side	43; 85
	Off	Side	
Single	High	Top	43; 85
		Side	43; 85
	Low	Top	43; 85
		Side	43; 85
	Off	Top	
		Side	

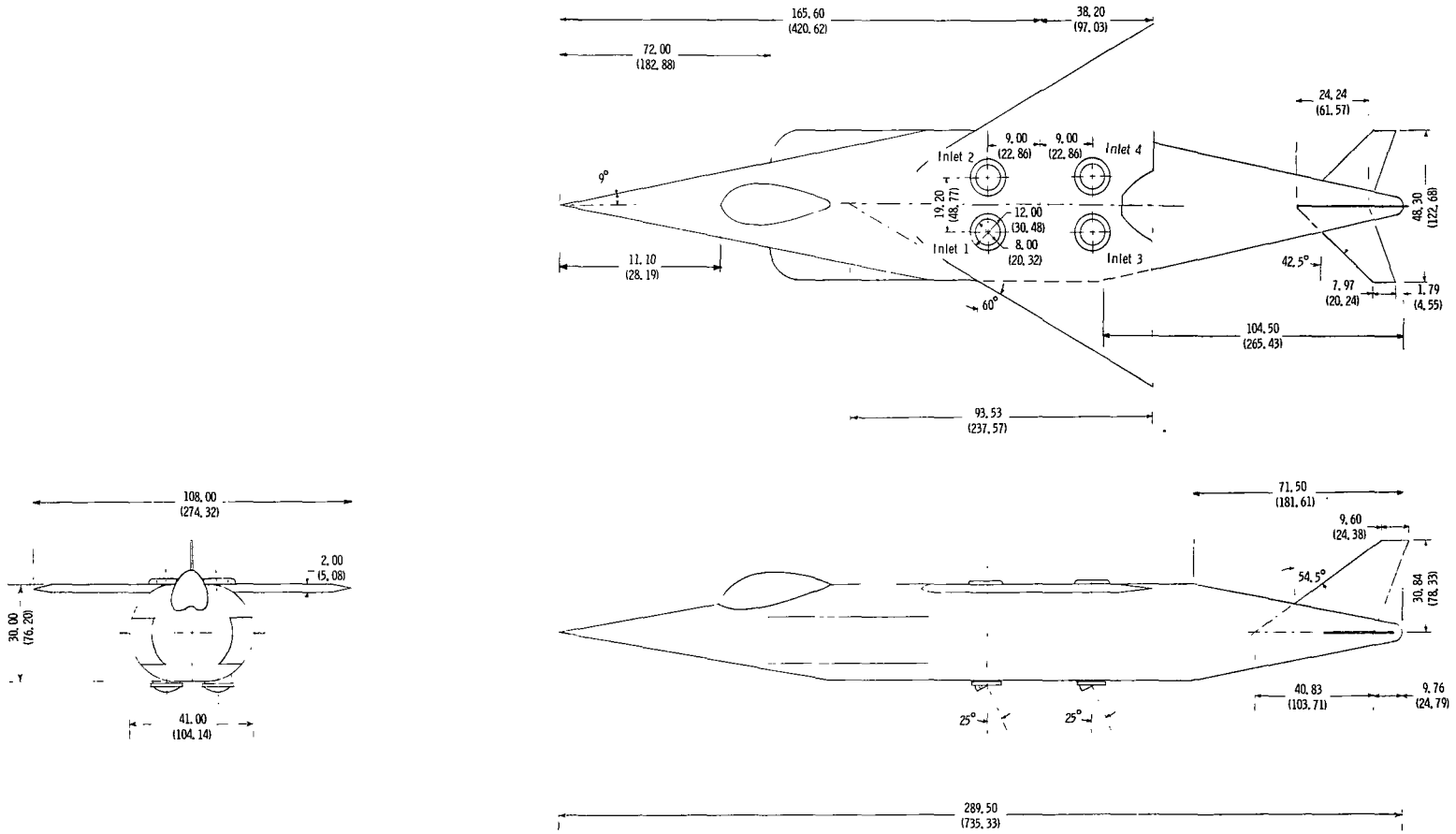

(a) Rectangular exhaust-nozzle arrangement with top inlets and small wing.

Figure 1.- General arrangement of model. (Dimensions are given in inches and parenthetically in centimeters.)

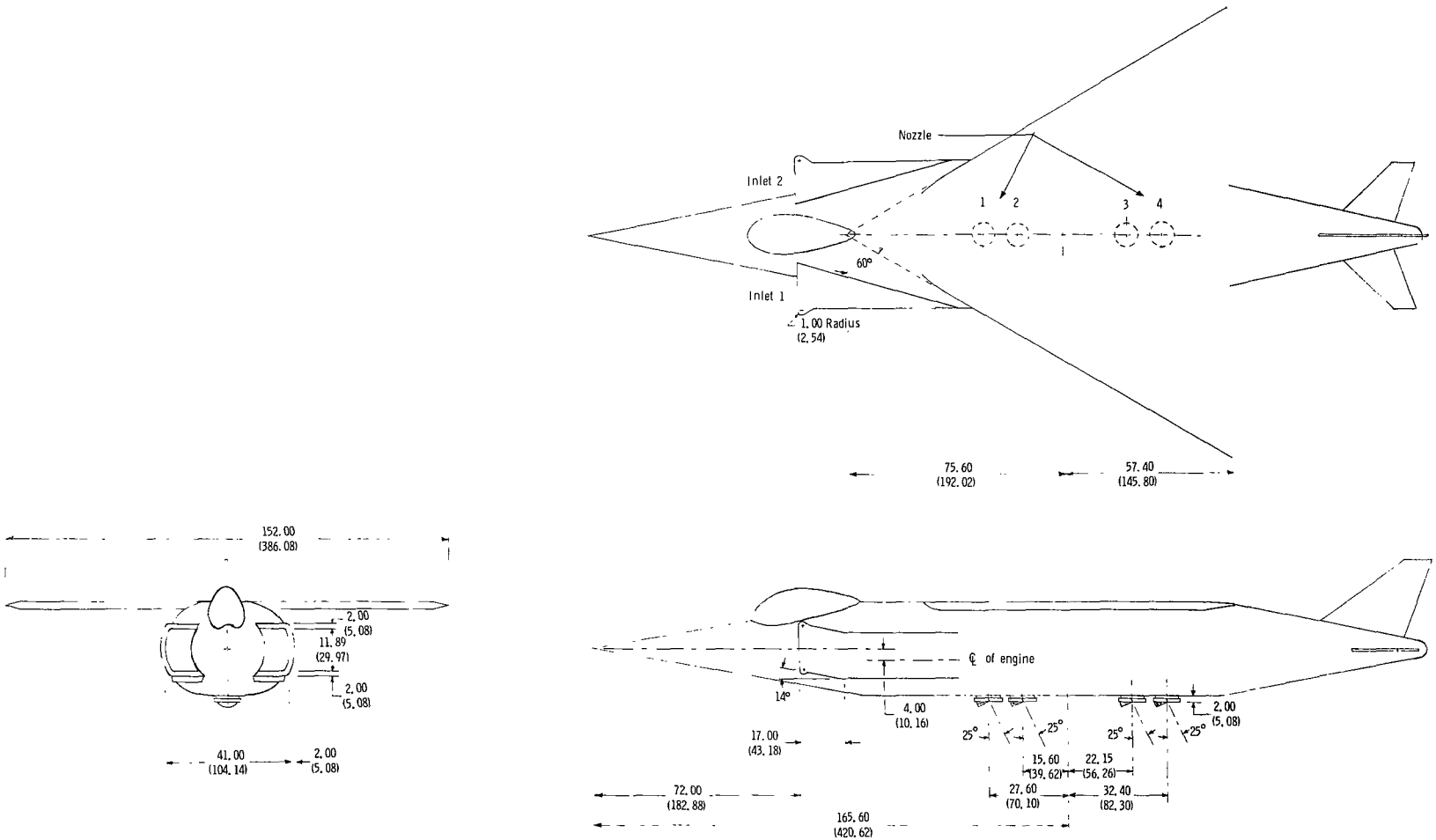

(b) In-line nozzle arrangement with forward-facing side inlets and large wing.

Figure 1.- Continued.

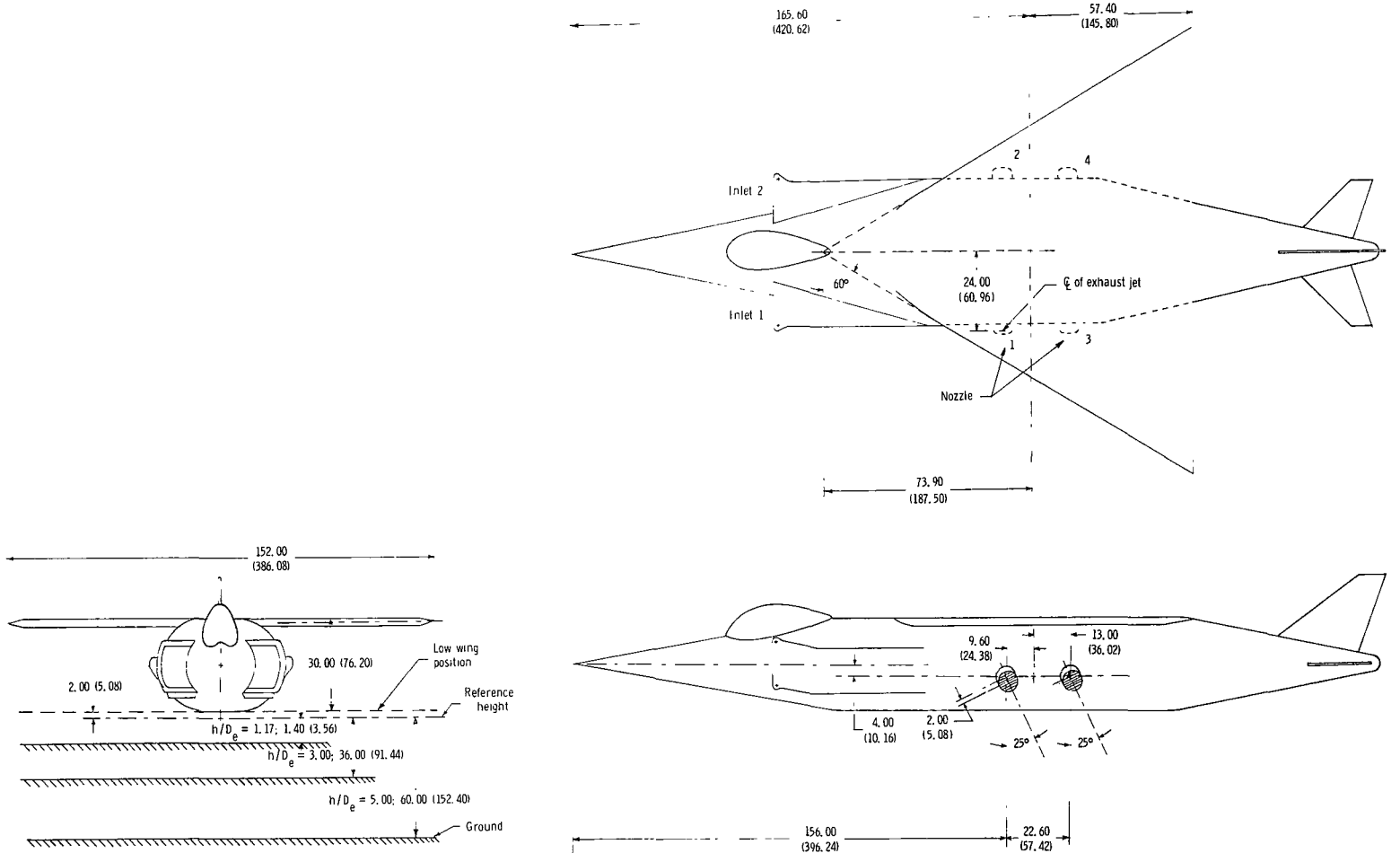

(c) Side nozzle arrangement with forward-facing side inlets and large wing.

Figure 1.- Continued.

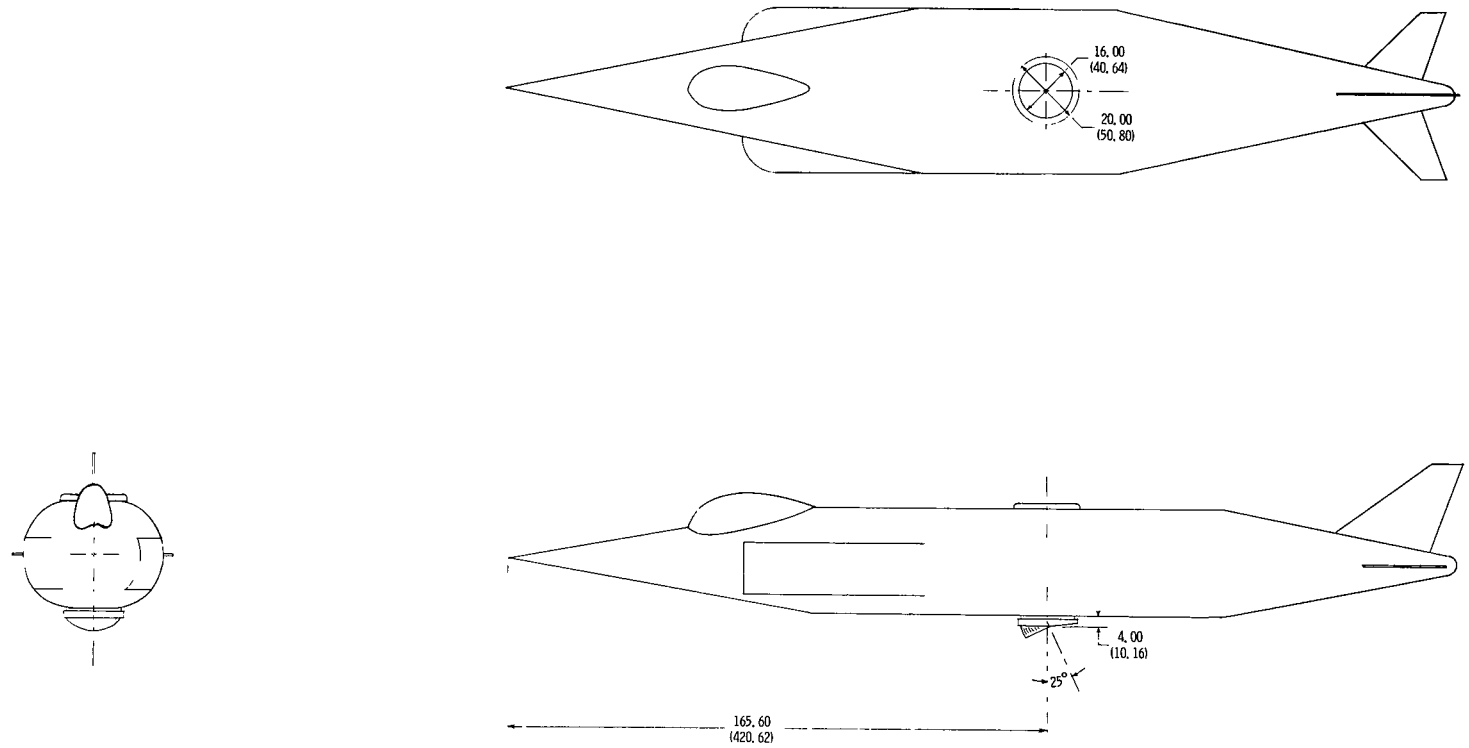

(d) Single-nozzle arrangement with top inlet and with wing removed.

Figure 1.- Concluded.

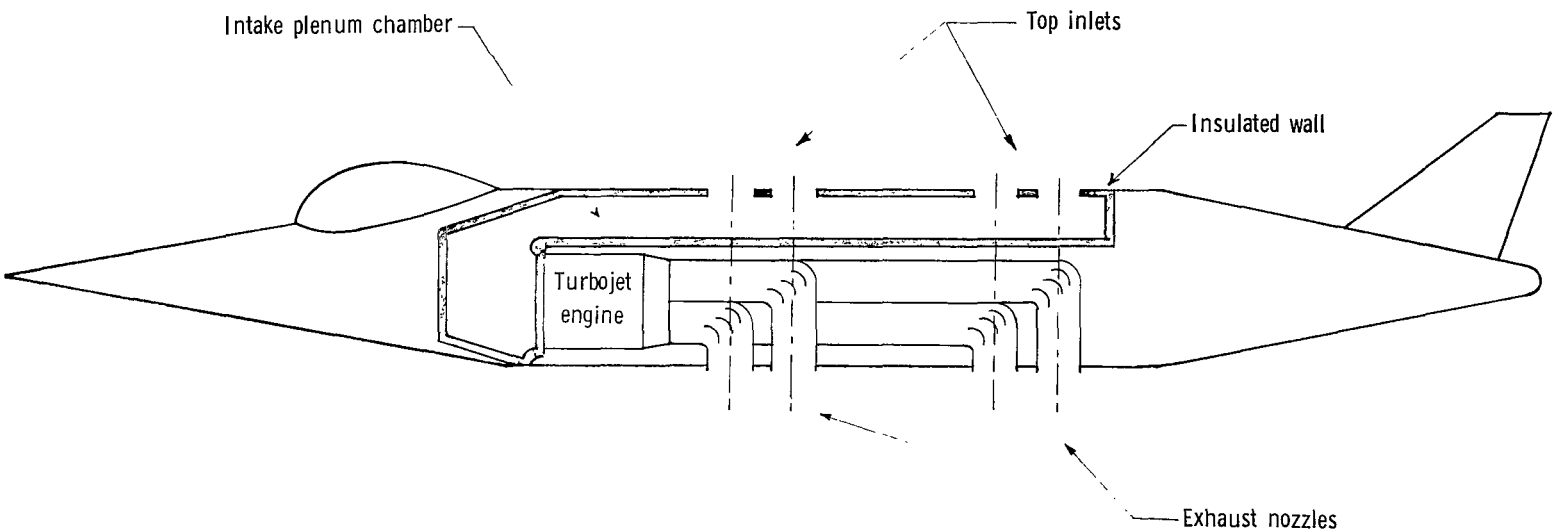

Figure 2.- Schematic arrangement of inlets, exhaust nozzles, and plenum chamber. (In-line lift-engine configuration illustrated.)

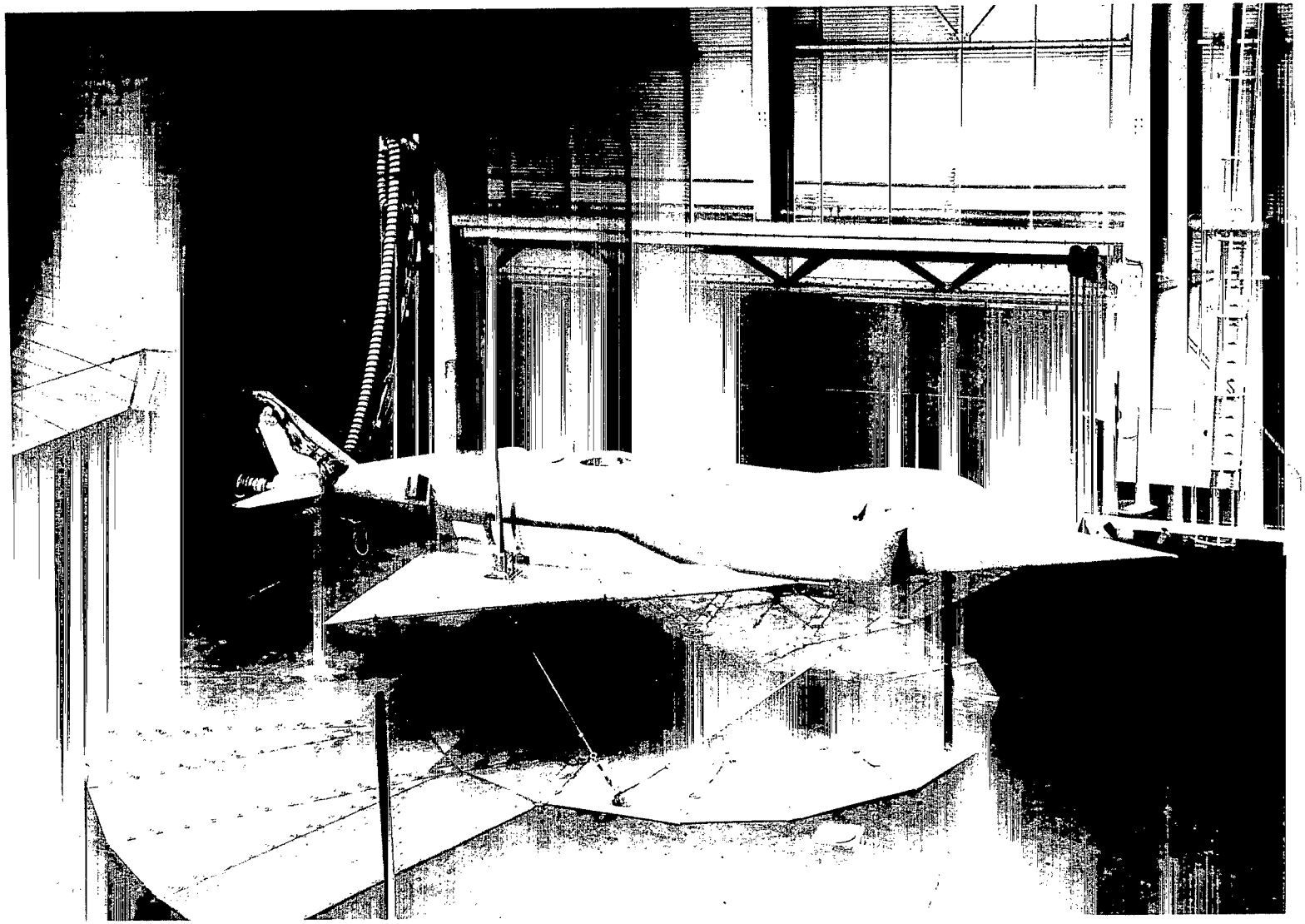

(a) Three-quarter front view of low-wing, single-nozzle, top-inlet configuration. L-67-3838

Figure 3.- Model and test setup in Langley full-scale tunnel.

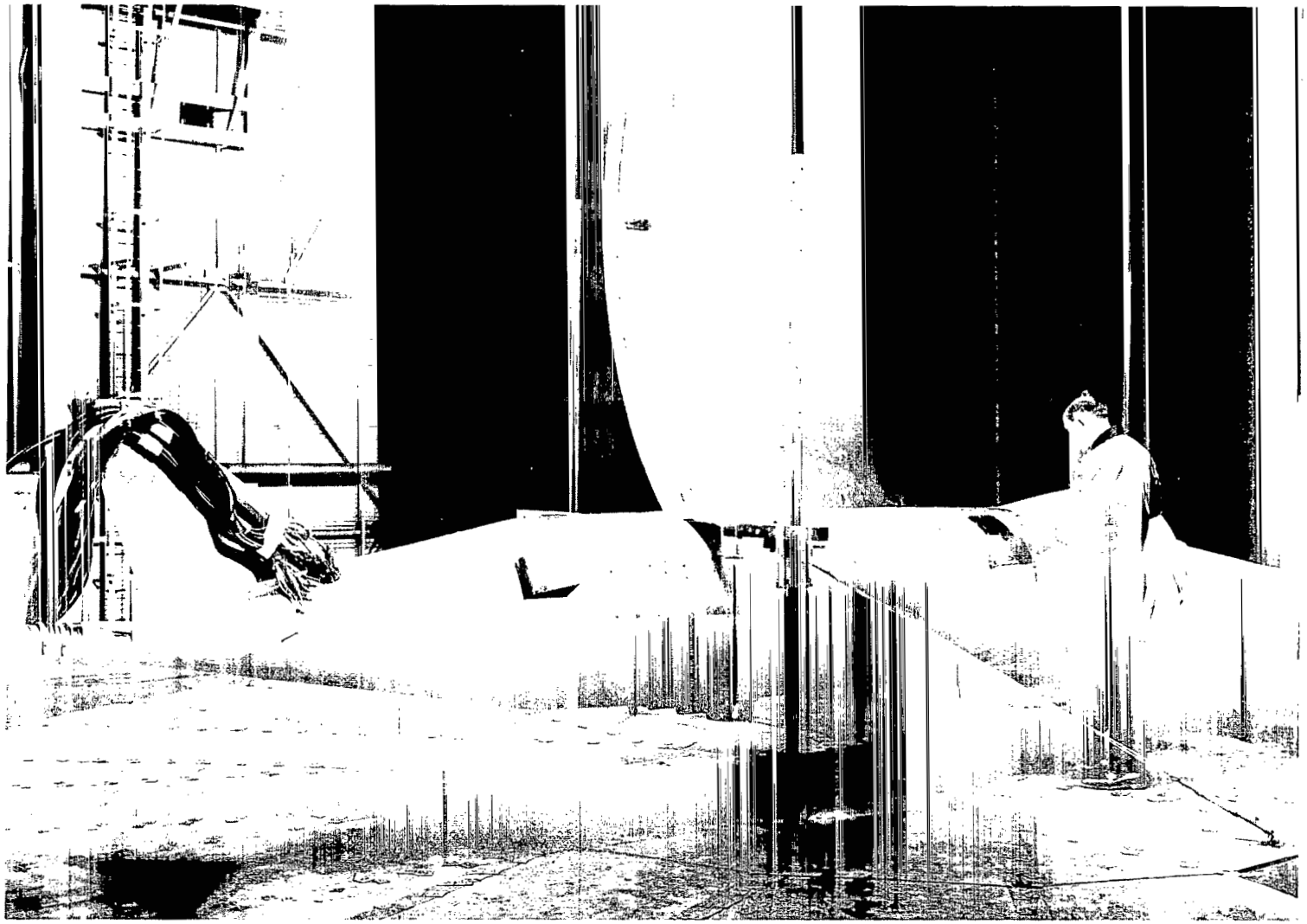

(b) Three-quarter rear view of rectangular-nozzle-arrangement configuration with side inlets and with wing removed. L-67-2963

Figure 3.- Continued.

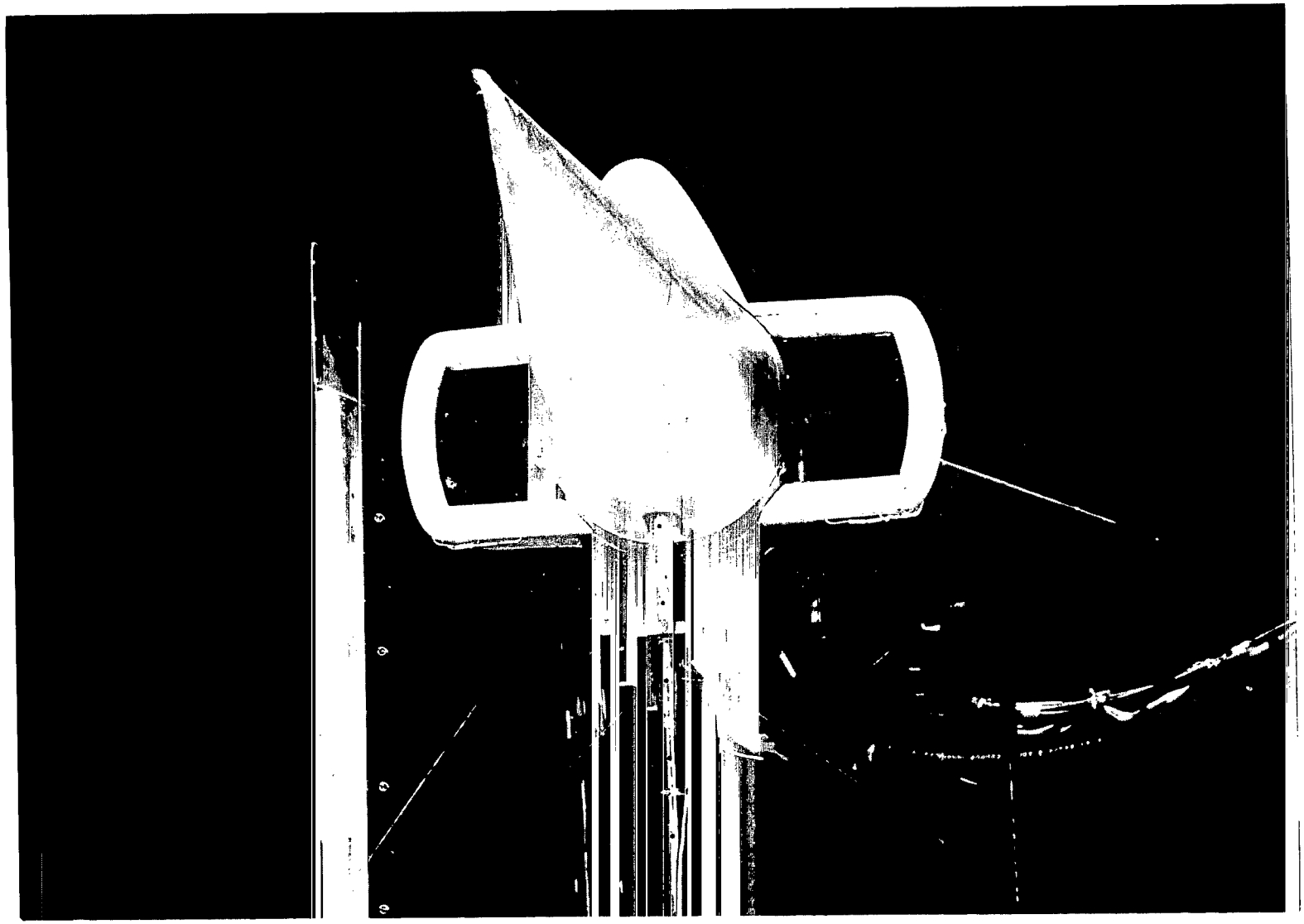

(c) Front view of side-inlet arrangement. L-67-2397

Figure 3.- Concluded.

(a) Two front inlets of in-line arrangement. L-66-5086

Figure 4.- Typical inlet-lip arrangements.

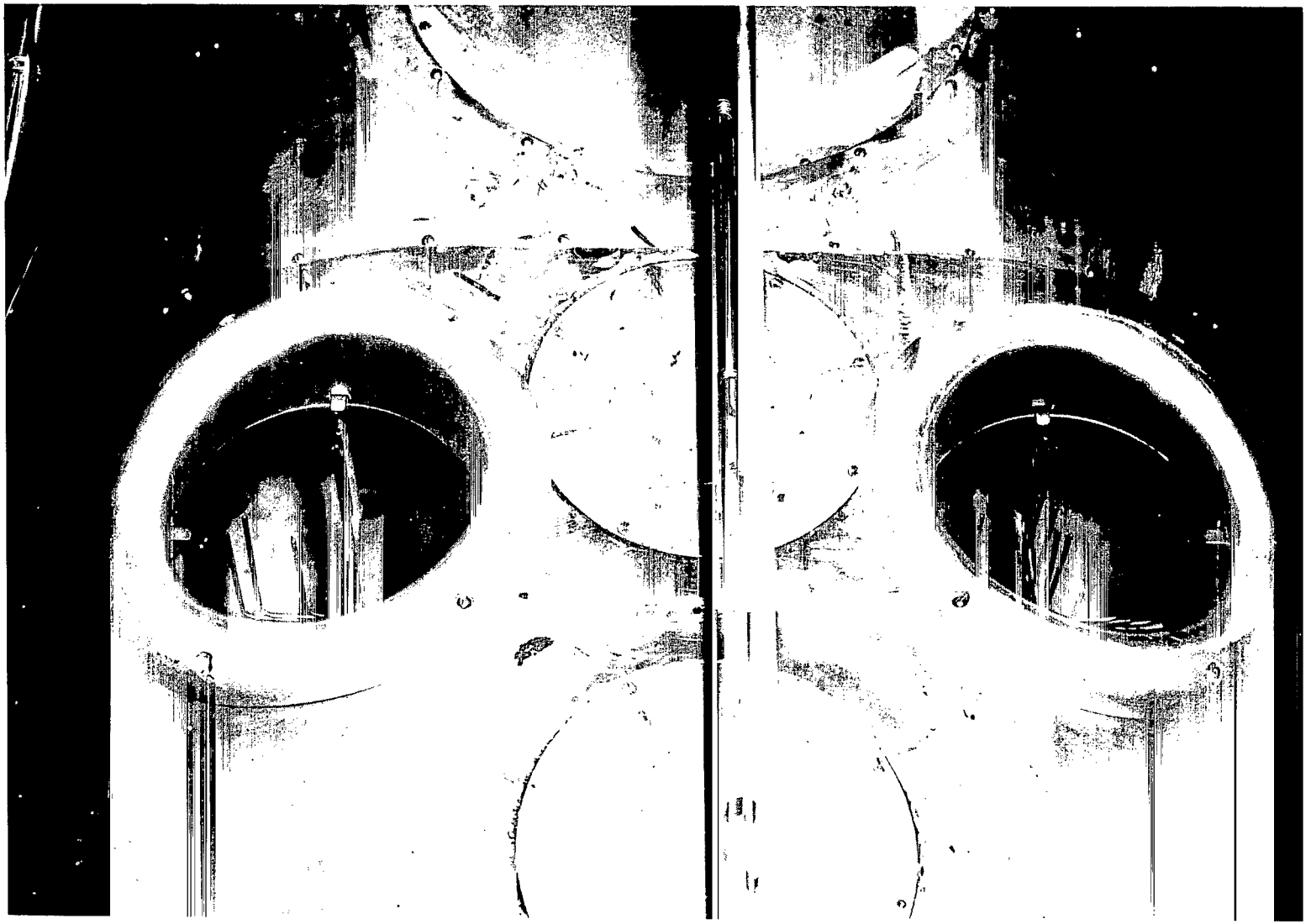

(b) Two front inlets of rectangular arrangement. L-66-5809

Figure 4.- Continued.

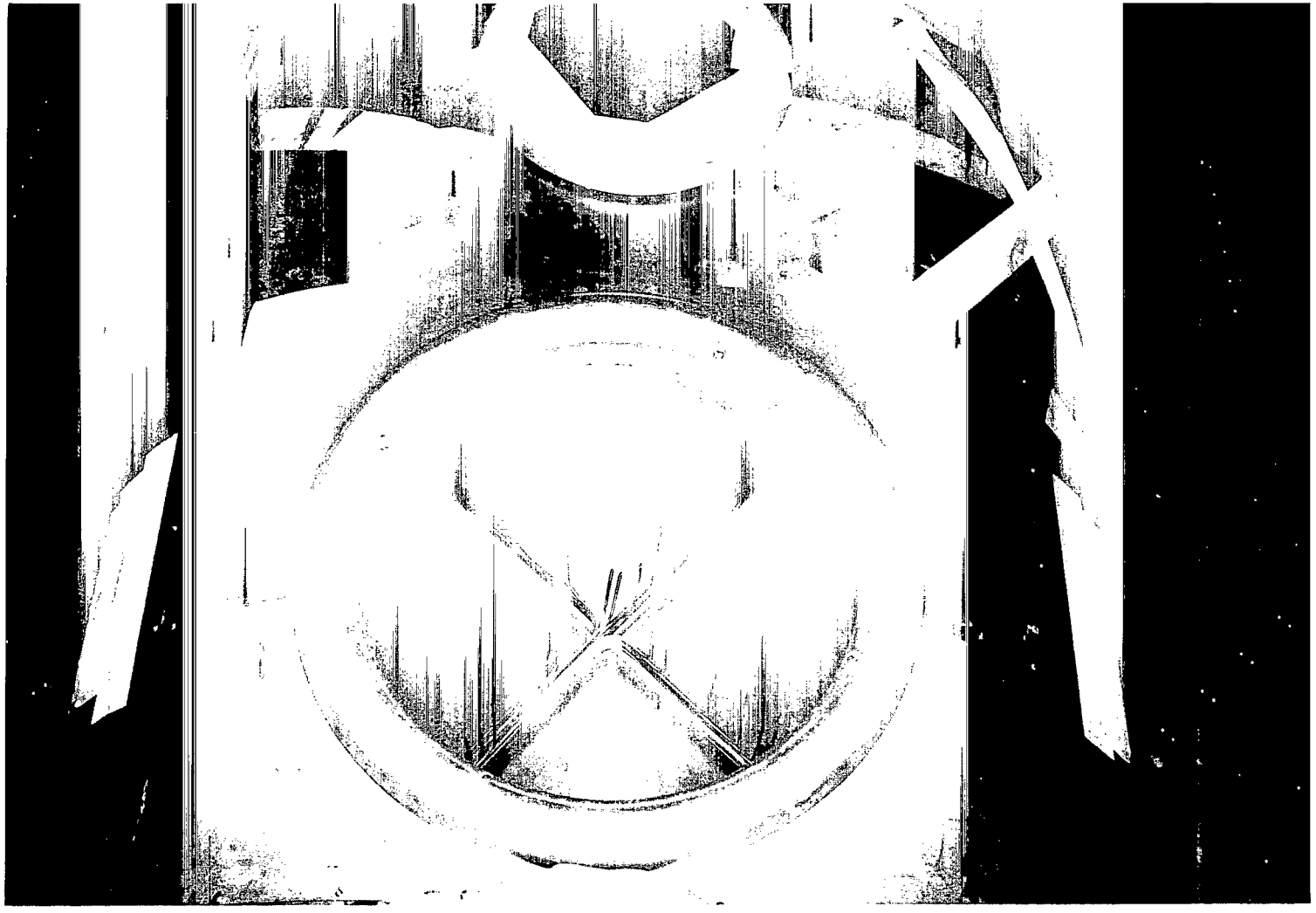

(c) Single-inlet arrangement.

L-67-3836

Figure 4.- Continued.

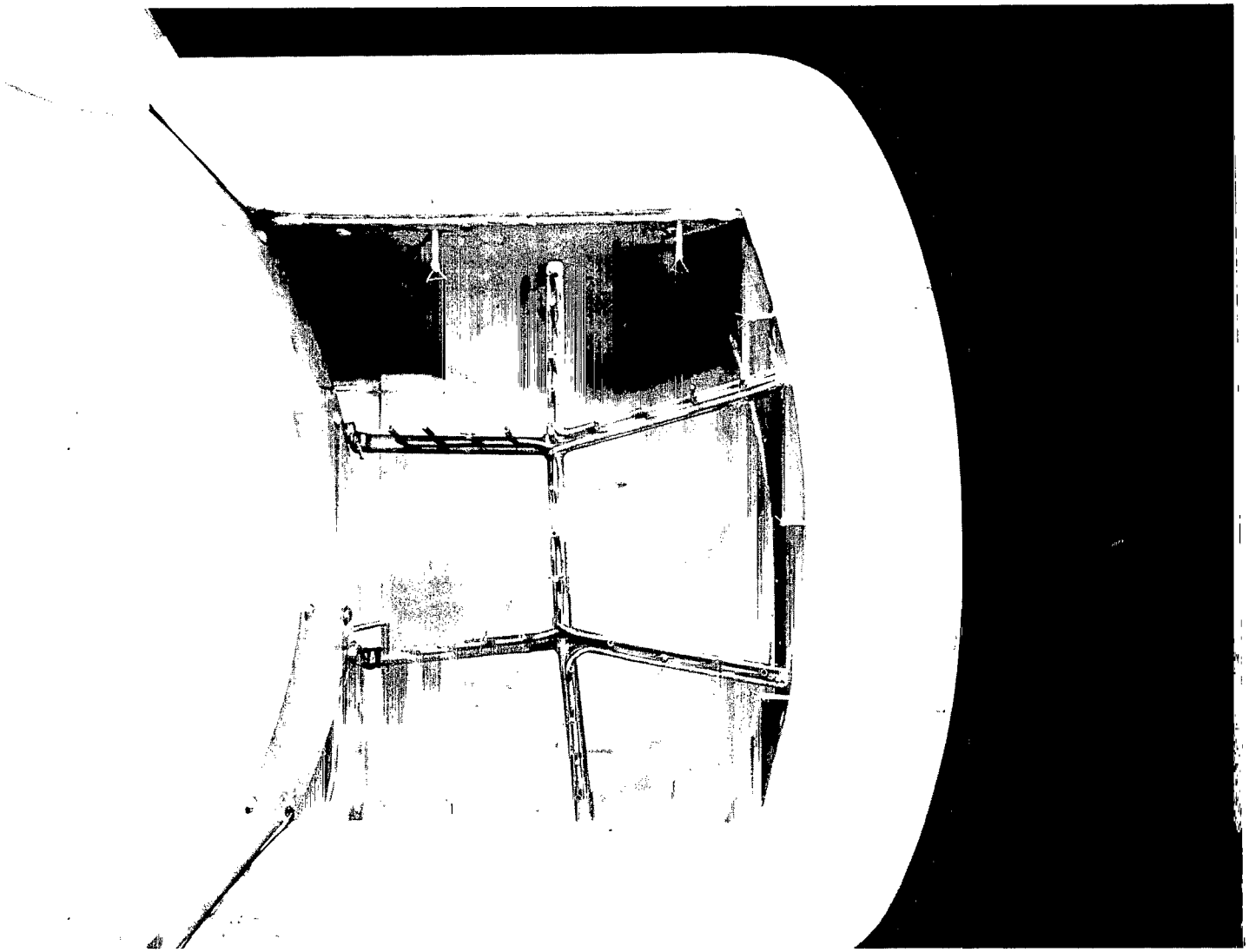

(d) Left-hand inlet of side-inlet arrangement. L-67-2396

Figure 4.- Concluded.

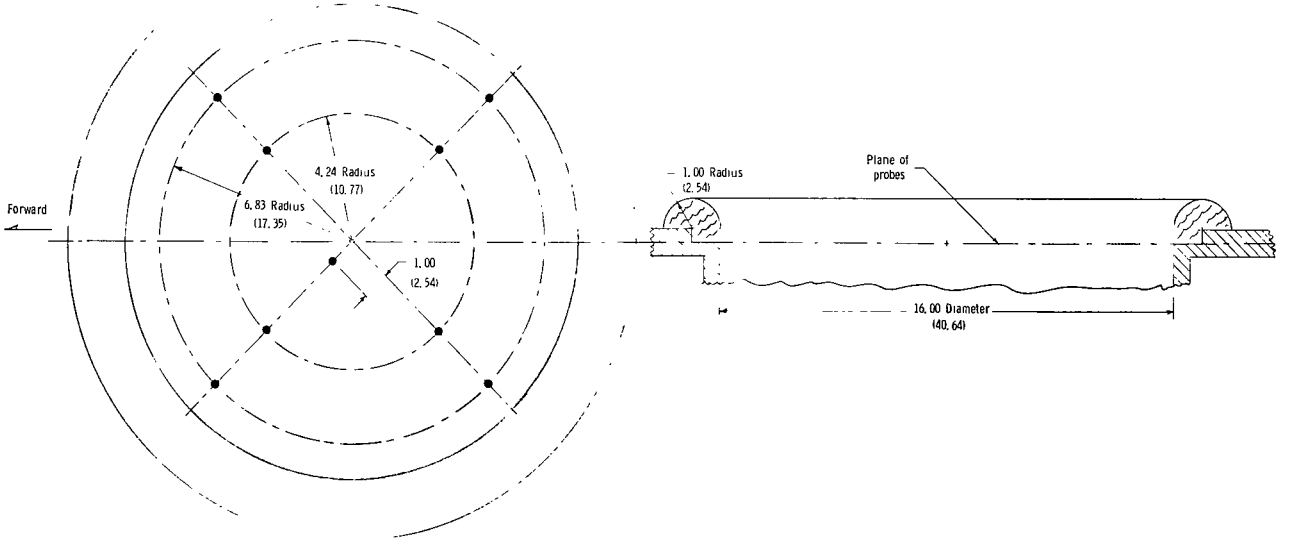

(a) Single top inlet.

● Denotes probe location

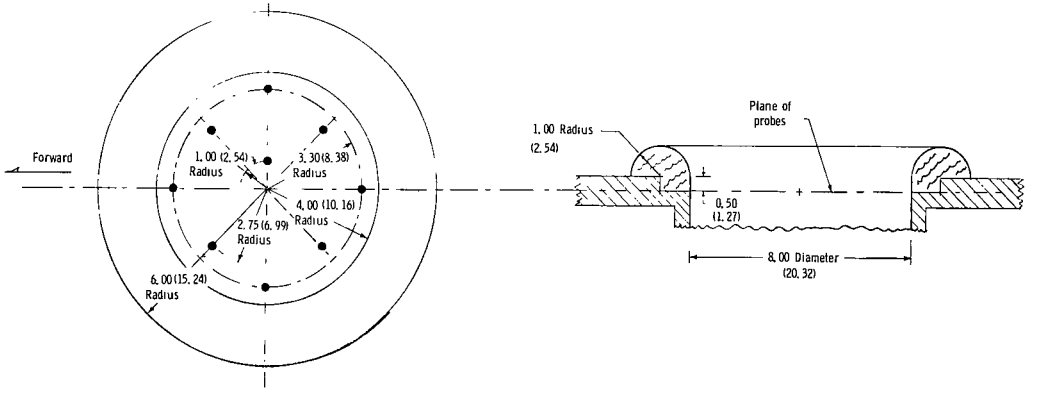

(b) Inlet 4 of in-line configuration.

Figure 5.- Sketch showing location of temperature probes in inlets. (All dimensions are given in inches and parenthetically in centimeters.)

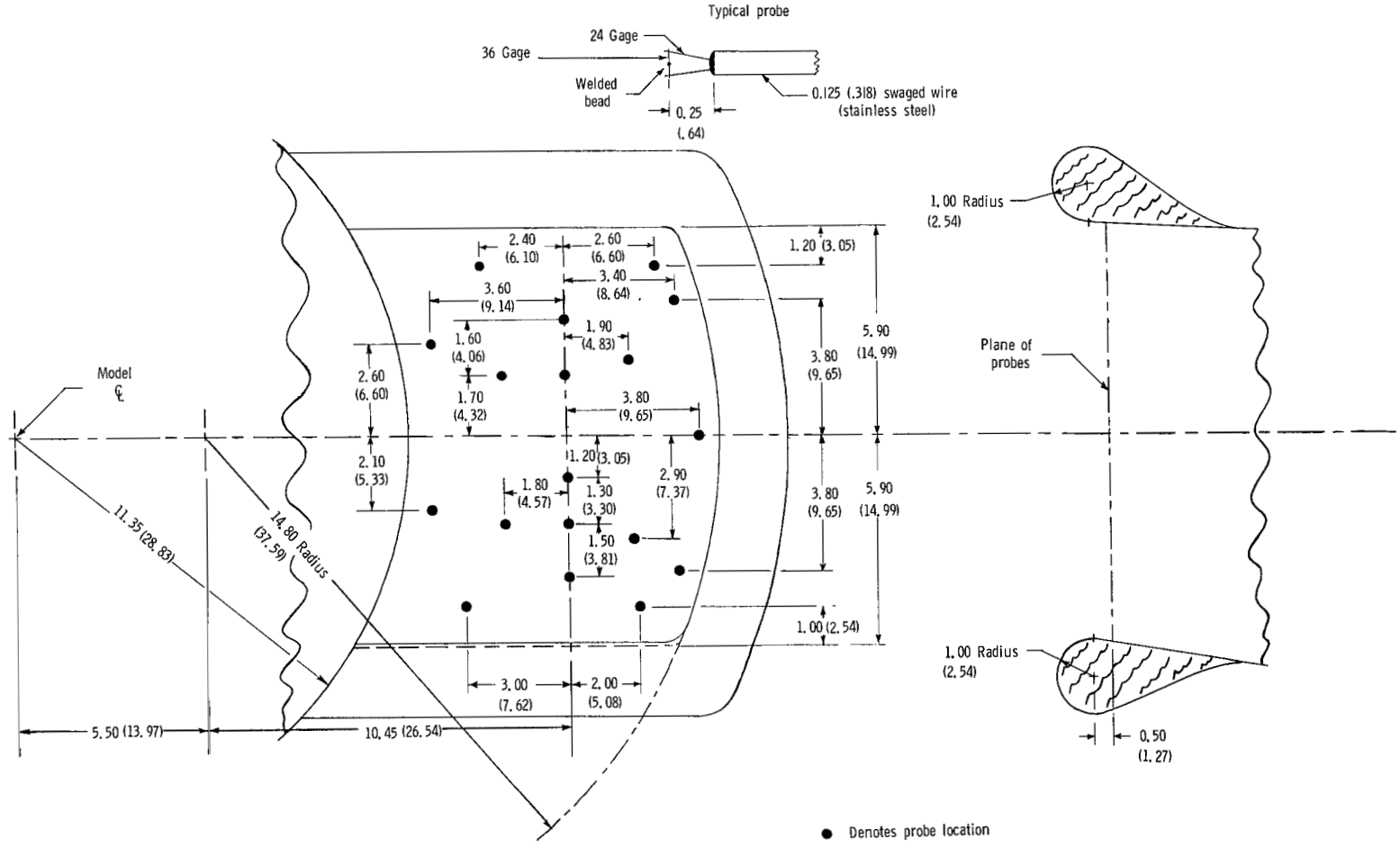

(c) Side inlet (inlet I).

Figure 5.- Concluded.

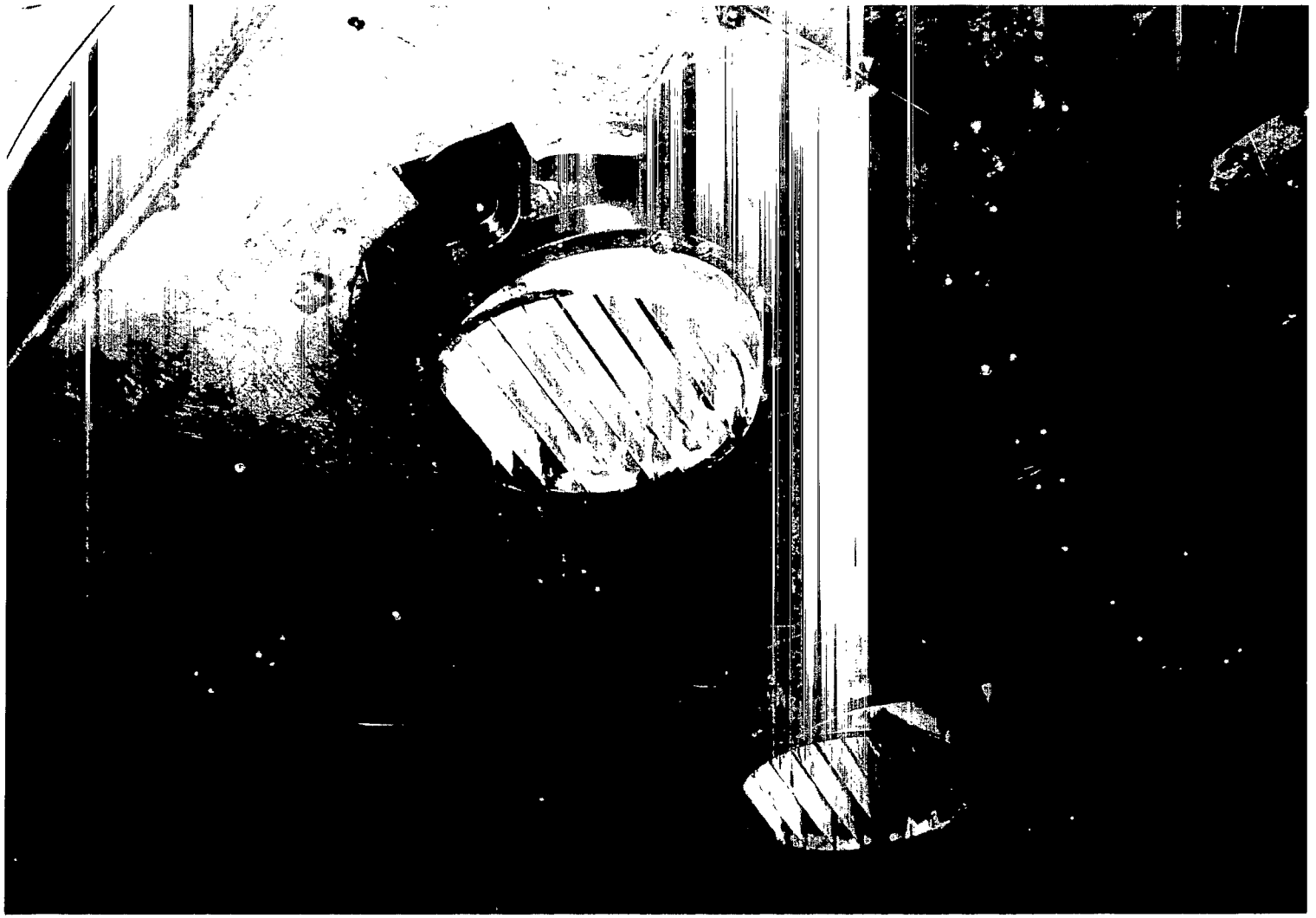

(a) Nozzles undeflected.

L-66-5805

Figure 6.- Two front nozzles of rectangular nozzle arrangement.

(b) Nozzles deflected 25° rearward. L-66-5803

Figure 6.- Concluded.

(a) Nozzles undeflected. L-66-5083

Figure 7.- Two rear nozzles of in-line nozzle arrangement.

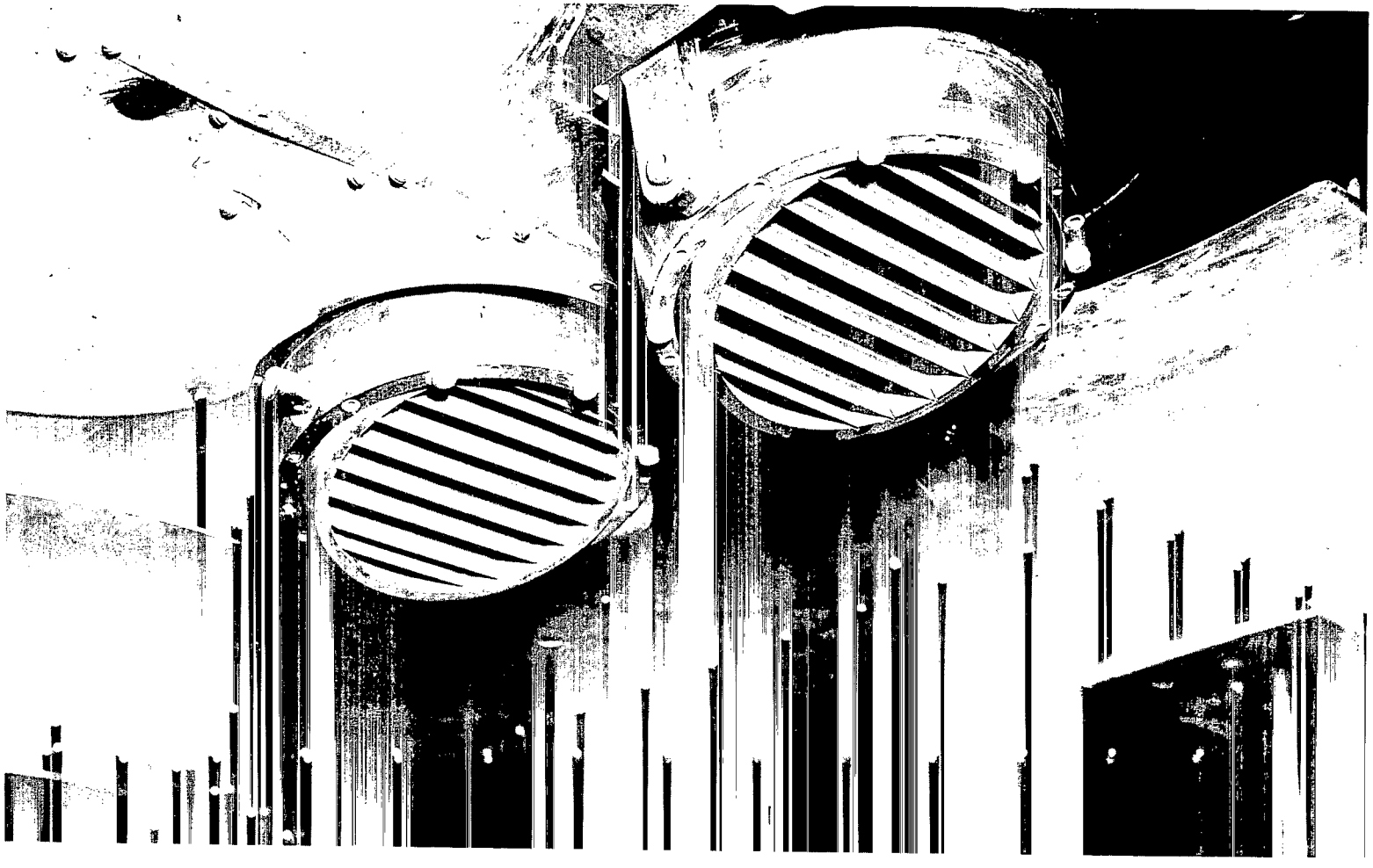

(b) Nozzles deflected 25^{0} rearward.

L-66-5082

Figure 7.- Concluded.

(a) Nozzles undeflected. L-67-2400.1

Figure 8.- Side nozzle arrangement.

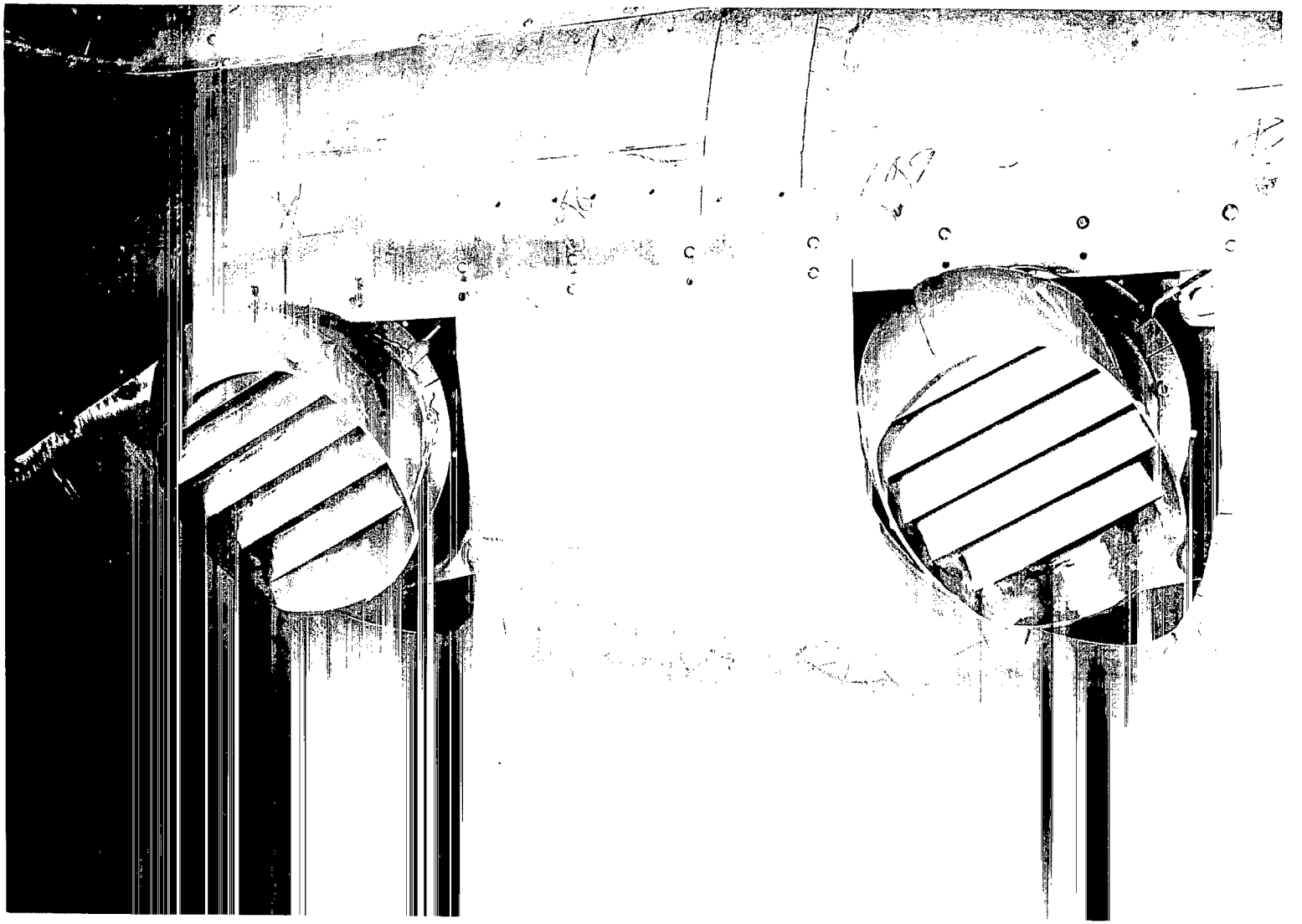

(b) Nozzles deflected 25° rearward. L-67-2399

Figure 8.- Concluded.

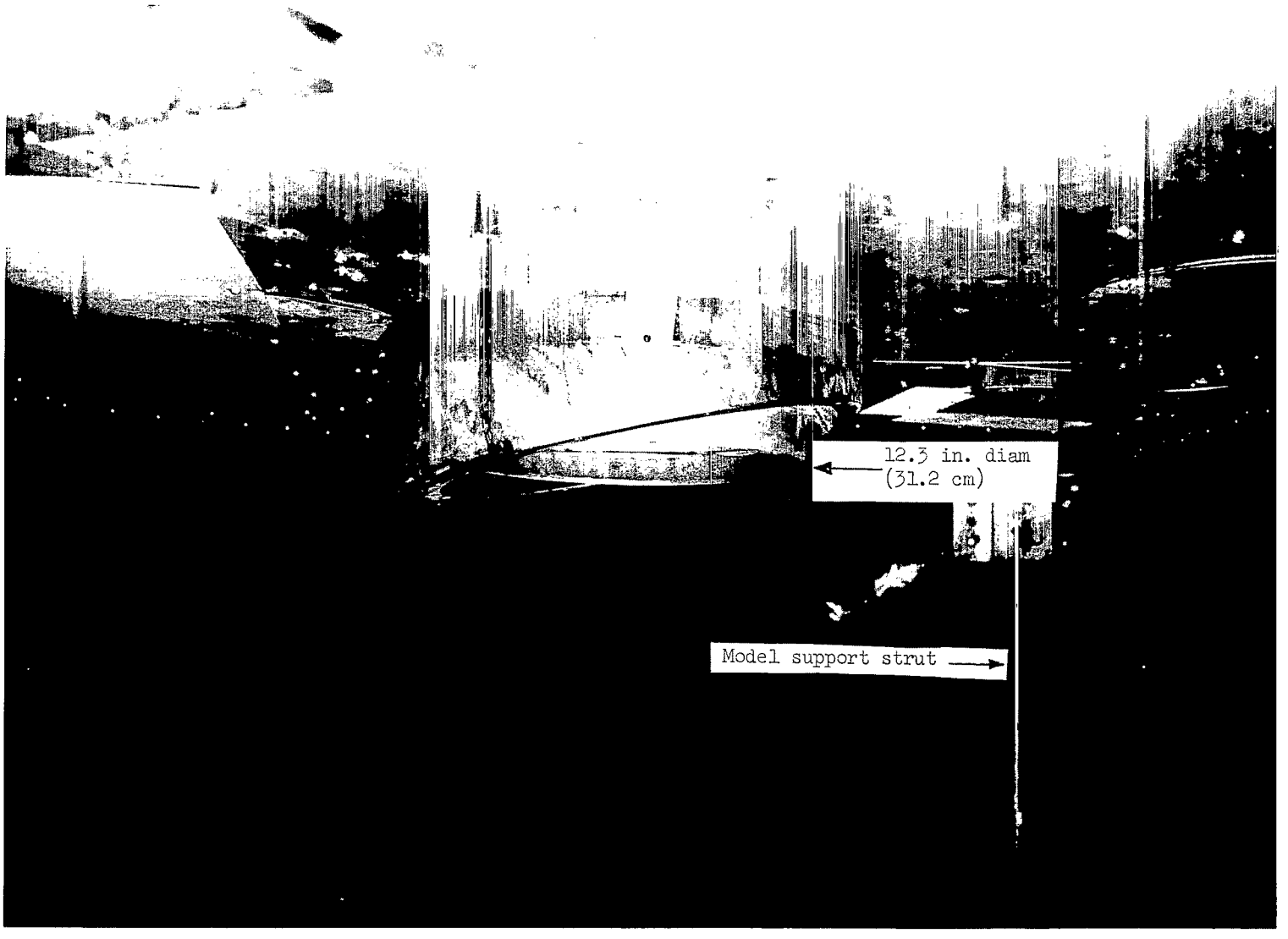

(a) Nozzle undeflected.

L-67-3839.1

Figure 9.- Single-nozzle arrangement.

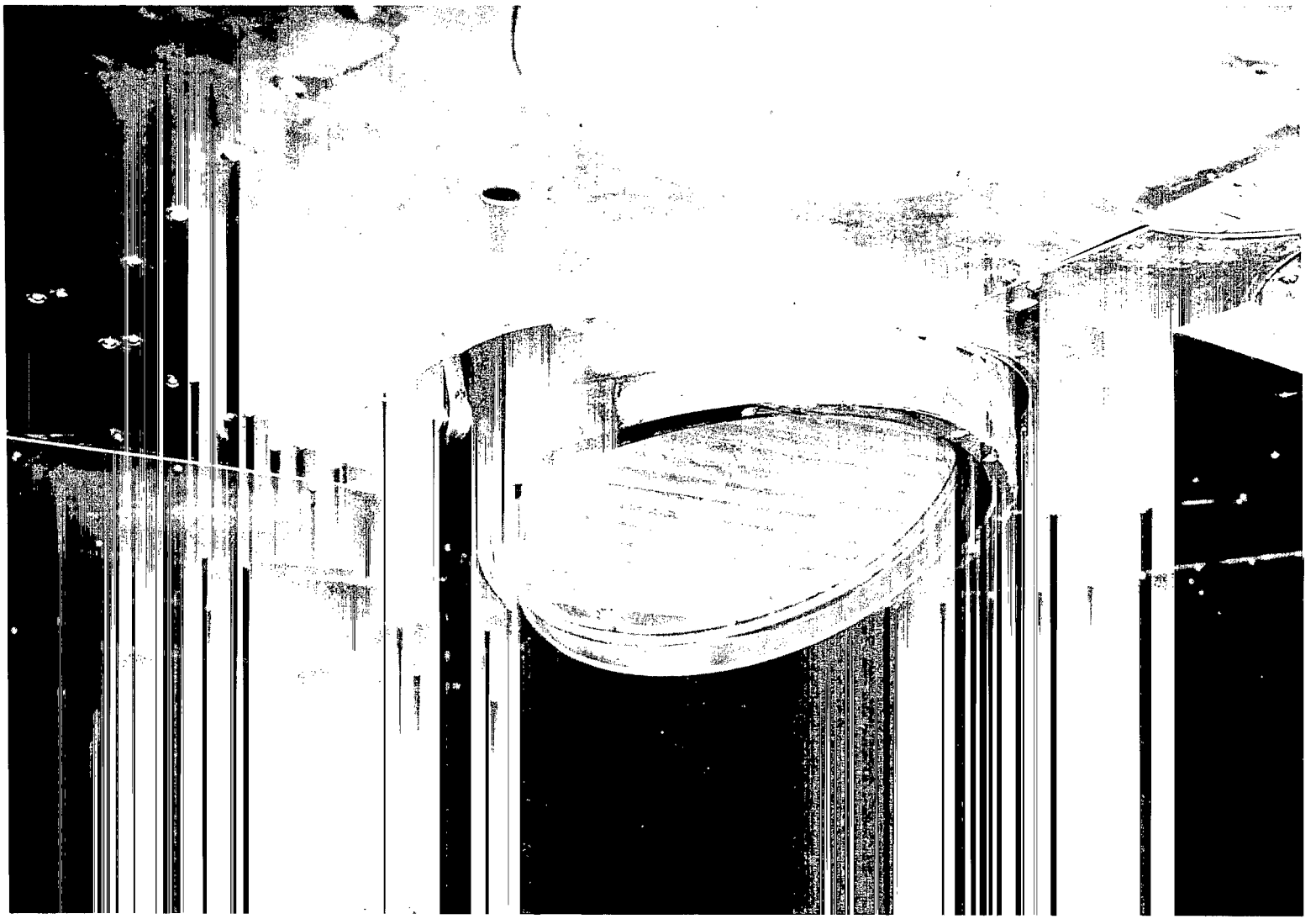

(b) Nozzle deflected 25^{0} rearward. L-67-3840

Figure 9.- Concluded.

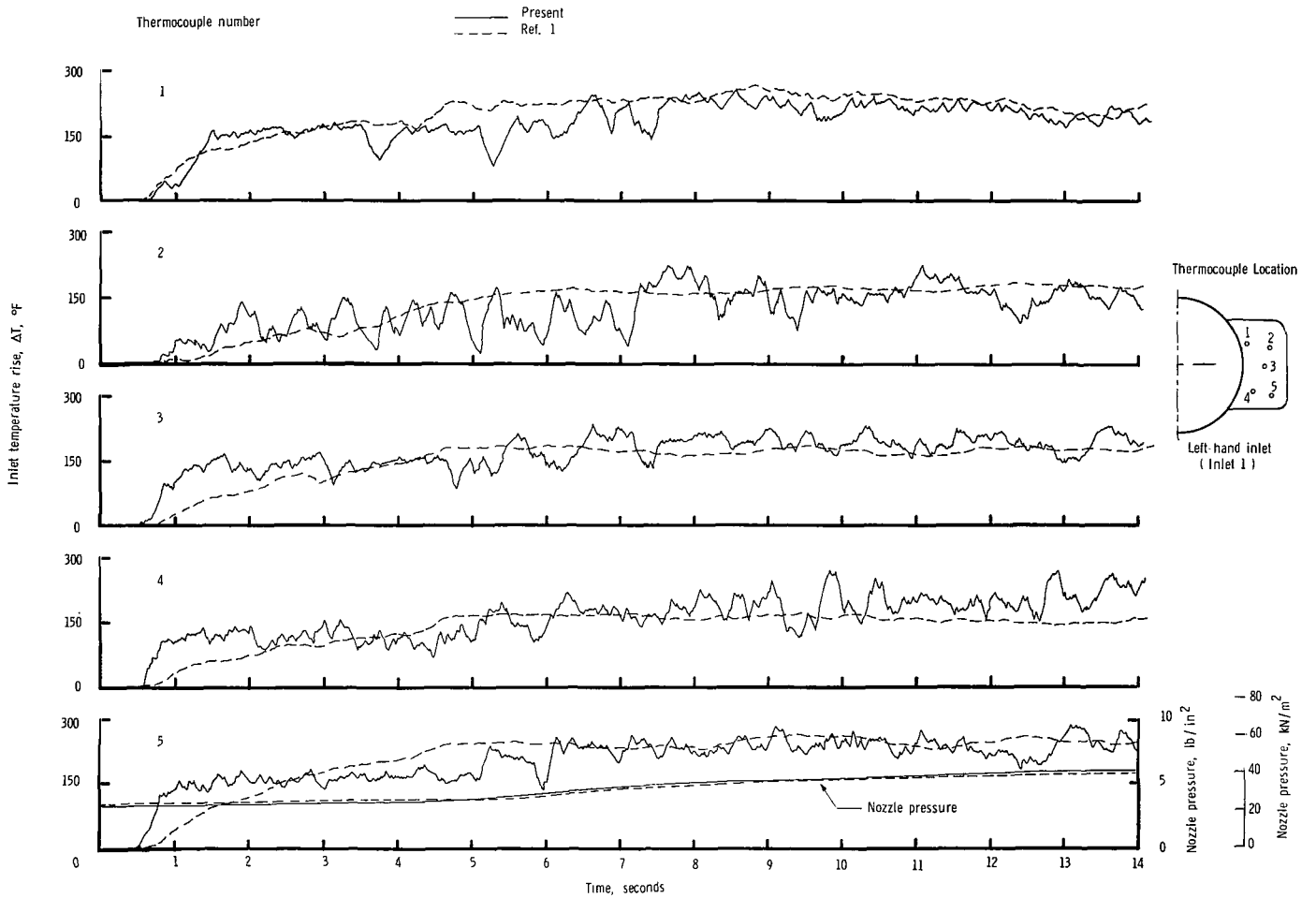

Figure 10.- Comparison of time-temperature histories of present and reference 1 tests of rectangular nozzle arrangement with side inlets. High wing; $S_W/S_J = 43$; $h/D_e = 1.17$; $V = 5.52$ knots. *(Values of ΔT in ^{o}C can be obtained by multiplying the ^{o}F values by 5/9.)*

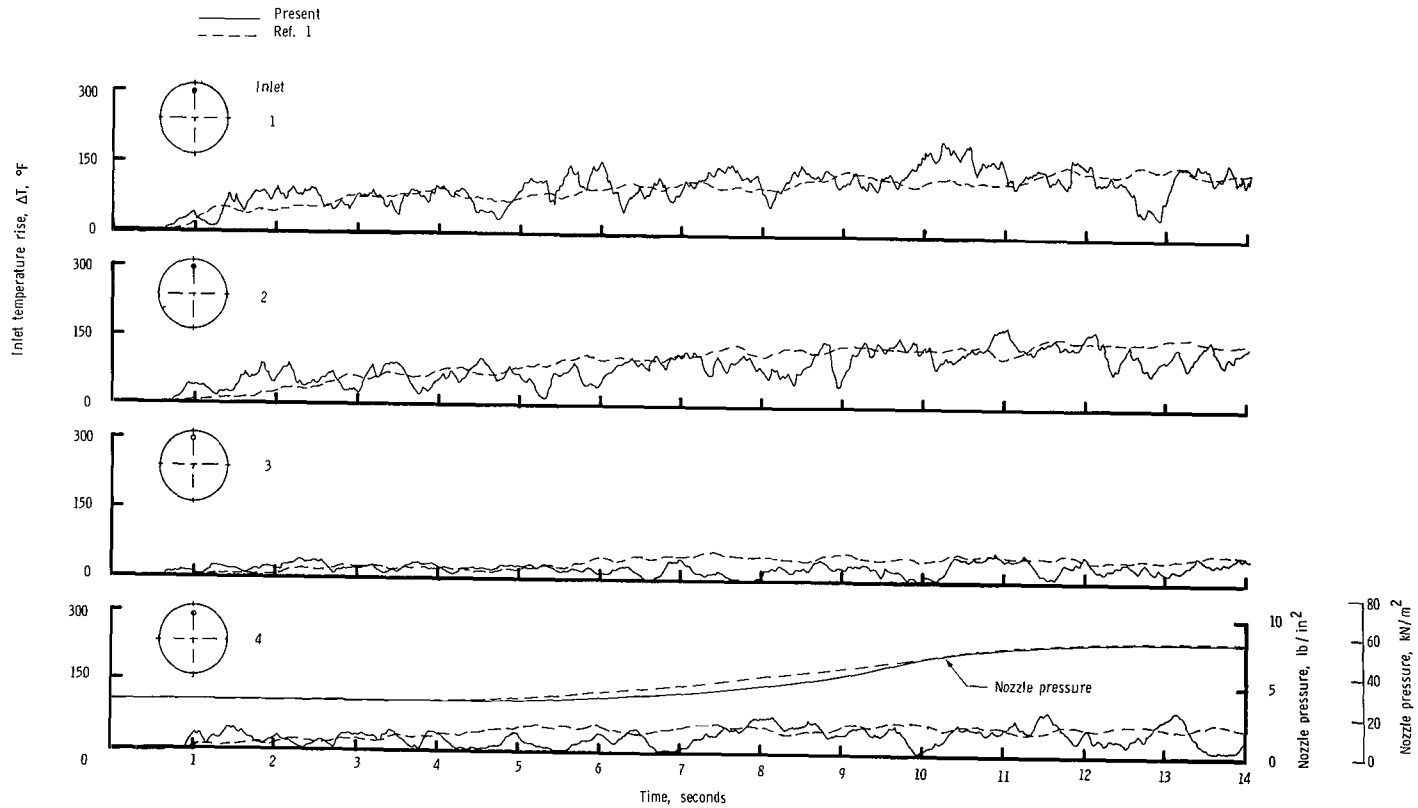

Figure 11.- Comparison of time-temperature histories of present and reference 1 tests of rectangular nozzle arrangement with top inlets. High wing; $S_W/S_J = 43$; $h/D_e = 3.00$; V = 5.92 knots. (Values of ΔT in °C can be obtained by multiplying the °F values by 5/9.)

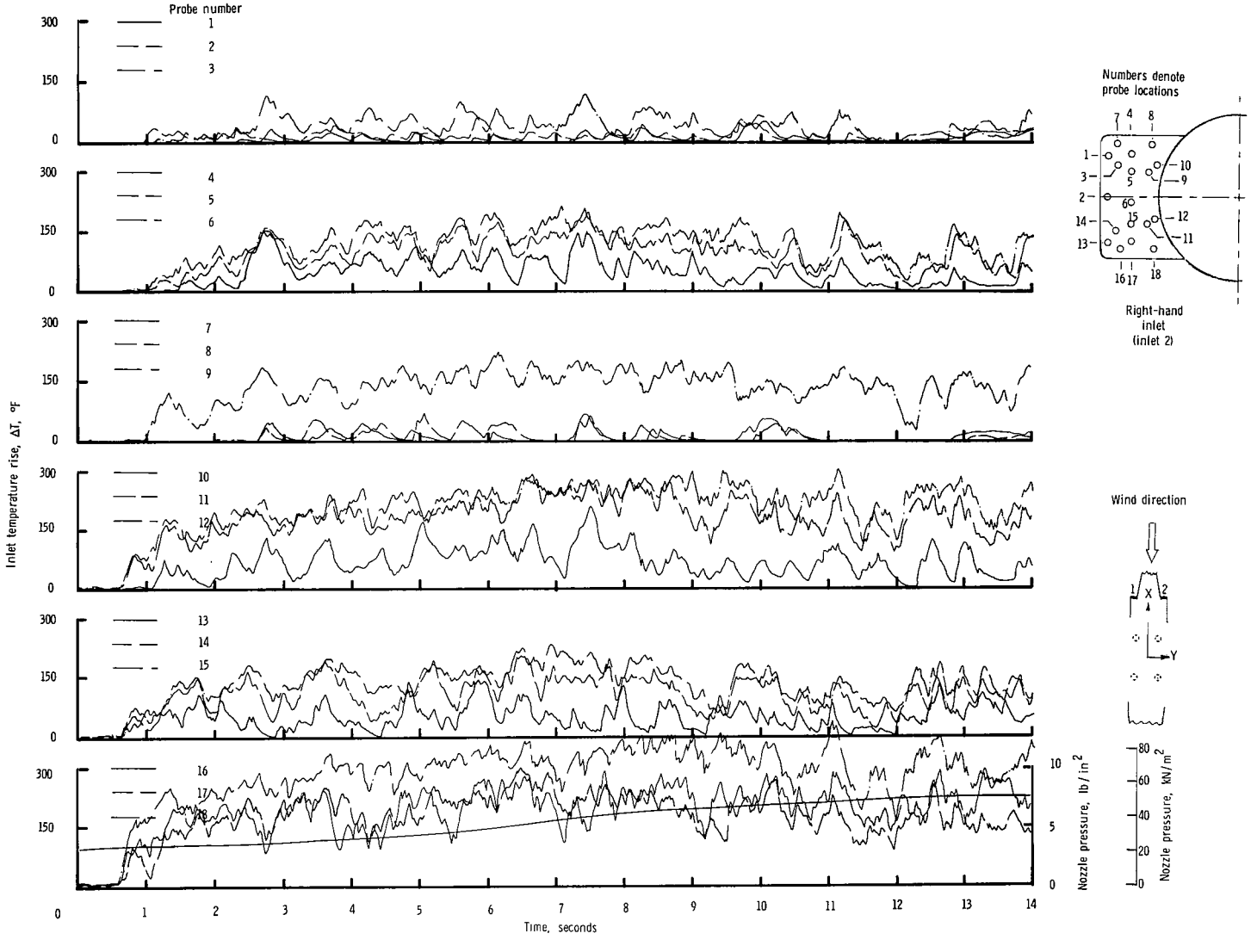

(a) $\psi = 0^{0}$; V = 0 knots.

Figure 12.- Variation of inlet-air temperature rise with time for the rectangular nozzle arrangement with side inlets and with wing removed. $h/D_e = 1.17$. (Values of ΔT in ^{0}C can be obtained by multiplying the ^{0}F values by 5/9.)

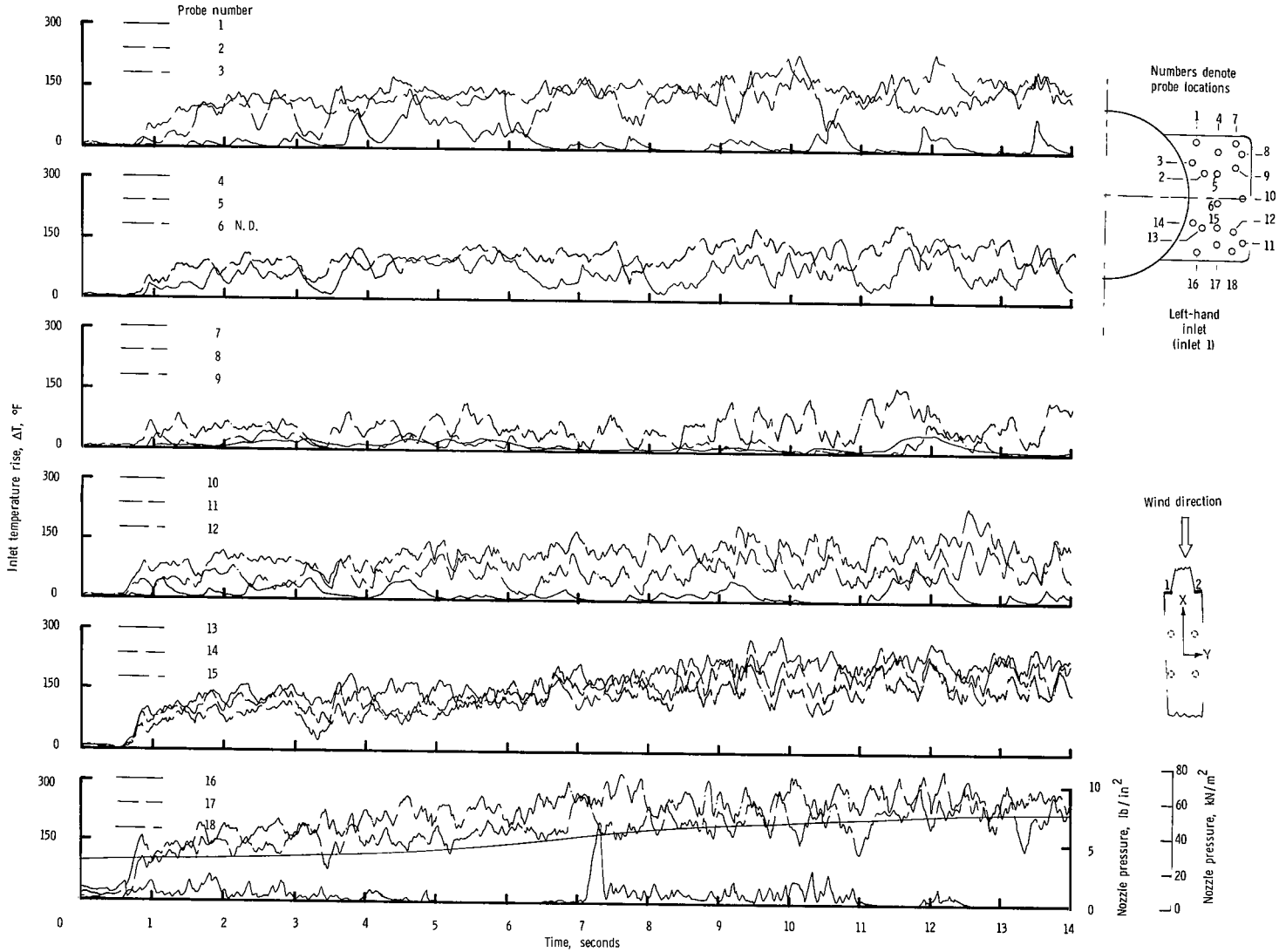

(a) Concluded.

Figure 12.- Continued.

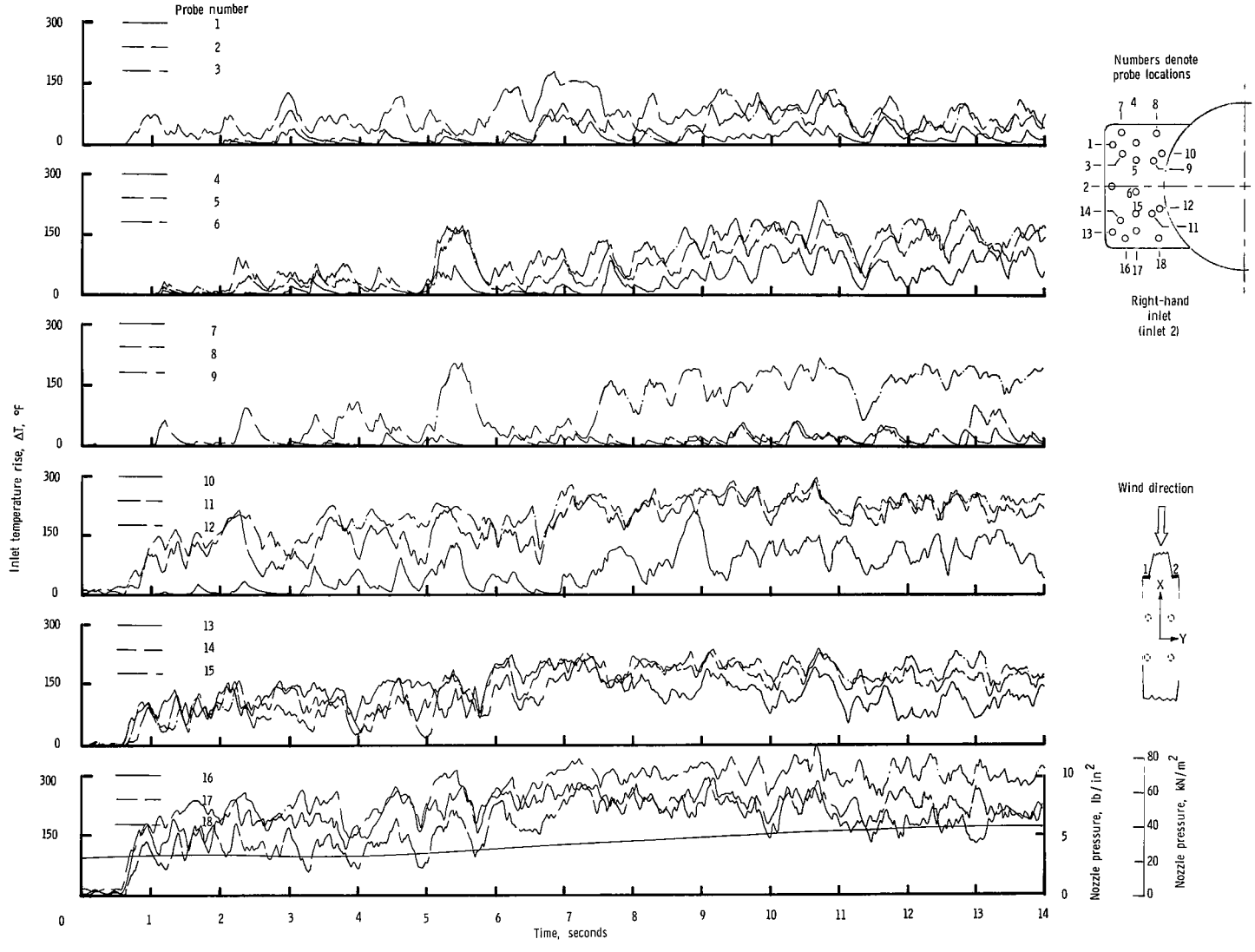

(b) $\psi = 0^0$; V = 5.92 knots.

Figure 12.- Continued.

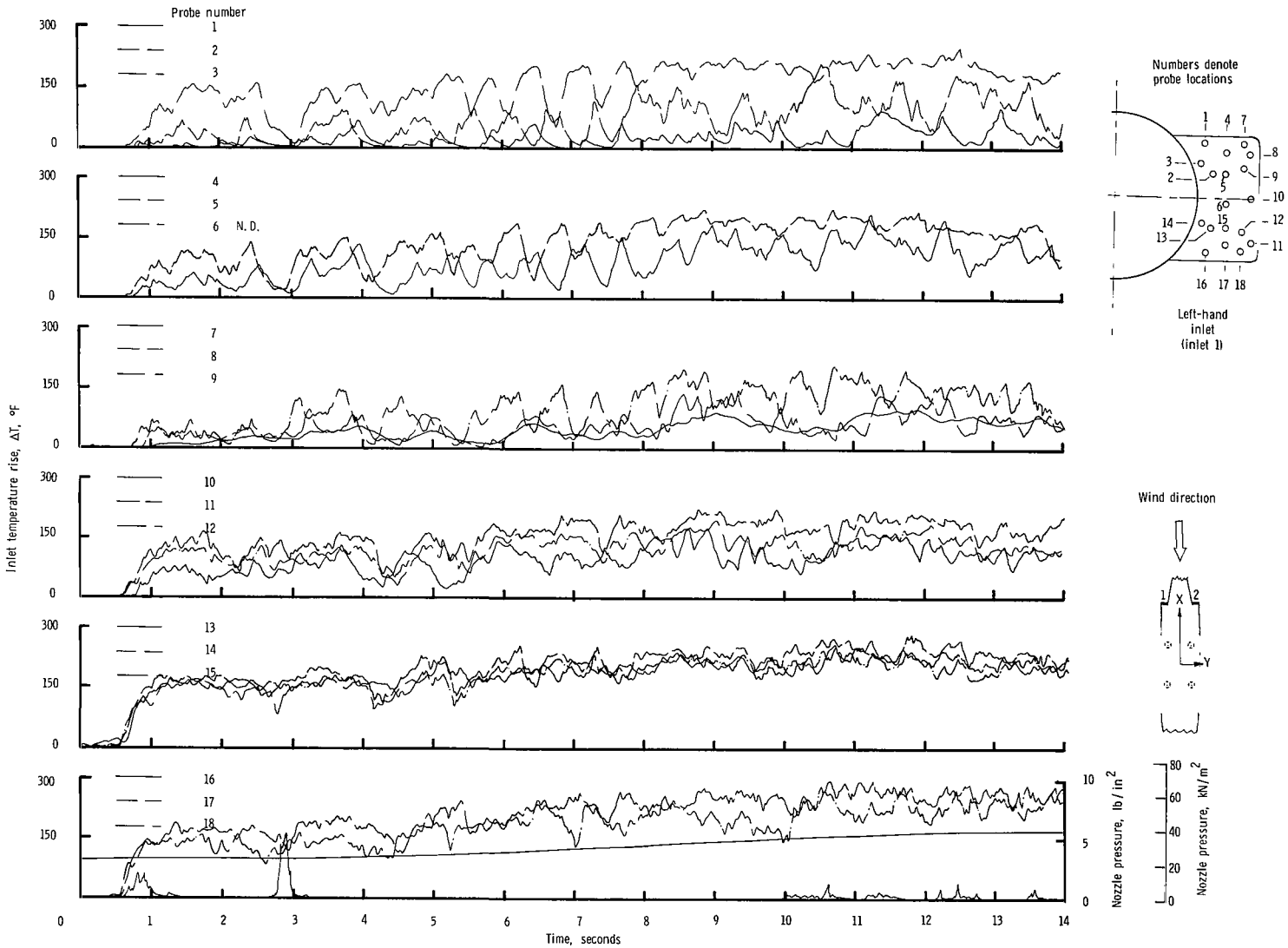

(b) Concluded.

Figure 12.- Continued.

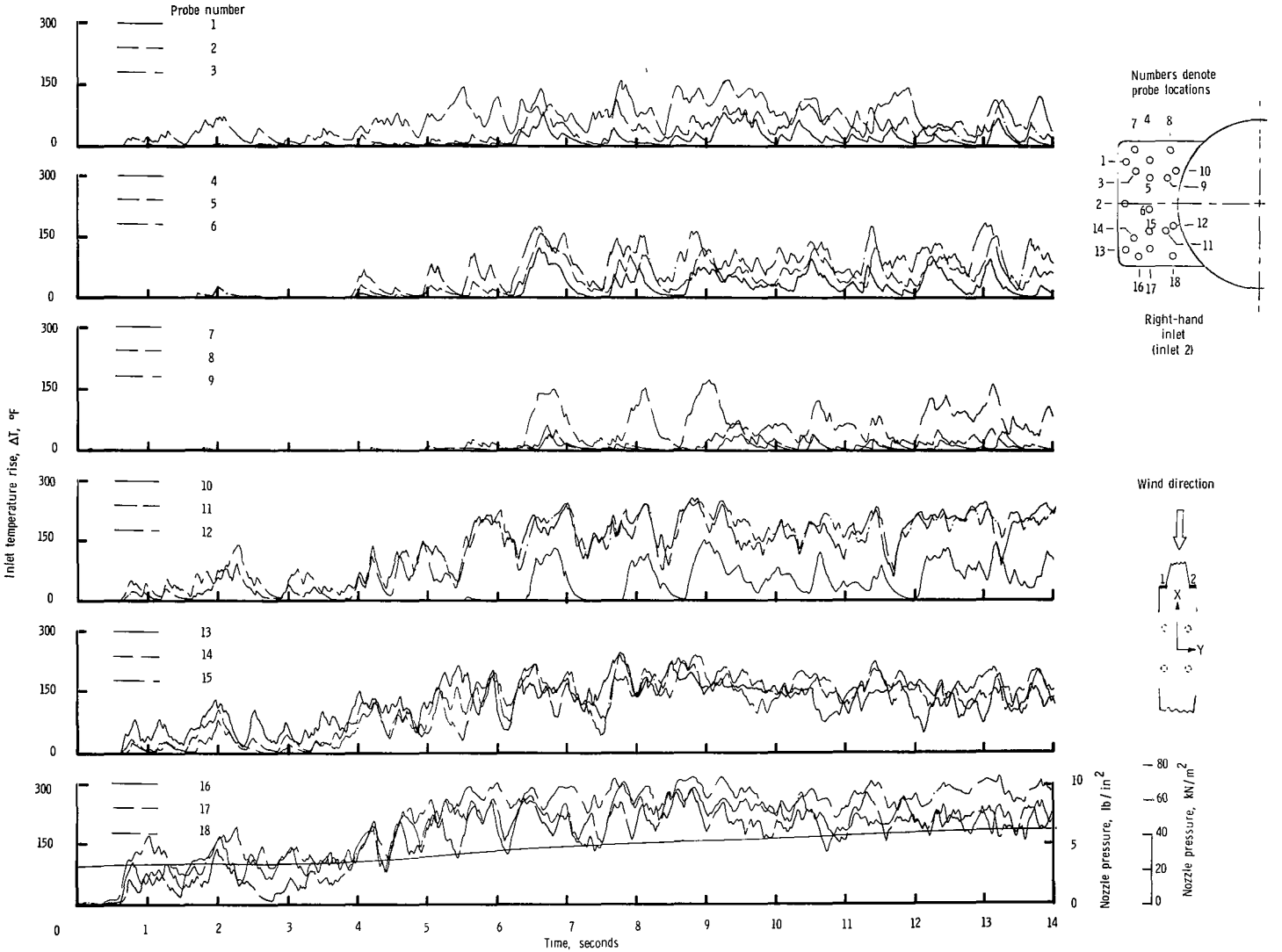

(c) $\psi = 0^0$; V = 11.85 knots.

Figure 12.- Continued.

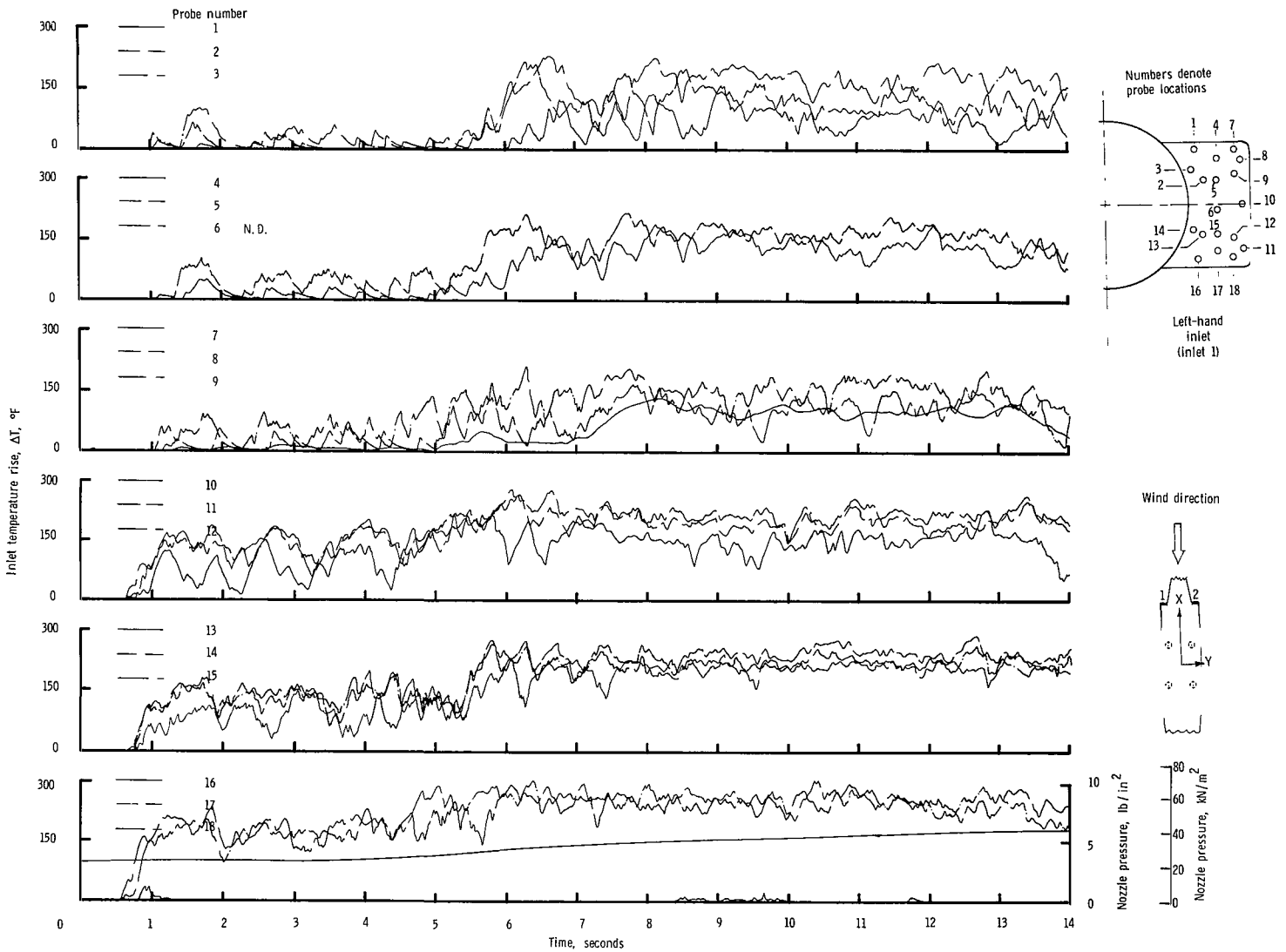

(c) Concluded.

Figure 12.- Continued.

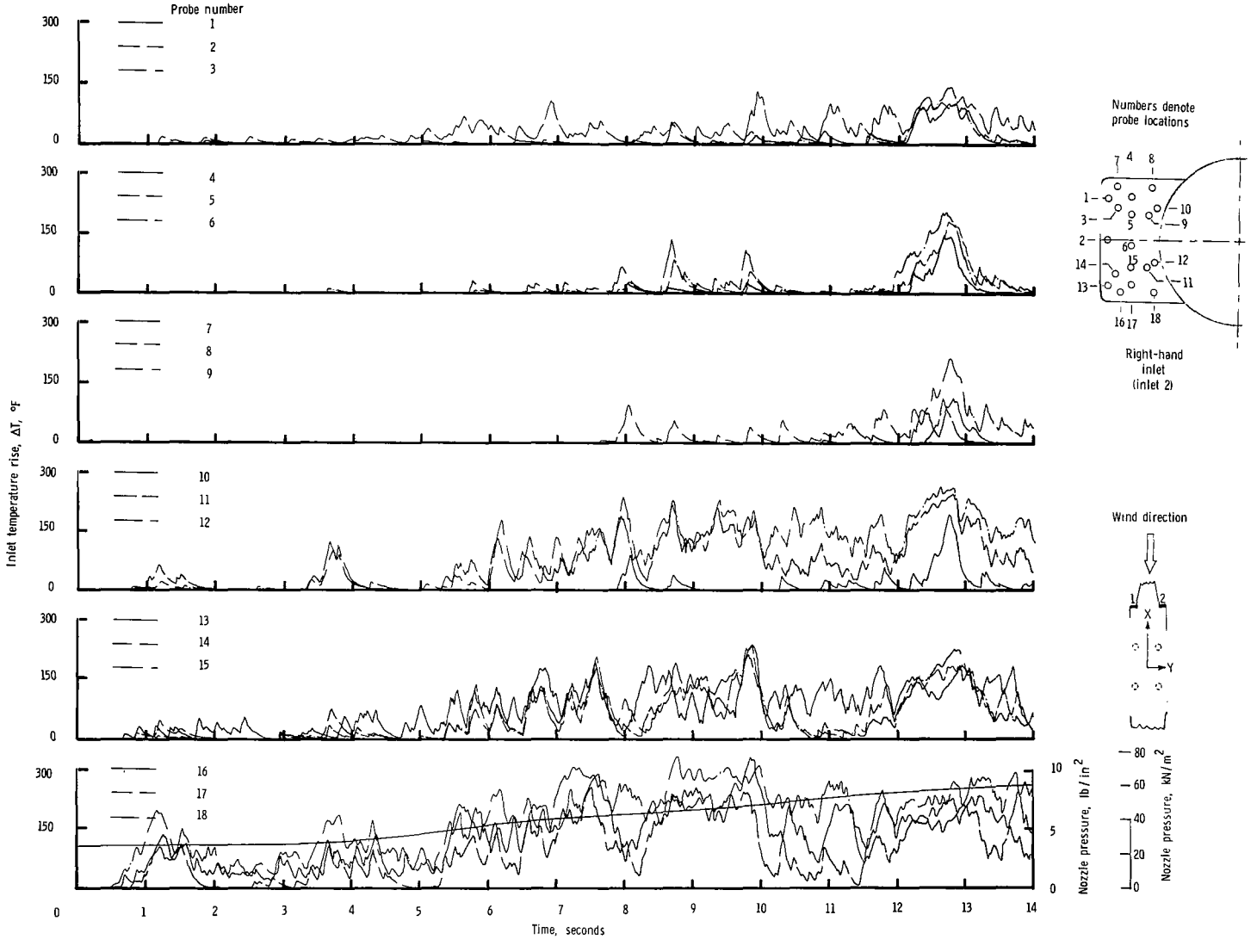

(d) $\psi = 0^0$; V = 17.78 knots.

Figure 12.- Continued.

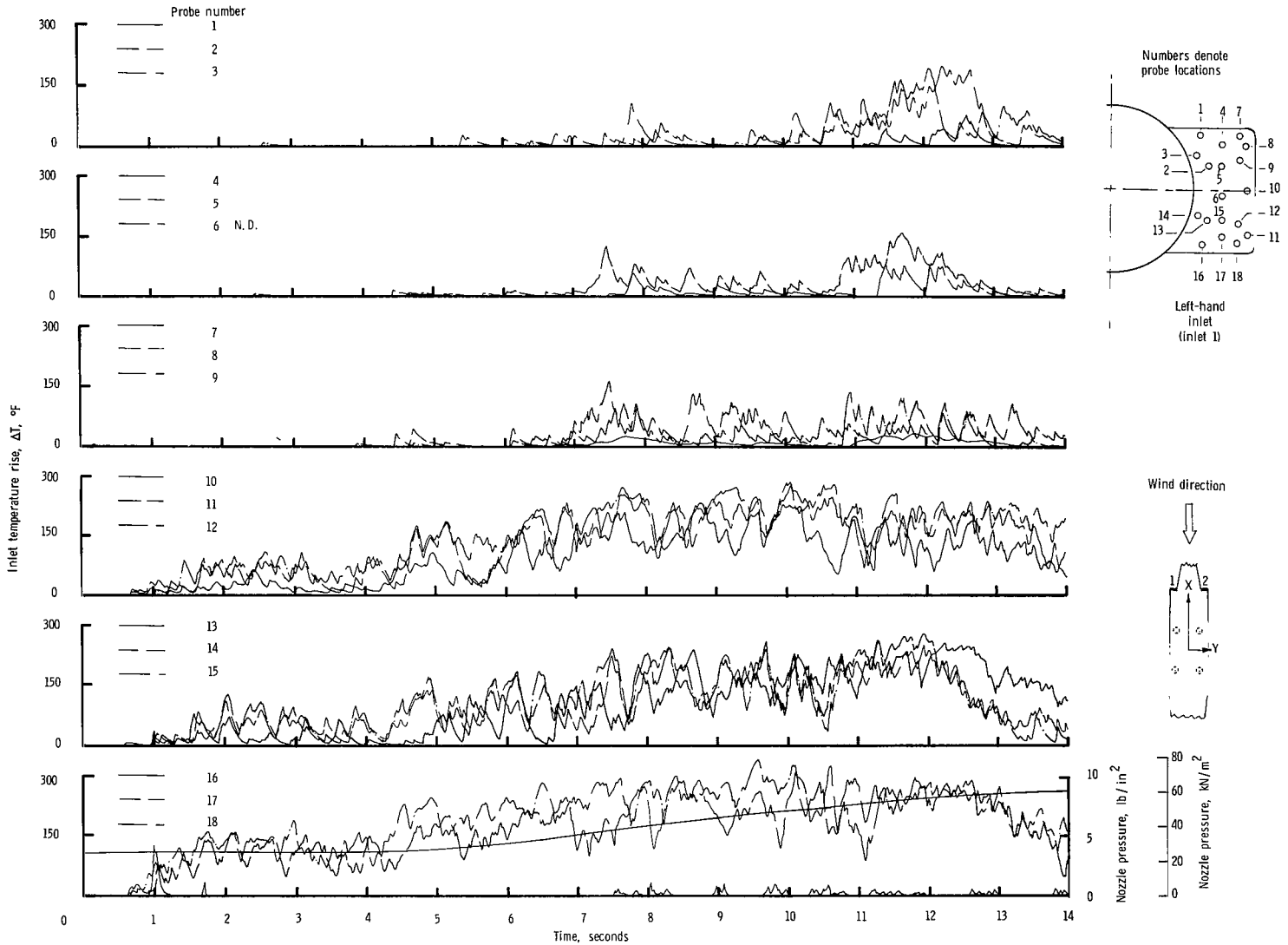

(d) Concluded.

Figure 12.- Continued.

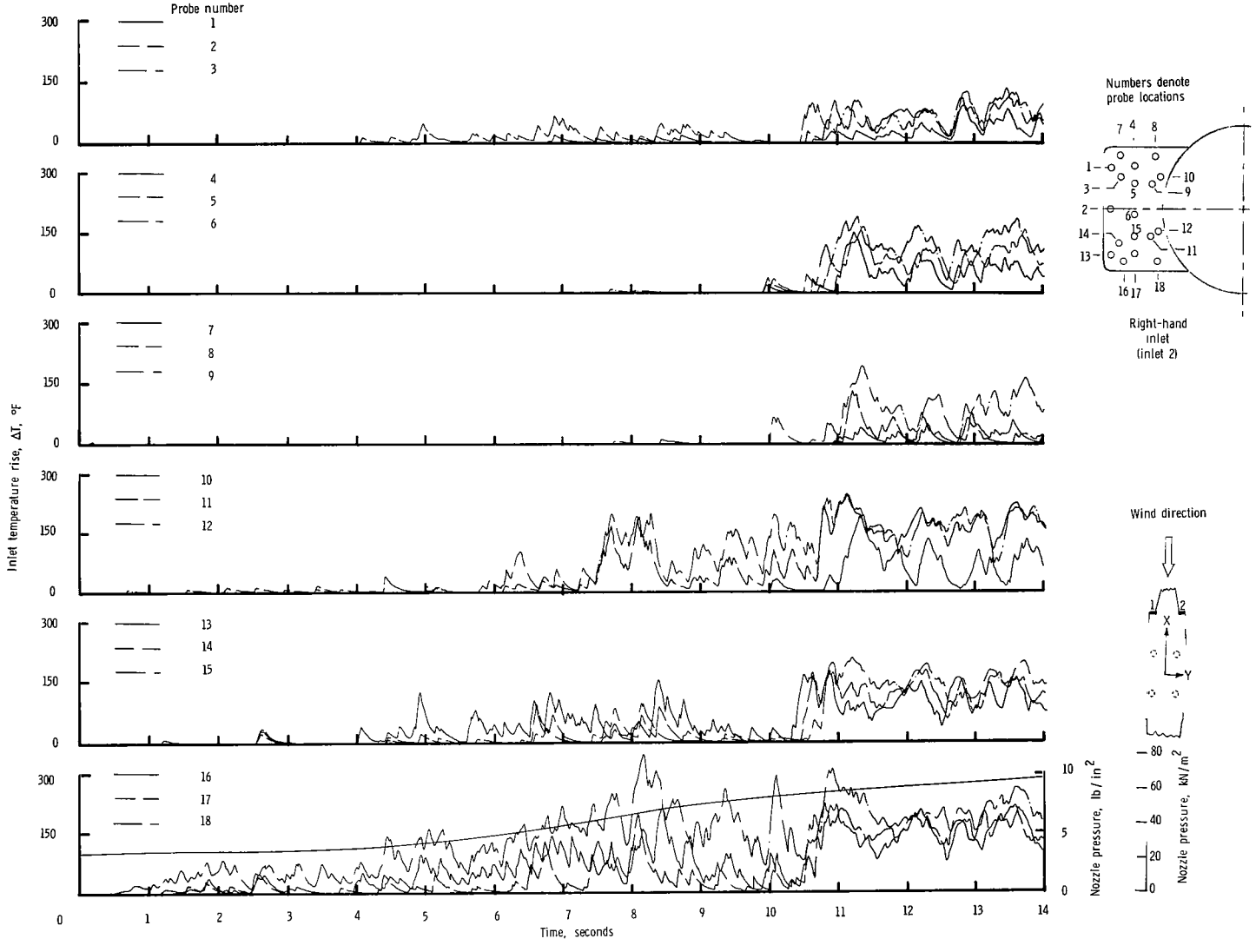

(e) $\psi = 0^{0}$; V = 23.70 knots.

Figure 12.- Continued.

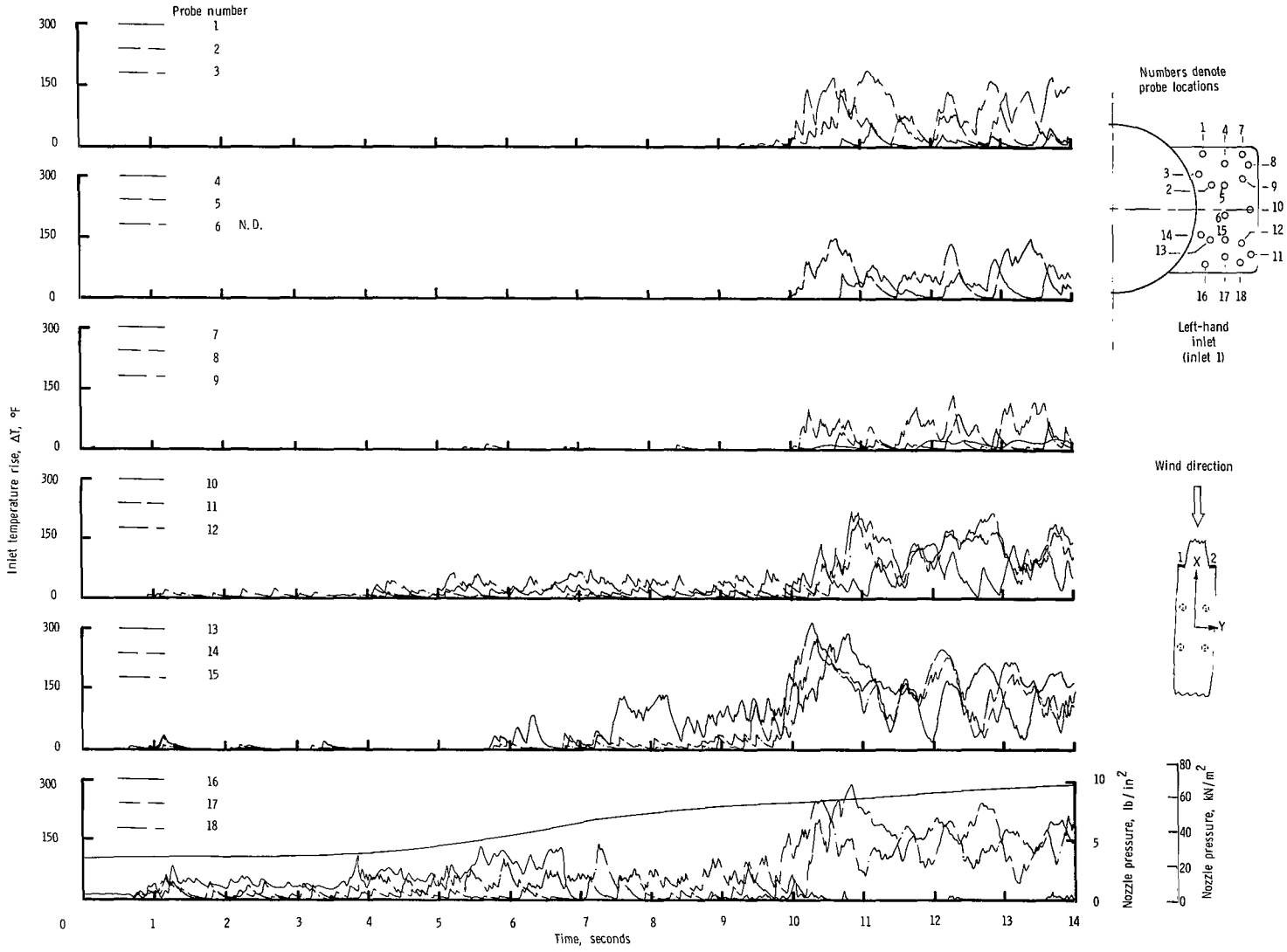

(e) Concluded.

Figure 12.- Continued.

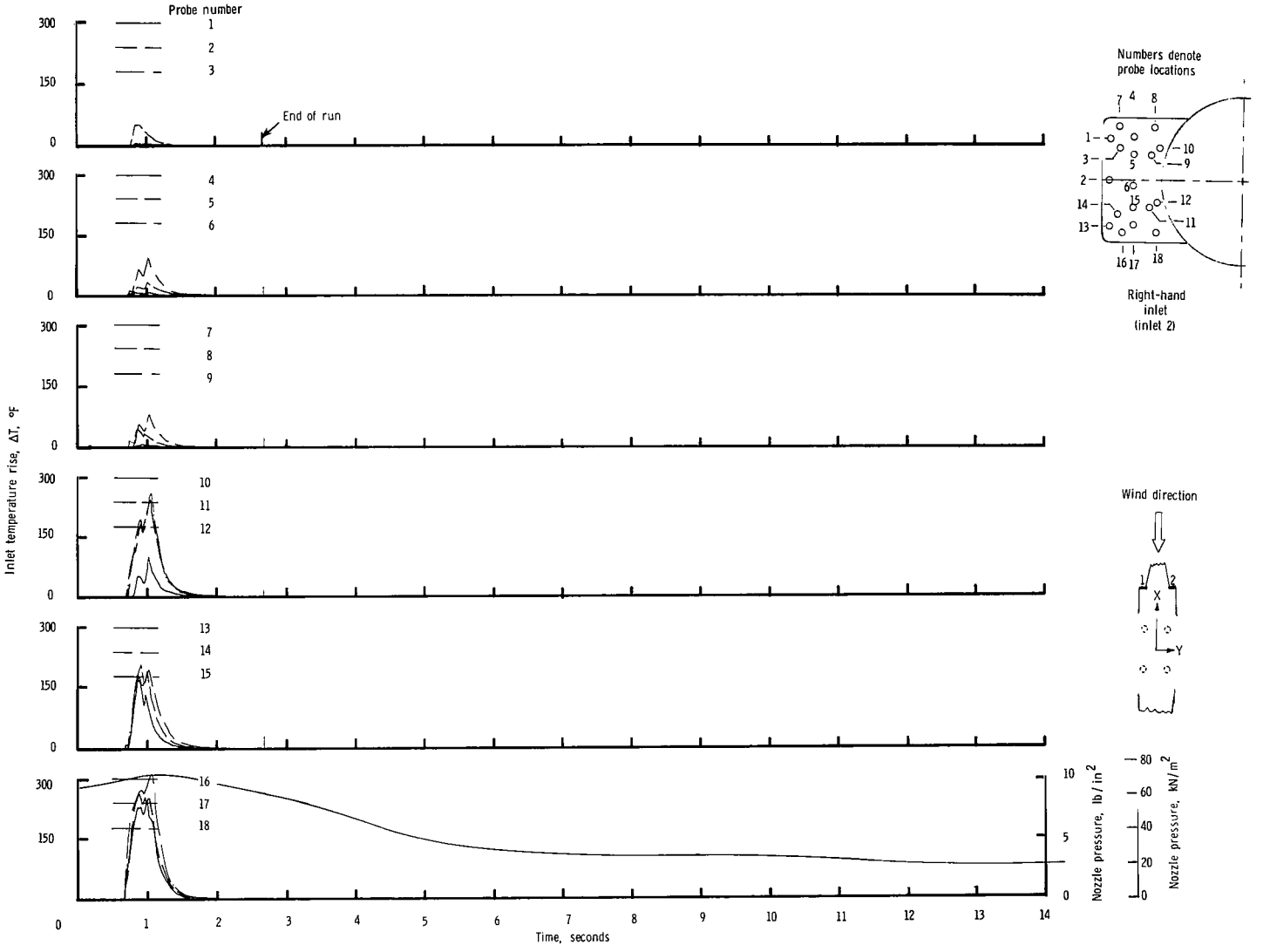

(f) $\psi = 0^{0}$; V = 26.93 knots.

Figure 12.- Continued.

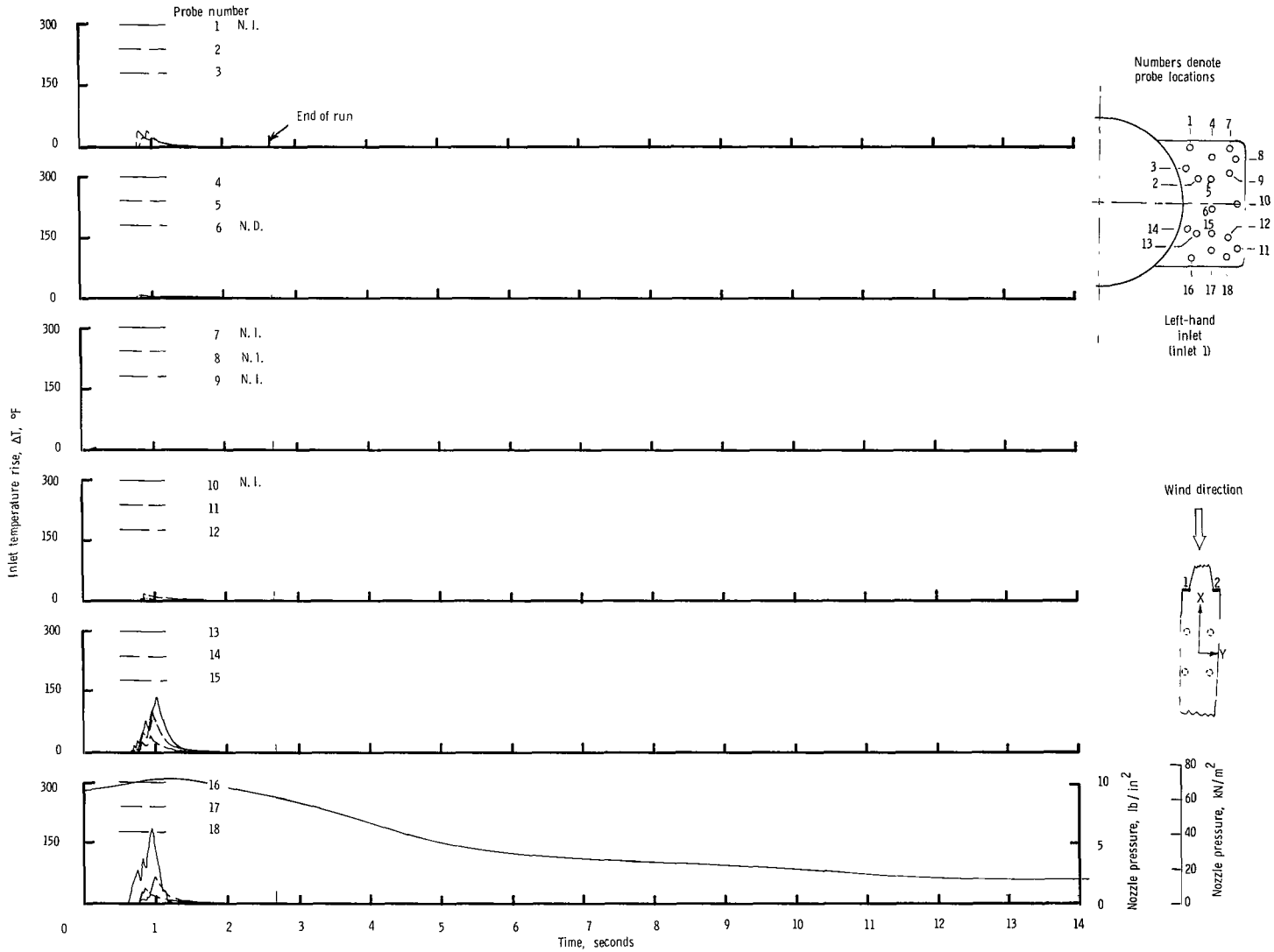

(f) Concluded.

Figure 12.- Continued.

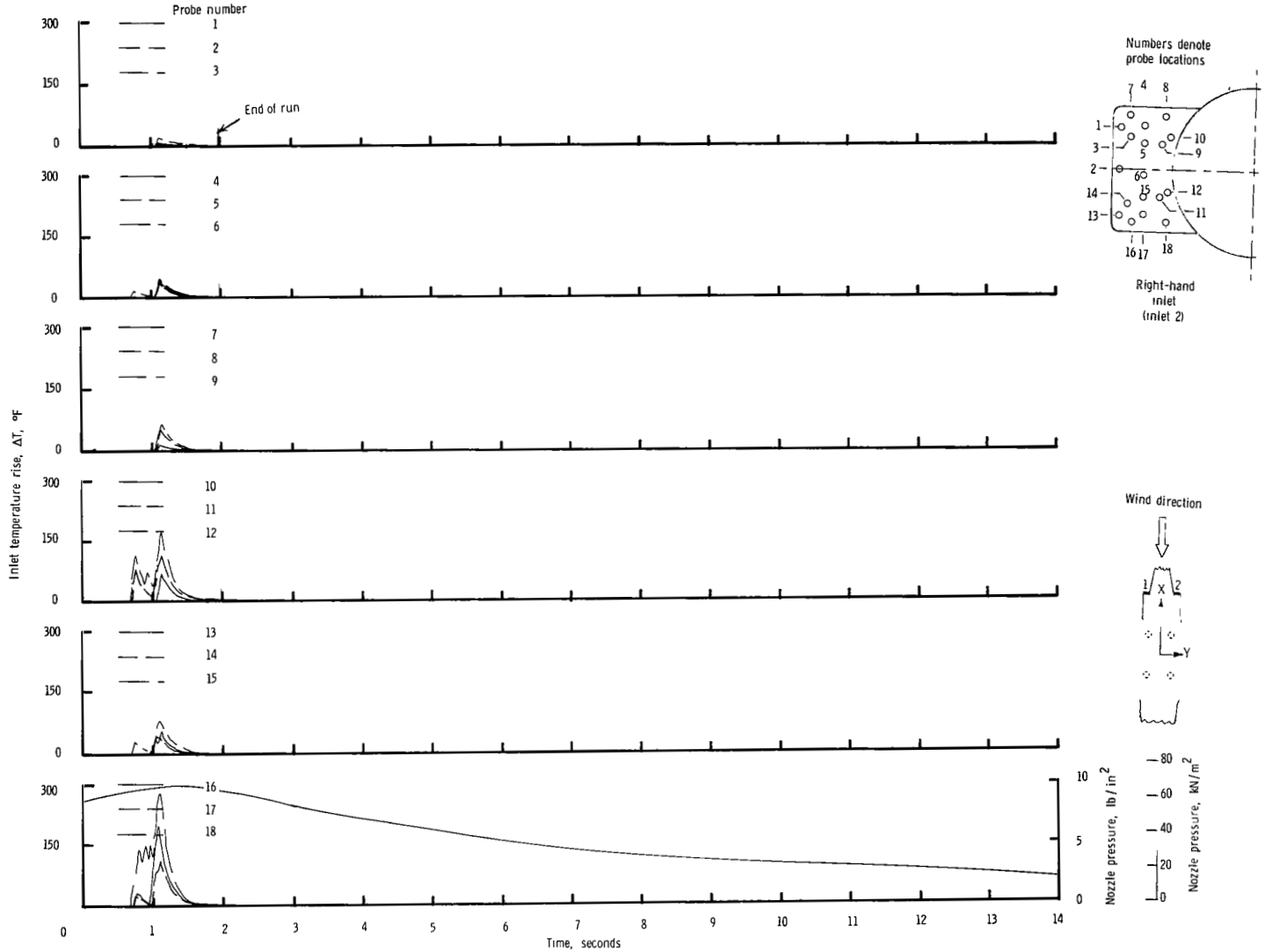

(g) $\psi = 0^0$; V = 35.55 knots.

Figure 12.- Continued.

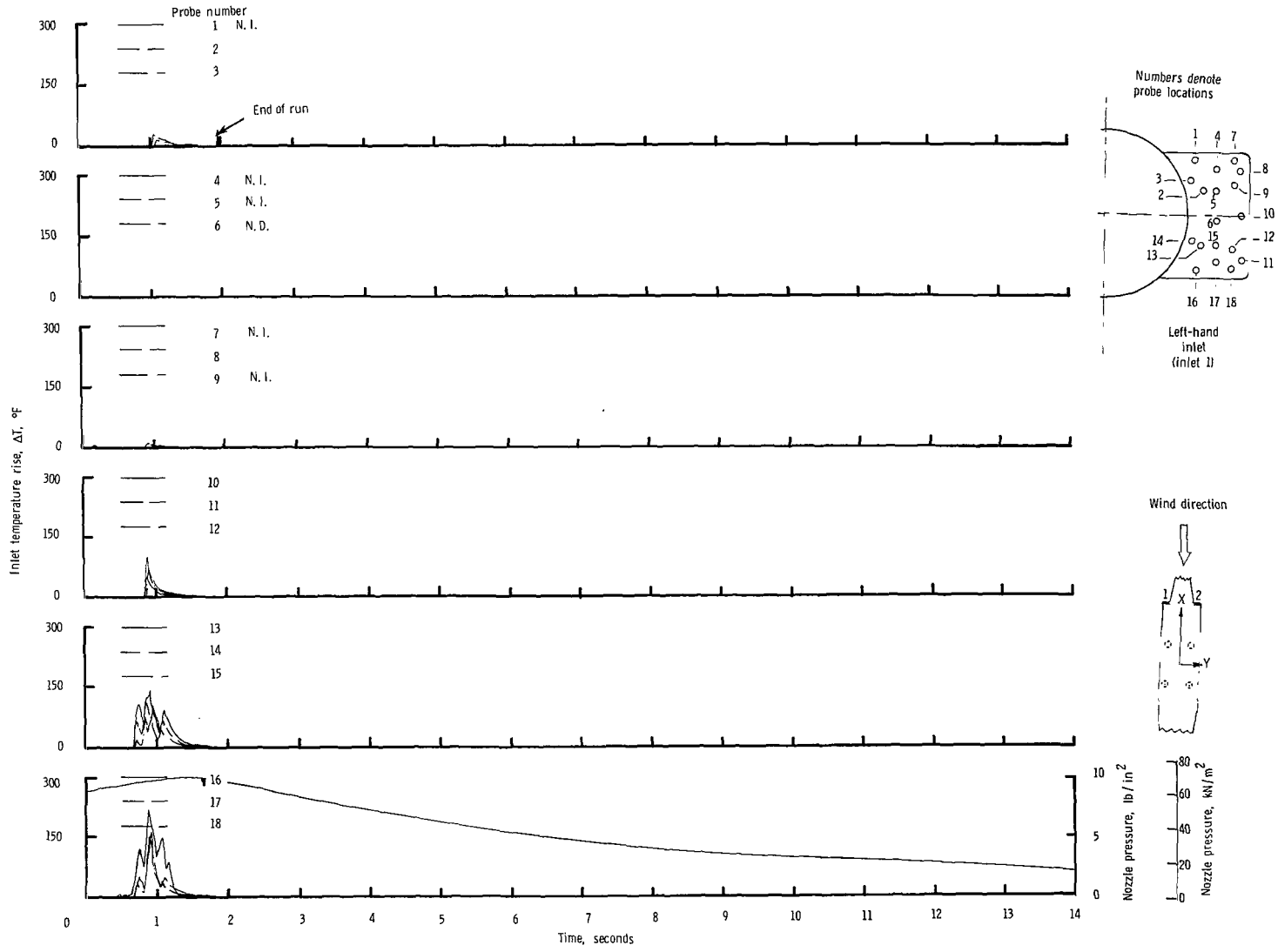

(g) Concluded.

Figure 12.- Continued.

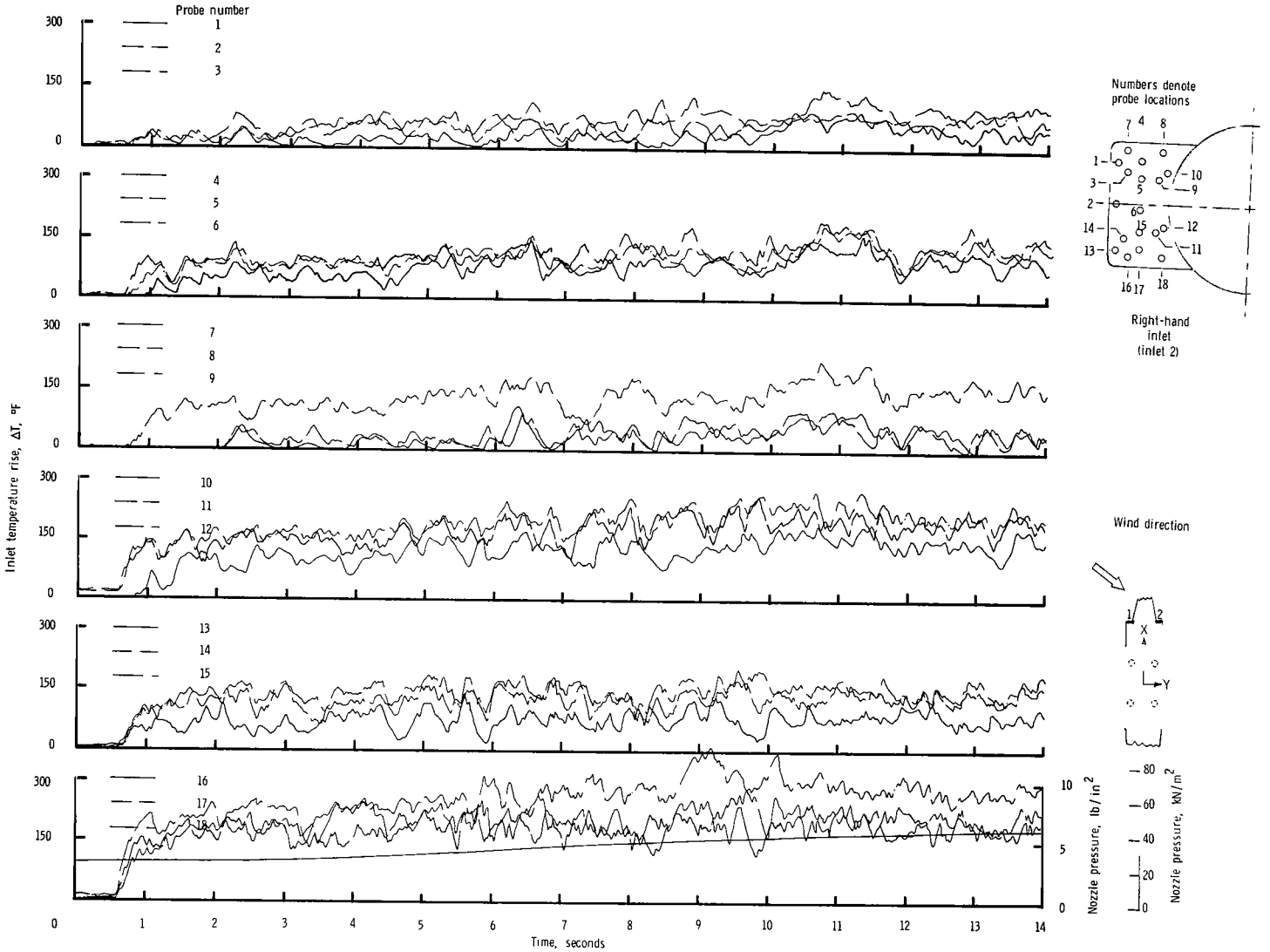

(h) $\psi = 45^0$; V = 5.92 knots.

Figure 12.- Continued.

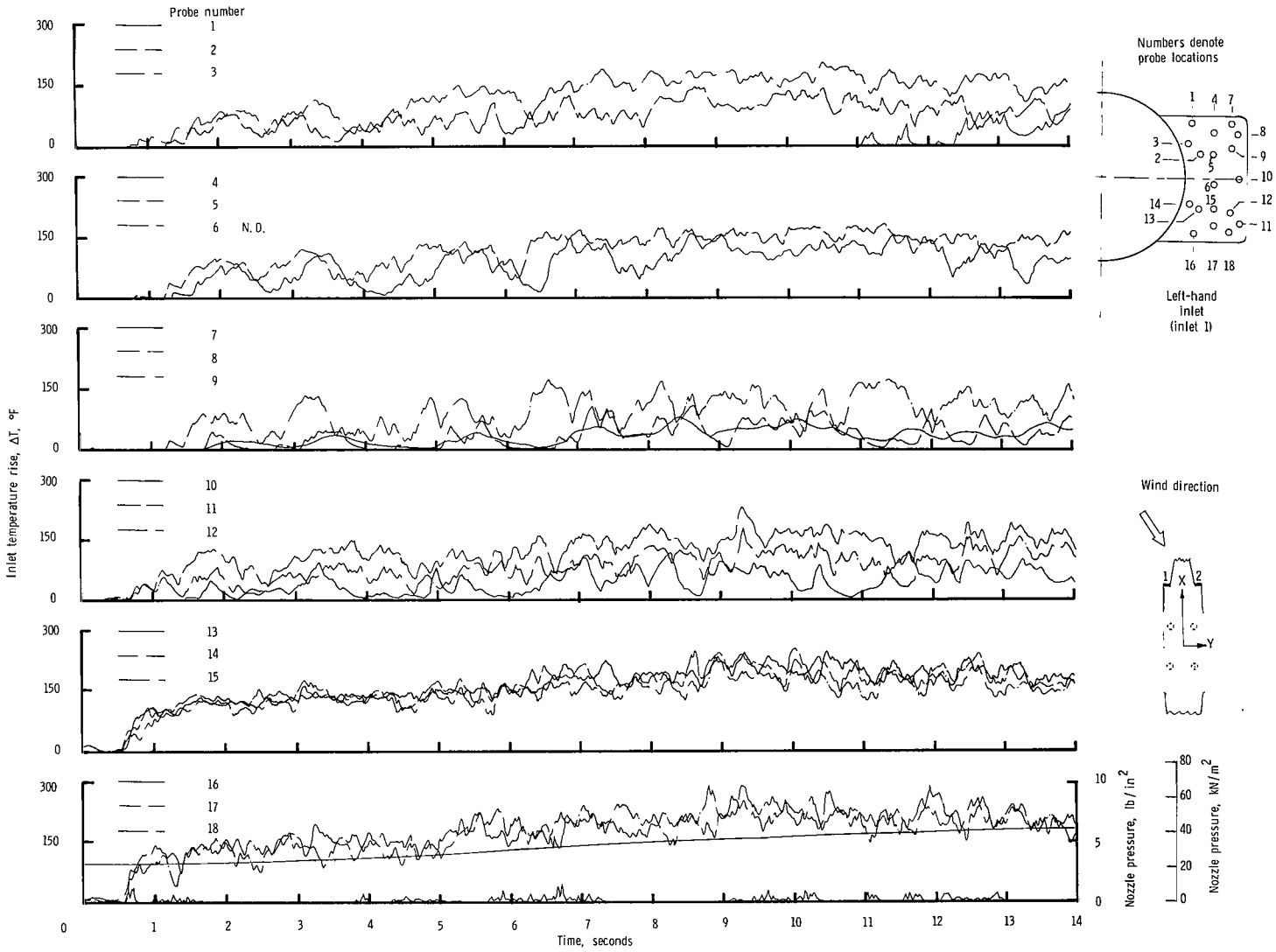

(h) Concluded.

Figure 12.- Continued.

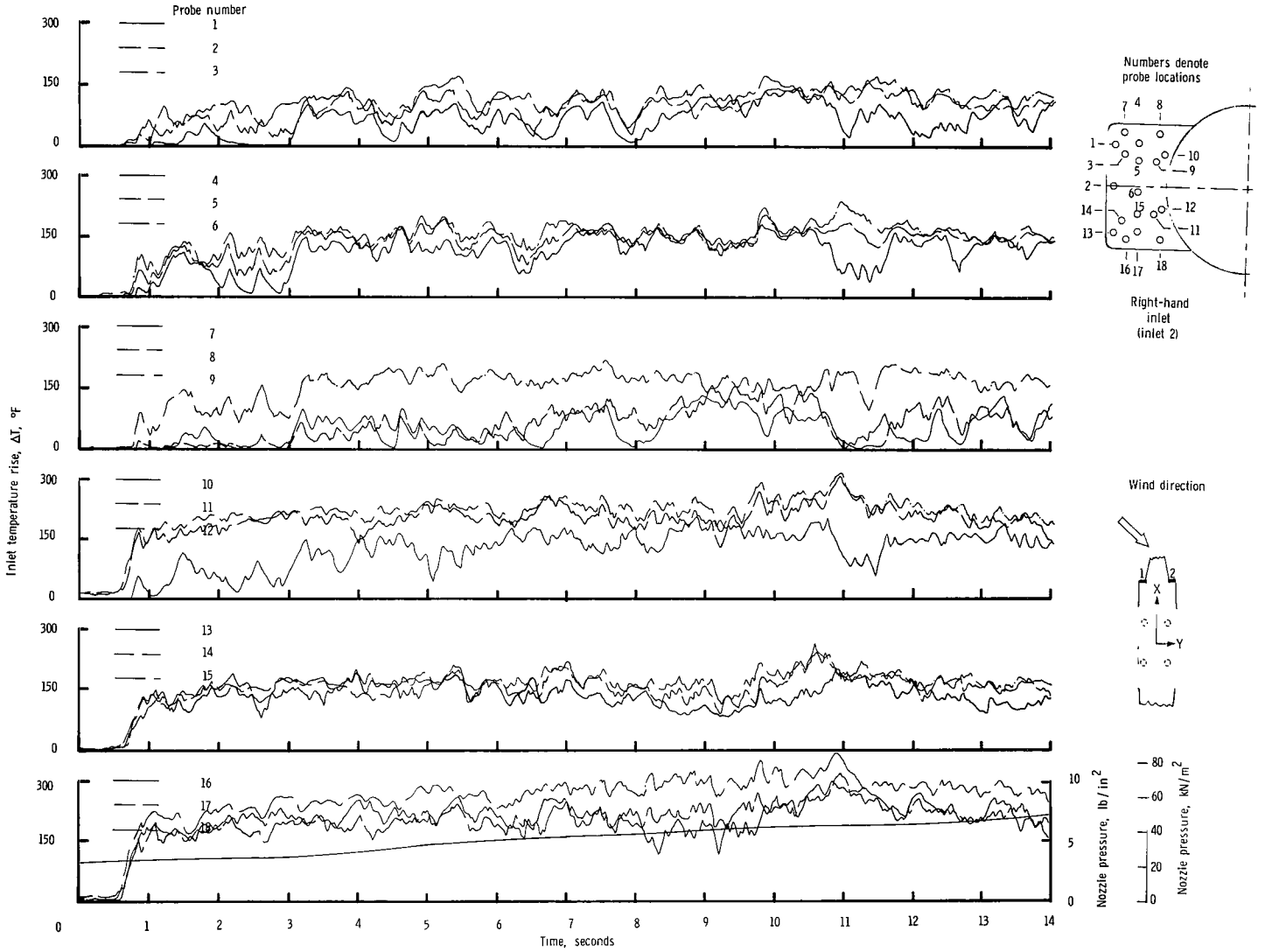

(i) $\psi = 45^0$; V = 11.85 knots.

Figure 12.- Continued.

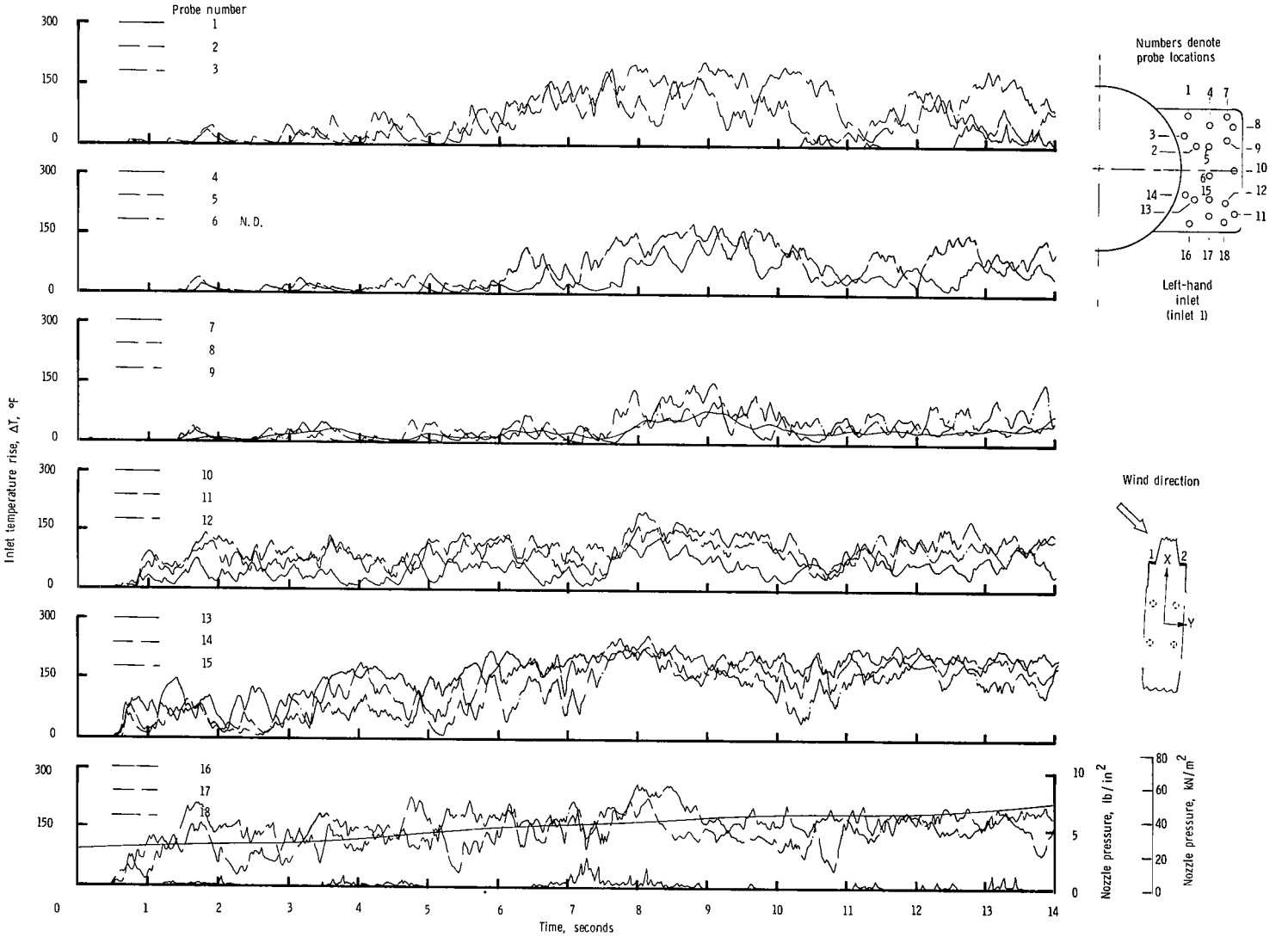

(i) Concluded.

Figure 12.- Continued.

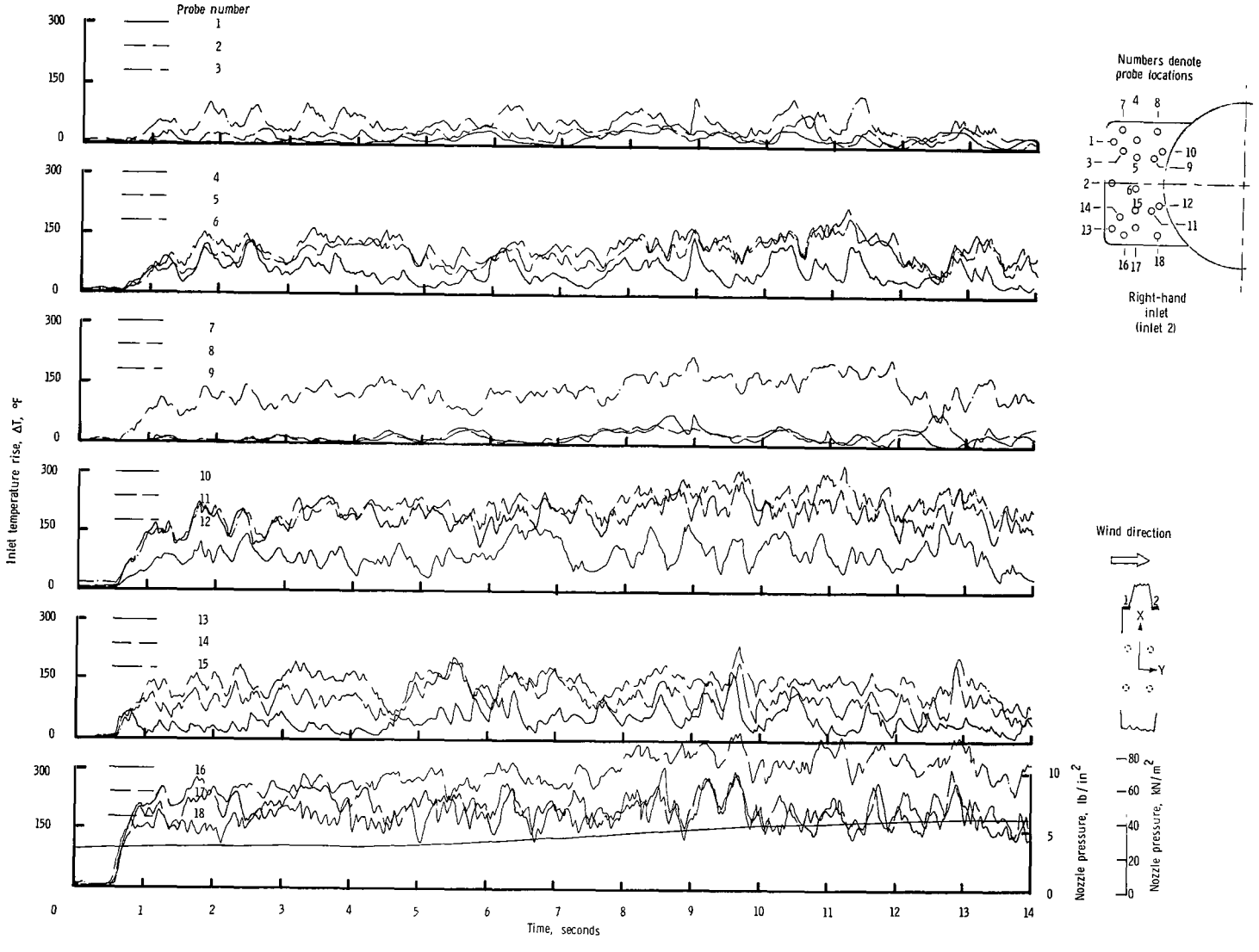

(j) $\psi = 90^0$; V = 5.92 knots.

Figure 12.- Continued.

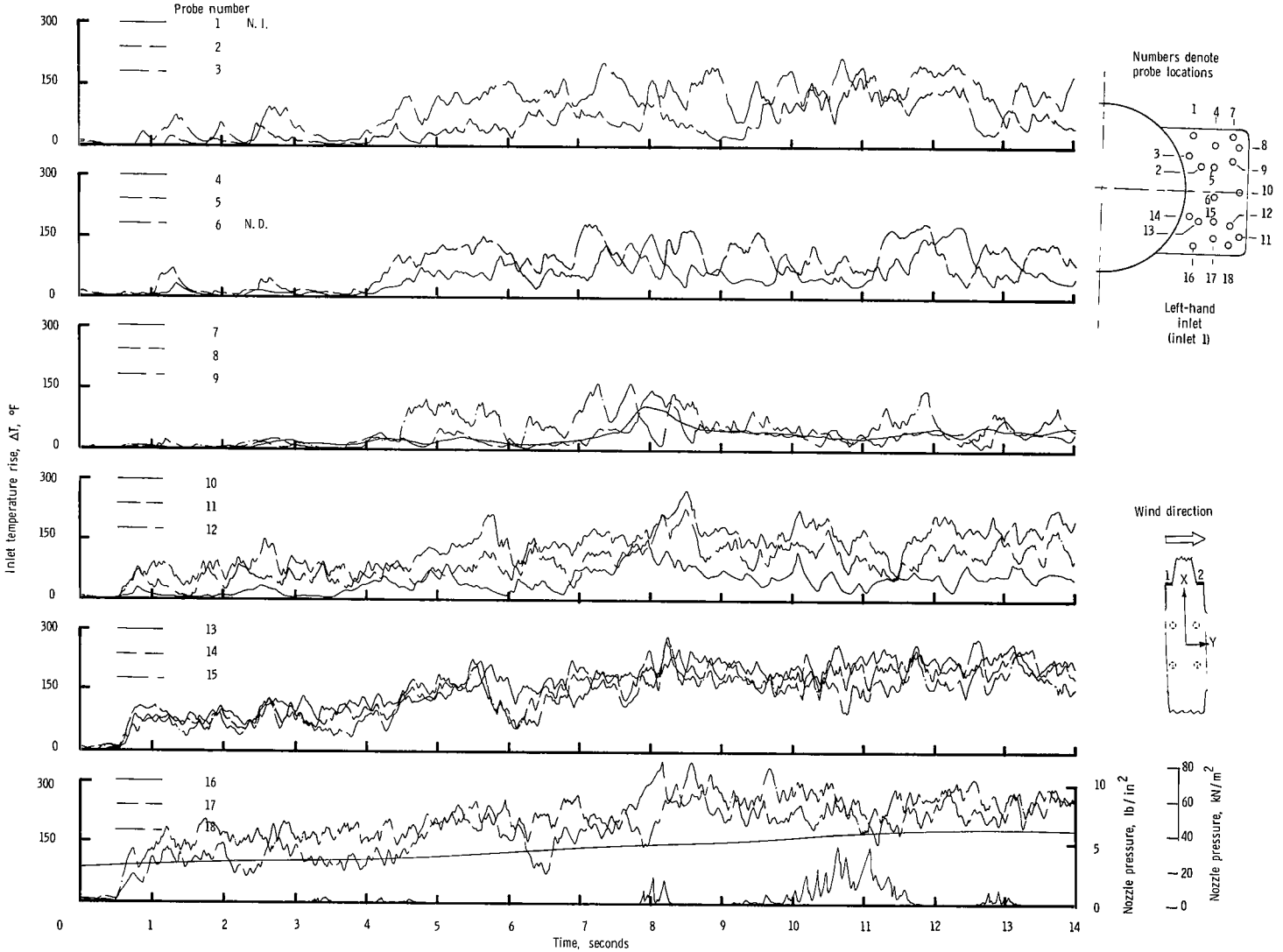

(j) Concluded.

Figure 12.- Continued.

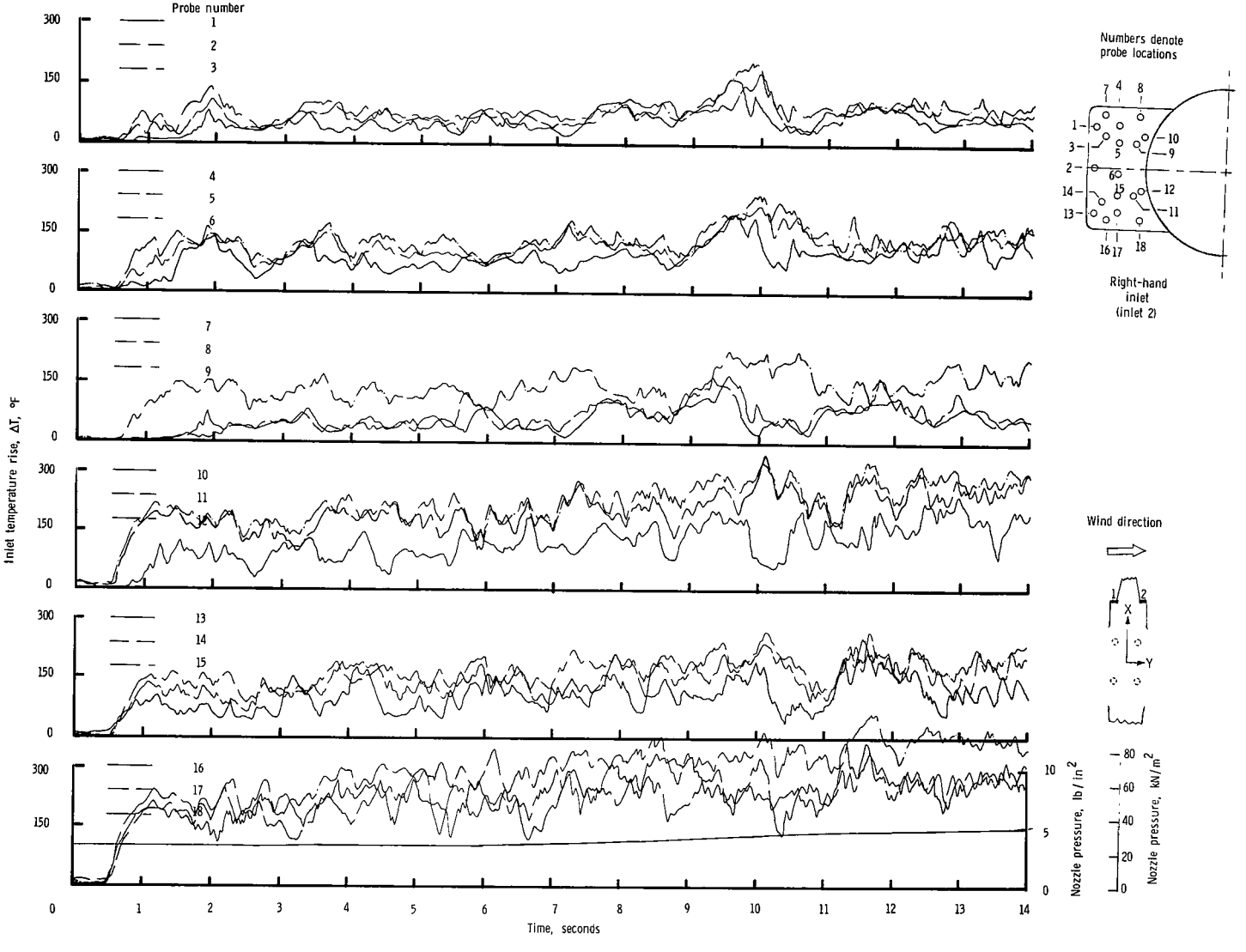

(k) $\psi = 90^0$; V = 11.85 knots.

Figure 12.- Continued.

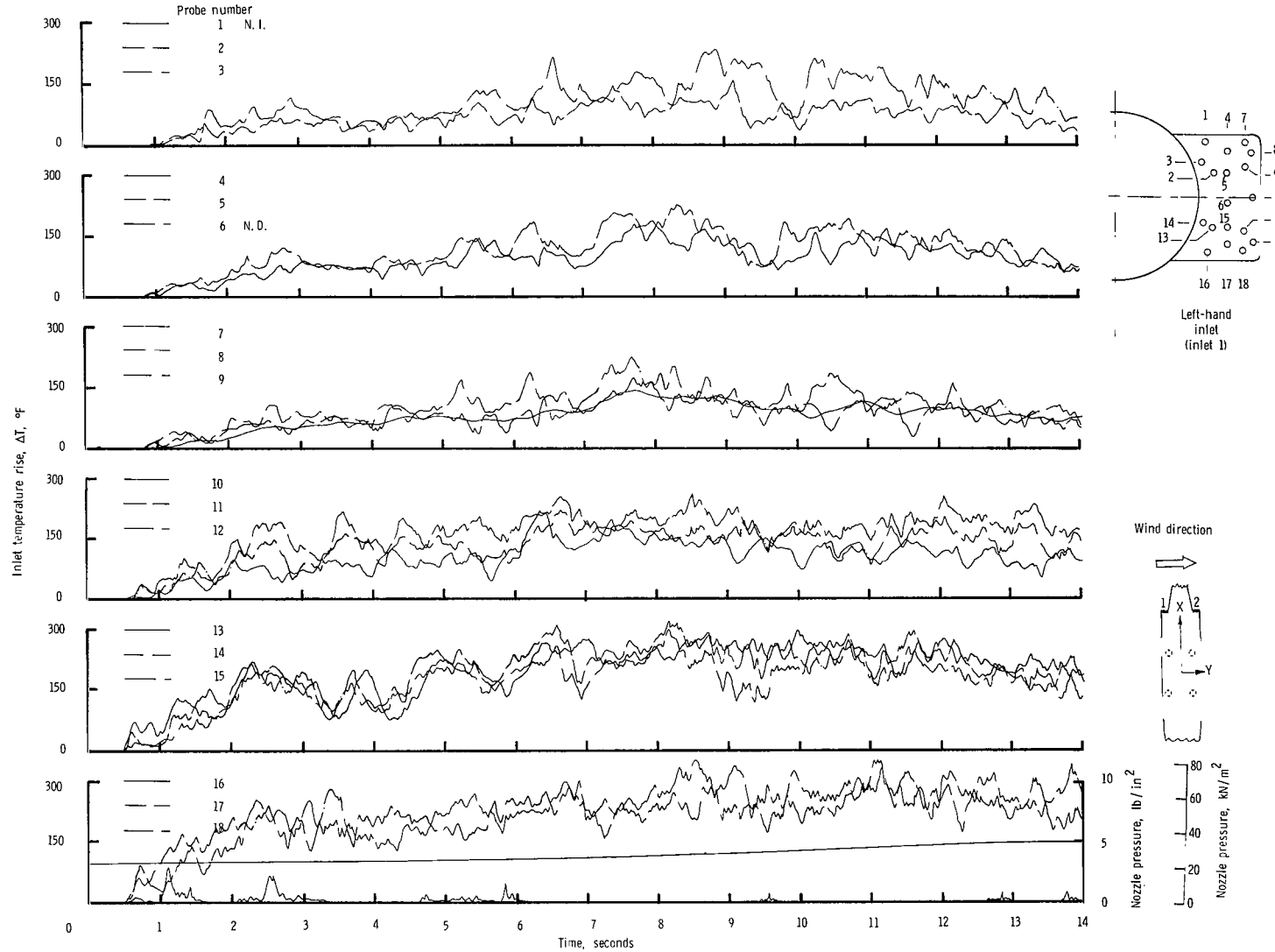

(k) Concluded.

Figure 12.- Concluded.

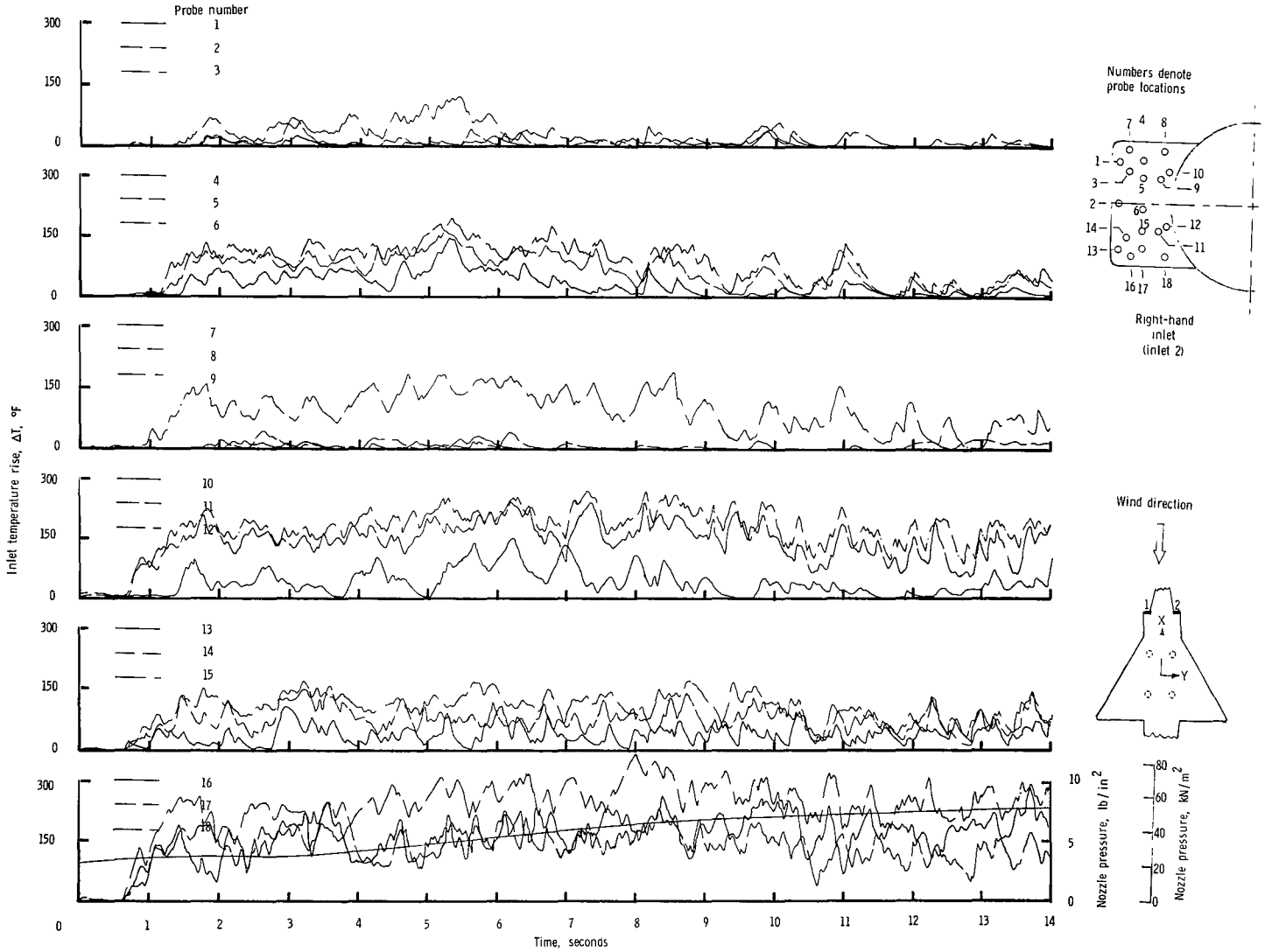

(a) $\psi = 0^0$; V = 0 knots.

Figure 13.- Variation of inlet-air temperature rise with time for the rectangular nozzle arrangement with side inlets and with small wing installed. $S_W/S_J = 43.00$; $h/D_e = 1.17$. (Values of ΔT in ^0C can be obtained by multiplying the ^0F values by 5/9.)

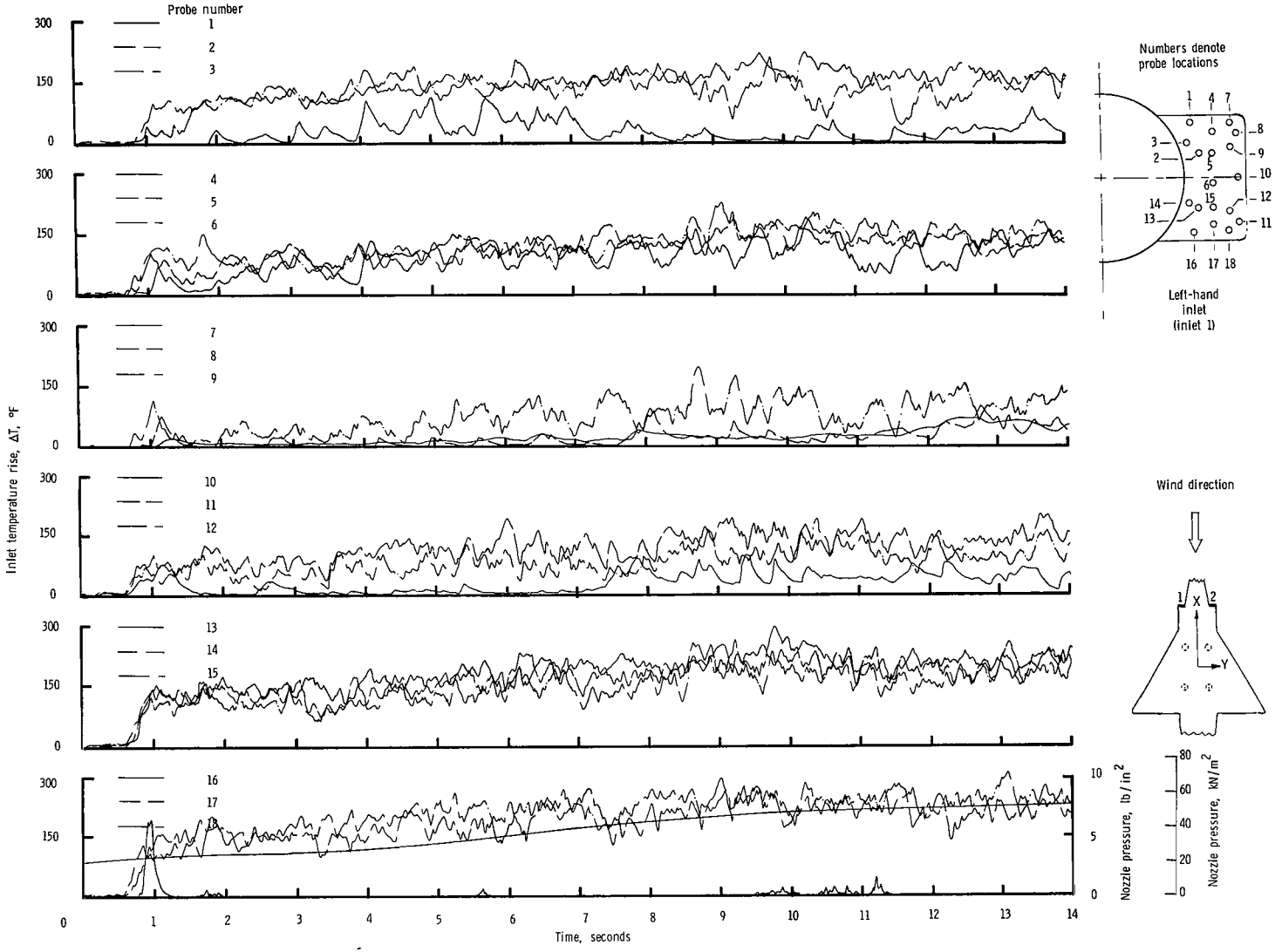

(a) Concluded.

Figure 13.- Continued.

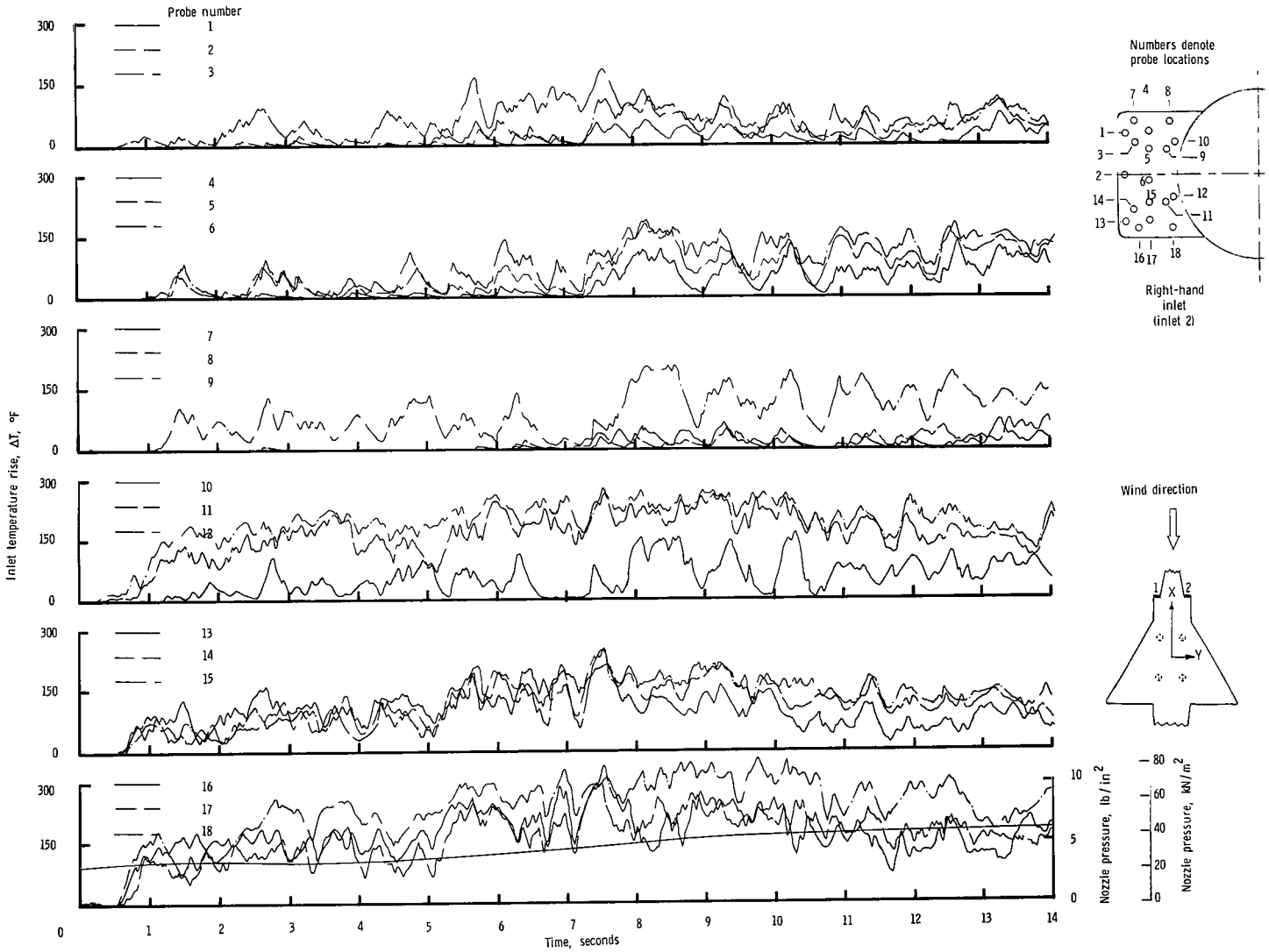

(b) $\psi = 0^0$; V = 5.92 knots.

Figure 13.- Continued.

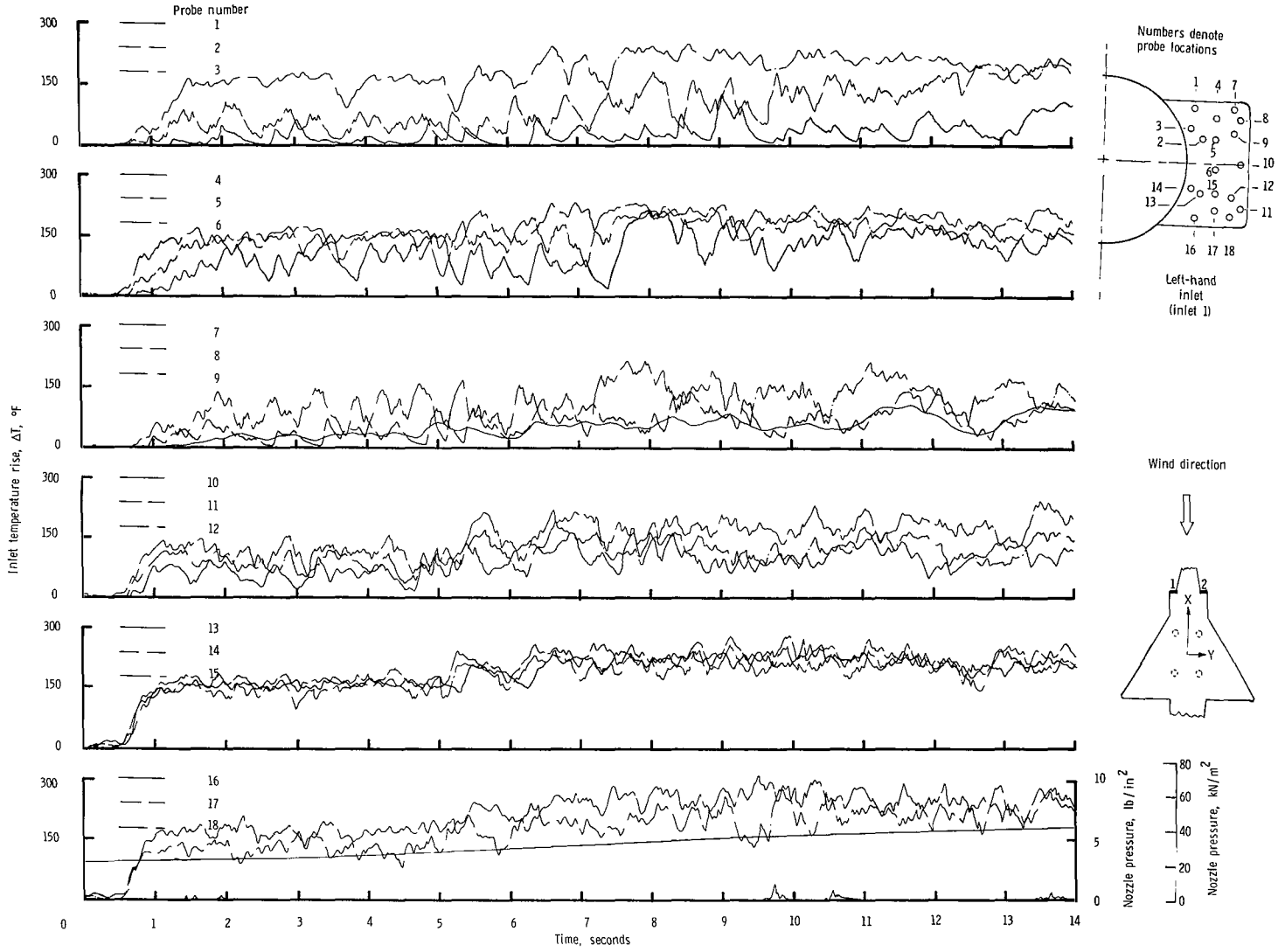

(b) Concluded.

Figure 13.- Continued.

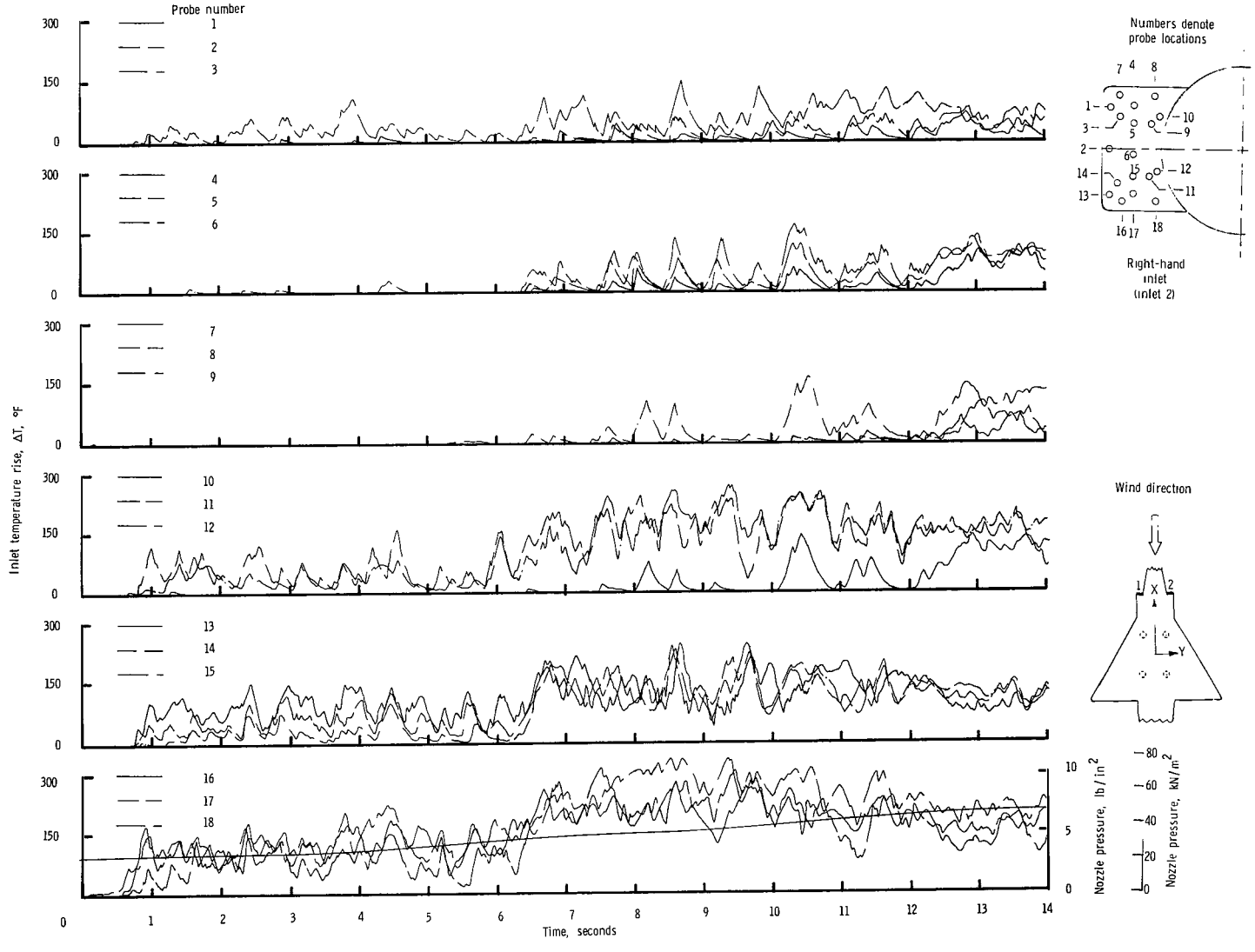

(c) $\psi = 0^{0}$; V = 11.85 knots.

Figure 13.- Continued.

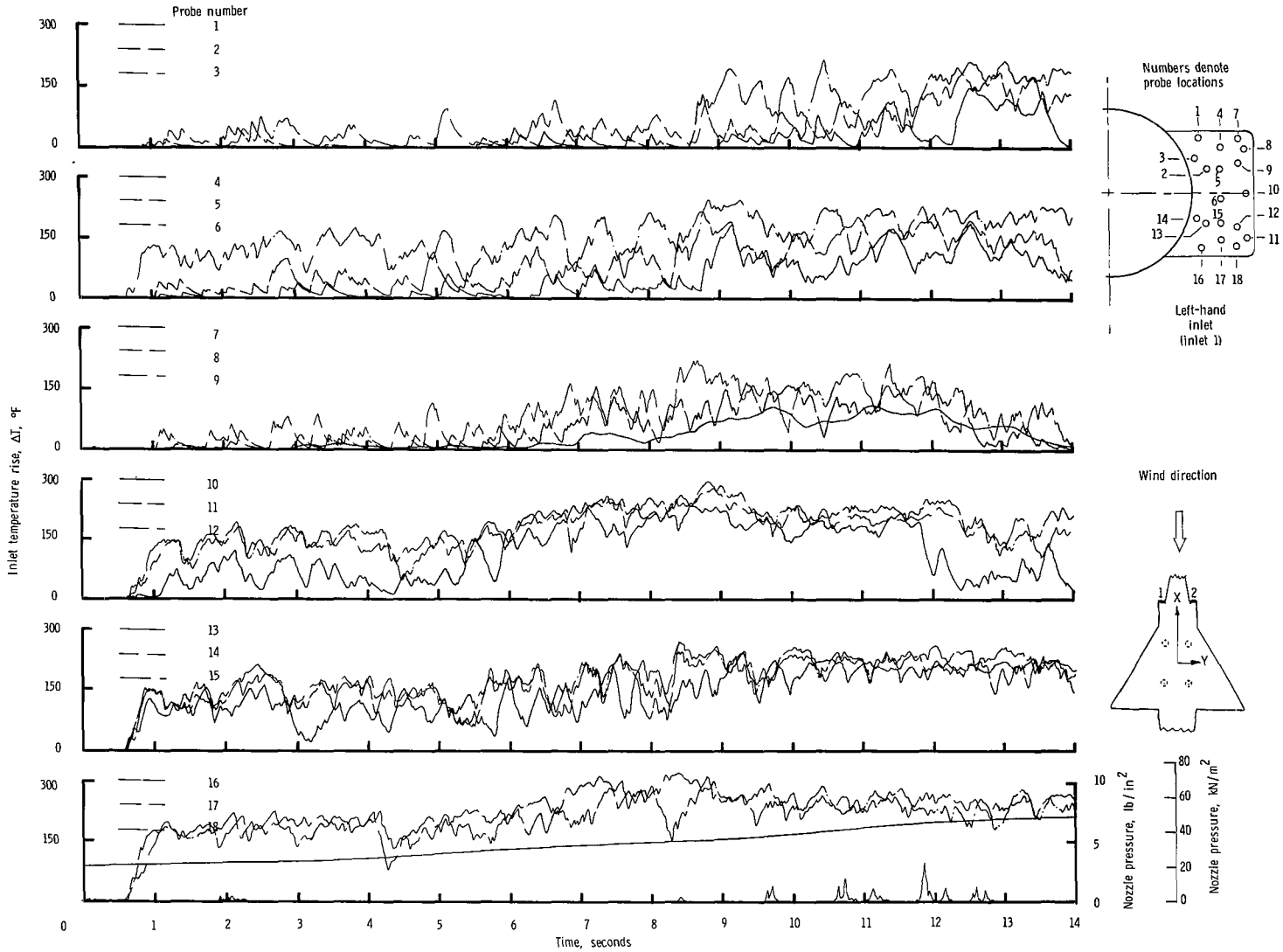

(c) Concluded.

Figure 13.- Continued.

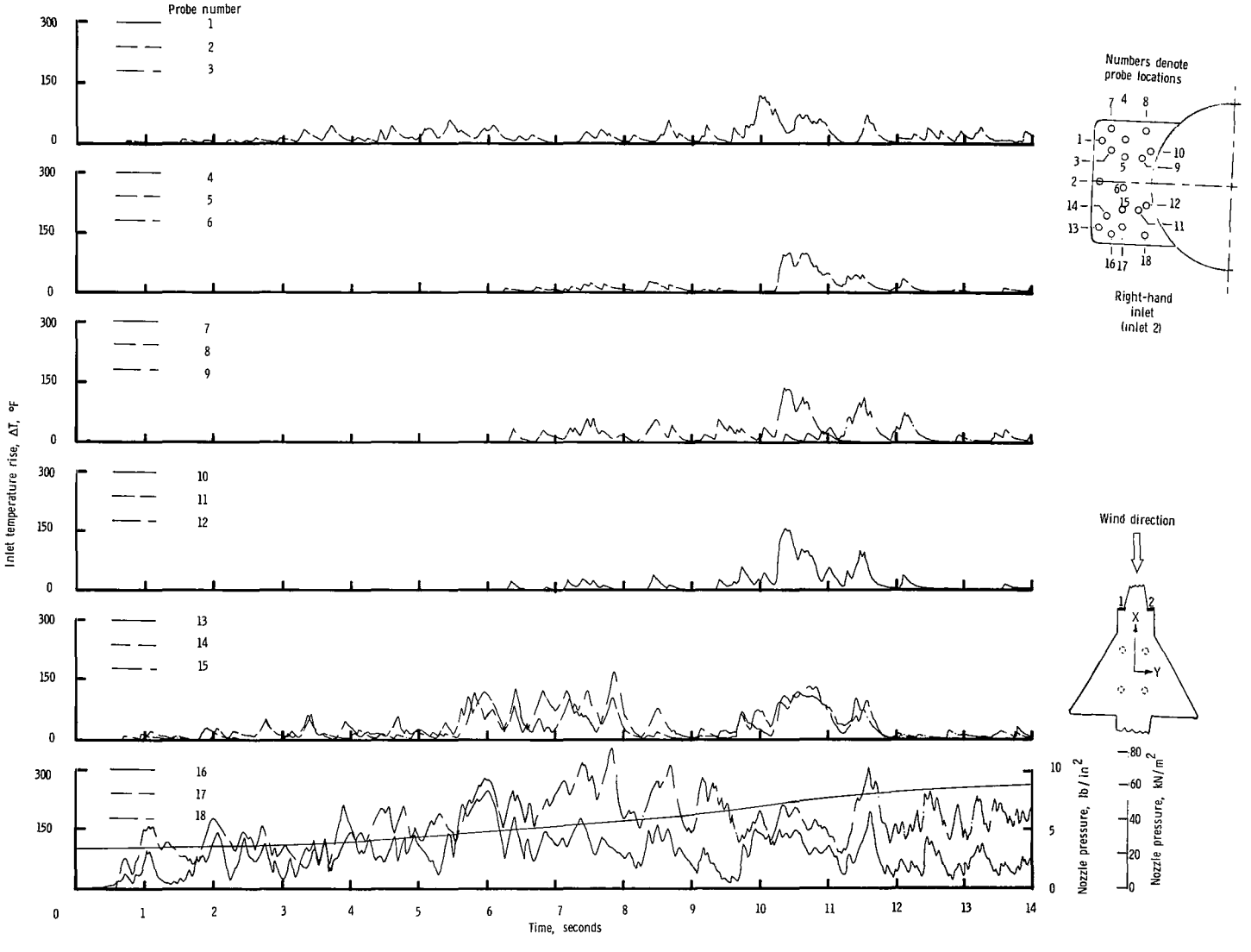

(d) $\psi = 0^0$; V = 17.78 knots.

Figure 13.- Continued.

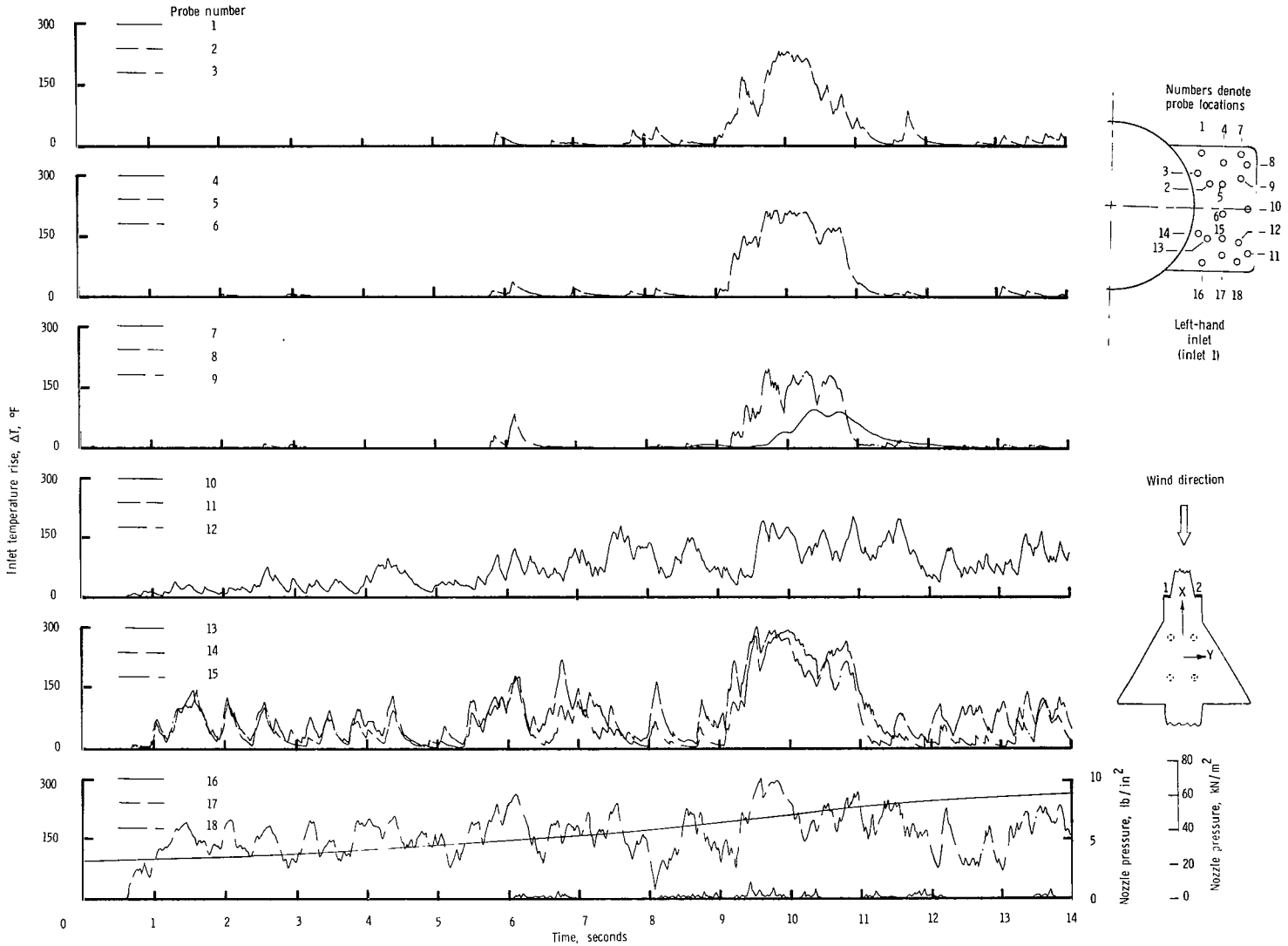

(d) Concluded.

Figure 13.- Continued.

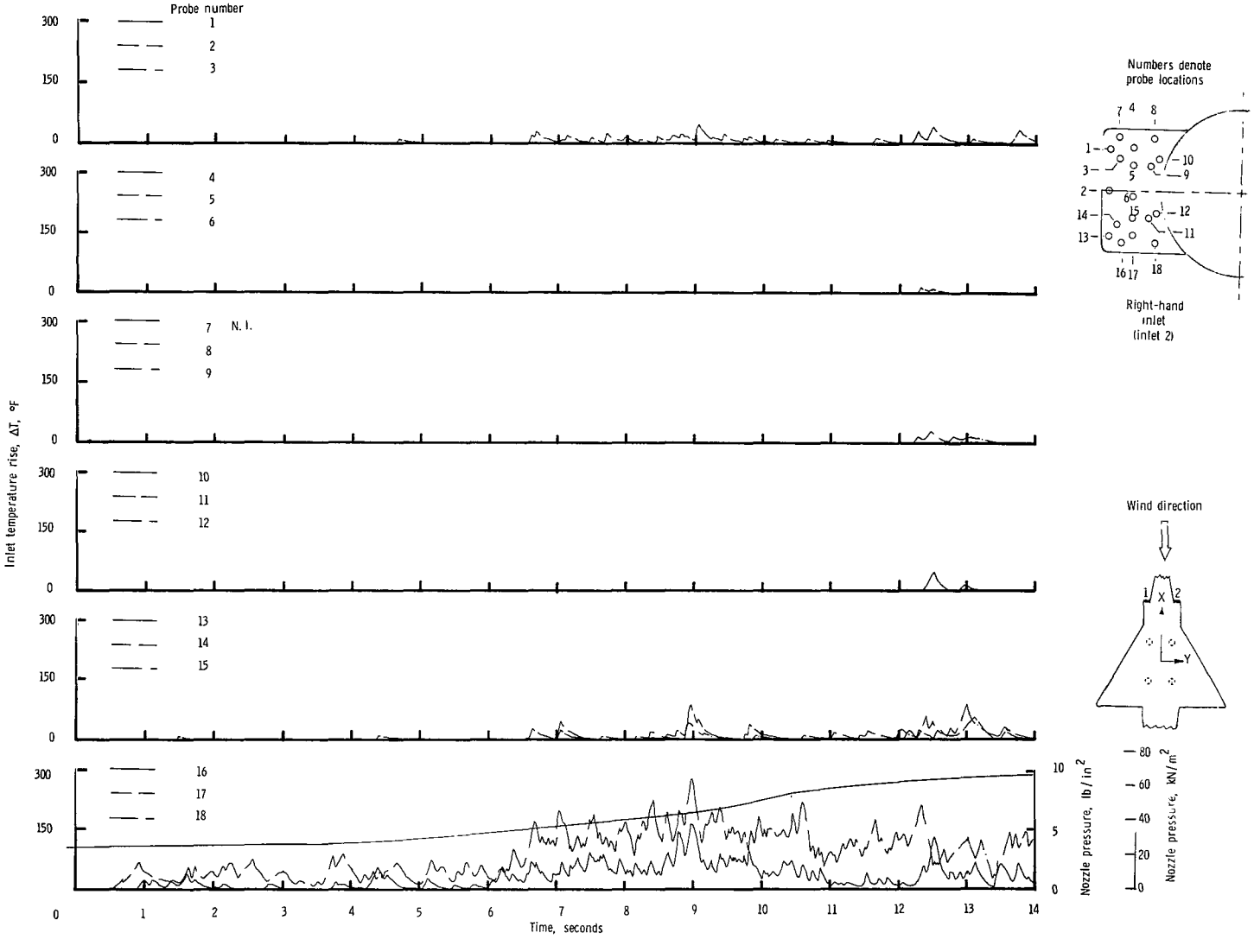

(e) $\psi = 0^{o}$; V = 23.70 knots.

Figure 13.- Continued.

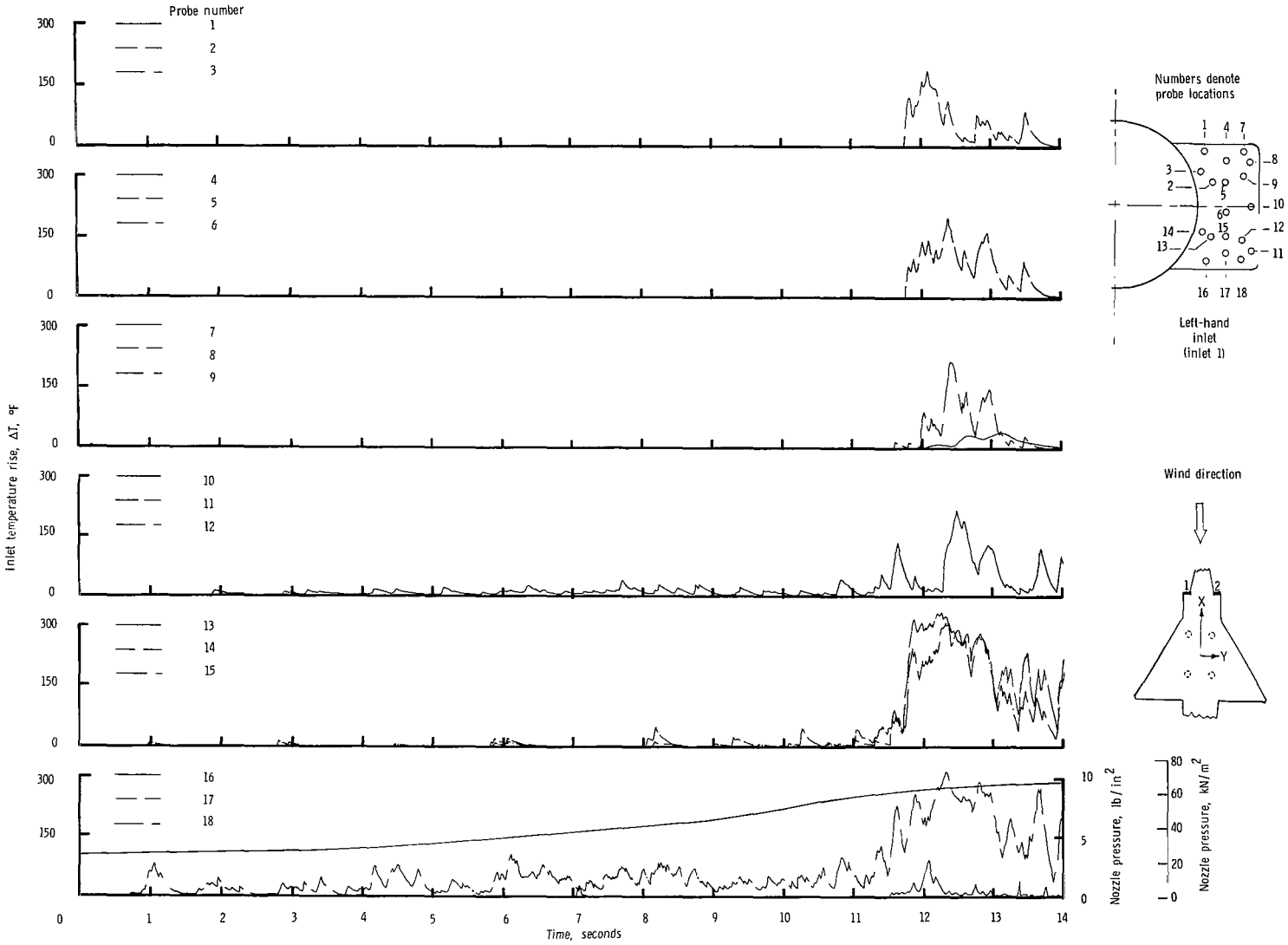

(e) Concluded.

Figure 13.- Continued.

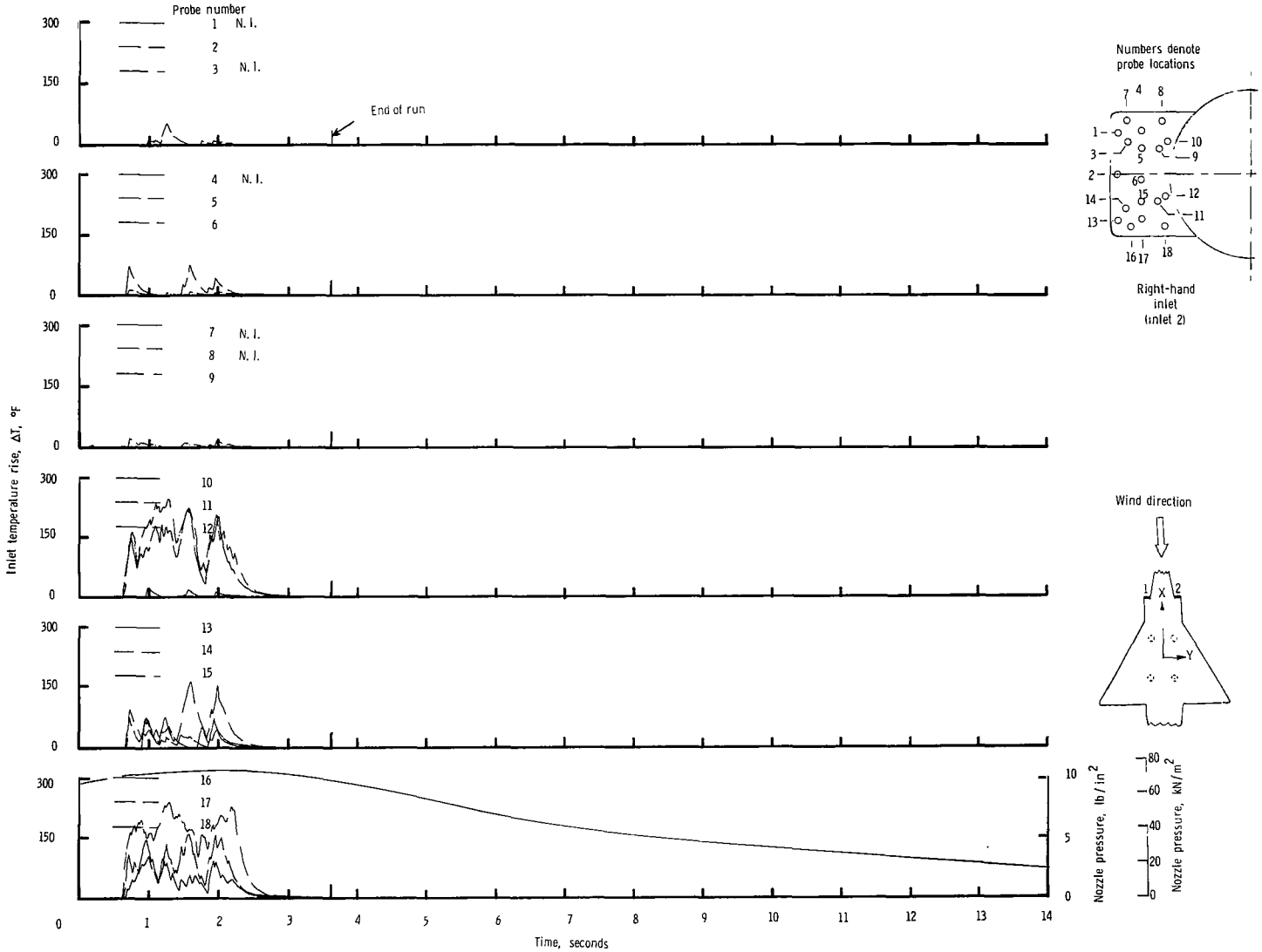

(f) $\psi = 0^0$; V = 26.93 knots.

Figure 13.- Continued.

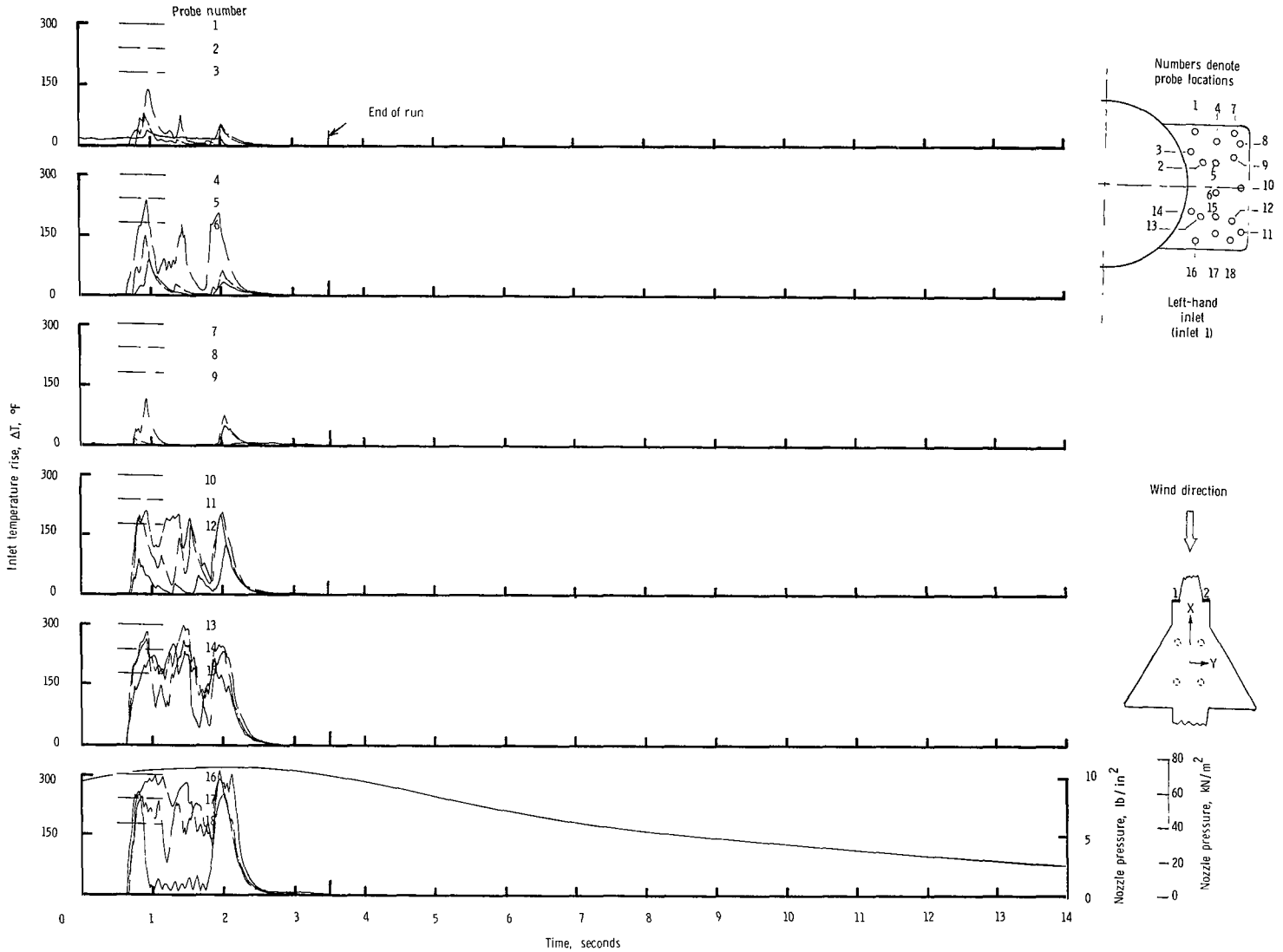

(f) Concluded.

Figure 13.- Continued.

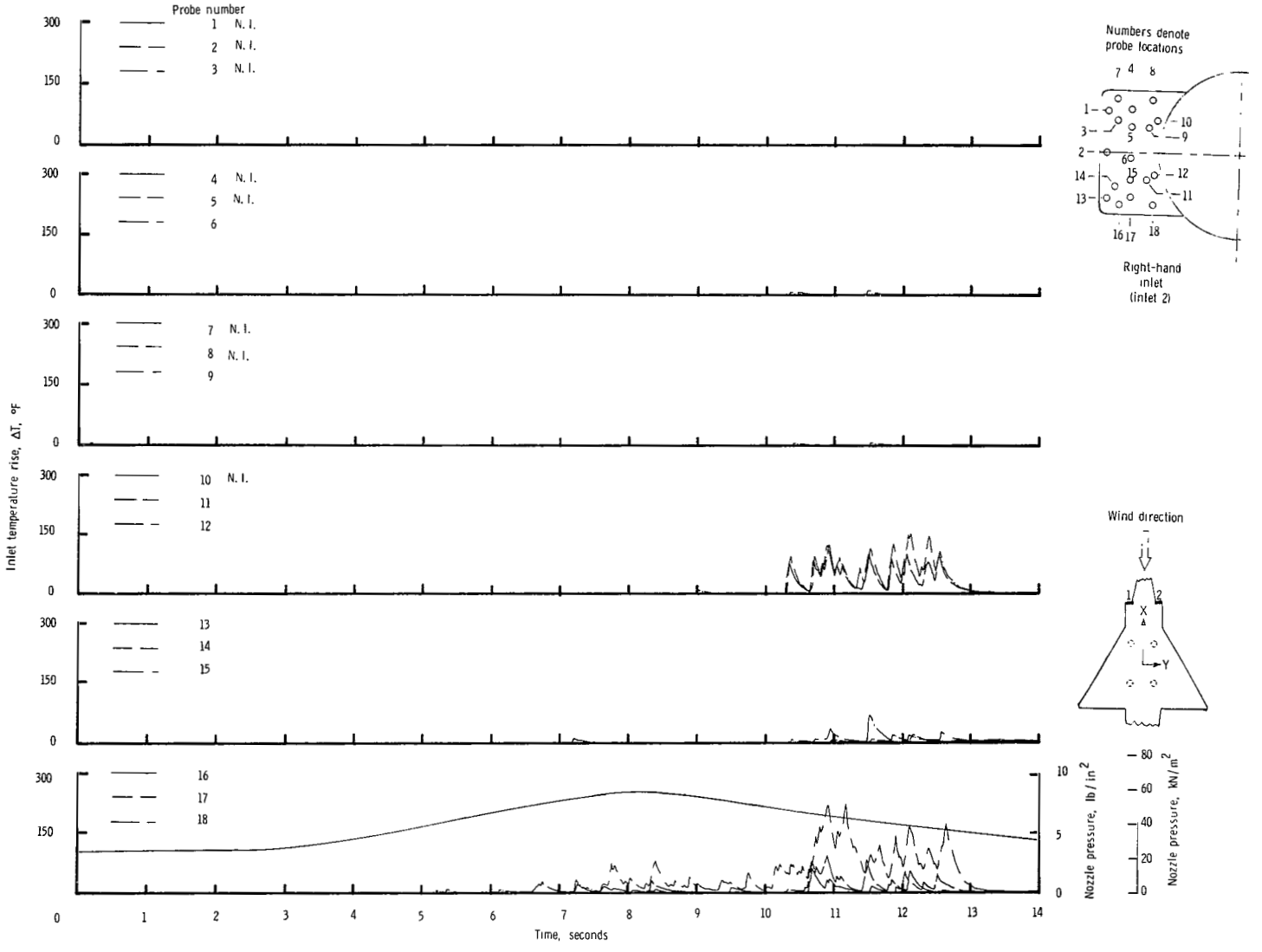

(g) $\psi = 0^{0}$; V = 35.55 knots.

Figure 13.- Continued.

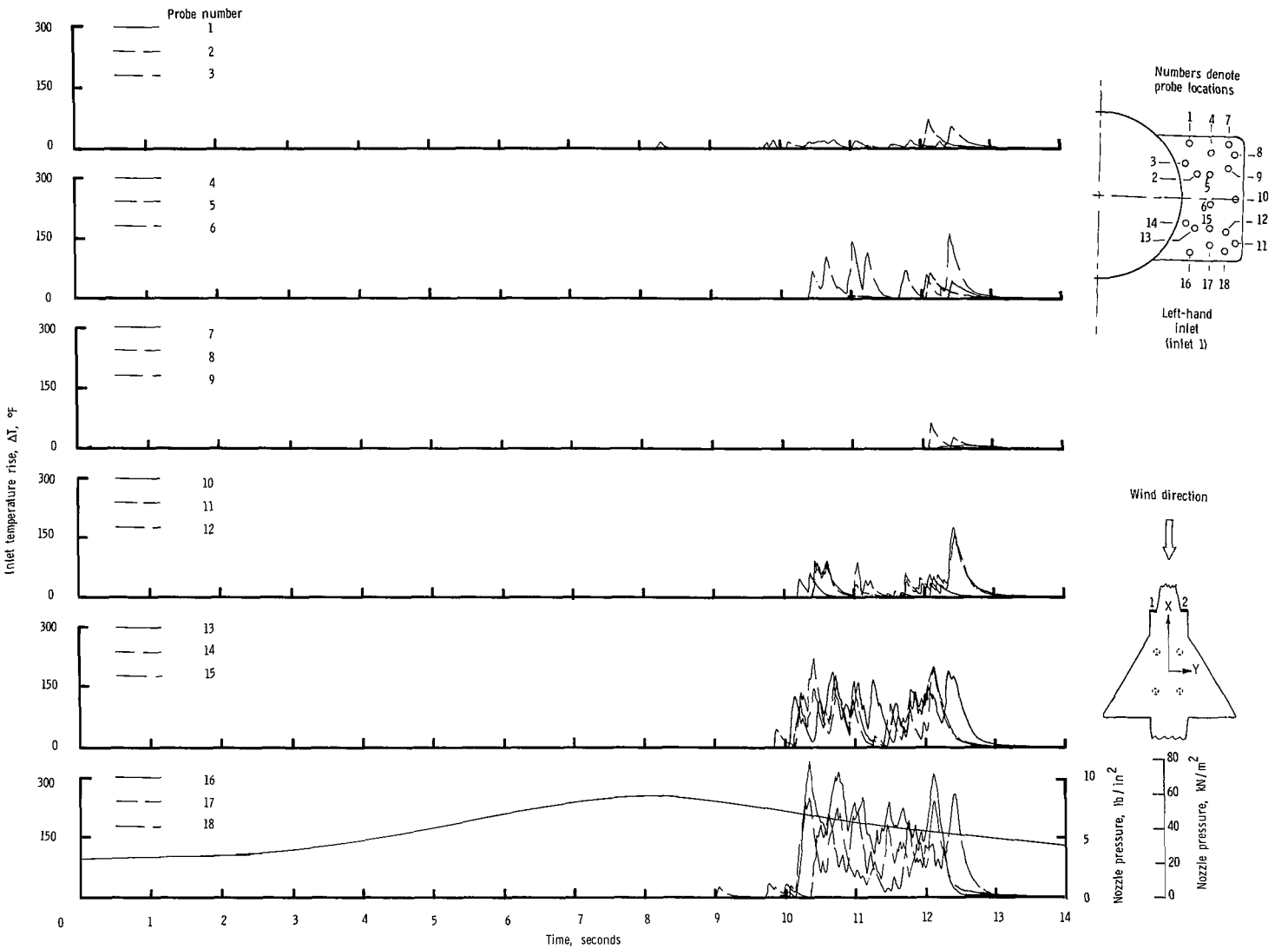

(g) Concluded.

Figure 13.- Continued.

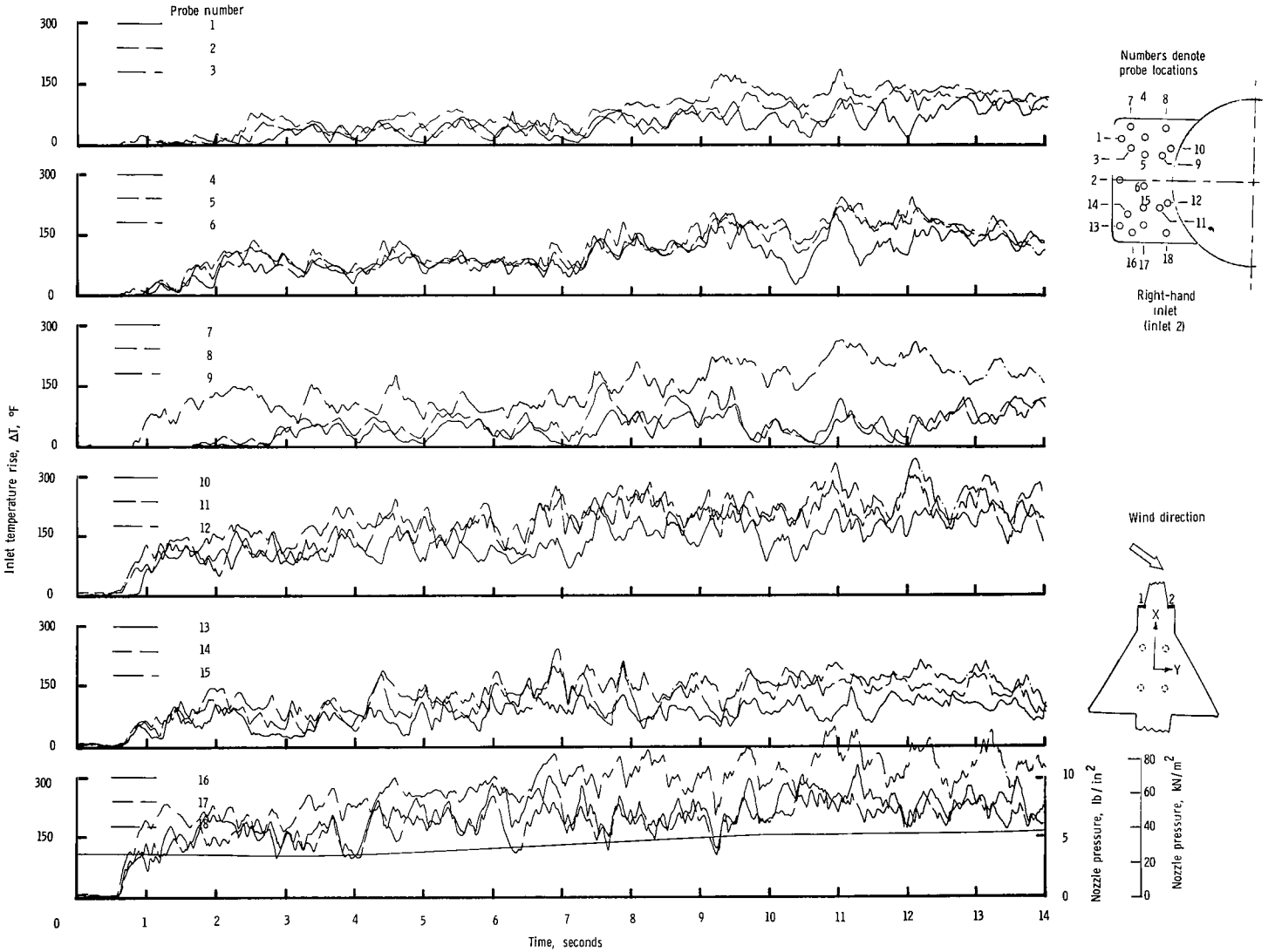

(h) $\psi = 45^{0}$; V = 5.92 knots.

Figure 13.- Continued.

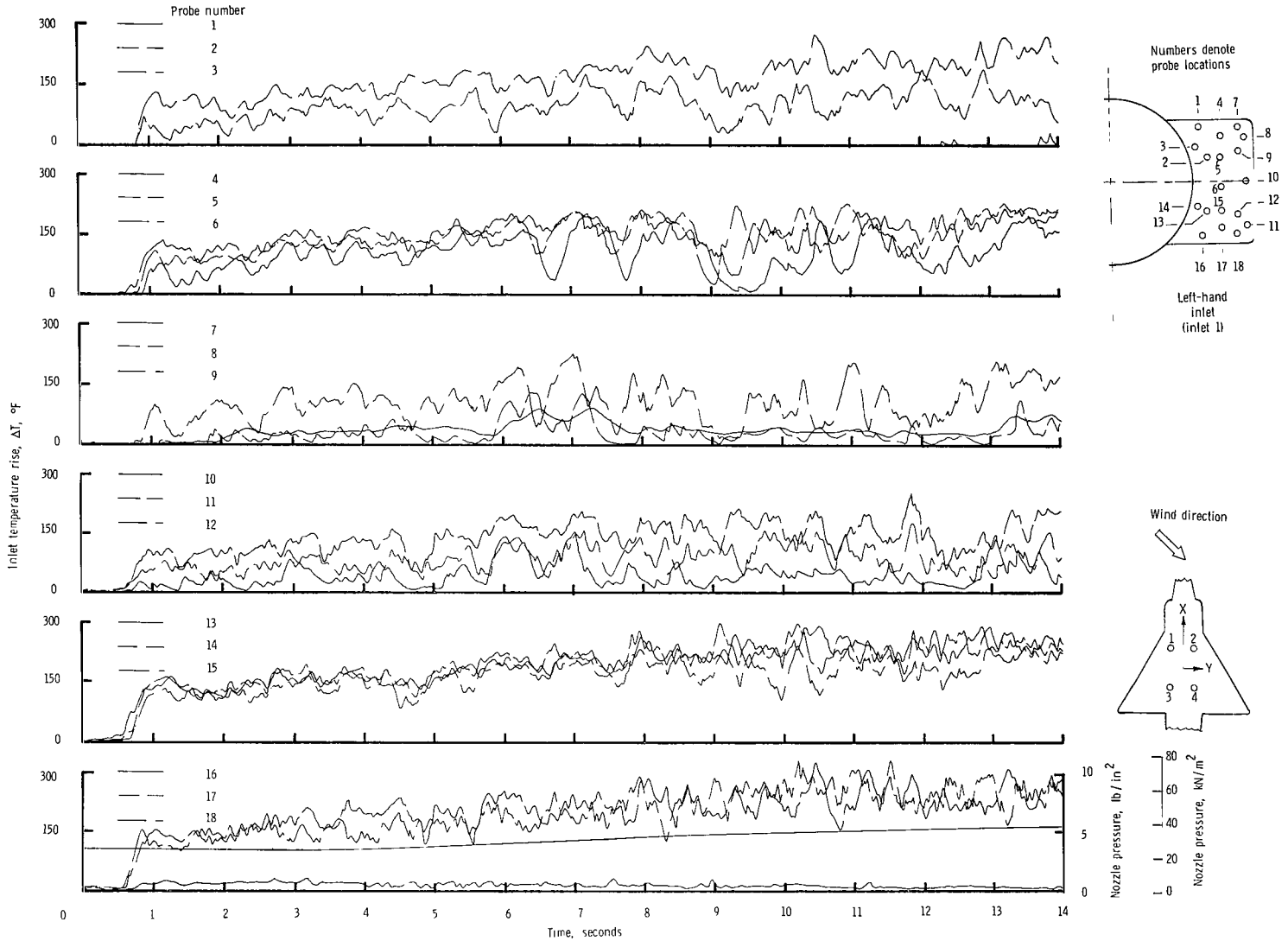

(h) Concluded.

Figure 13.- Continued.

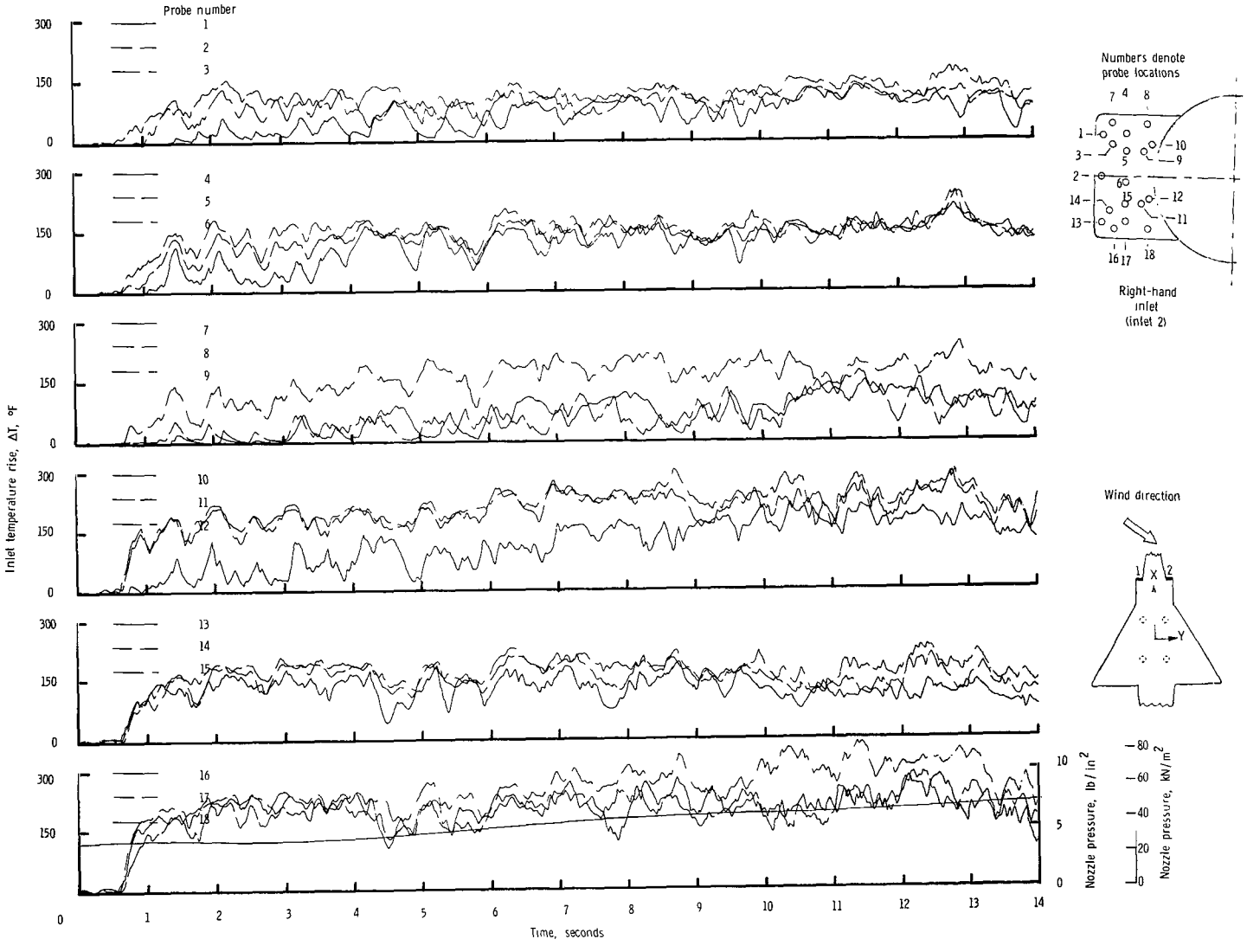

(i) $\psi = 45^{0}$; V = 11.85 knots.

Figure 13.- Continued.

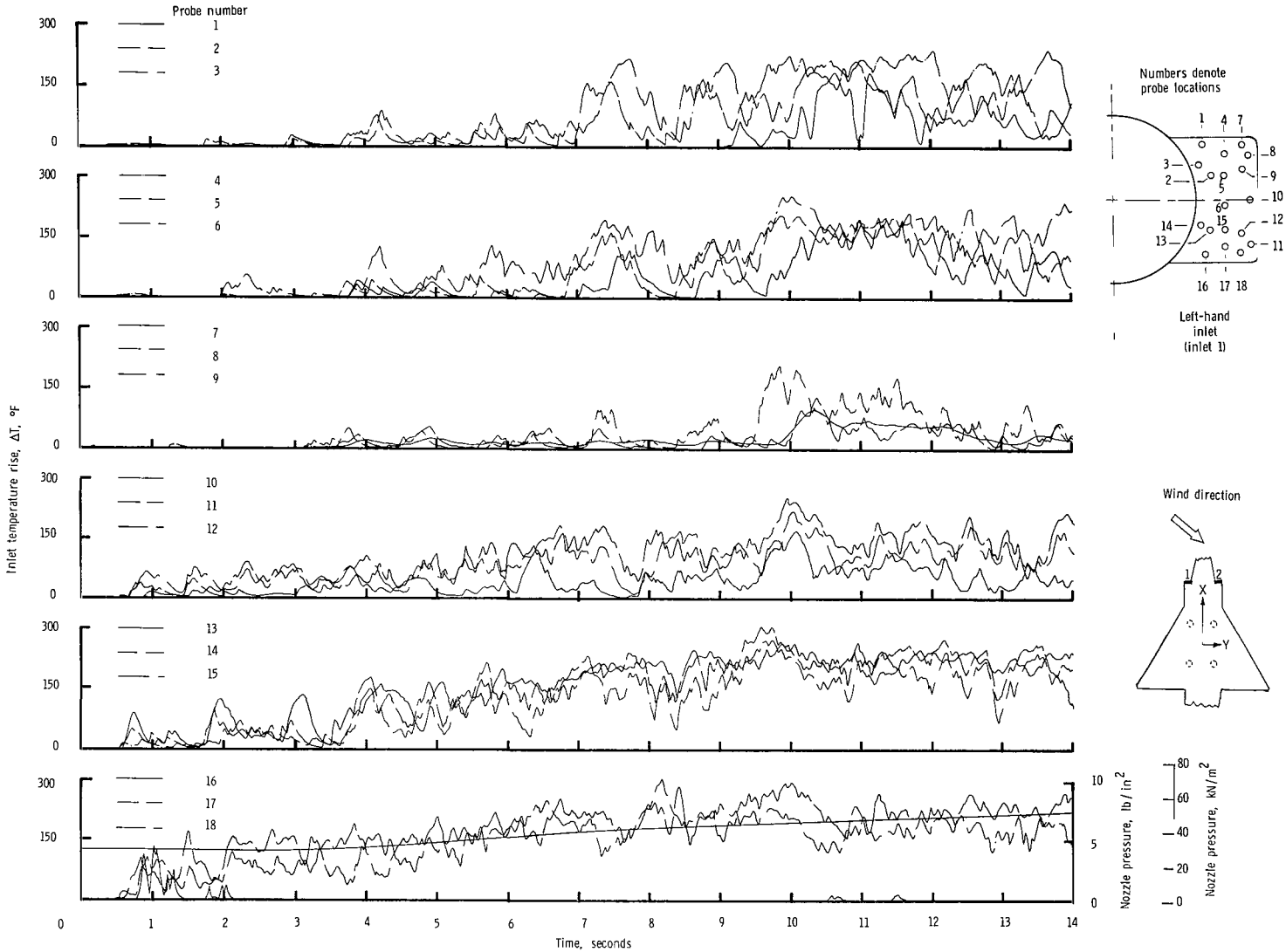

(i) Concluded.

Figure 13.- Continued.

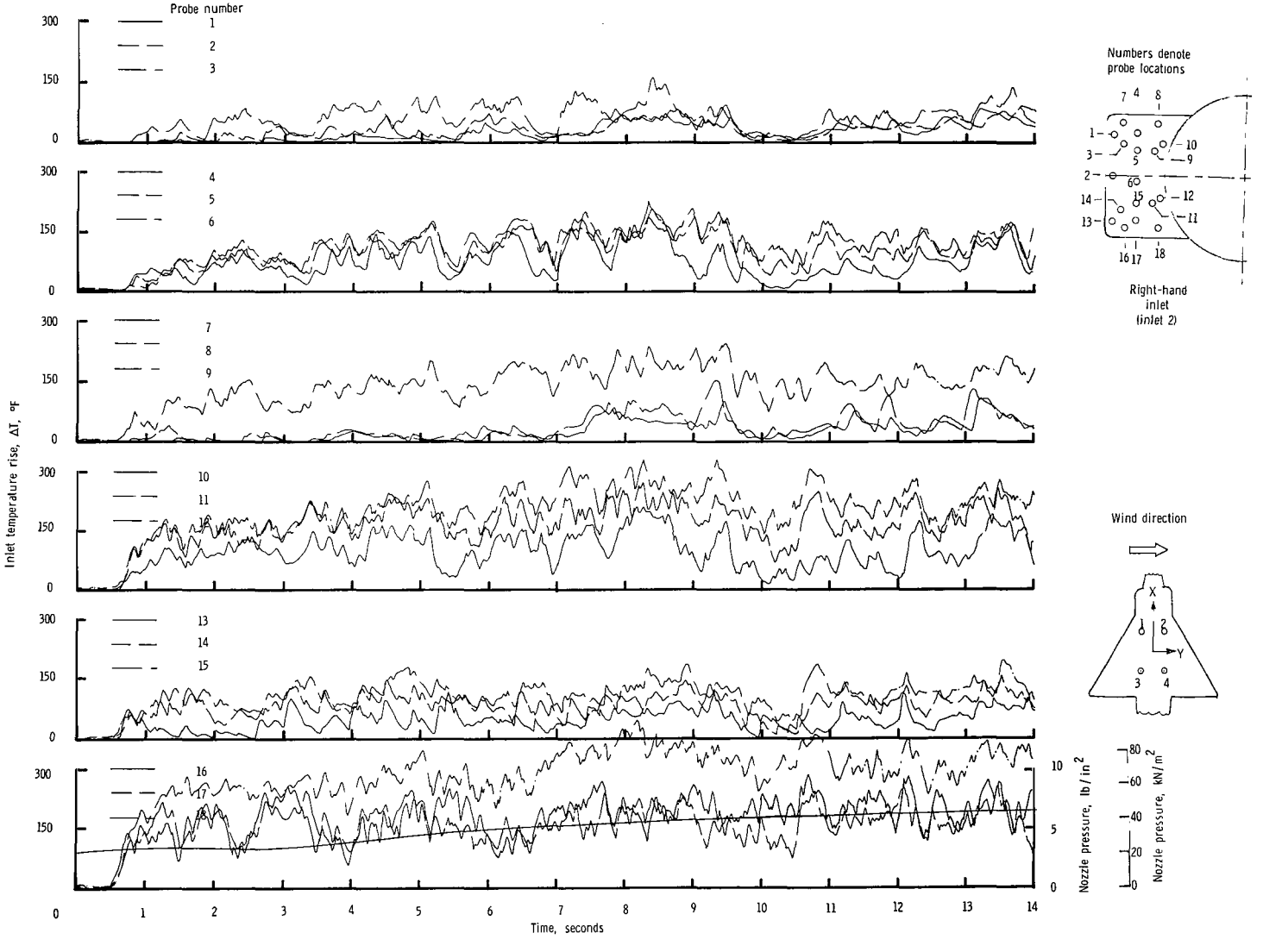

(j) $\psi = 90^0$; V = 5.92 knots.

Figure 13.- Continued.

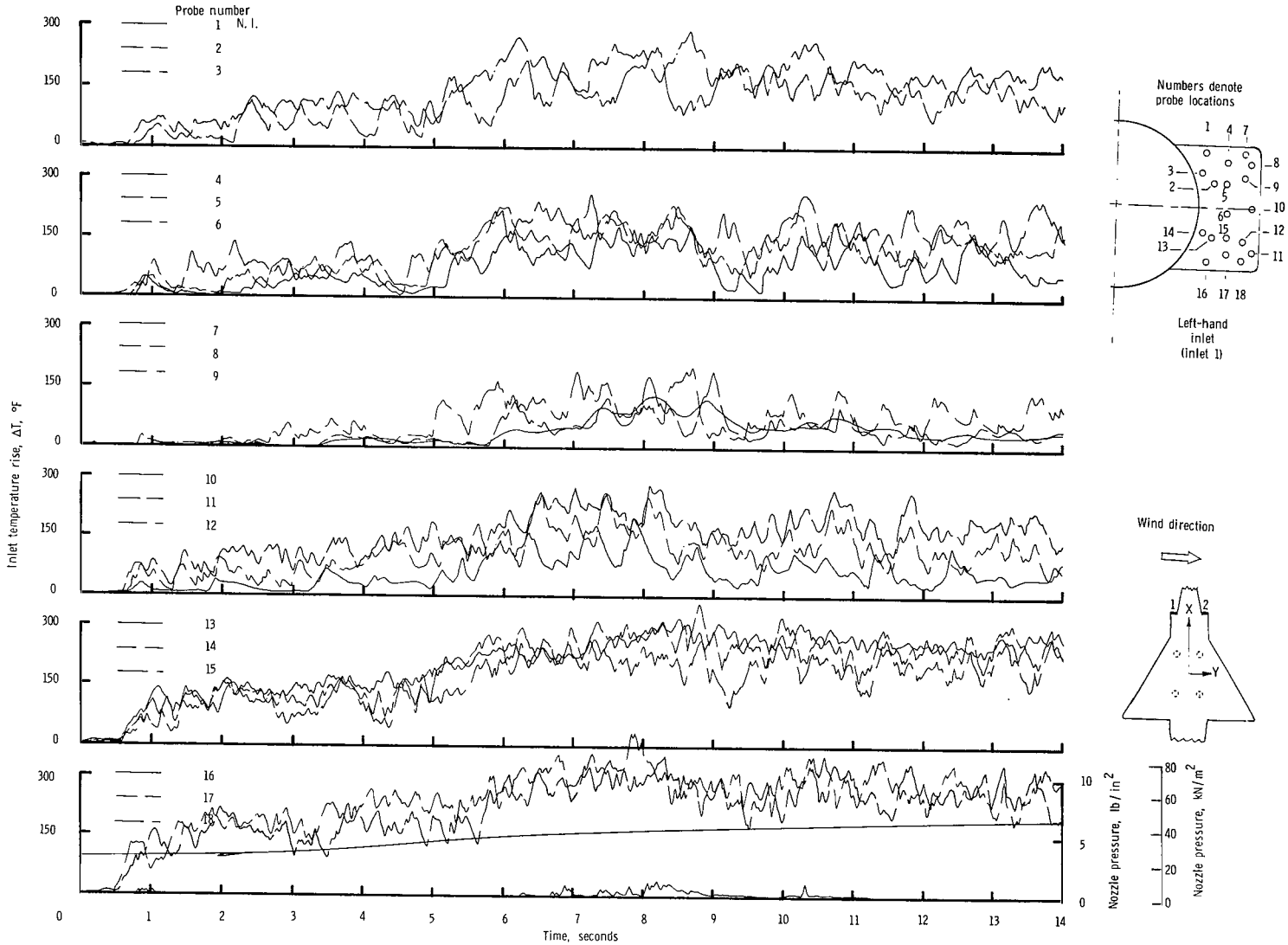

(j) Concluded.

Figure 13.- Continued.

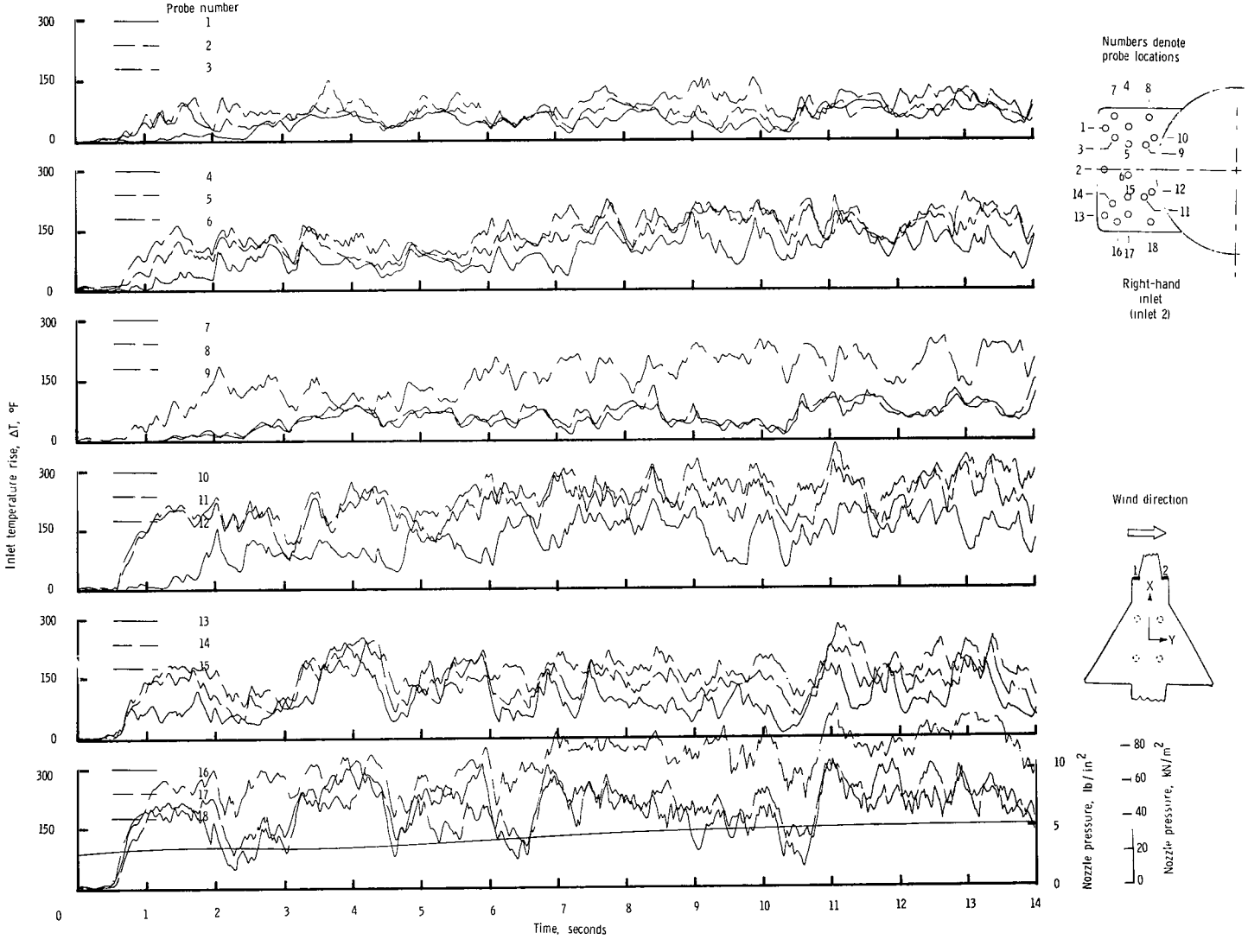

(k) $\psi = 90^{0}$; V = 11.85 knots.

Figure 13.- Continued.

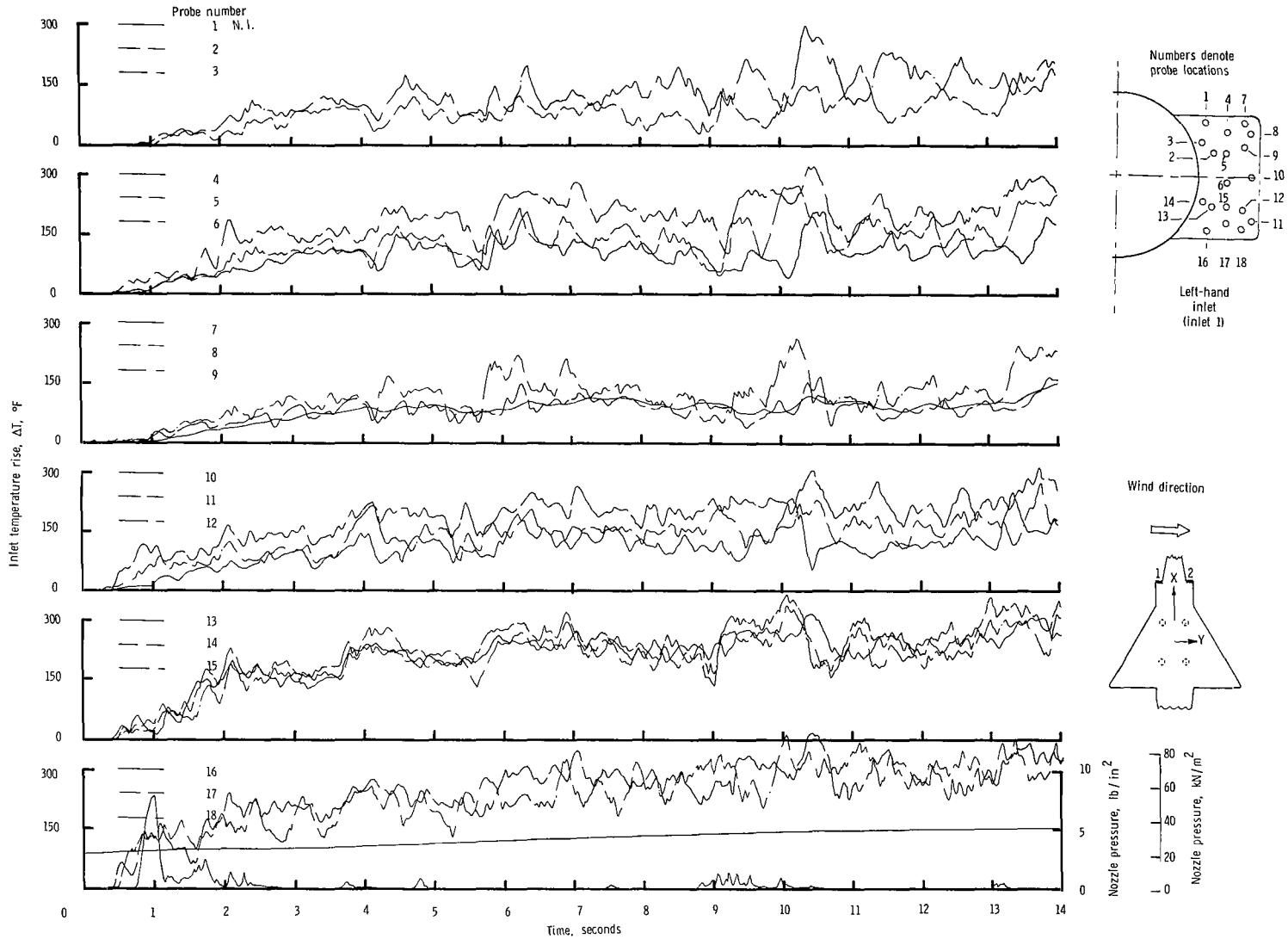

(k) Concluded.

Figure 13.- Concluded.

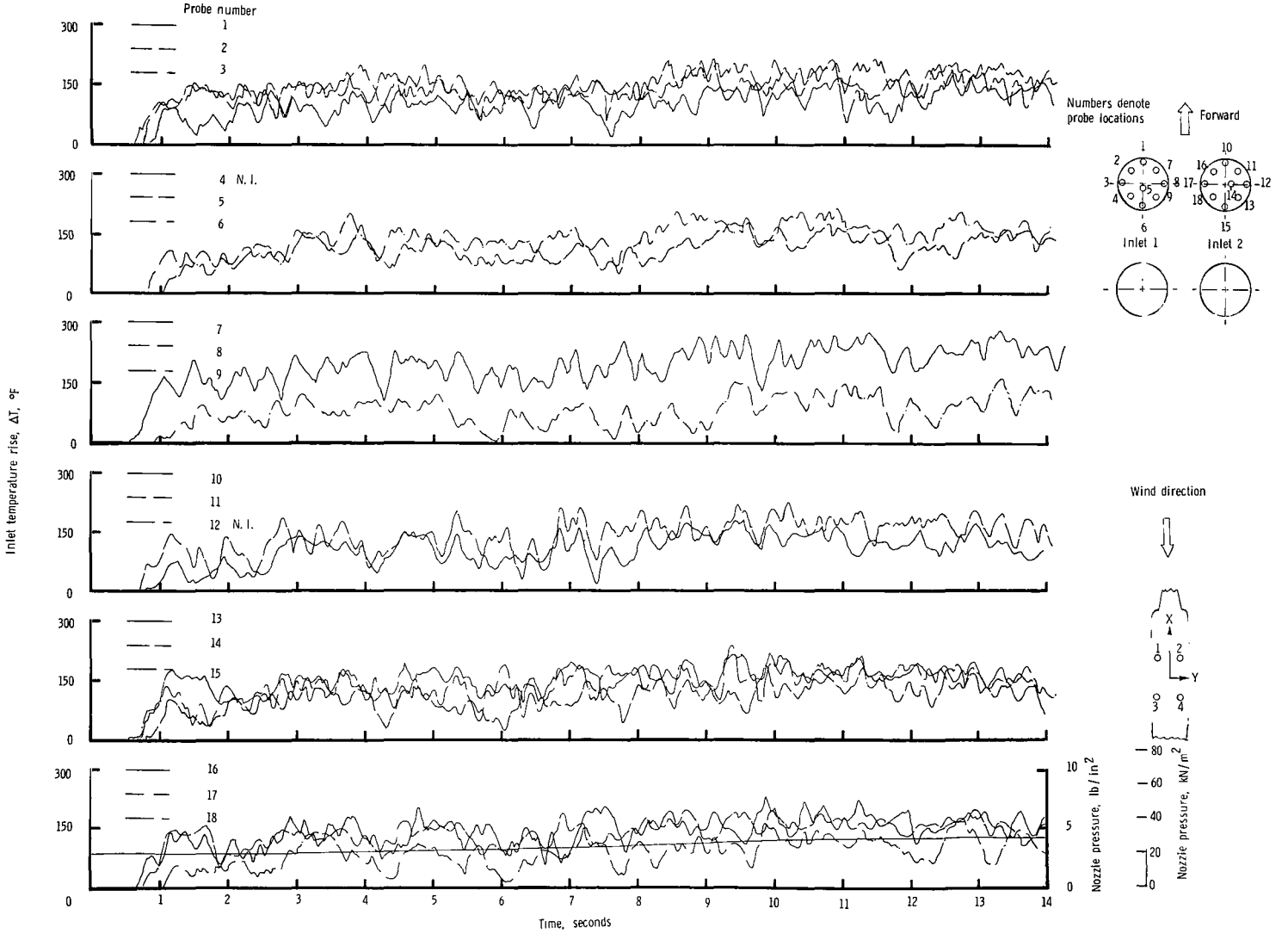

(a) $\psi = 0^0$; V = 0 knots.

Figure 14.- Variation of inlet-air temperature rise with time for the rectangular nozzle arrangement with top inlets and with wing removed. $h/D_e = 3.00$. (Values of ΔT in ^0C can be obtained by multiplying the ^0F values by 5/9.)

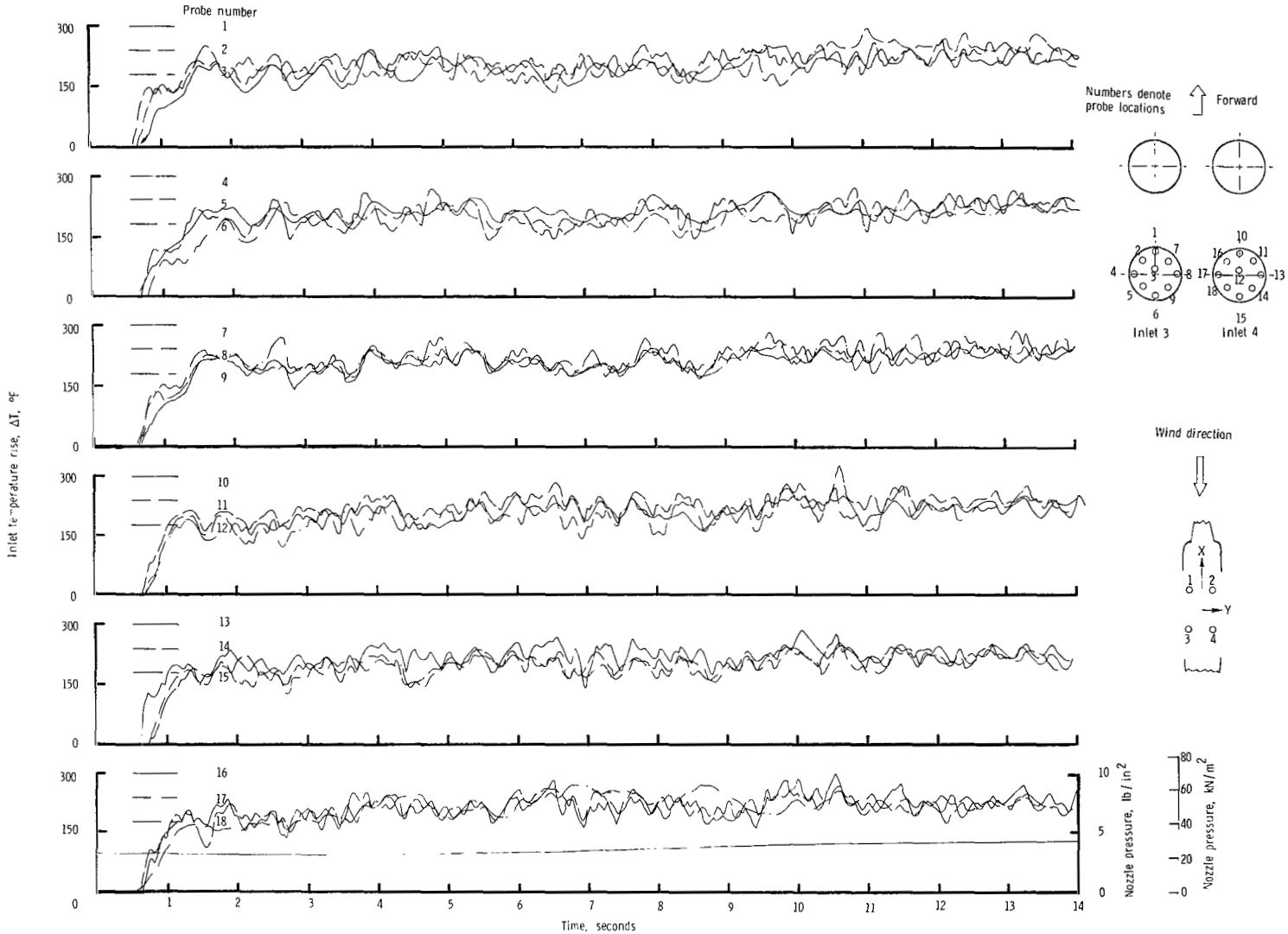

(a) Concluded.

Figure 14.- Continued.

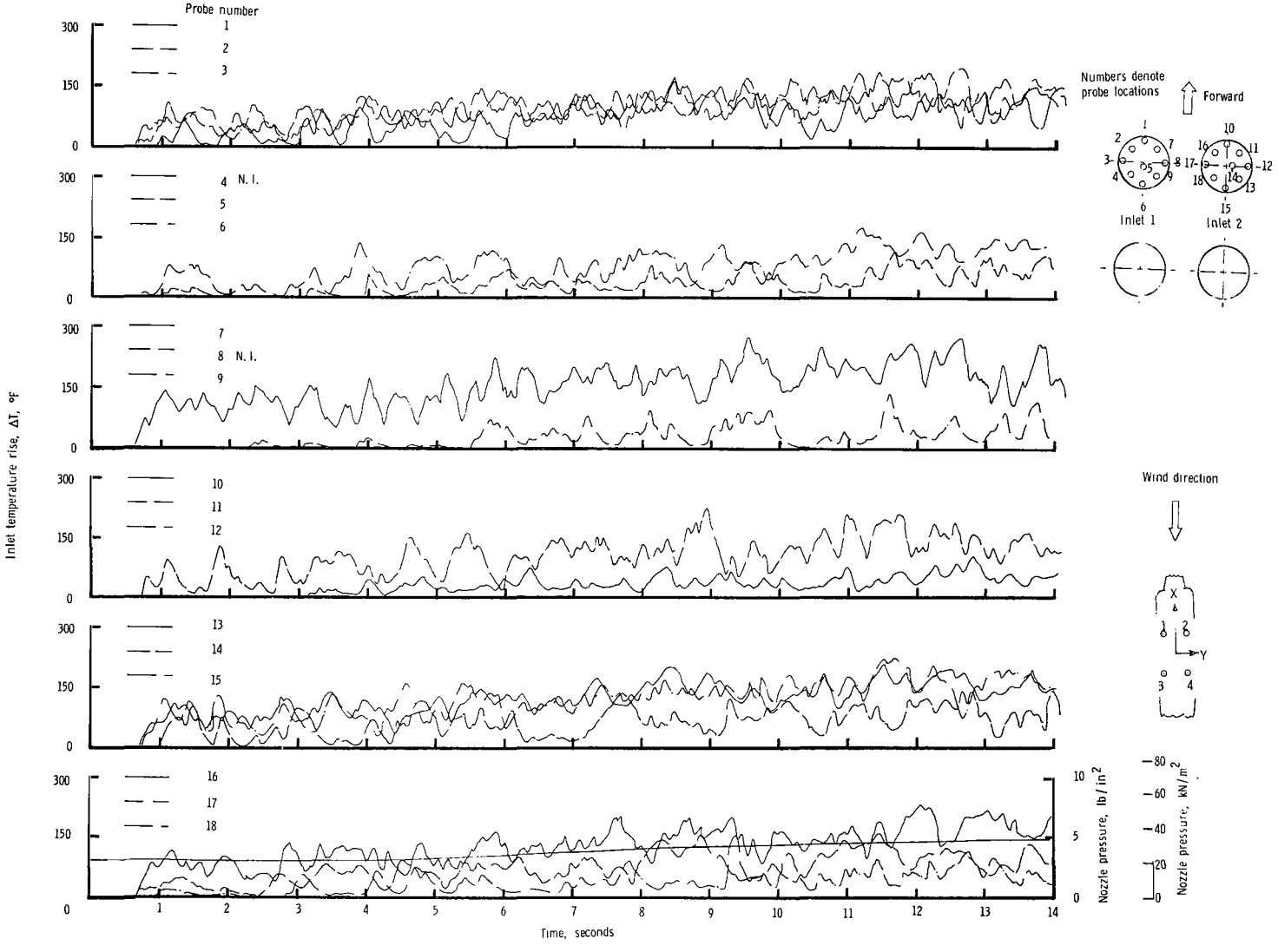

(b) $\psi = 0^0$; V = 5.92 knots.

Figure 14.- Continued.

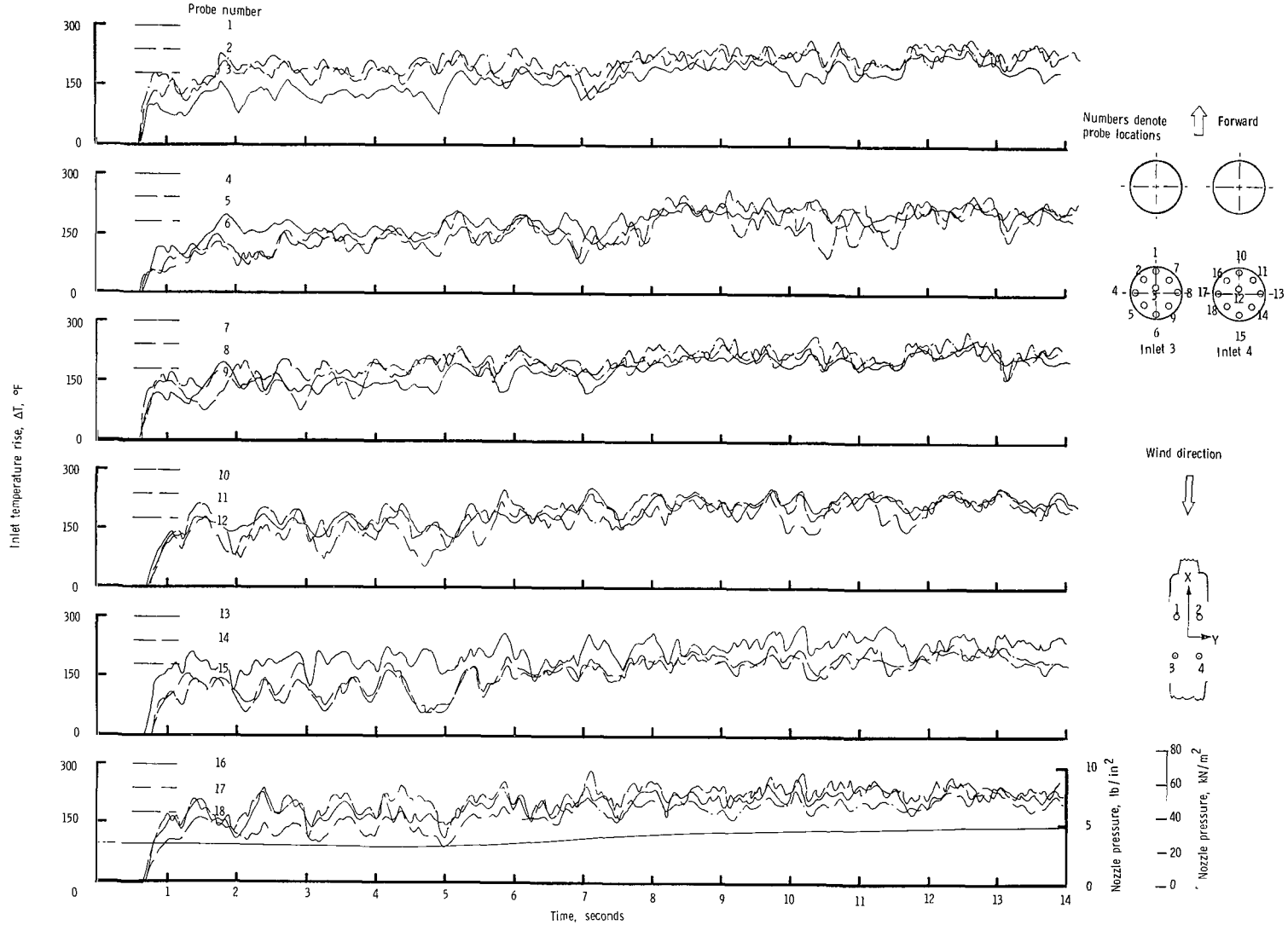

(b) Concluded.

Figure 14.- Continued.

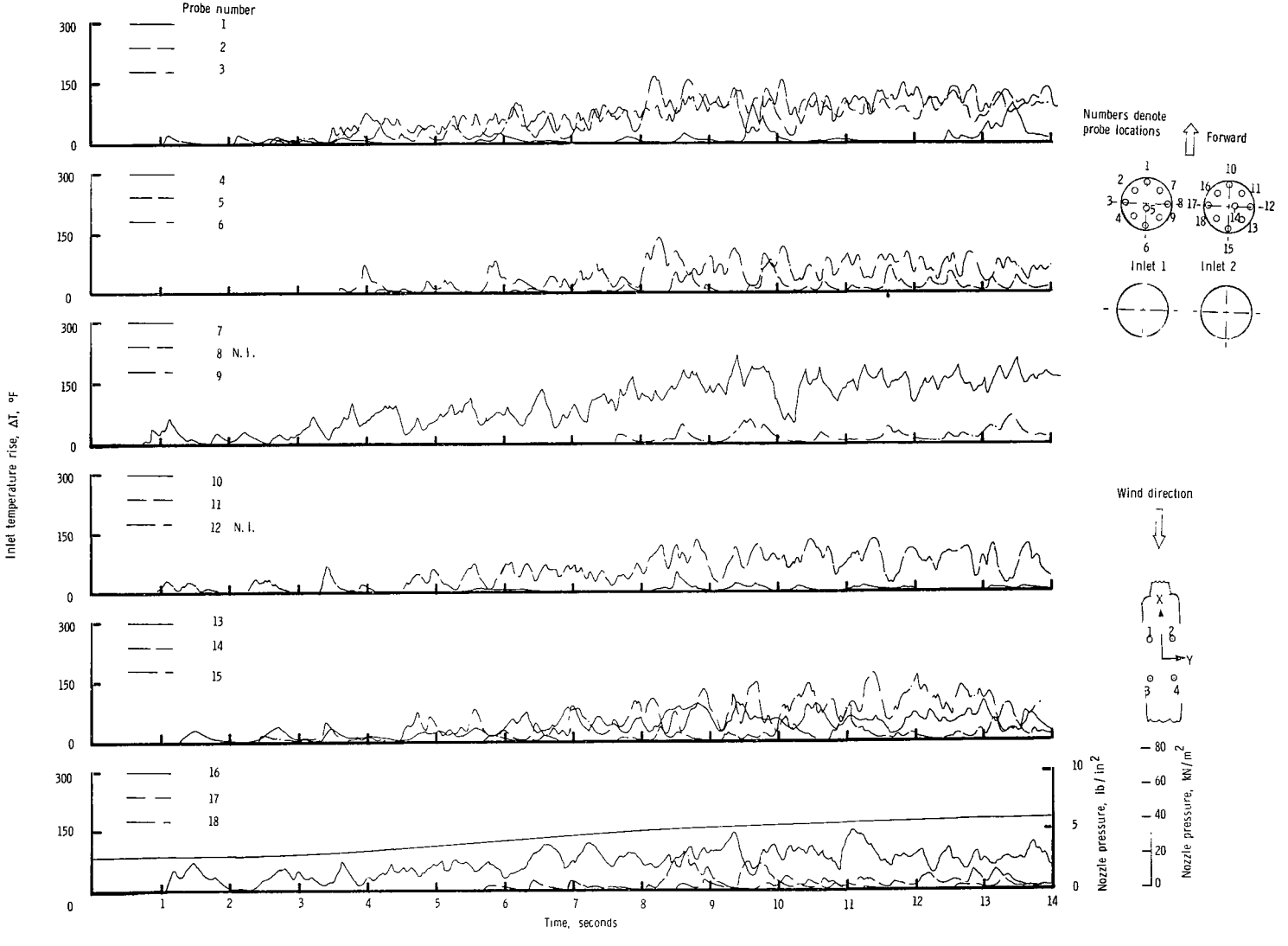

(c) $\psi = 0^0$; V = 11.85 knots.

Figure 14.- Continued.

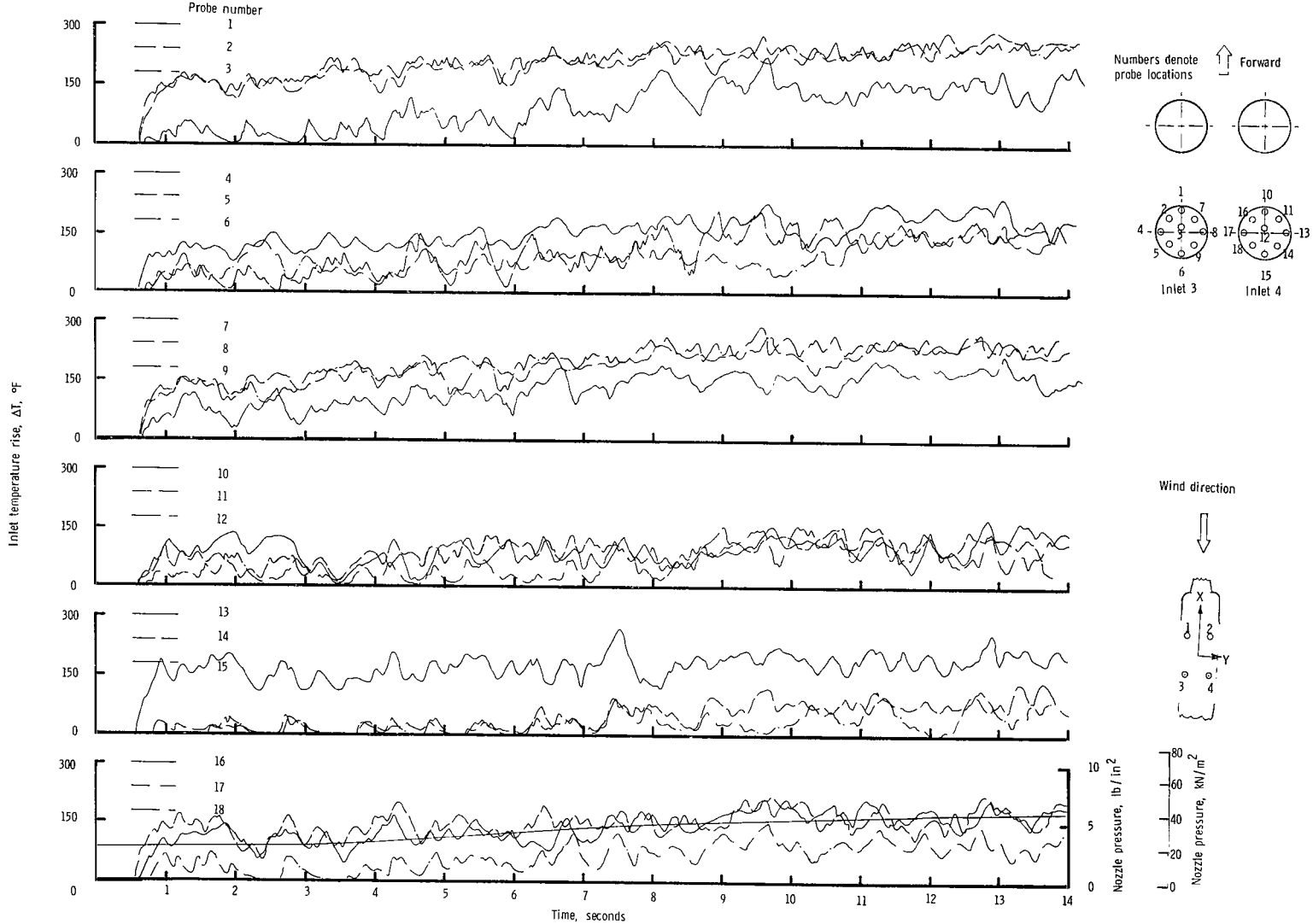

(c) Concluded.

Figure 14.- Continued.

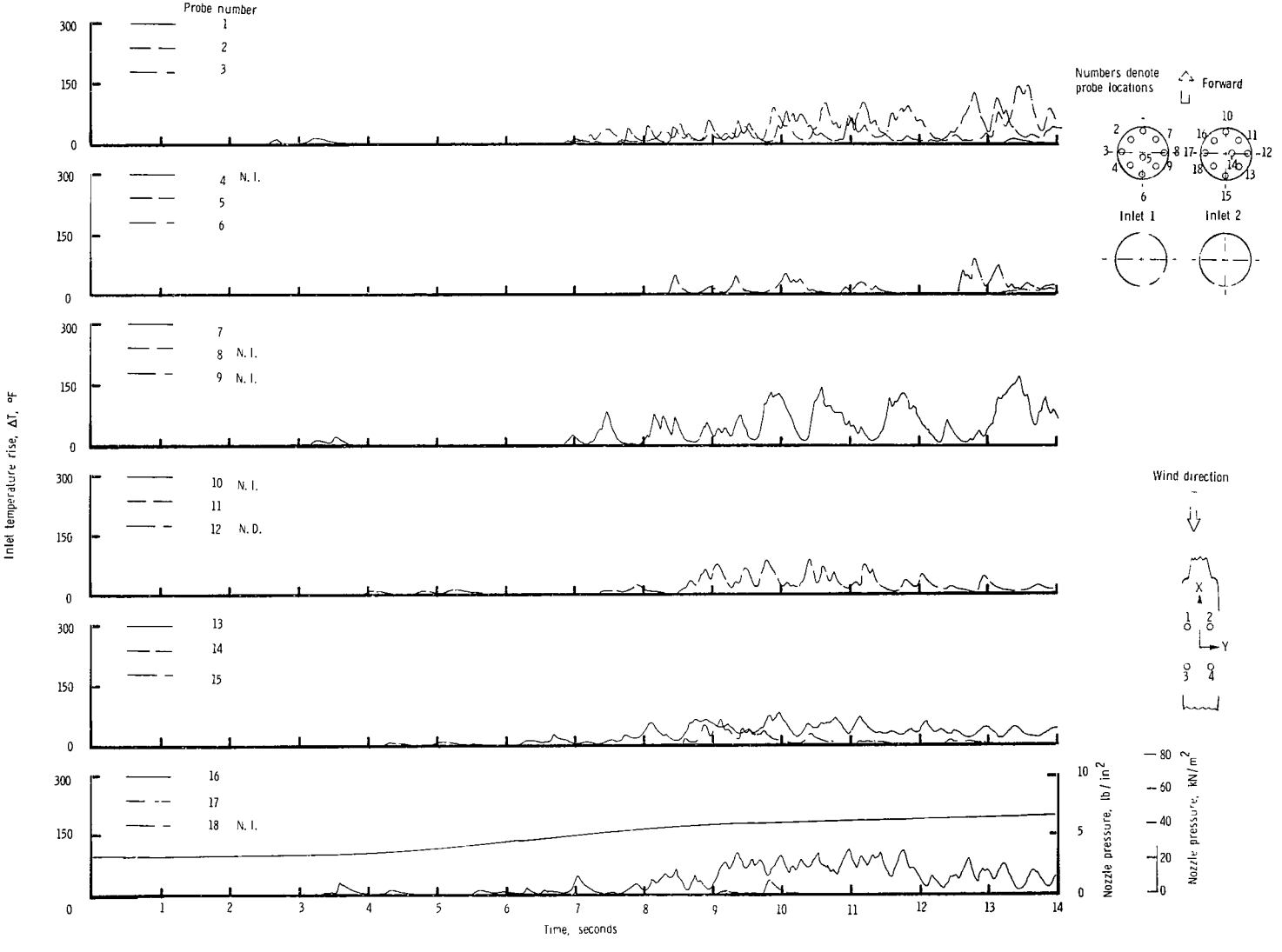

(d) $\psi = 0^0$; V = 17.78 knots.

Figure 14.- Continued.

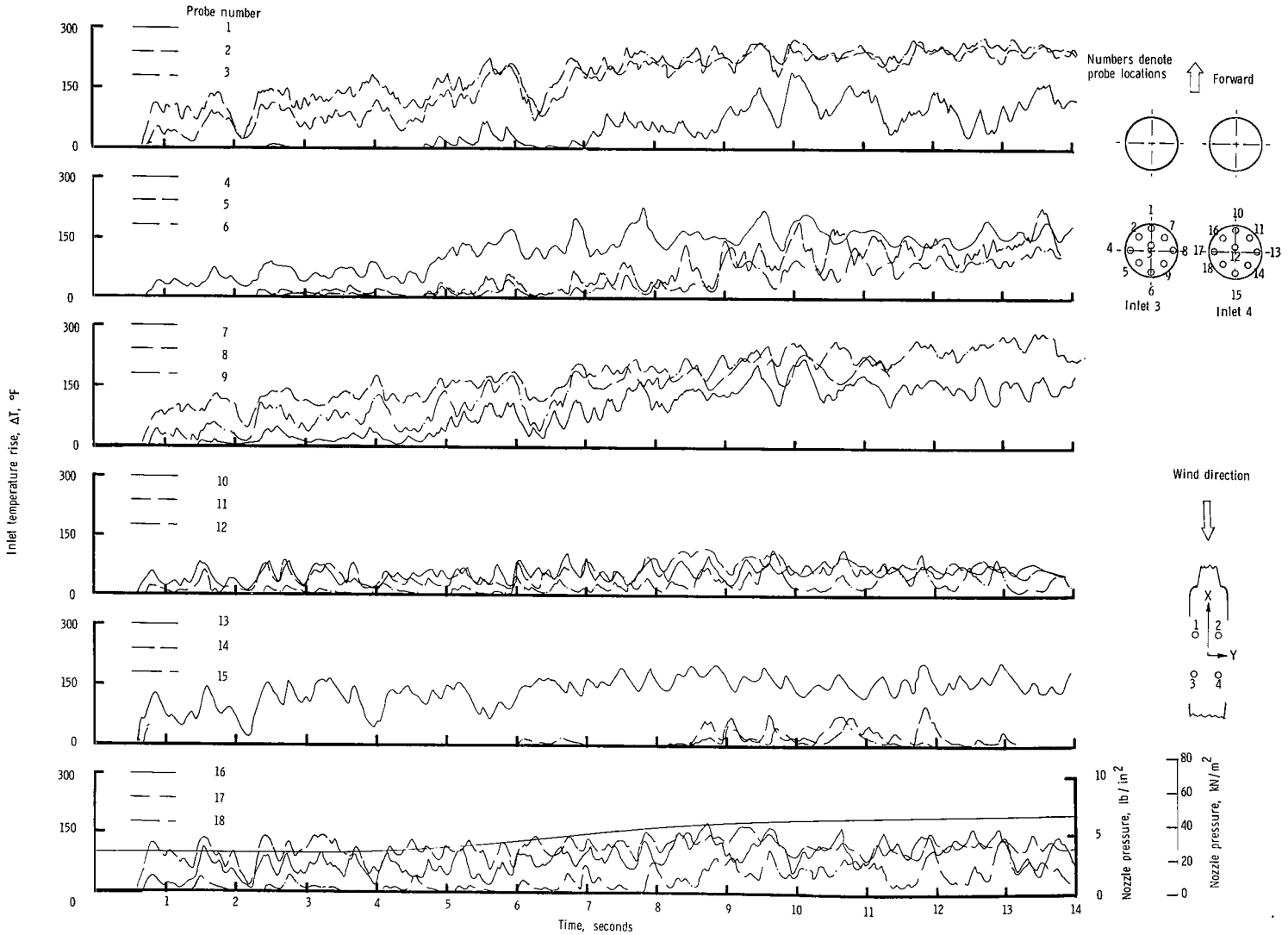

(d) Concluded.

Figure 14.- Continued.

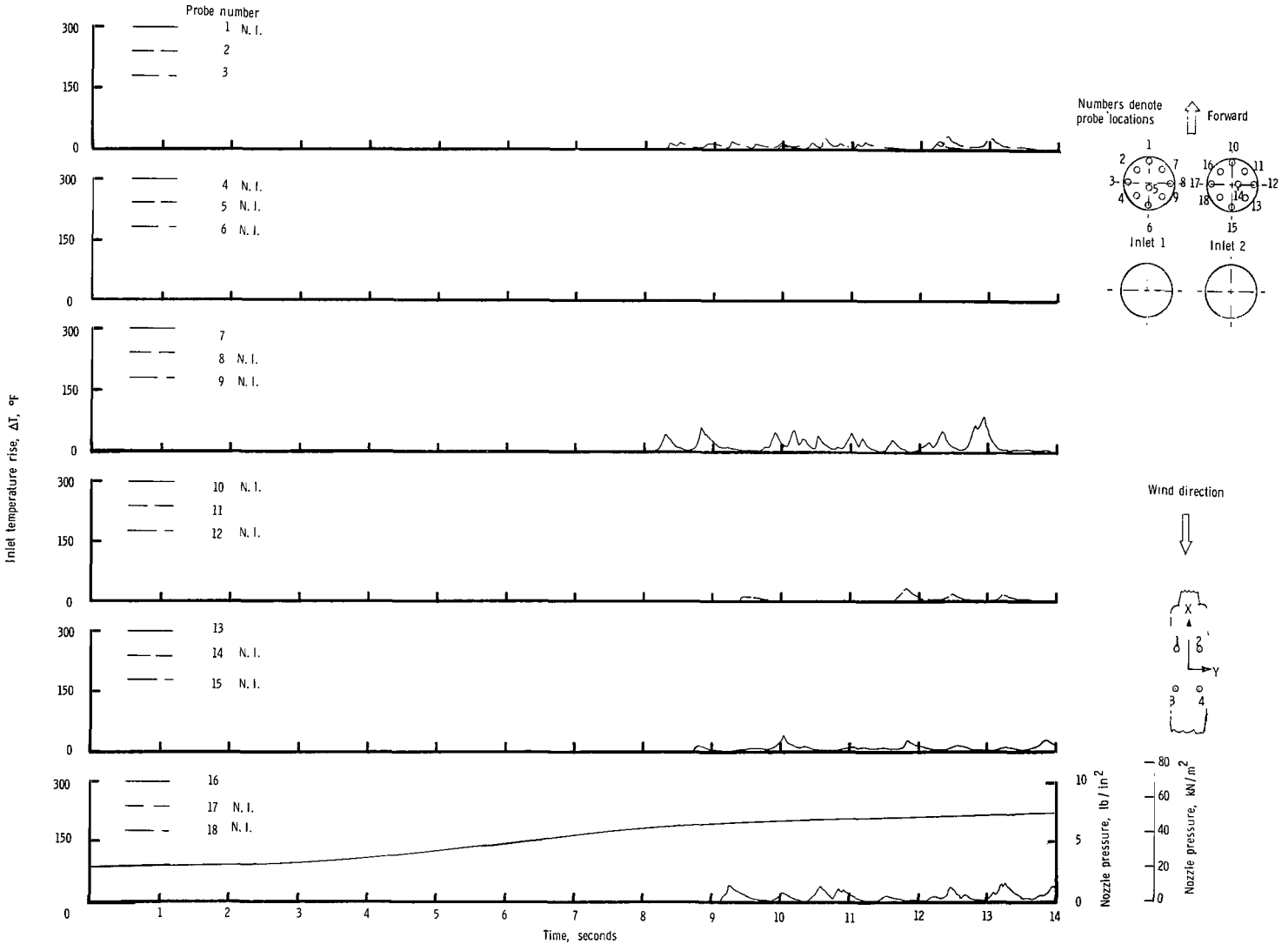

(e) $\psi = 0^0$; V = 23.70 knots.

Figure 14.- Continued.

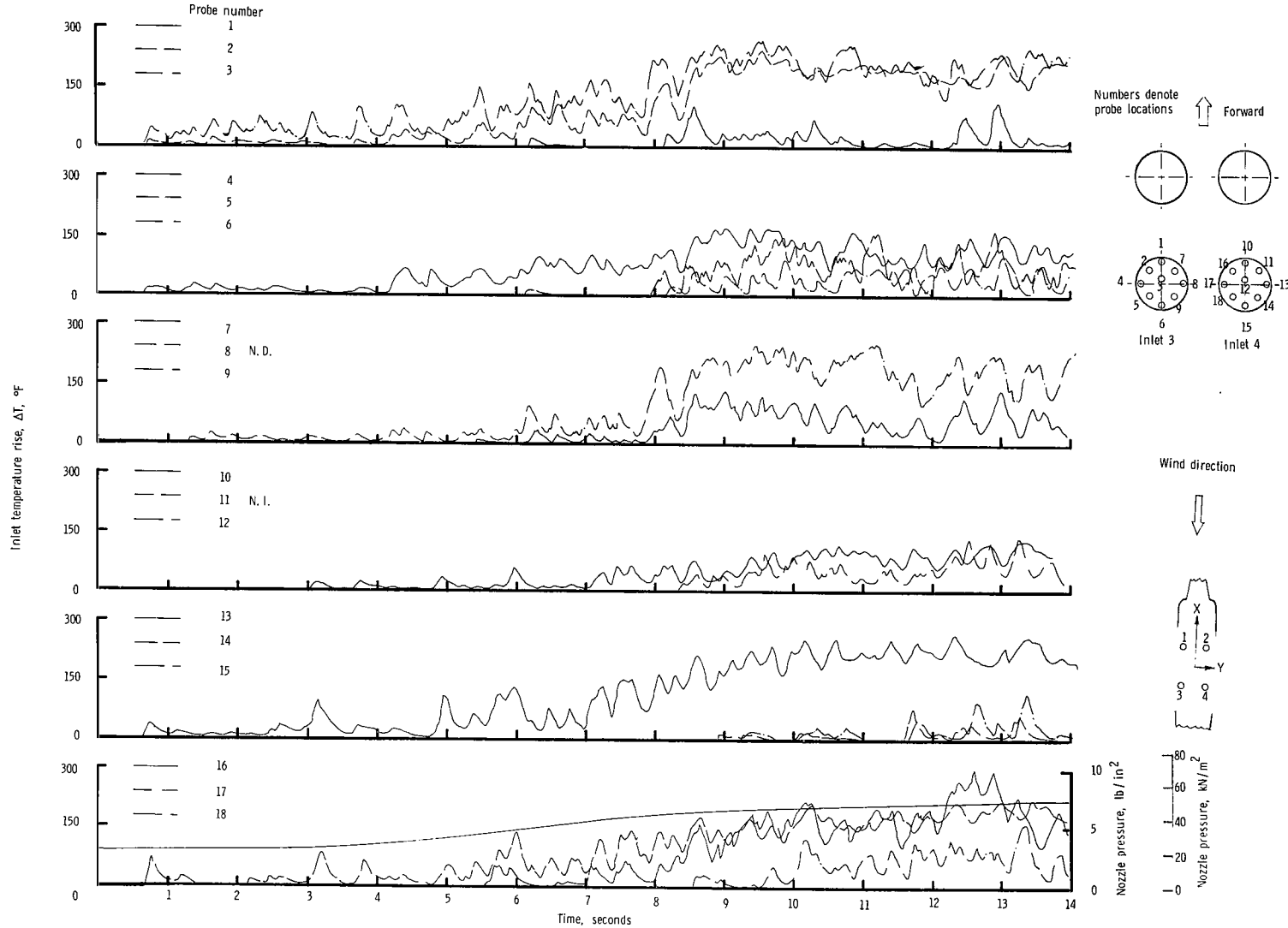

(e) Concluded.

Figure 14.- Continued.

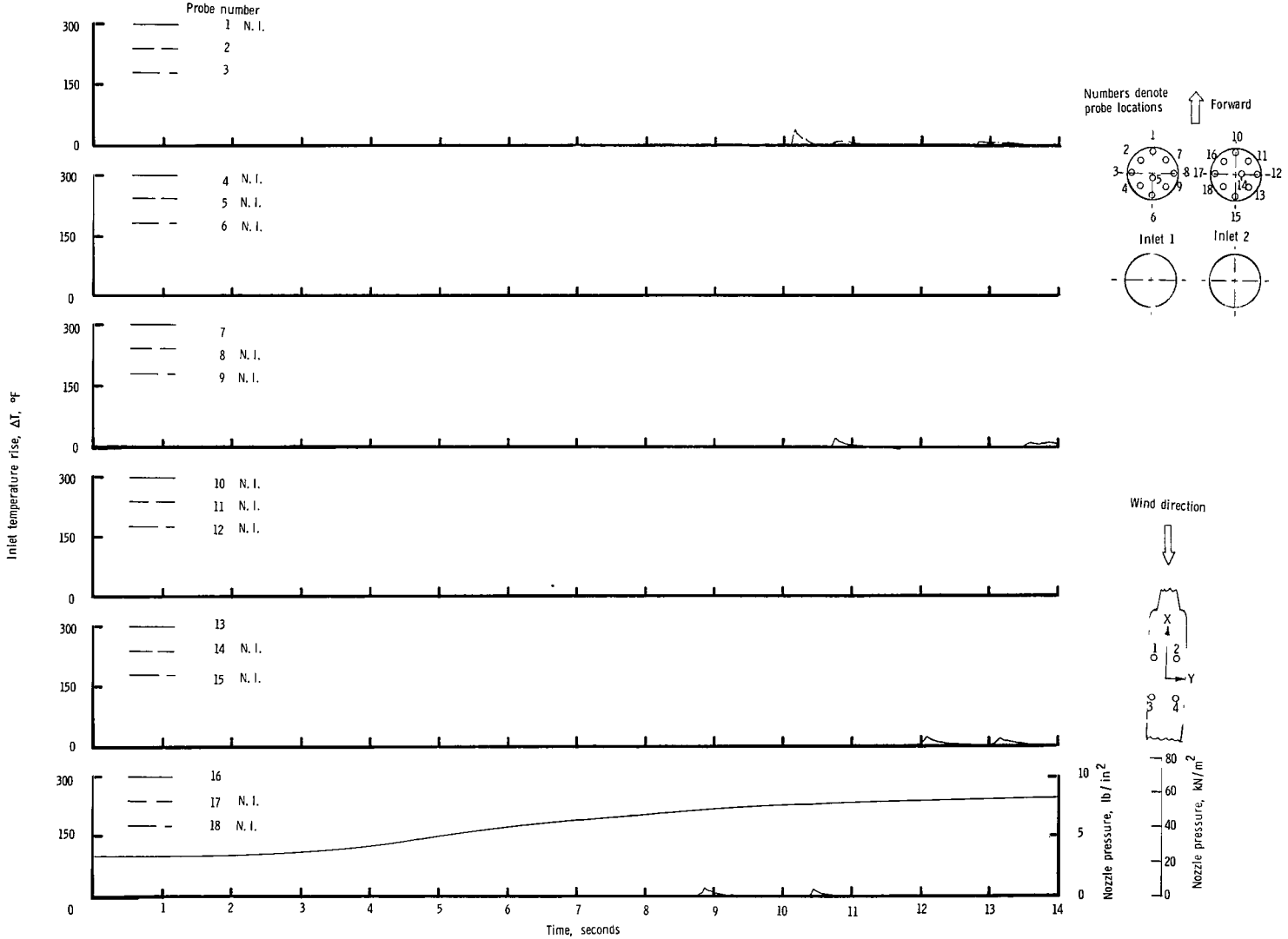

(f) $\psi = 0^0$; V = 26.93 knots.

Figure 14.- Continued.

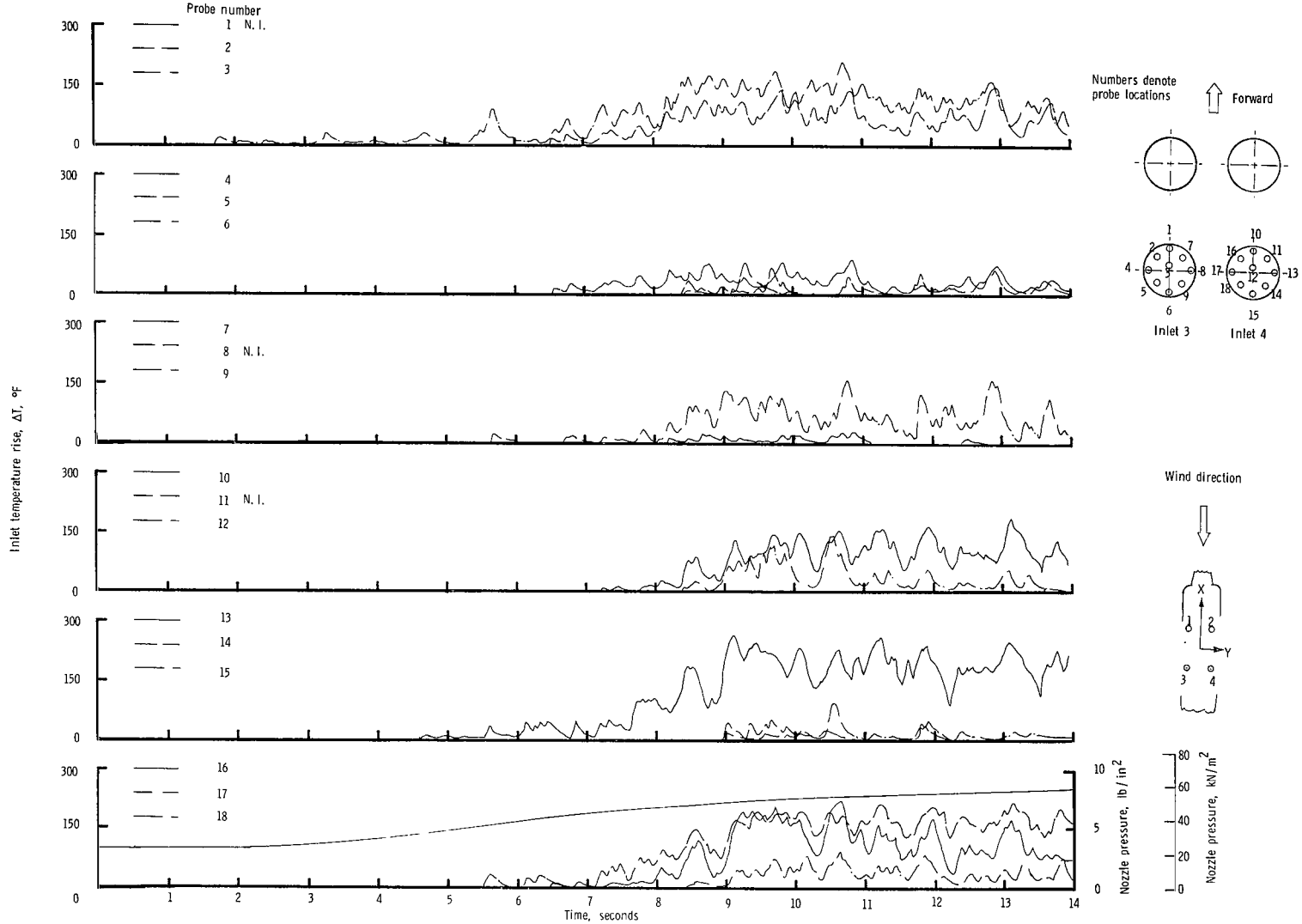

(f) Concluded.

Figure 14.- Continued.

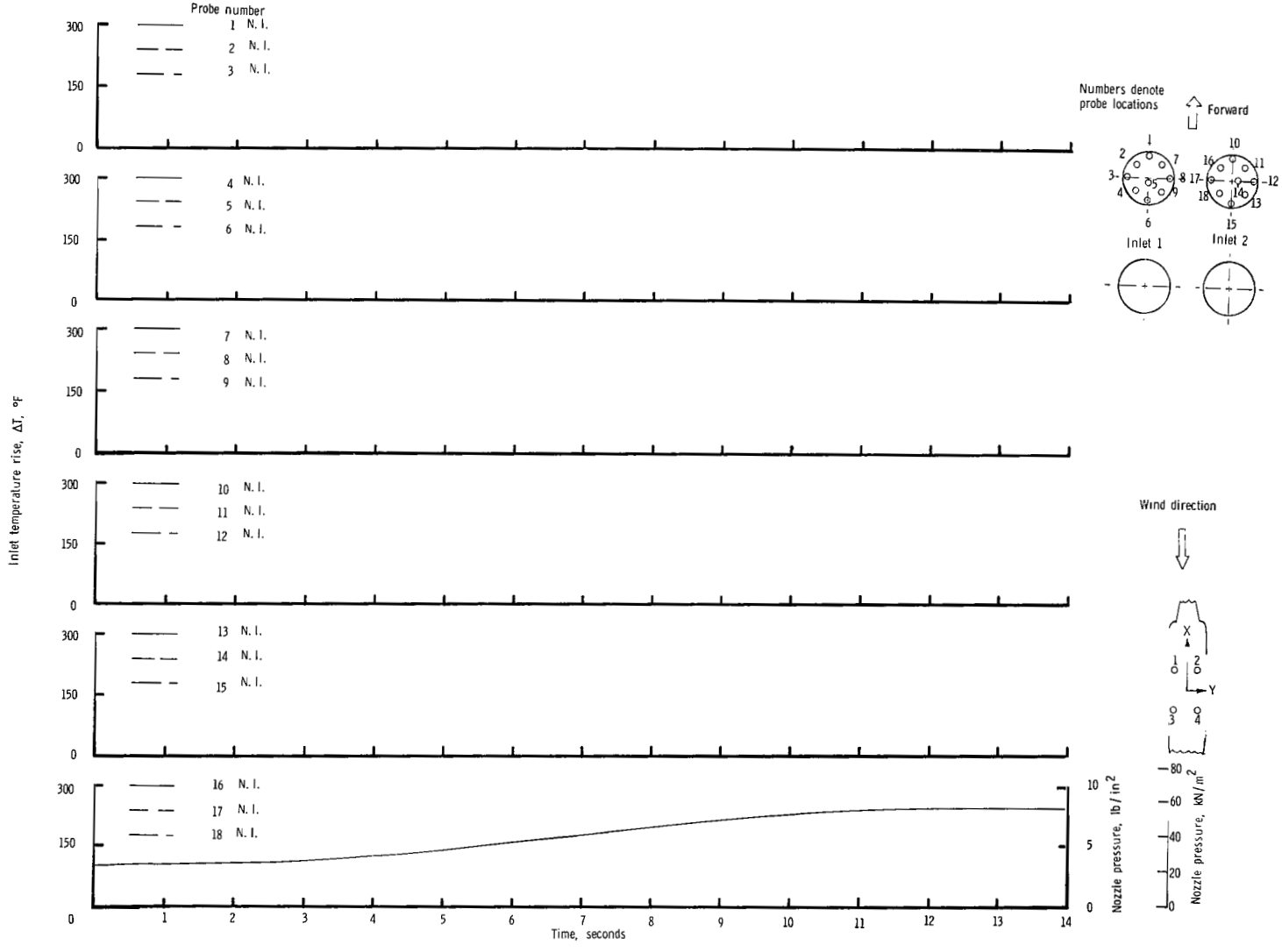

(g) $\psi = 0^0$; V = 35.55 knots.

Figure 14.- Continued.

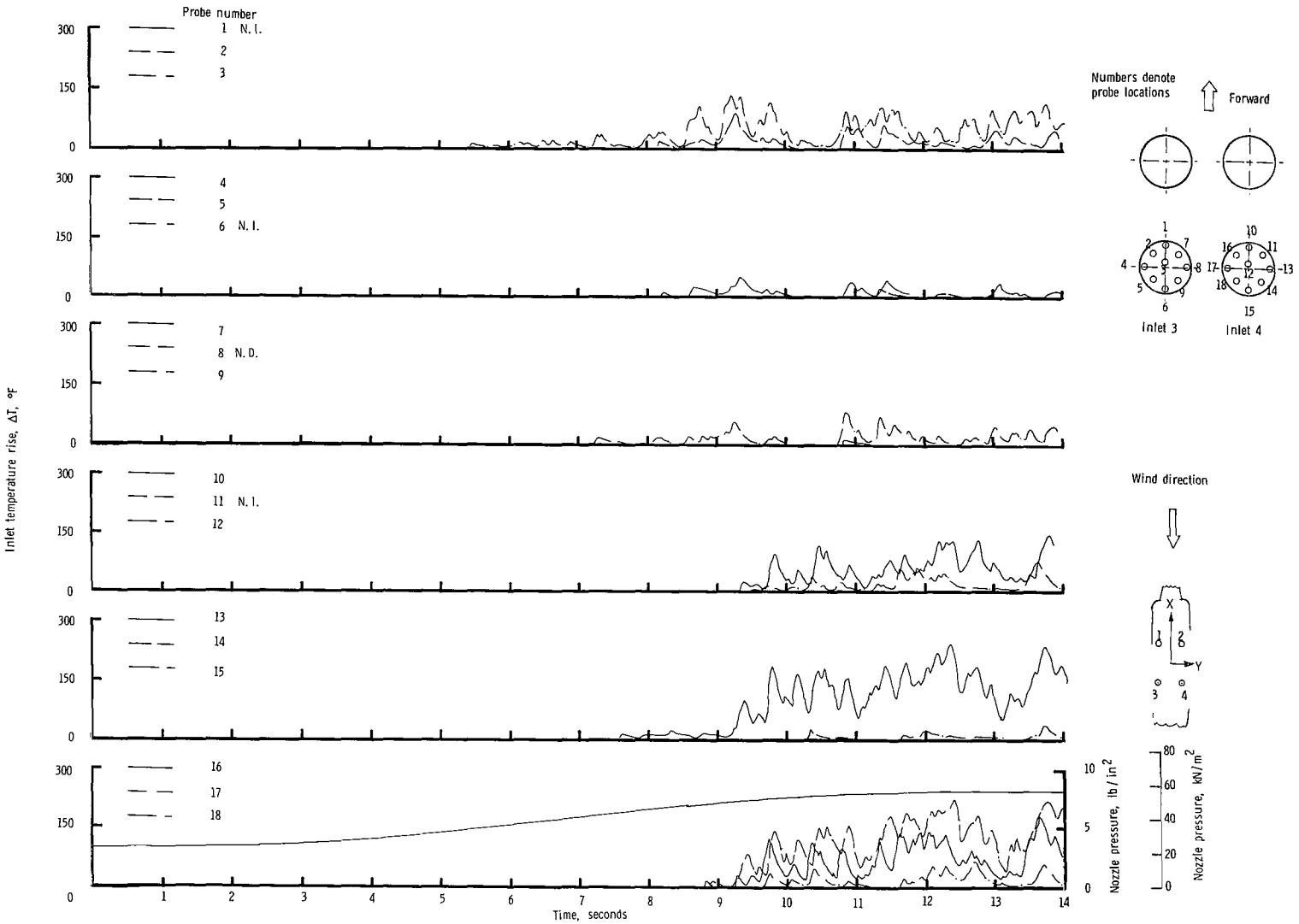

(g) Concluded.

Figure 14.- Continued.

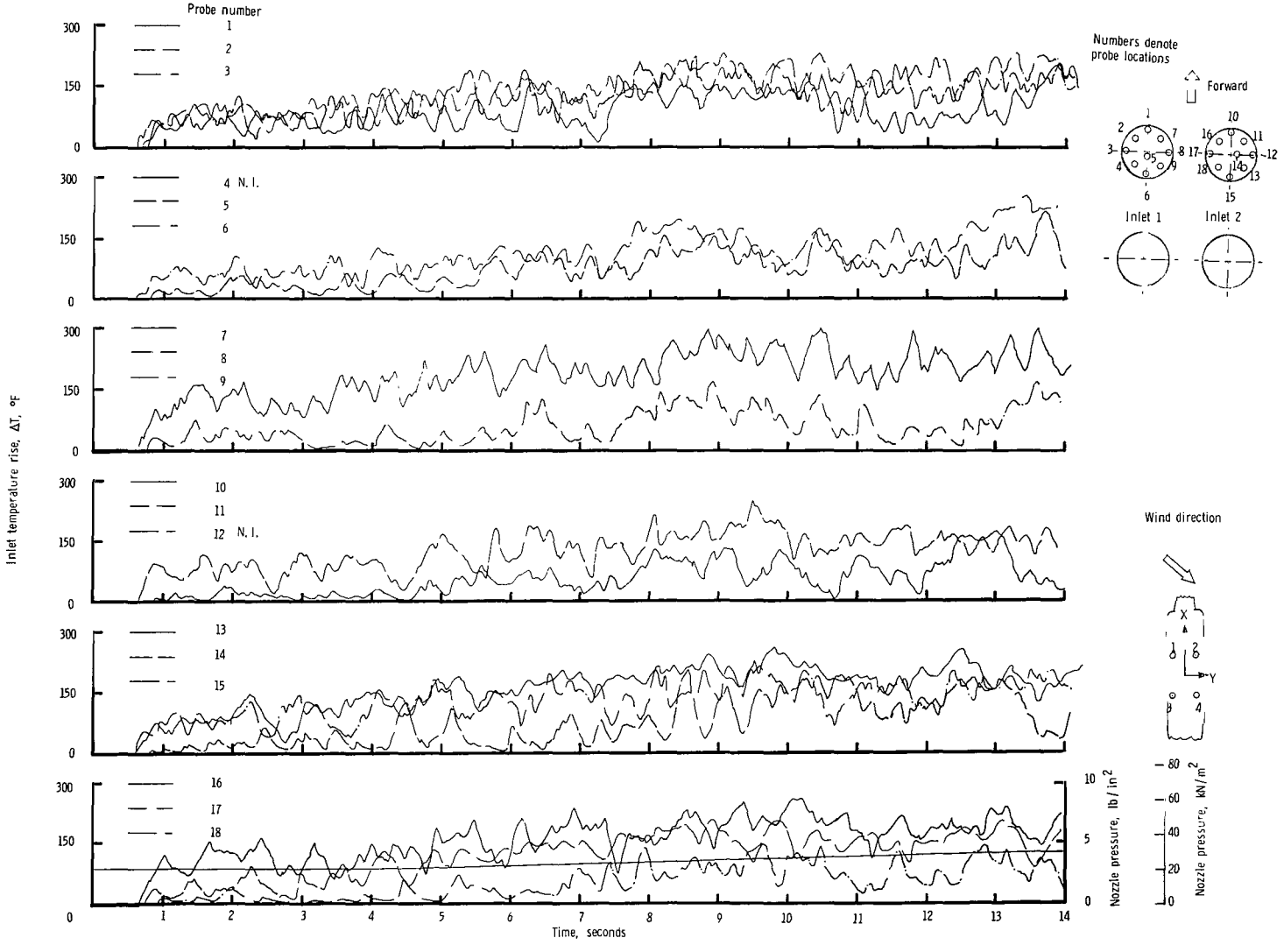

(h) $\psi = 45^{0}$; V = 5.92 knots.

Figure 14.- Continued.

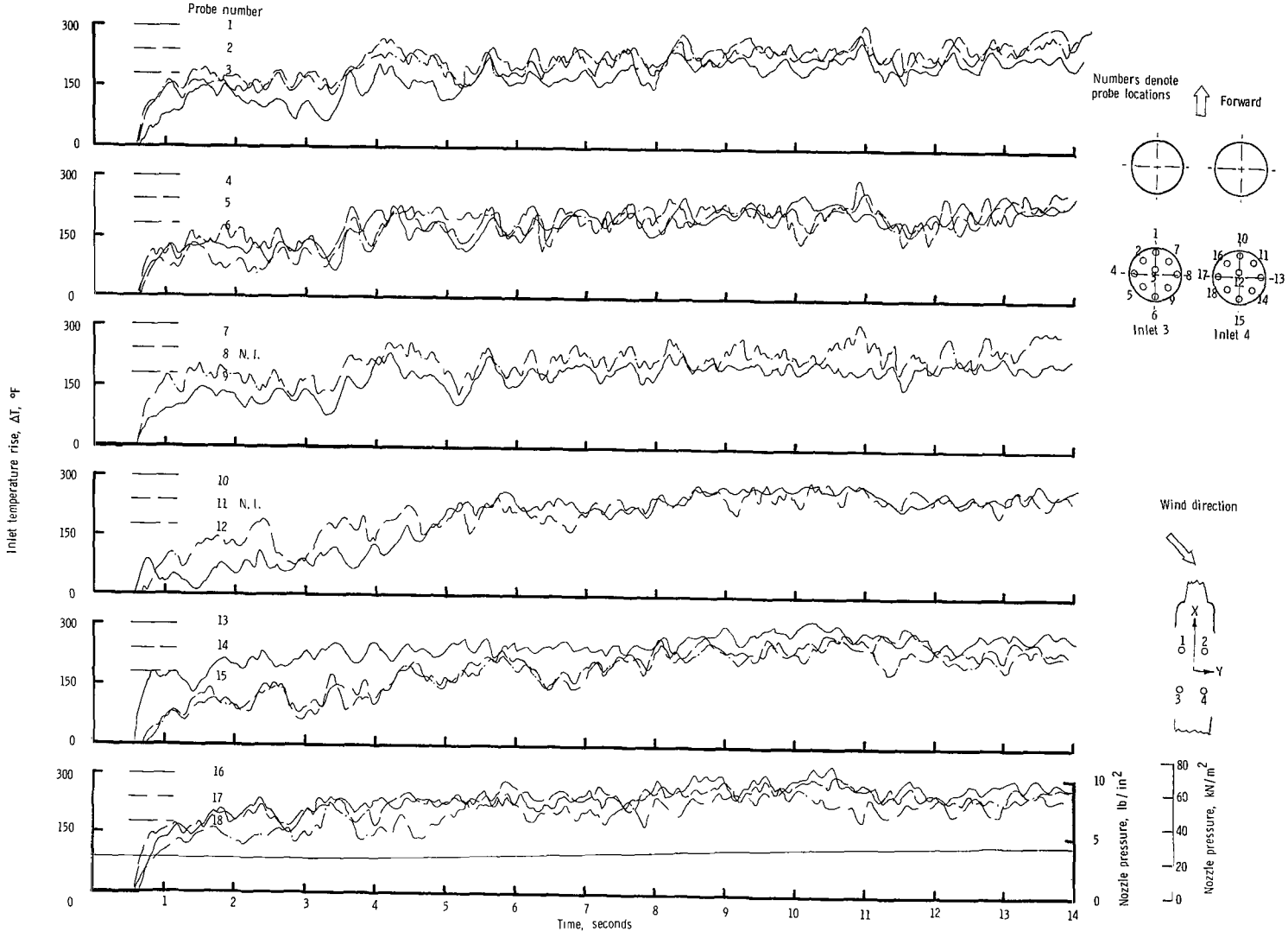

(h) Concluded.

Figure 14.- Continued.

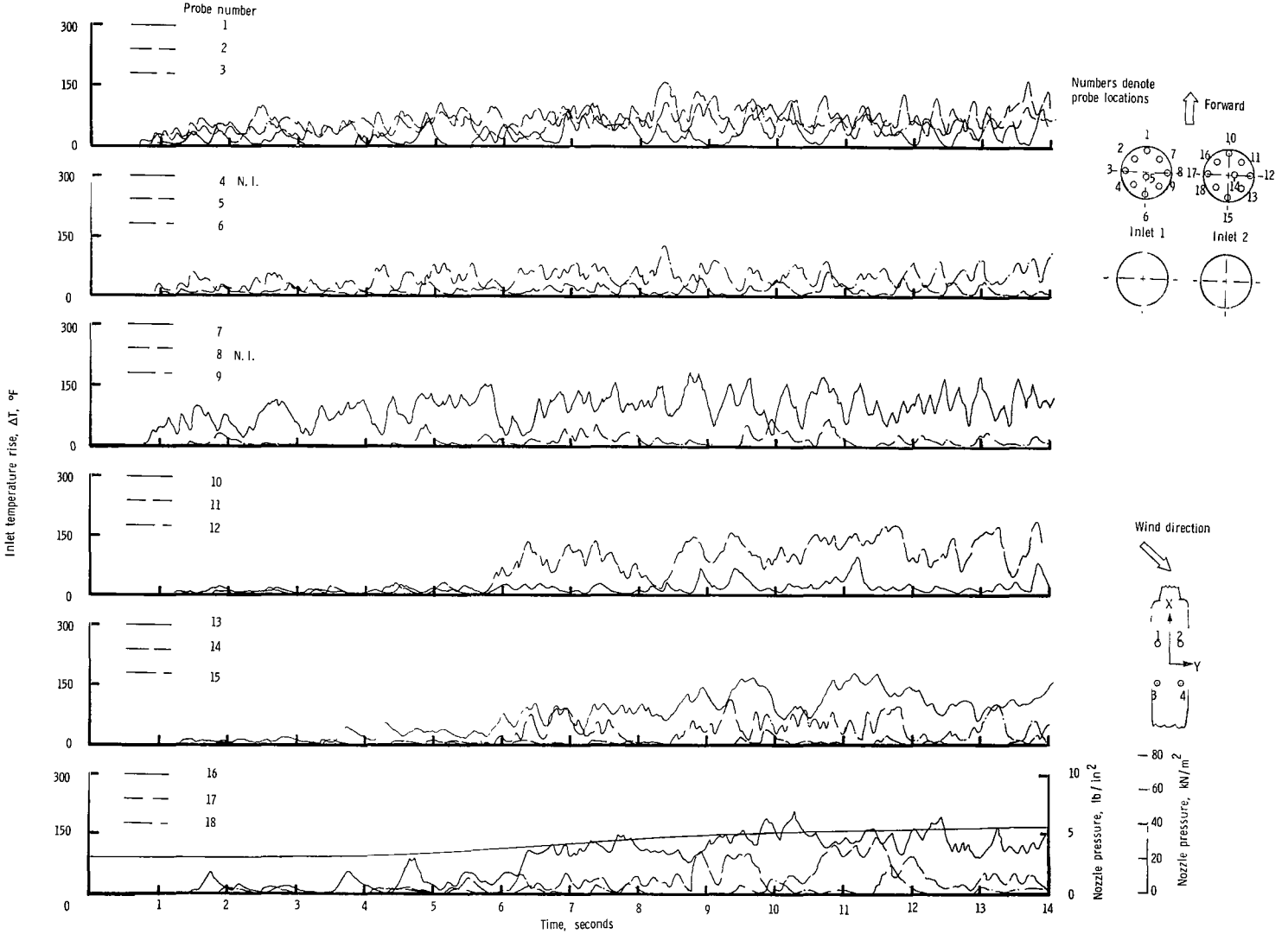

(i) $\psi = 45^{0}$; V = 11.85 knots.

Figure 14.- Continued.

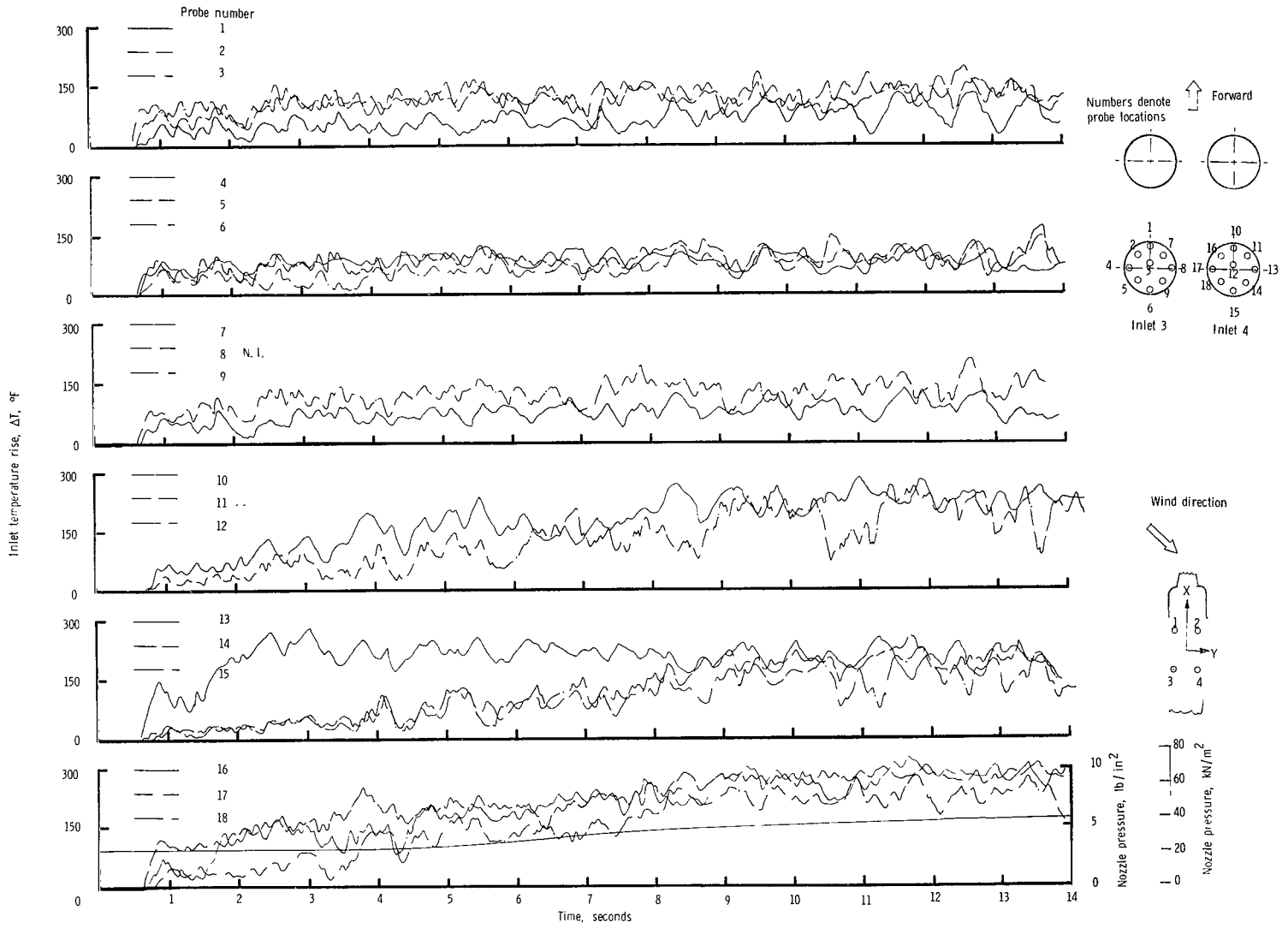

(i) Concluded.

Figure 14.- Continued.

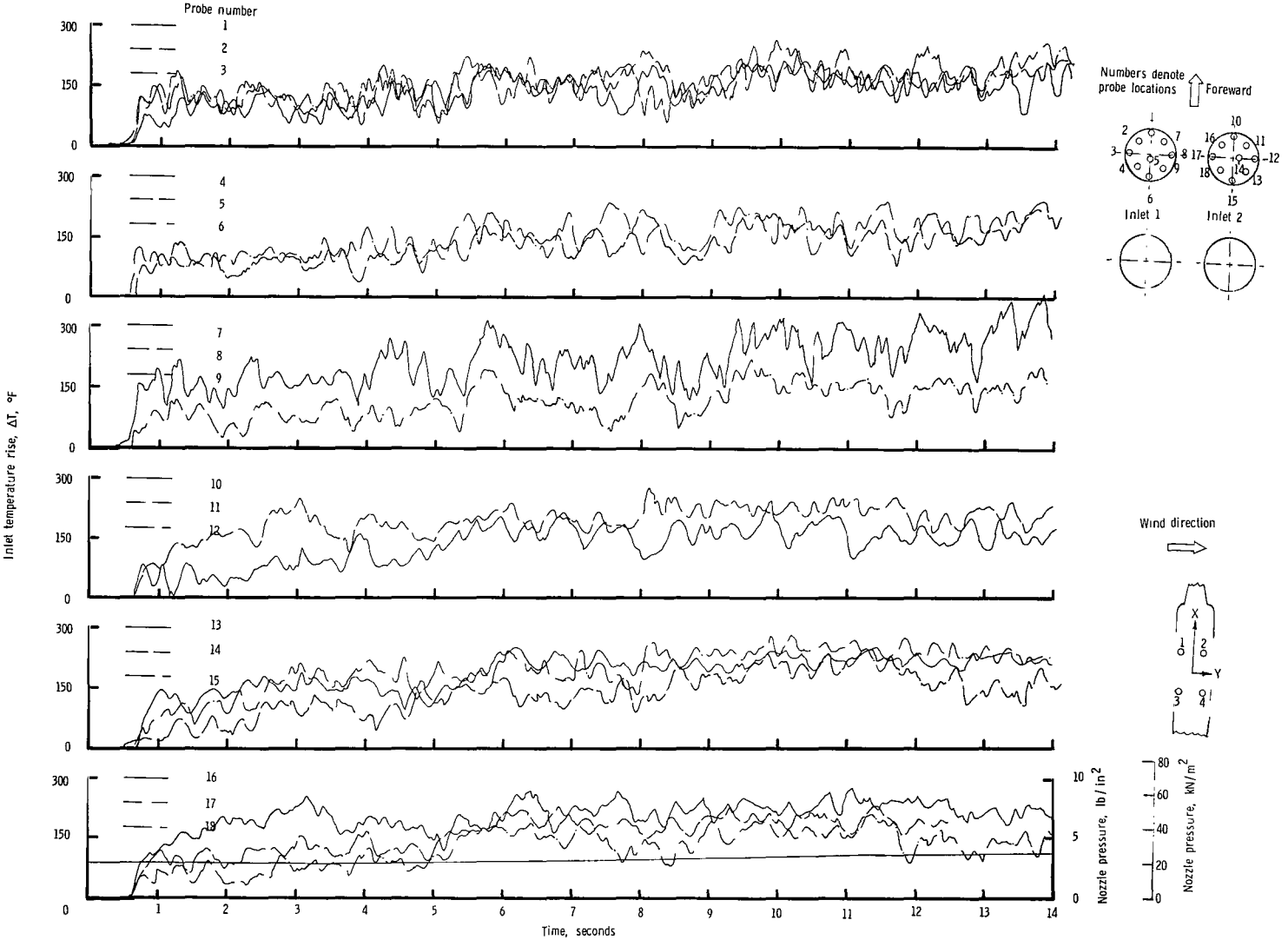

(j) $\psi = 90^0$; V = 5.92 knots.

Figure 14.- Continued.

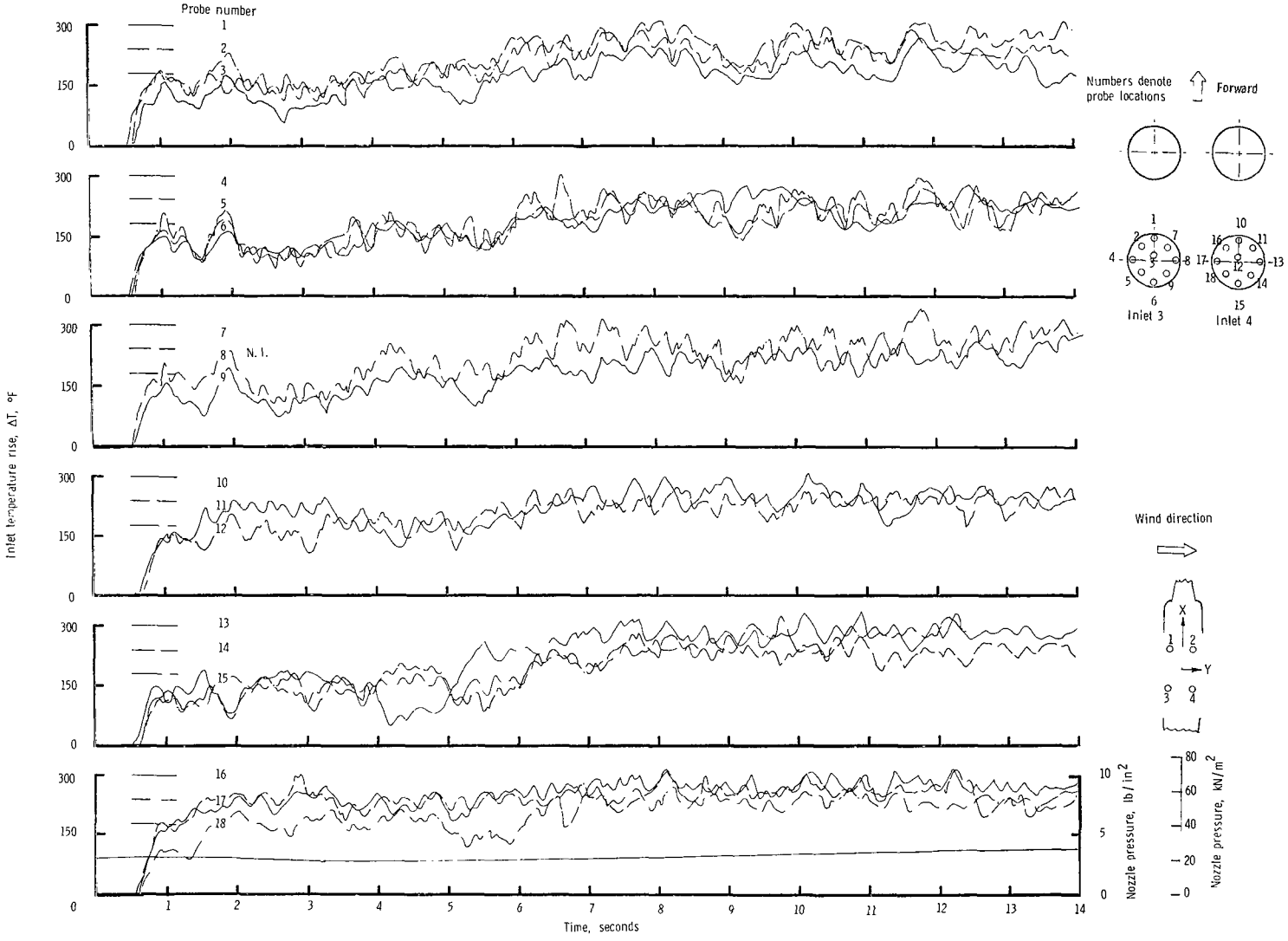

(j) Concluded.

Figure 14.- Continued.

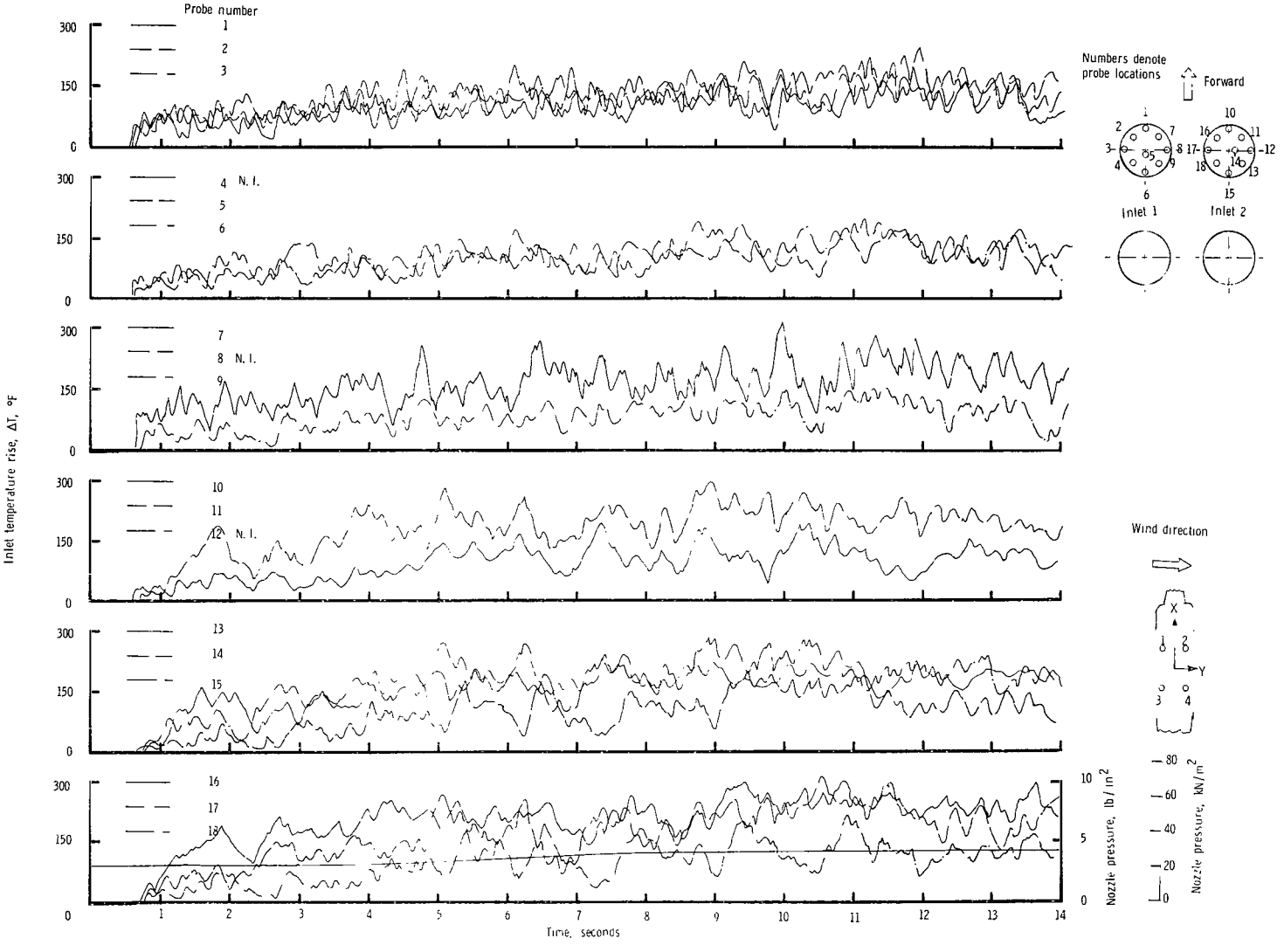

(k) $\psi = 90^{0}$; V = 11.85 knots.

Figure 14.- Continued.

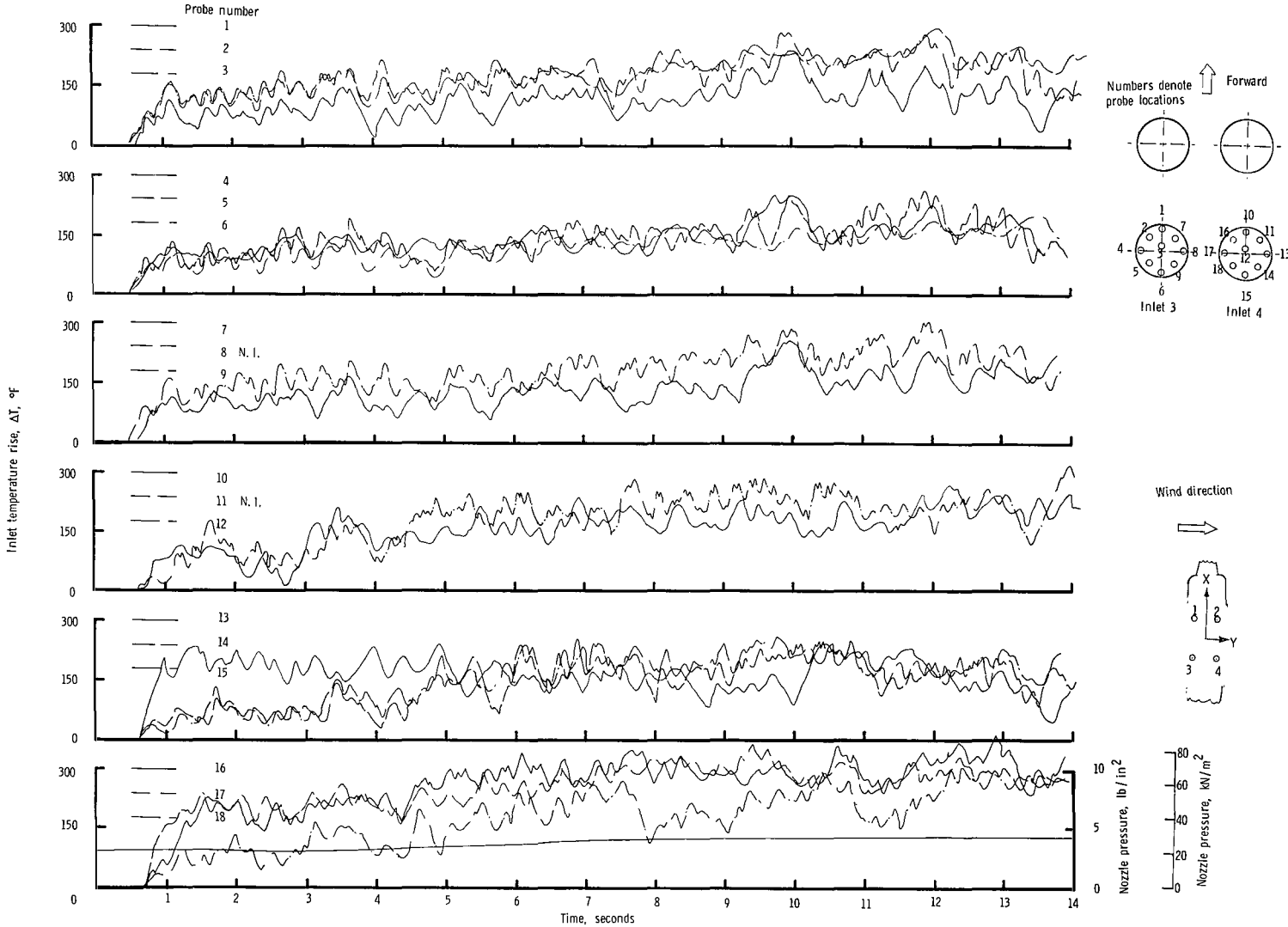

(k) Concluded.

Figure 14.- Concluded.

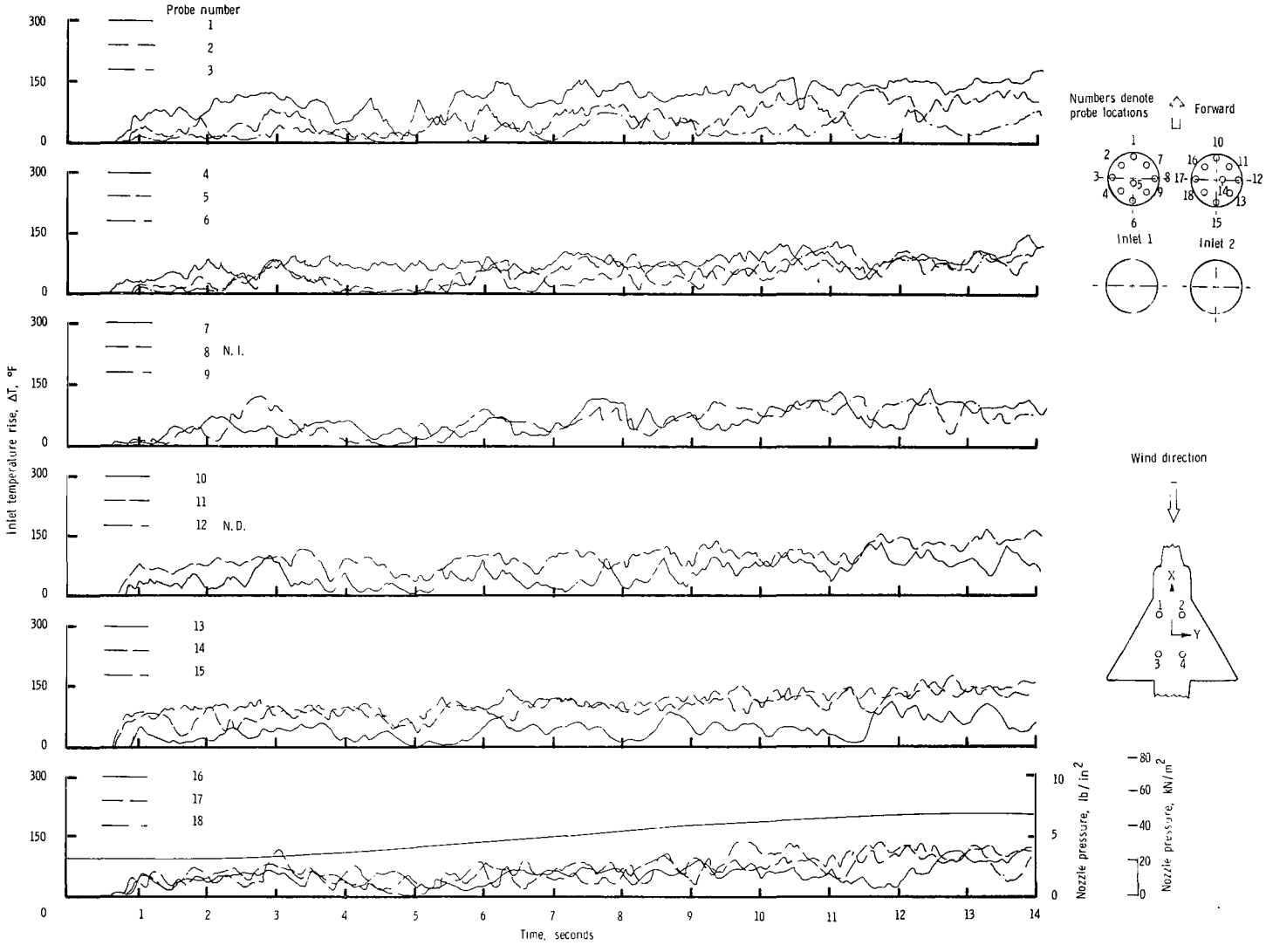

(a) $\psi = 0^0$; V = 0 knots.

Figure 15.- Variation of inlet-air temperature rise with time for the rectangular nozzle arrangement with top inlets and with the small wing installed. $S_W/S_J = 43.00$; $h/D_e = 3.00$. (Values of ΔT in ^0C can be obtained by multiplying the ^0F values by 5/9.)

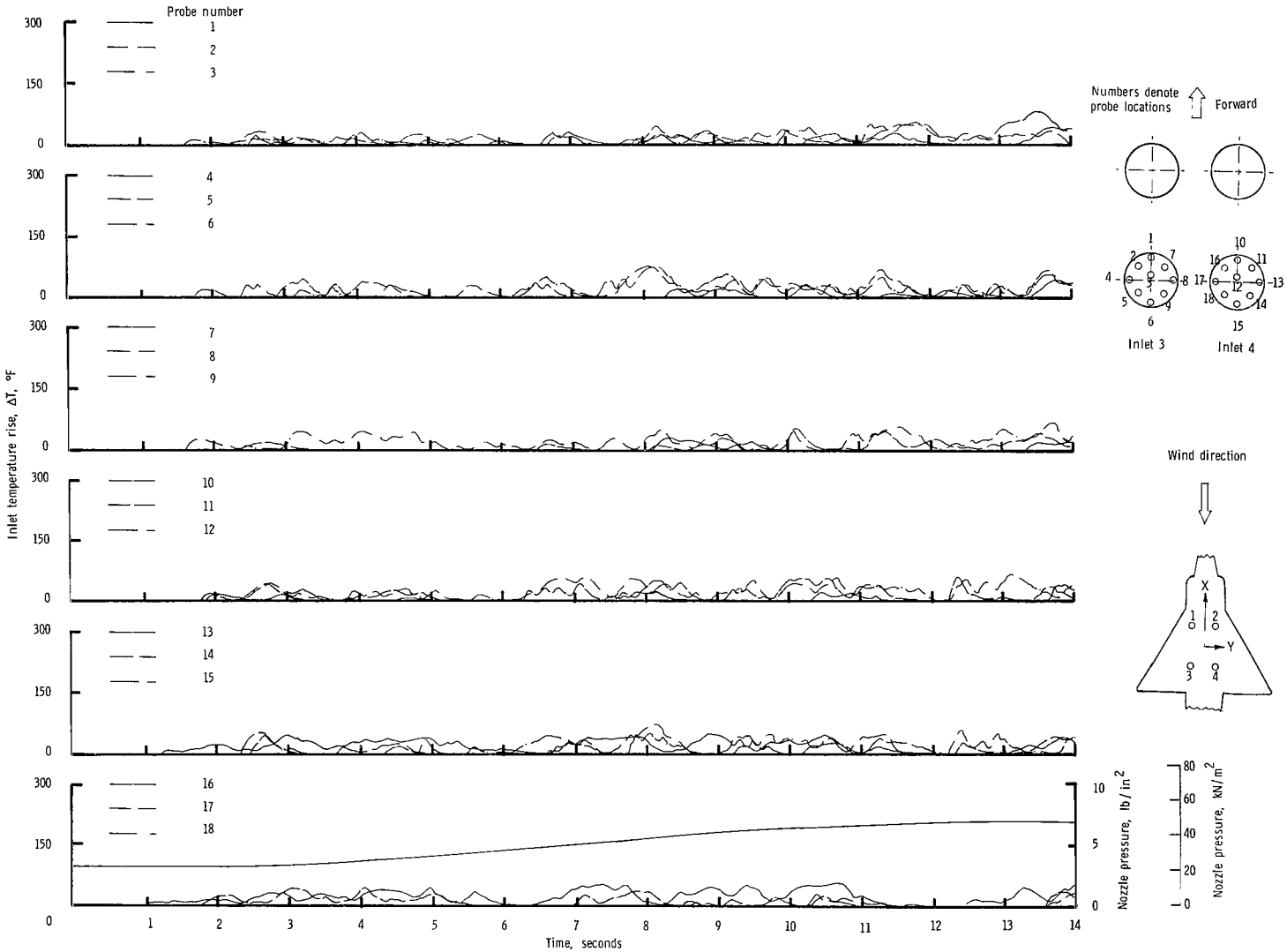

(a) Concluded.

Figure 15.- Continued.

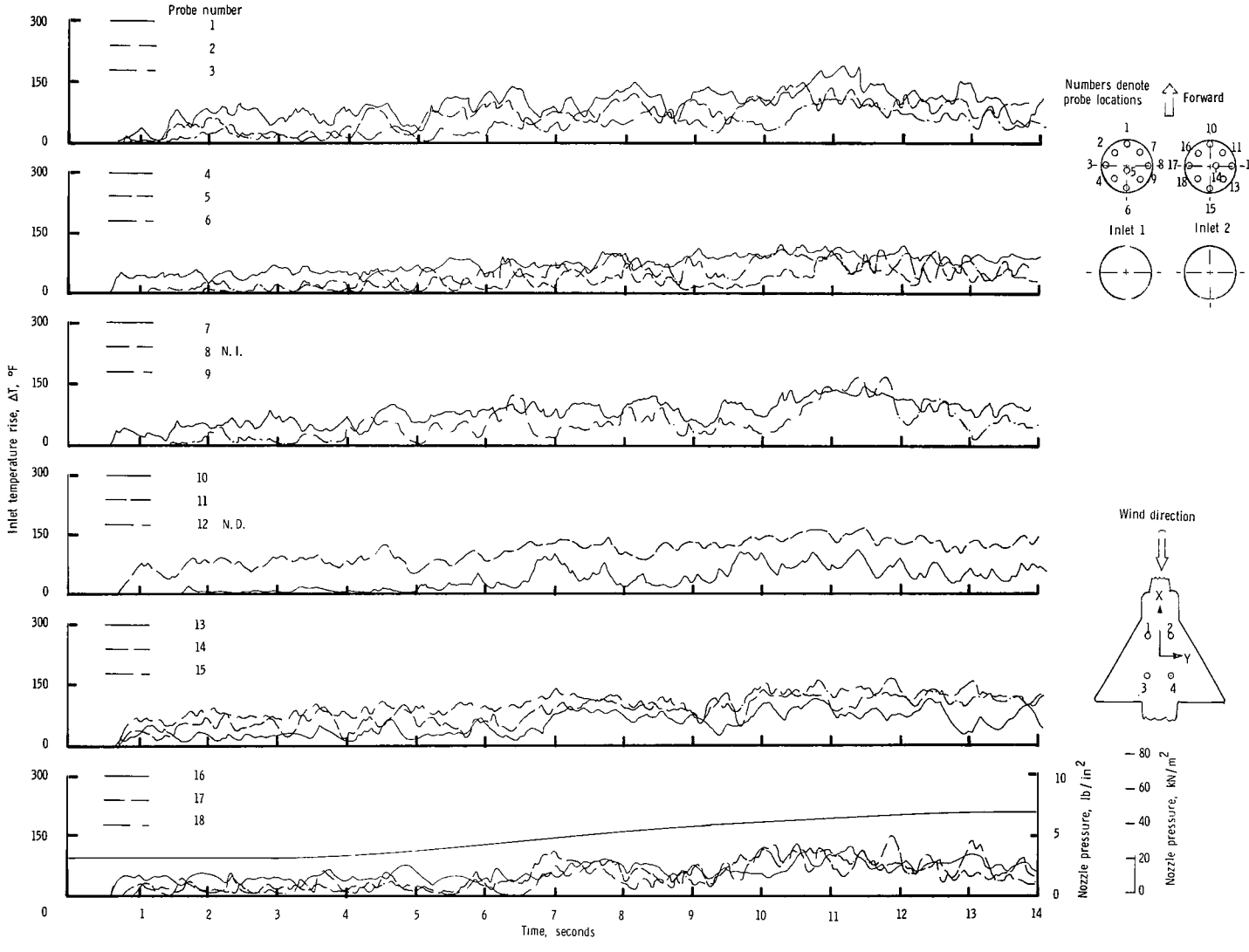

(b) $\psi = 0^0$; V = 5.92 knots.

Figure 15.- Continued.

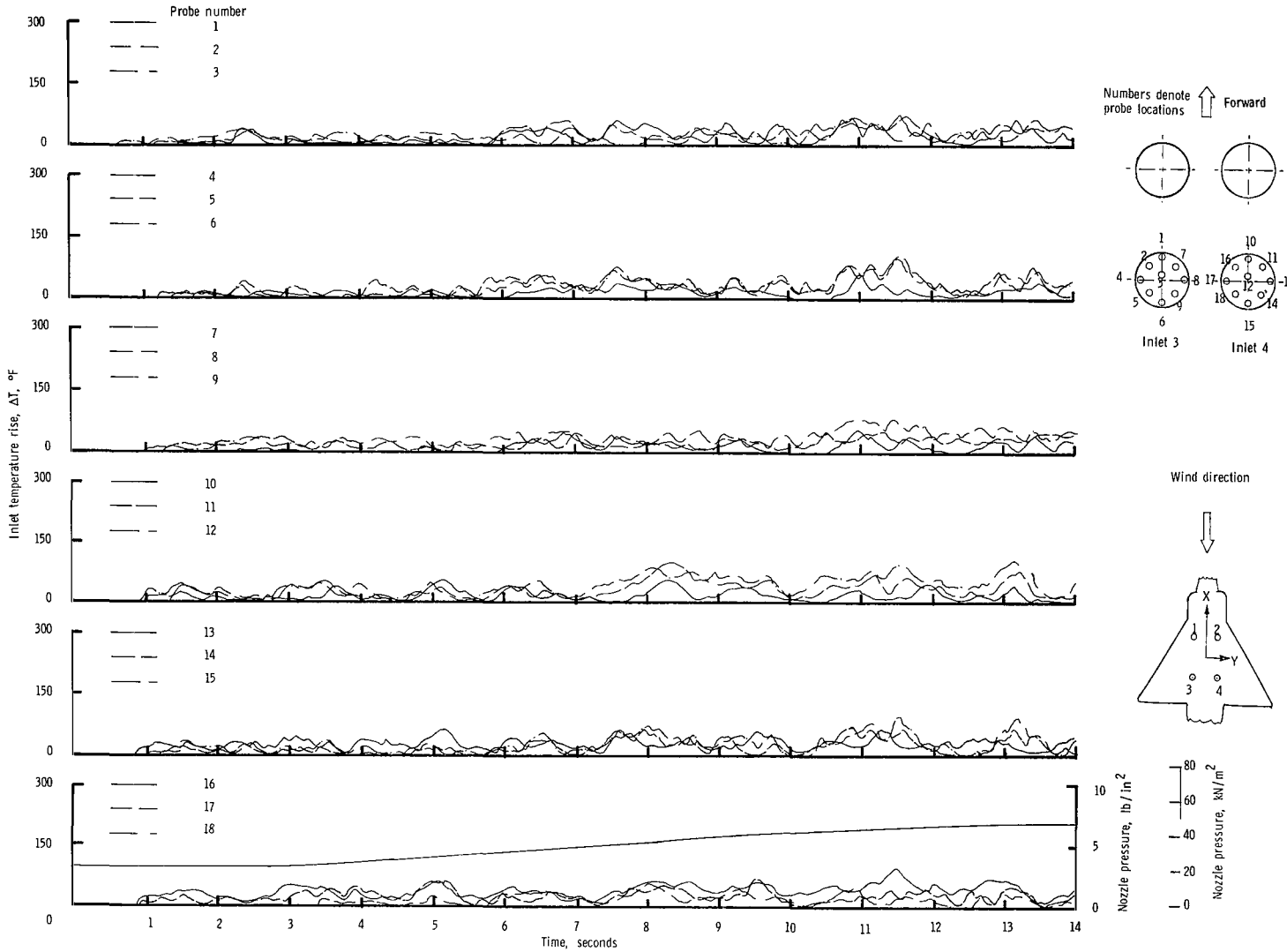

(b) Concluded.

Figure 15.- Continued.

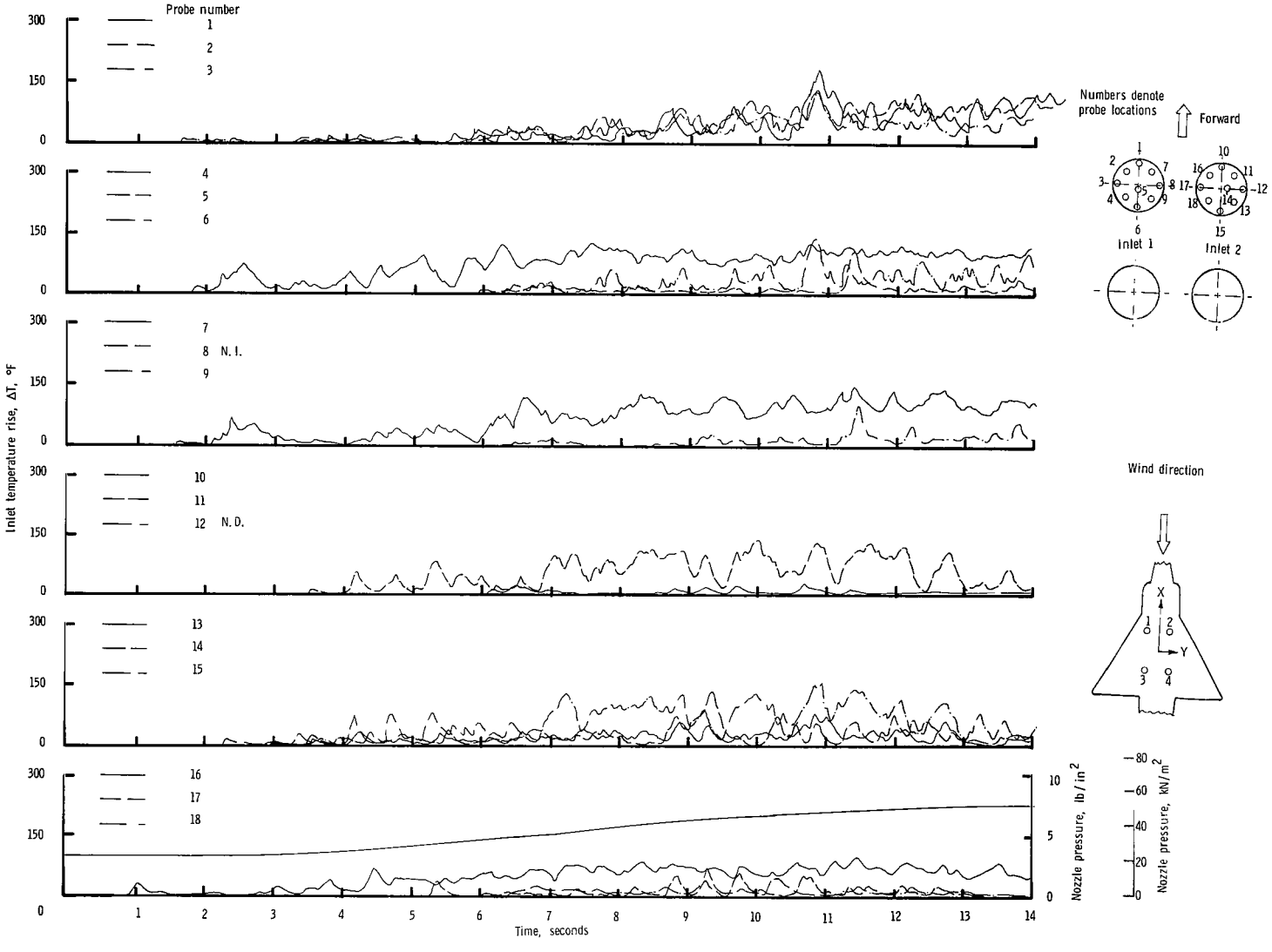

(c) $\psi = 0^0$; V = 11.85 knots.

Figure 15.- Continued.

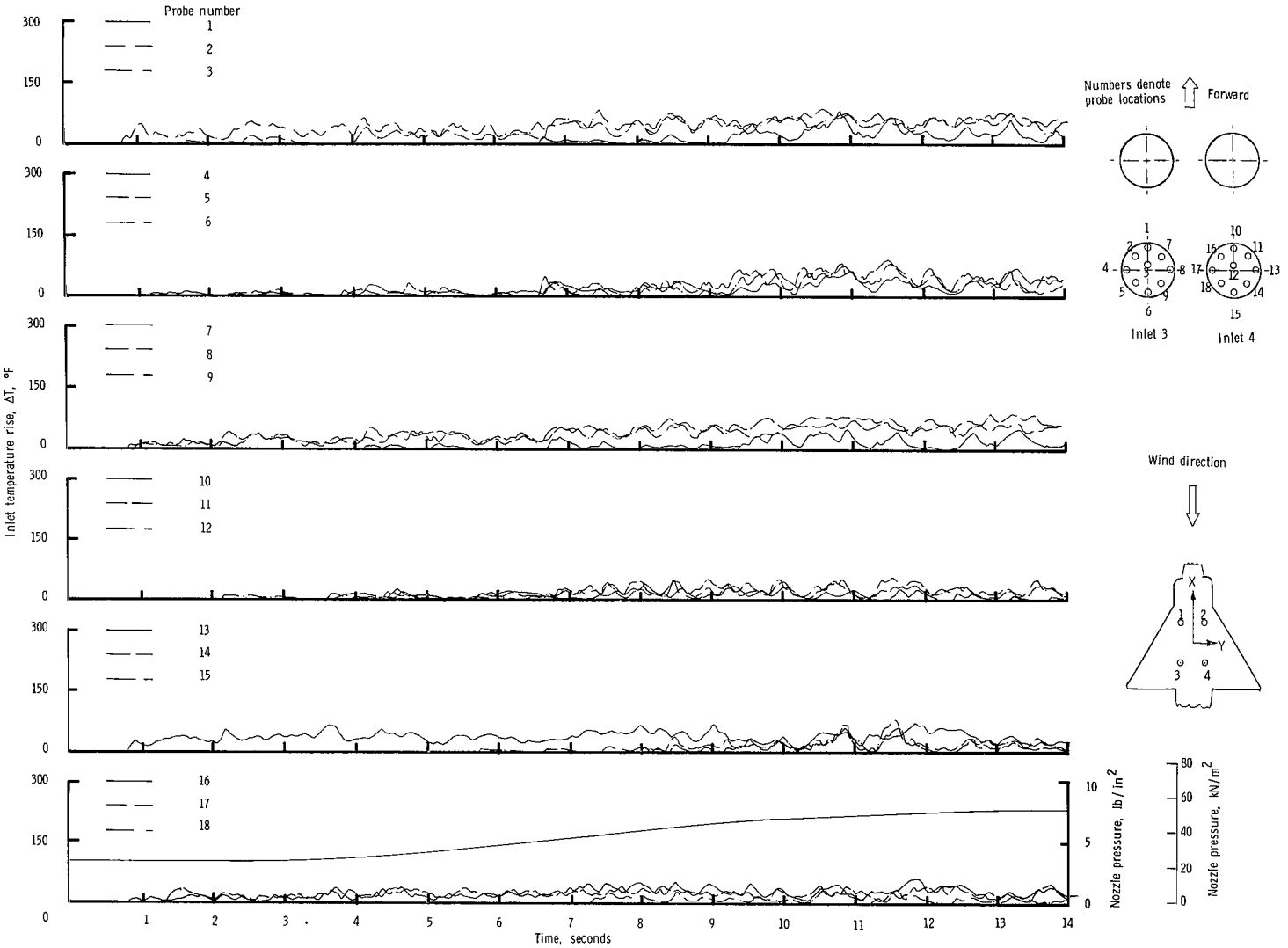

(c) Concluded.

Figure 15.- Continued.

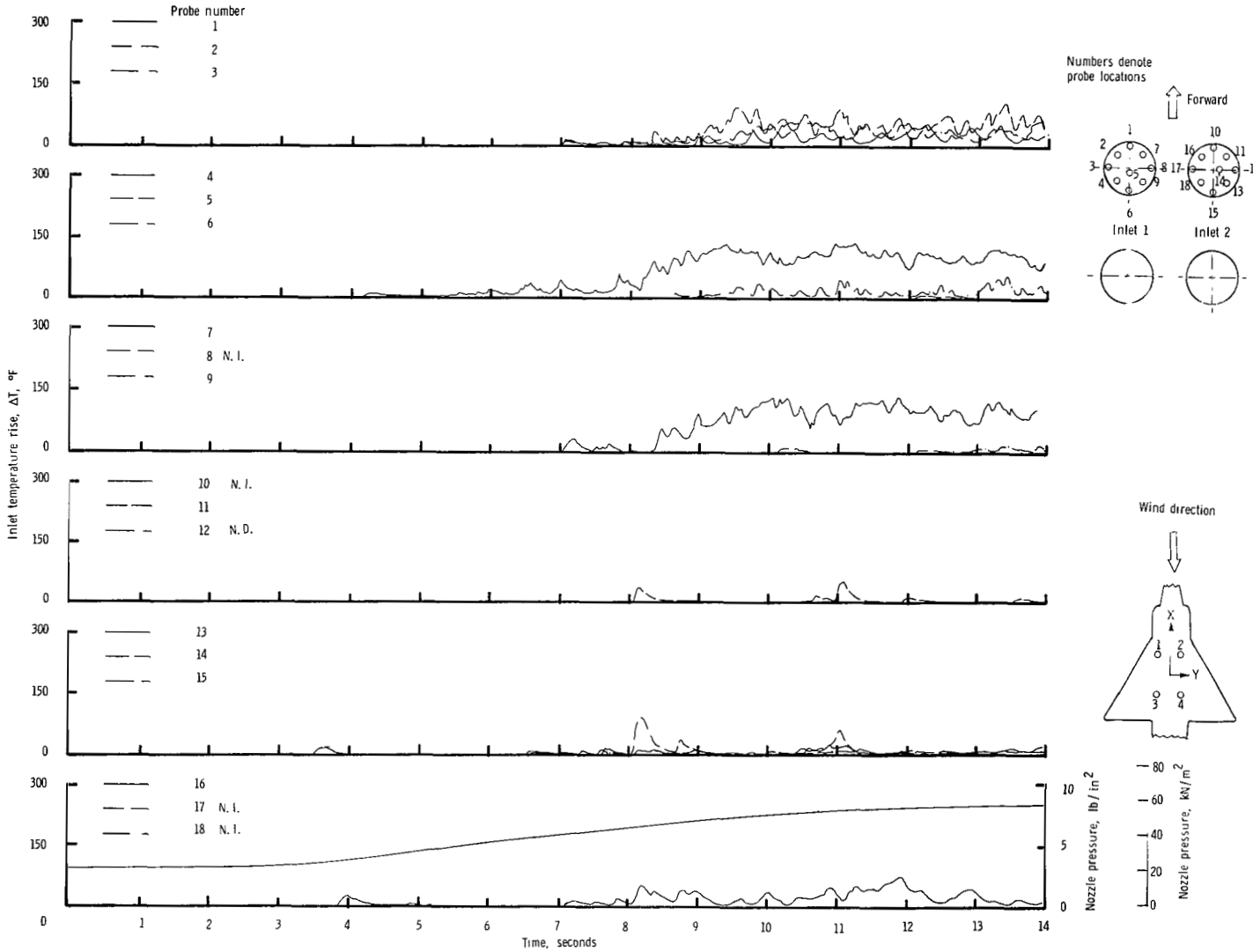

(d) $\psi = 0^0$; V = 17.78 knots.

Figure 15.- Continued.

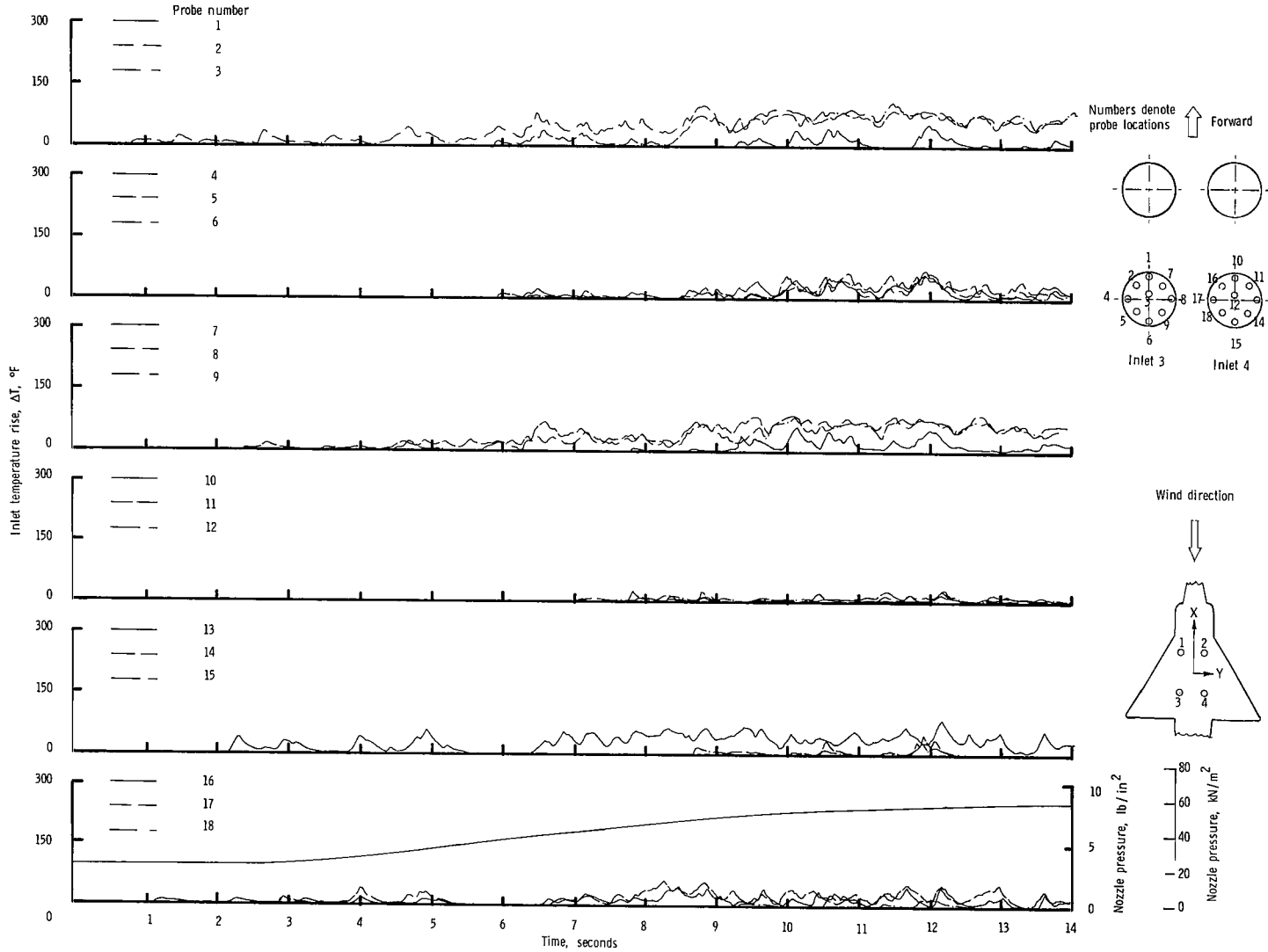

(d) Concluded.

Figure 15.- Continued.

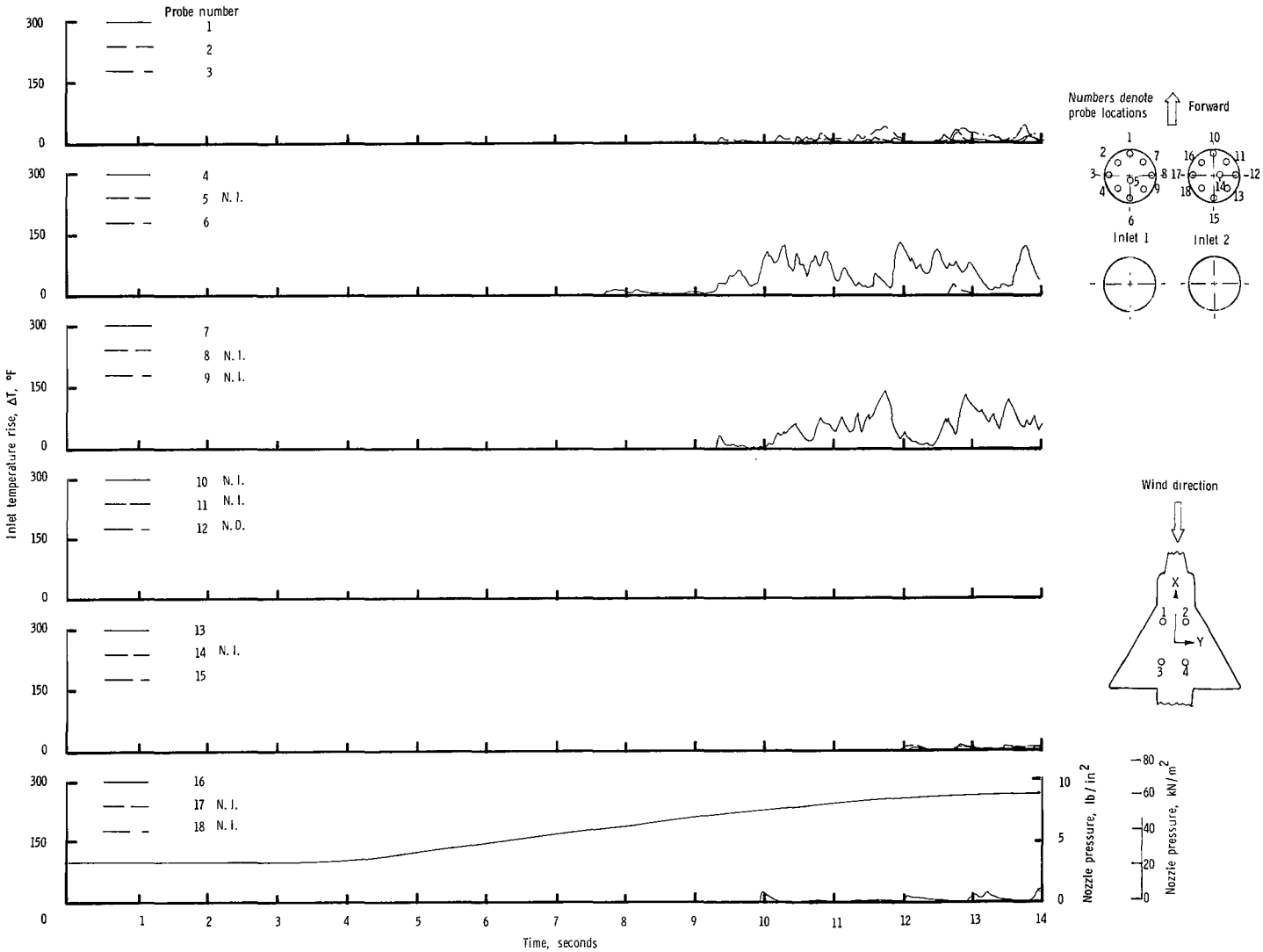

(e) $\psi = 0^0$; V = 23.70 knots.

Figure 15.- Continued.

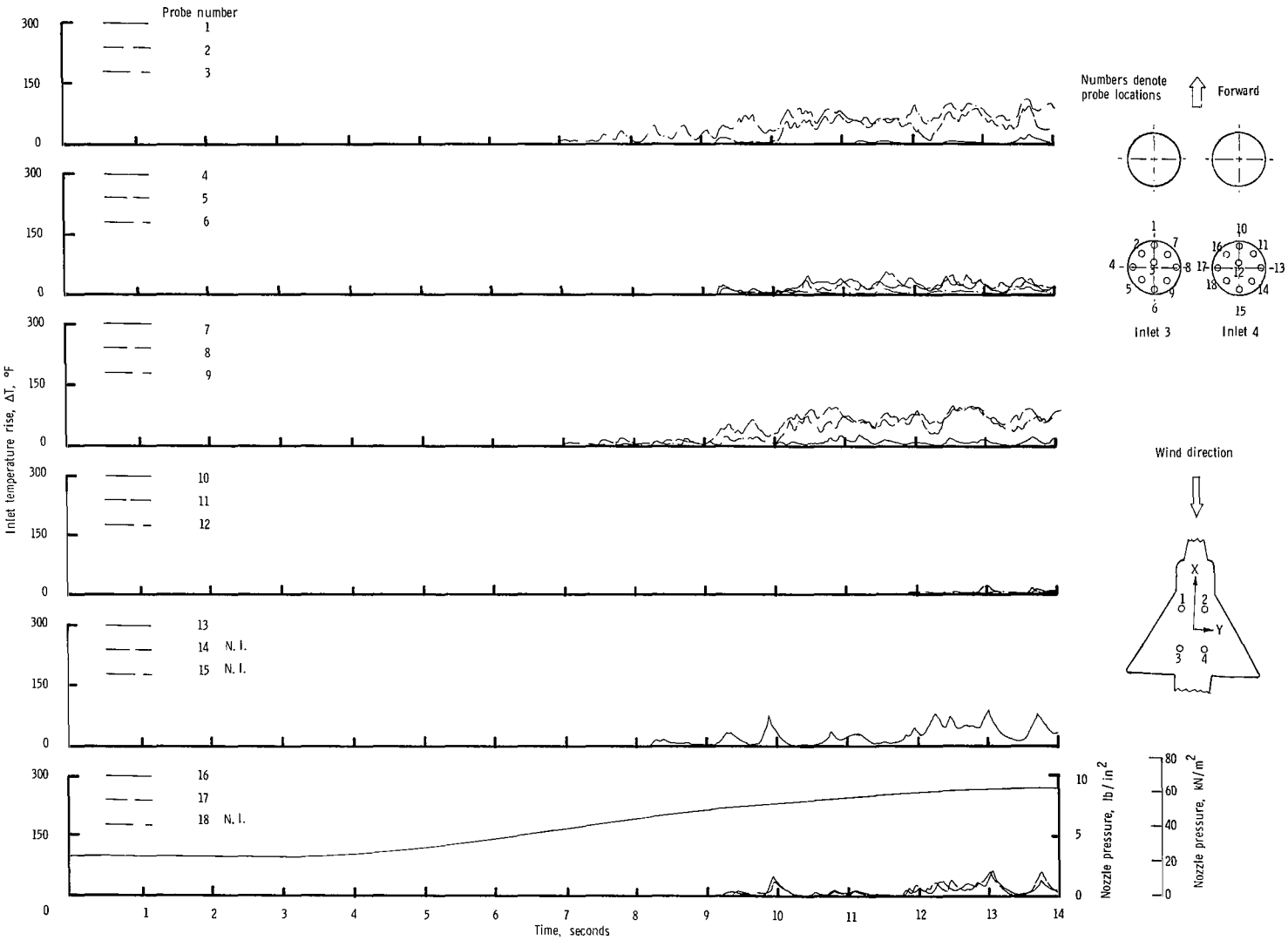

(e) Concluded.

Figure 15.- Continued.

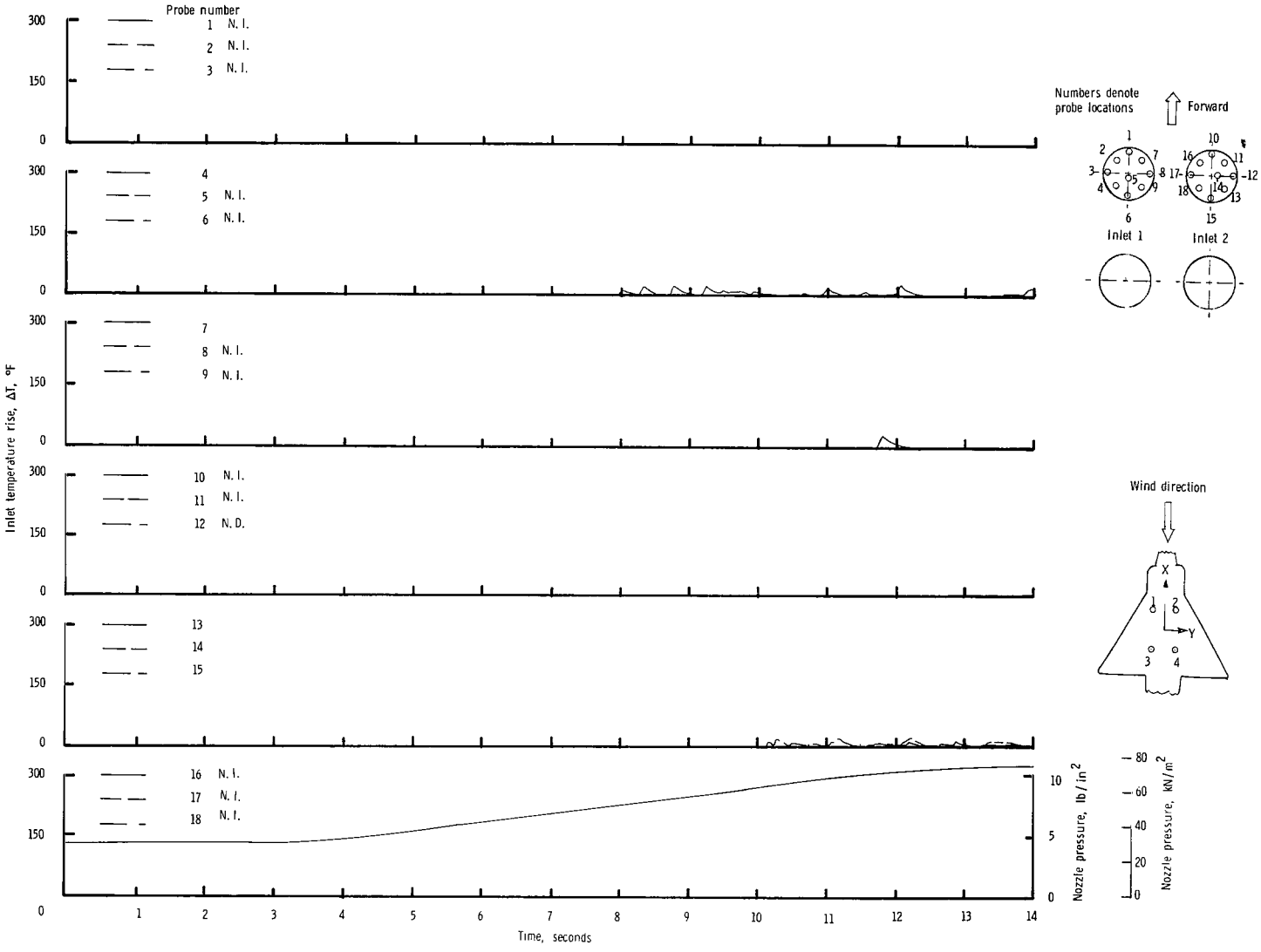

(f) $\psi = 0^{0}$; V = 26.93 knots.

Figure 15.- Continued.

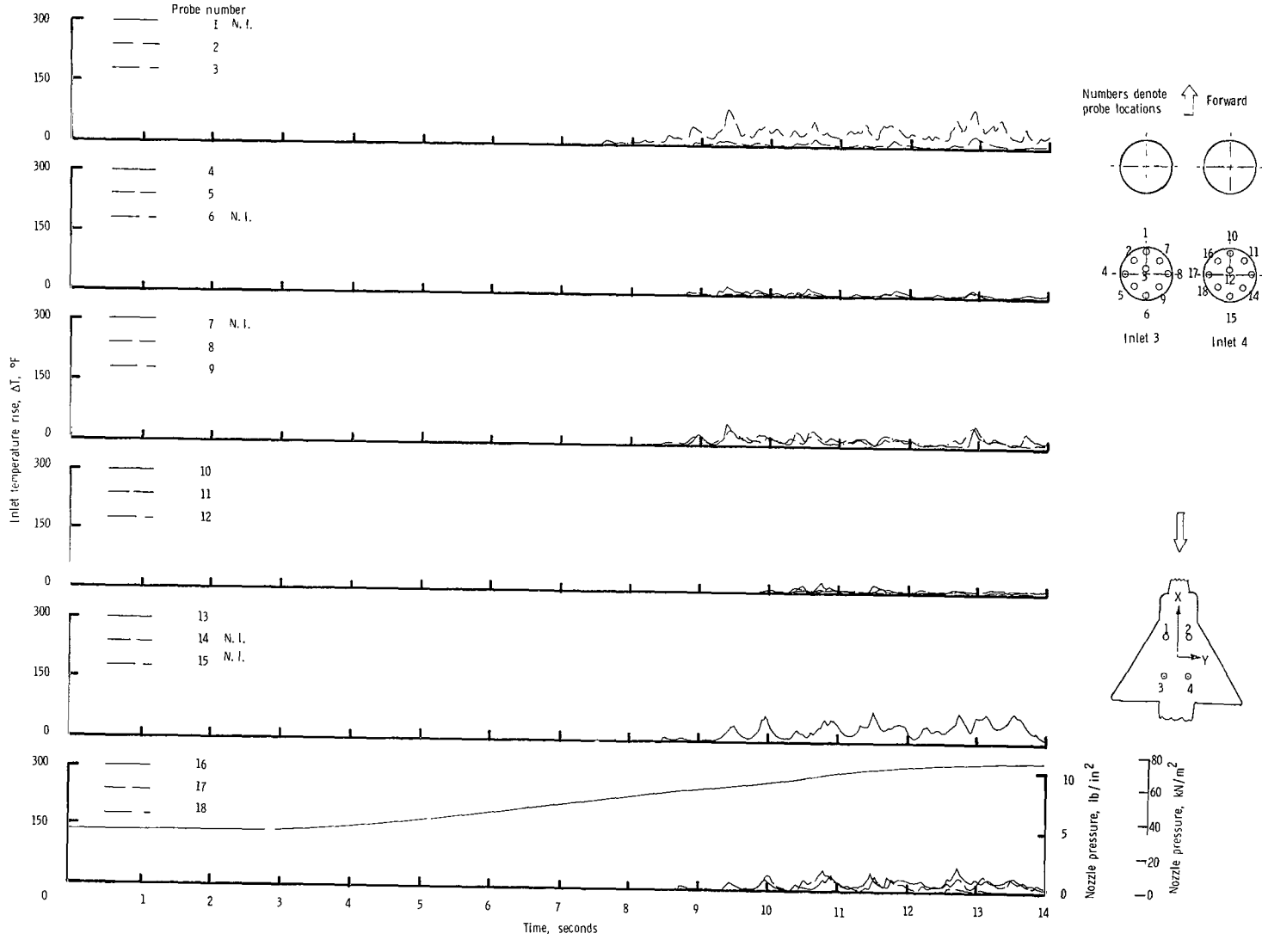

(f) Concluded.

Figure 15.- Continued.

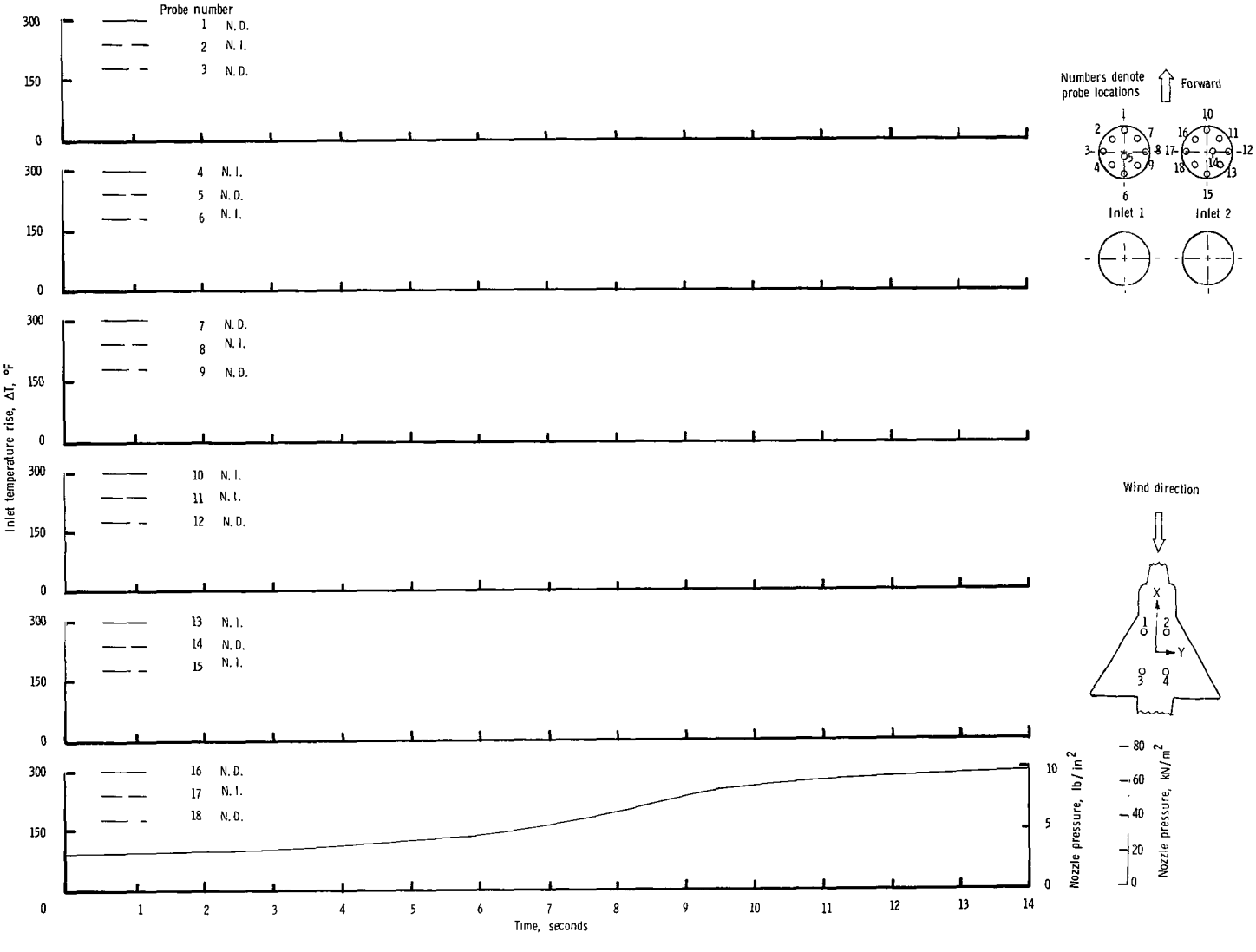

(g) $\psi = 0^{0}$; V = 35.55 knots.

Figure 15.- Continued.

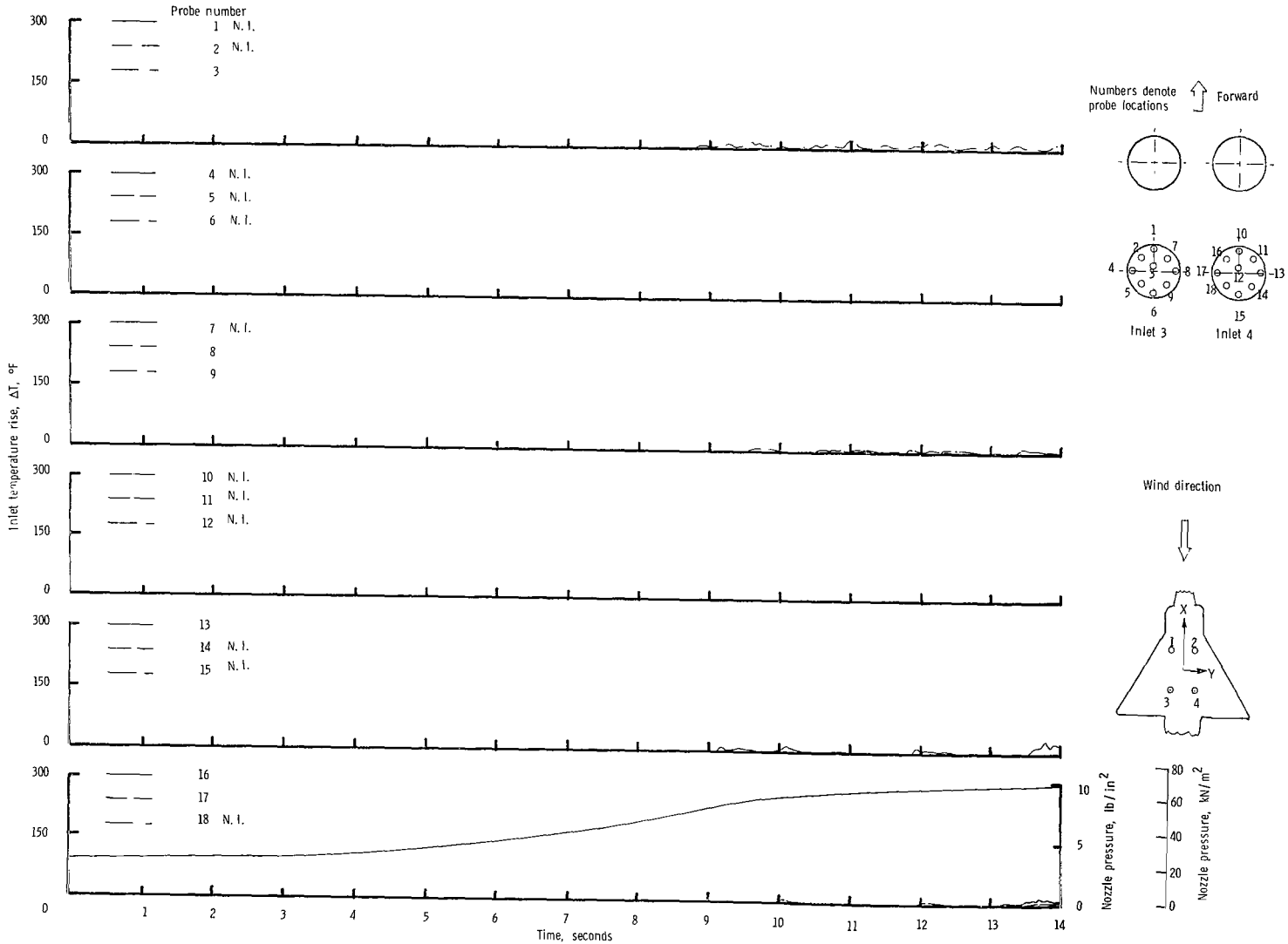

(g) Concluded.

Figure 15.- Continued.

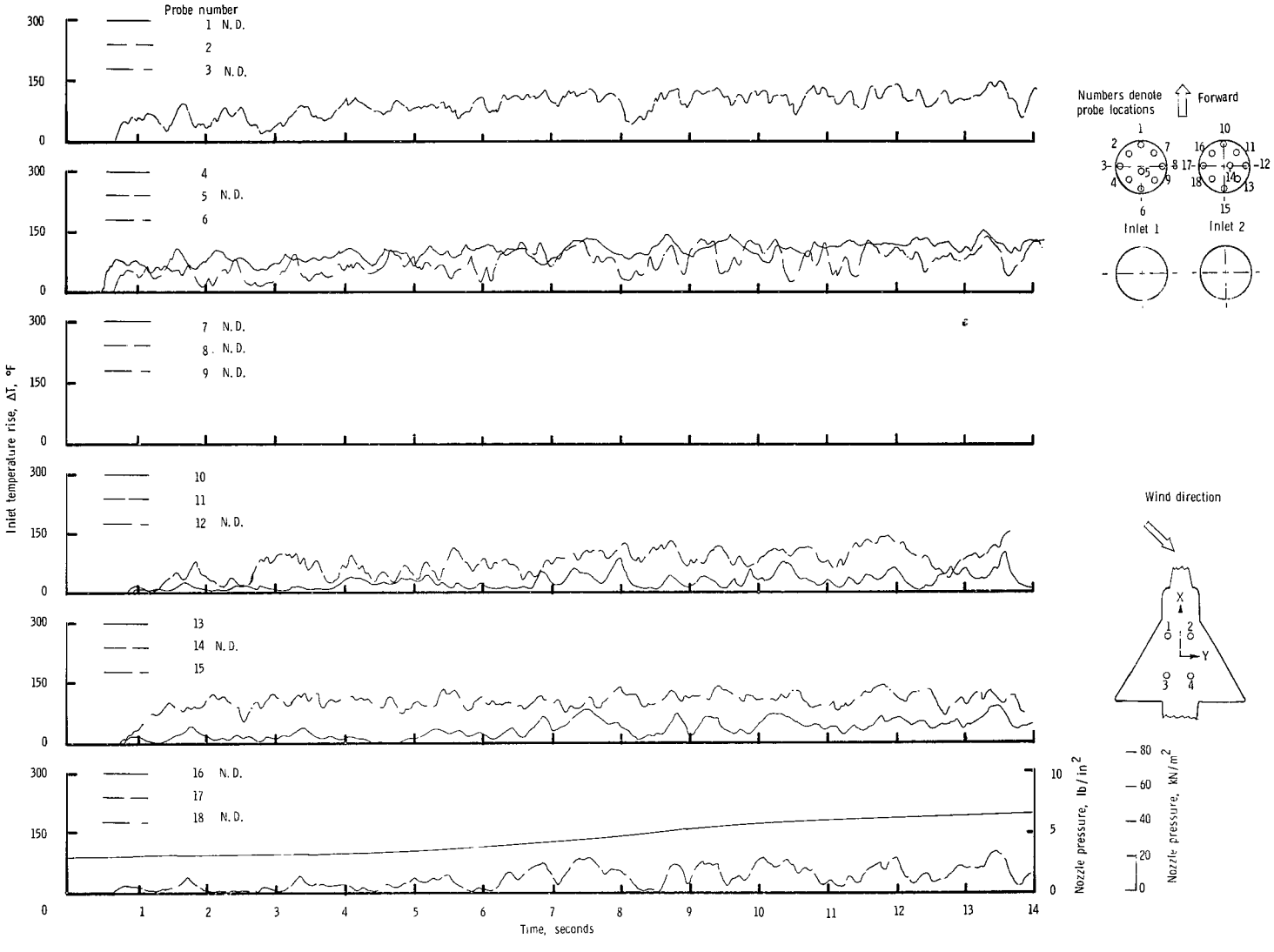

(h) $\psi = 45^{0}$; V = 5.92 knots.

Figure 15.- Continued.

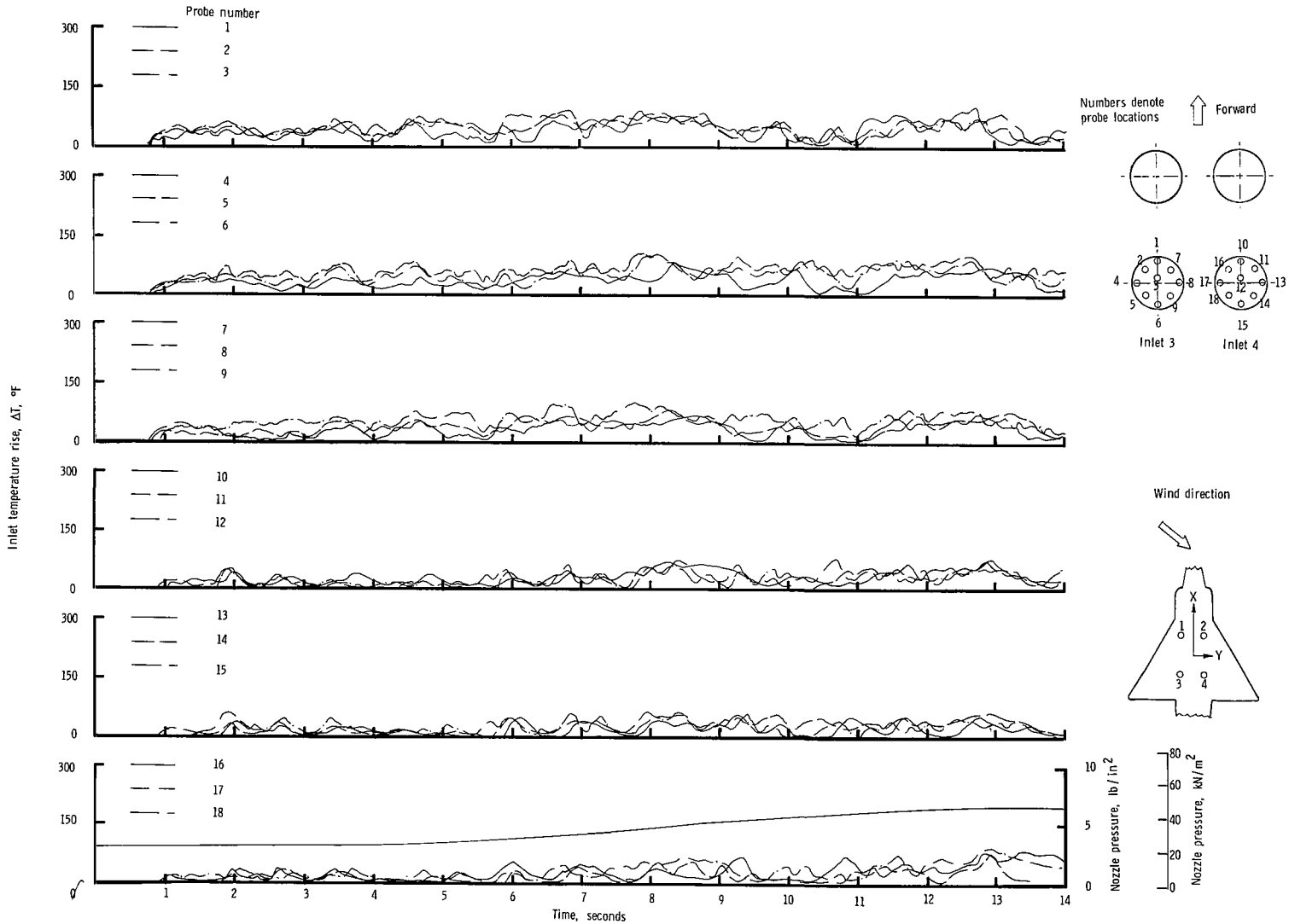

(h) Concluded.

Figure 15.- Continued.

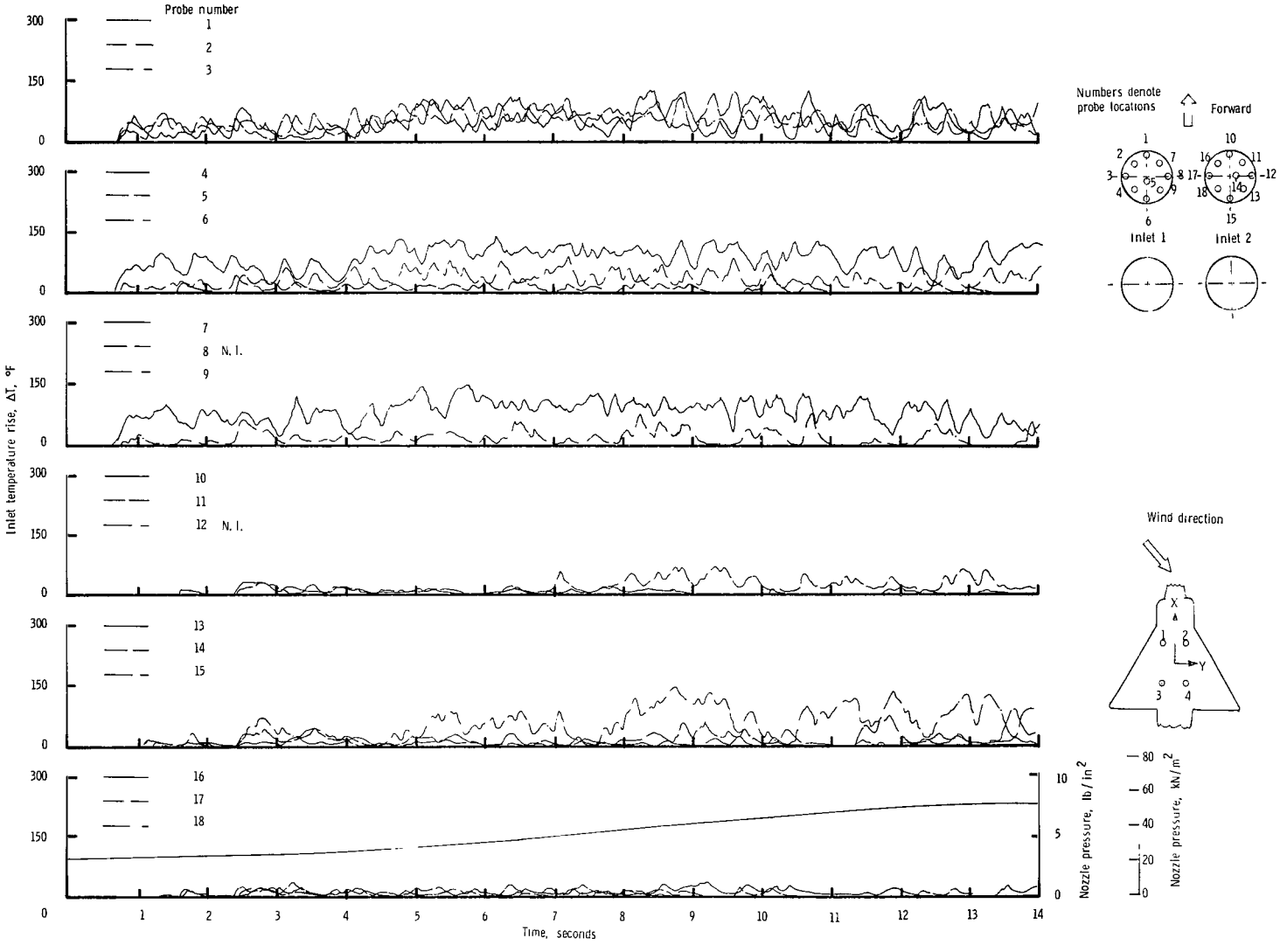

(i) $\psi = 45^{0}$; V = 11.85 knots.

Figure 15.- Continued.

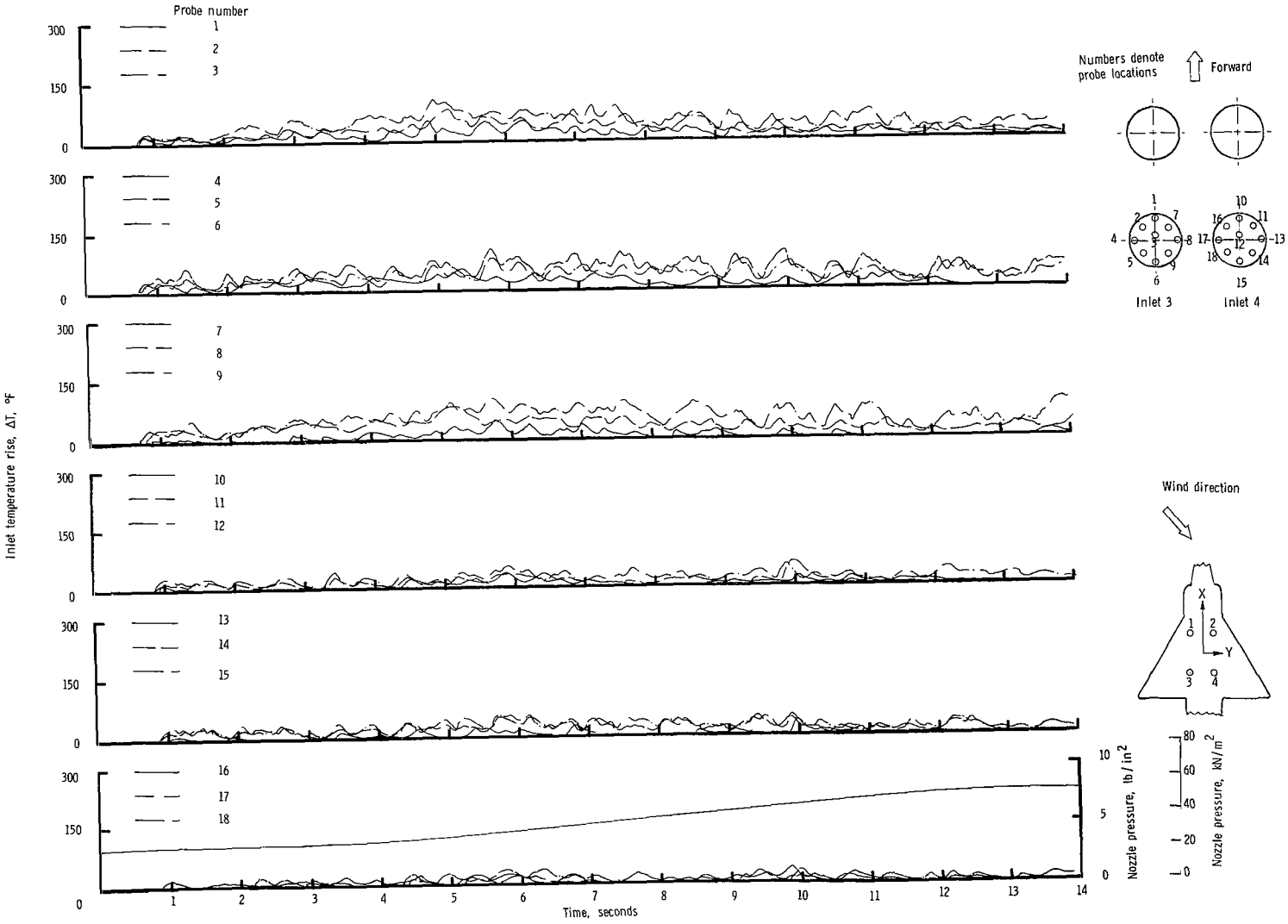

(i) Concluded.

Figure 15.- Continued.

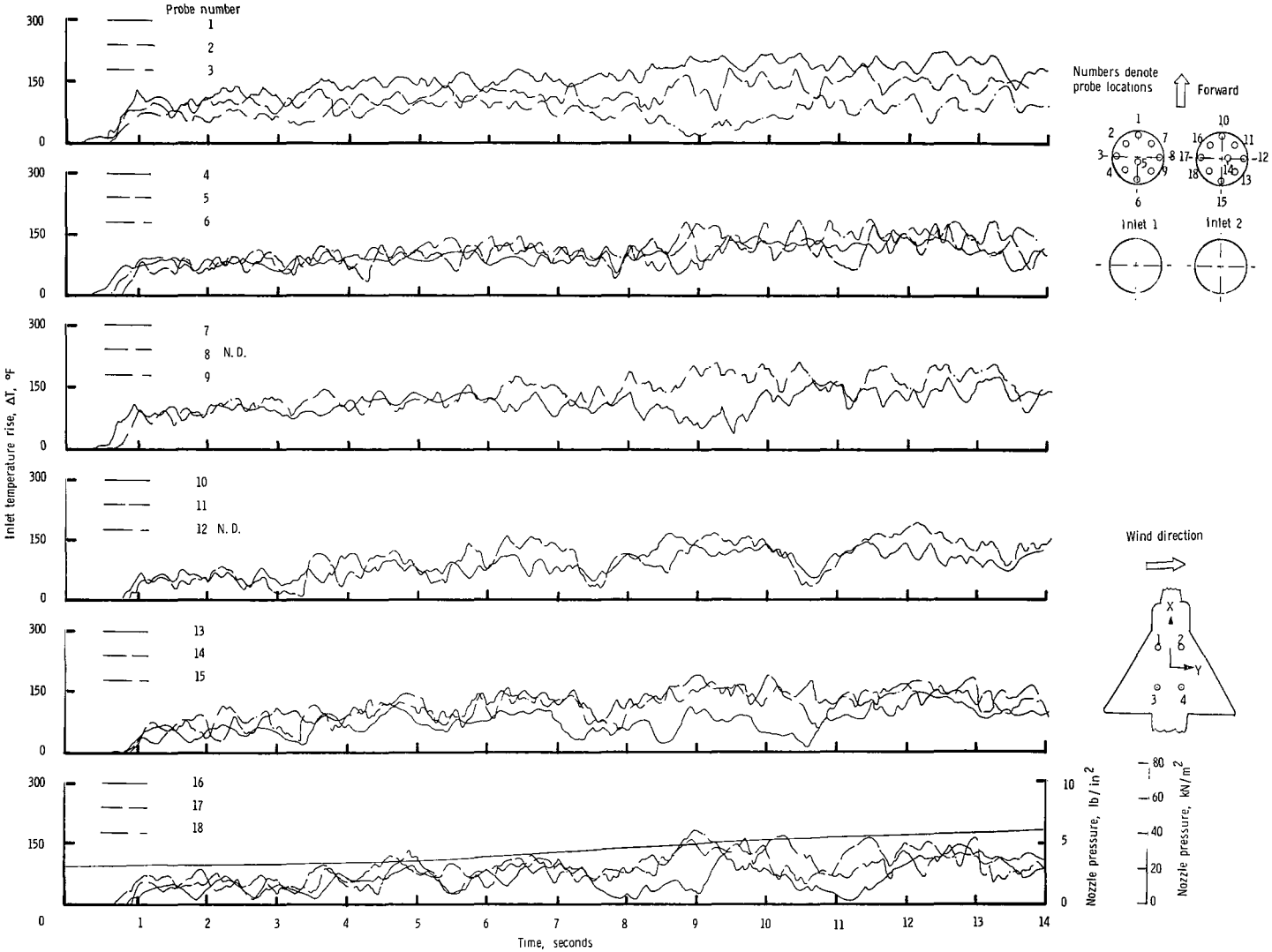

(j) $\psi = 90^0$; V = 5.92 knots.

Figure 15.- Continued.

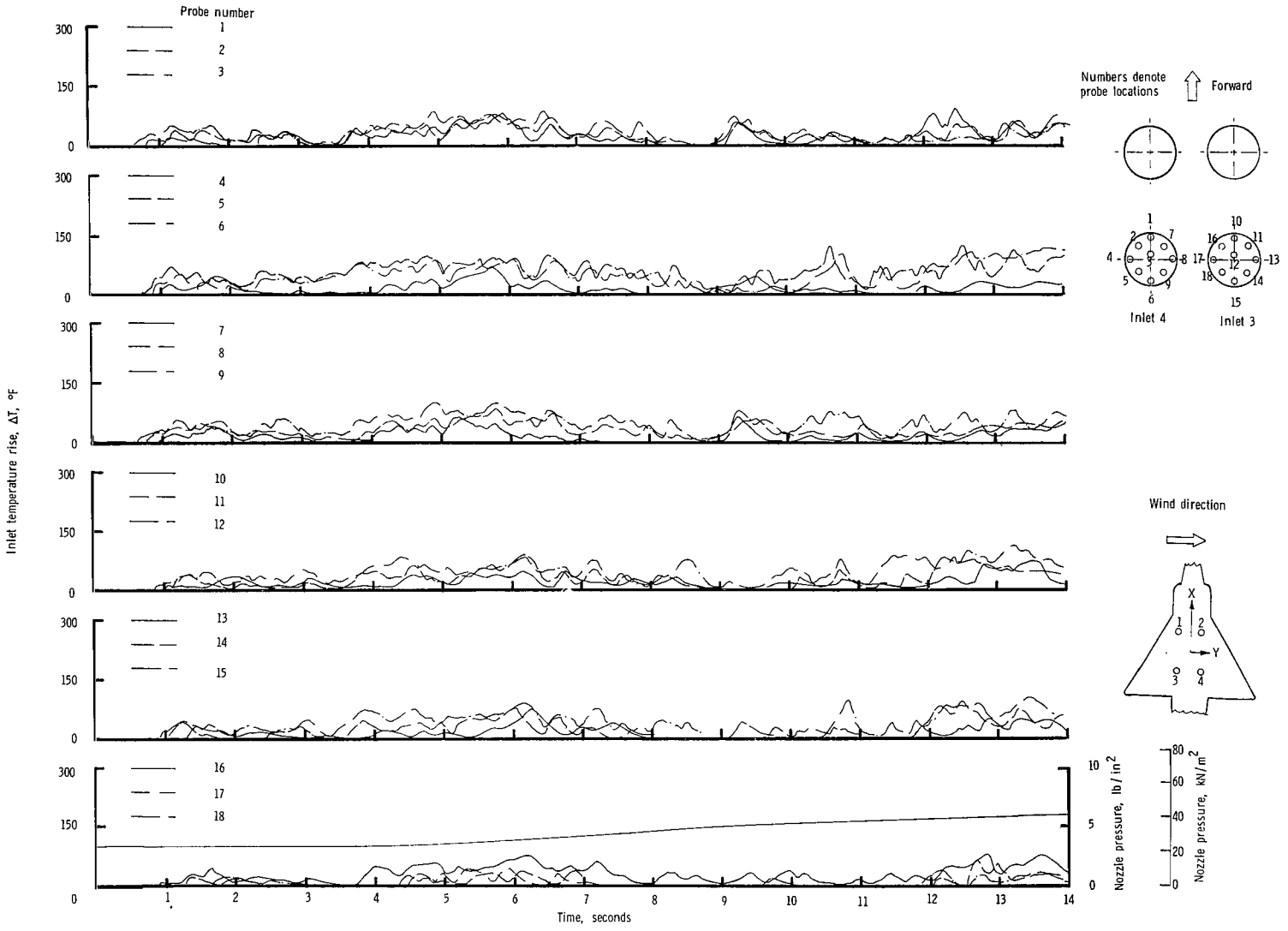

(j) Concluded.

Figure 15.- Continued.

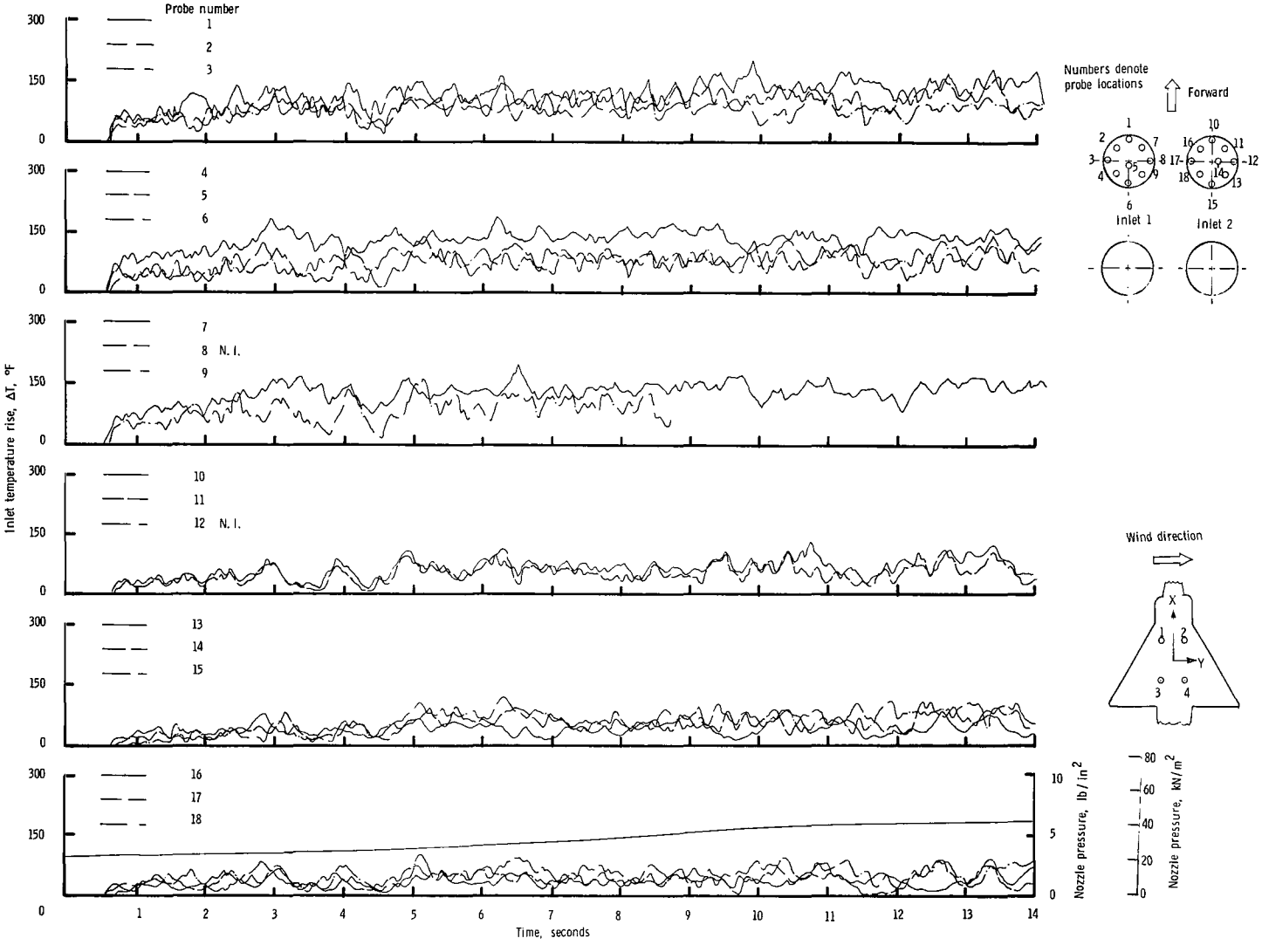

(k) $\psi = 90^0$; V = 11.85 knots.

Figure 15.- Continued.

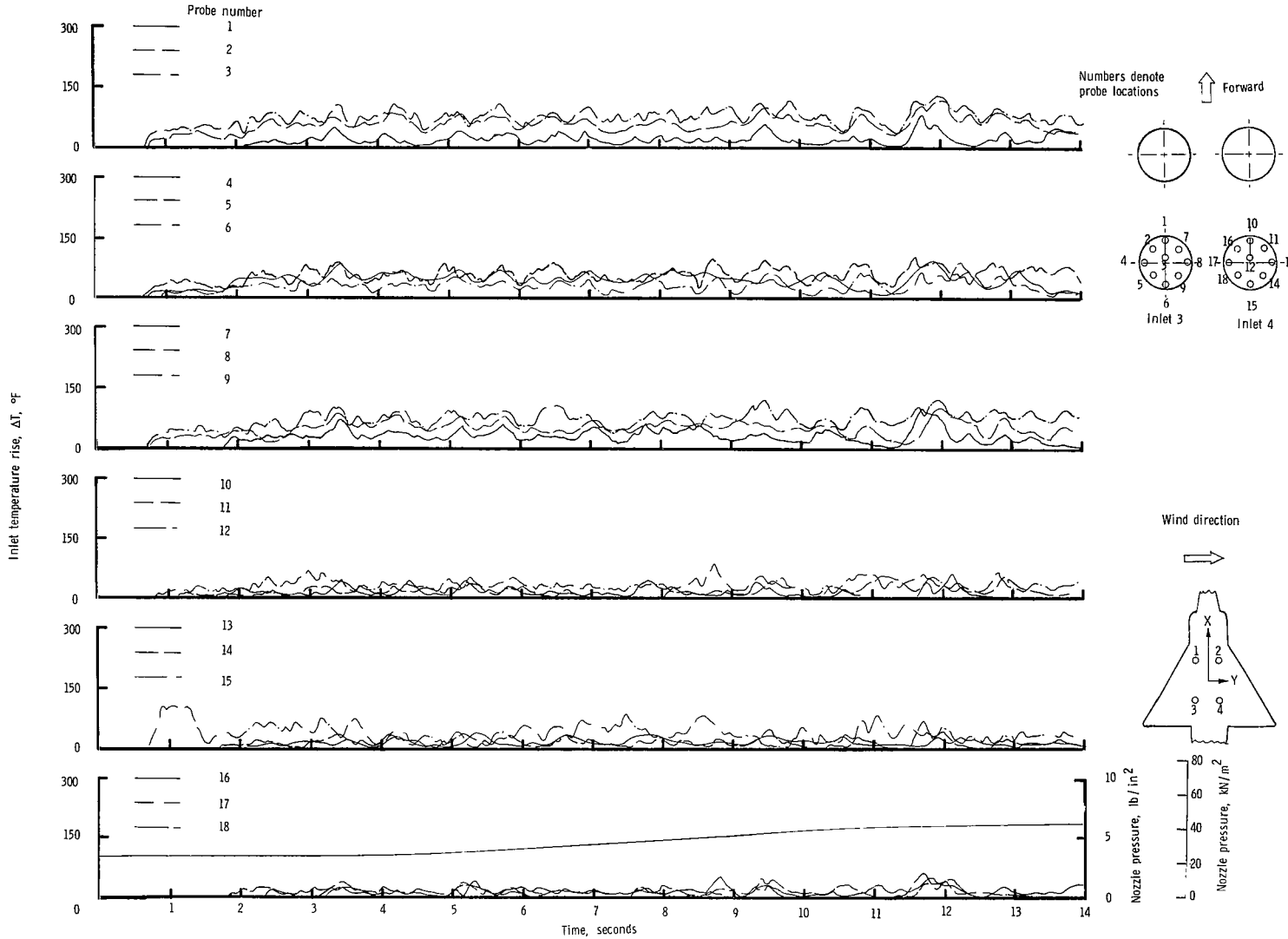

(k) Concluded.

Figure 15.- Concluded.

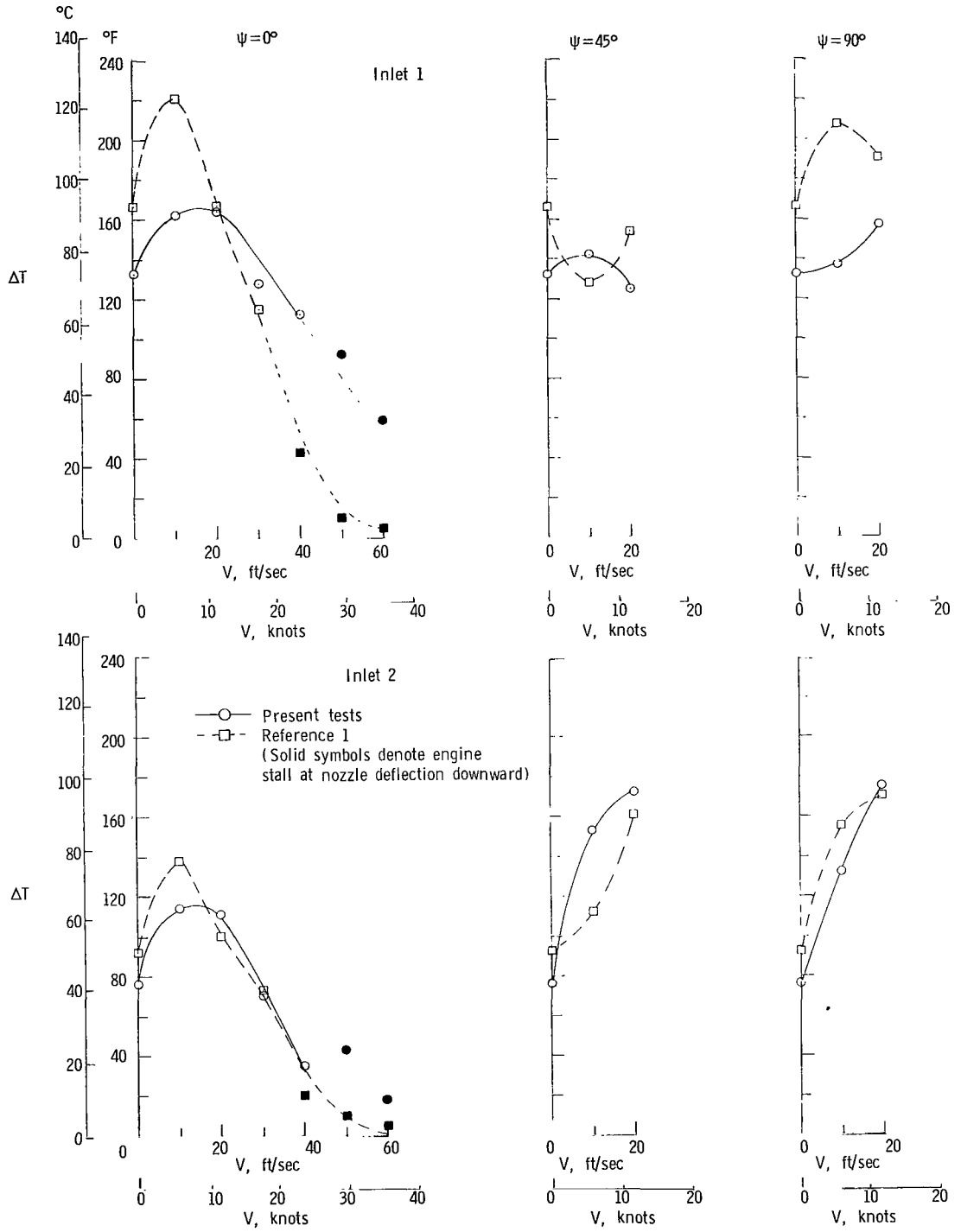

Figure 16.- Comparison of previous and present data on the variation of average inlet-air temperature rise with windspeed for the rectangular nozzle arrangement with side inlets. High wing; $S_W/S_J = 43$; $h/D_e = 1.17$.

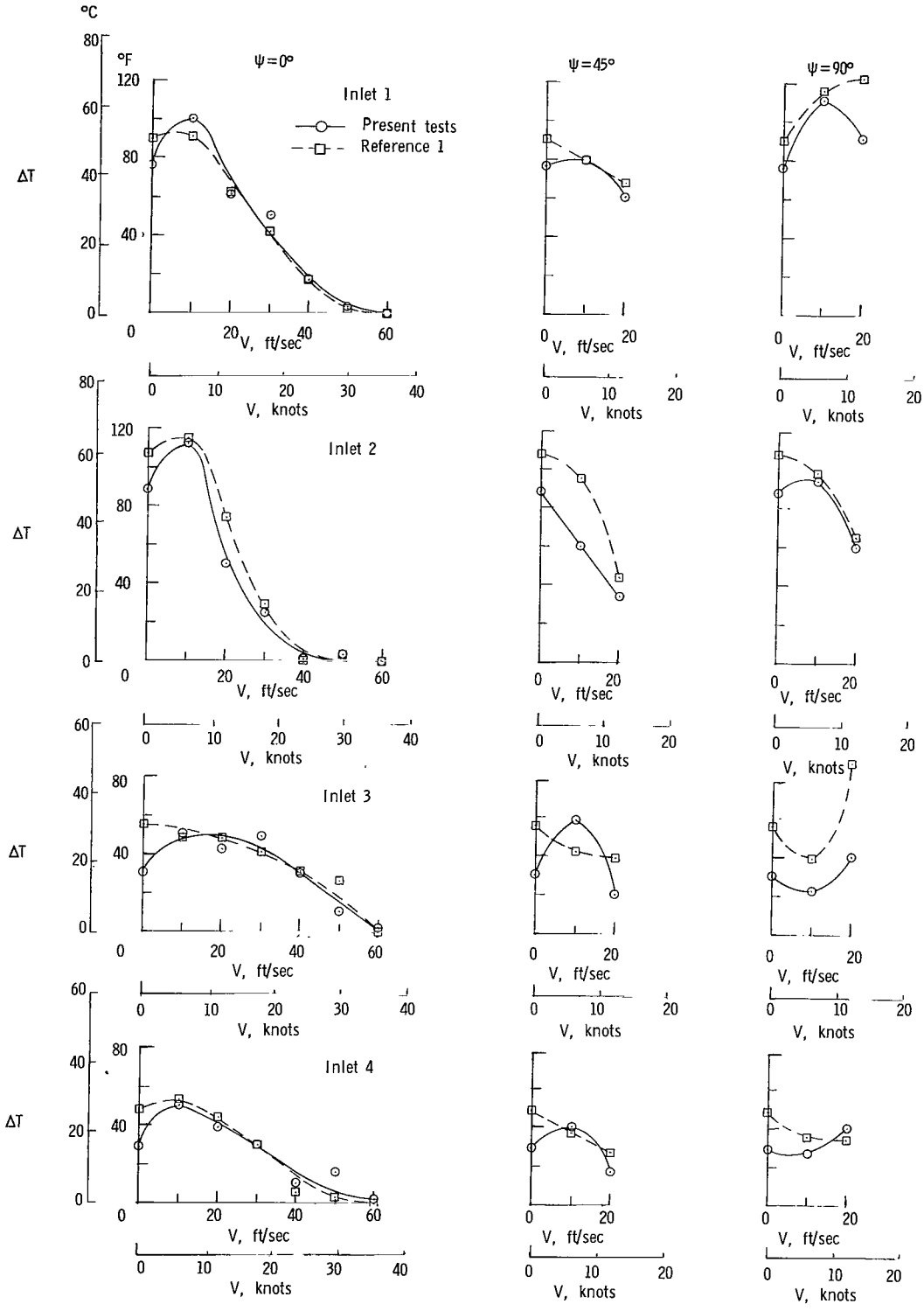

Figure 17.- Comparison of previous and present data on the variation of average inlet-air temperature rise with windspeed for the rectangular nozzle arrangement with top inlets. High wing; $S_W/S_J = 43$; $h/D_e = 3.00$.

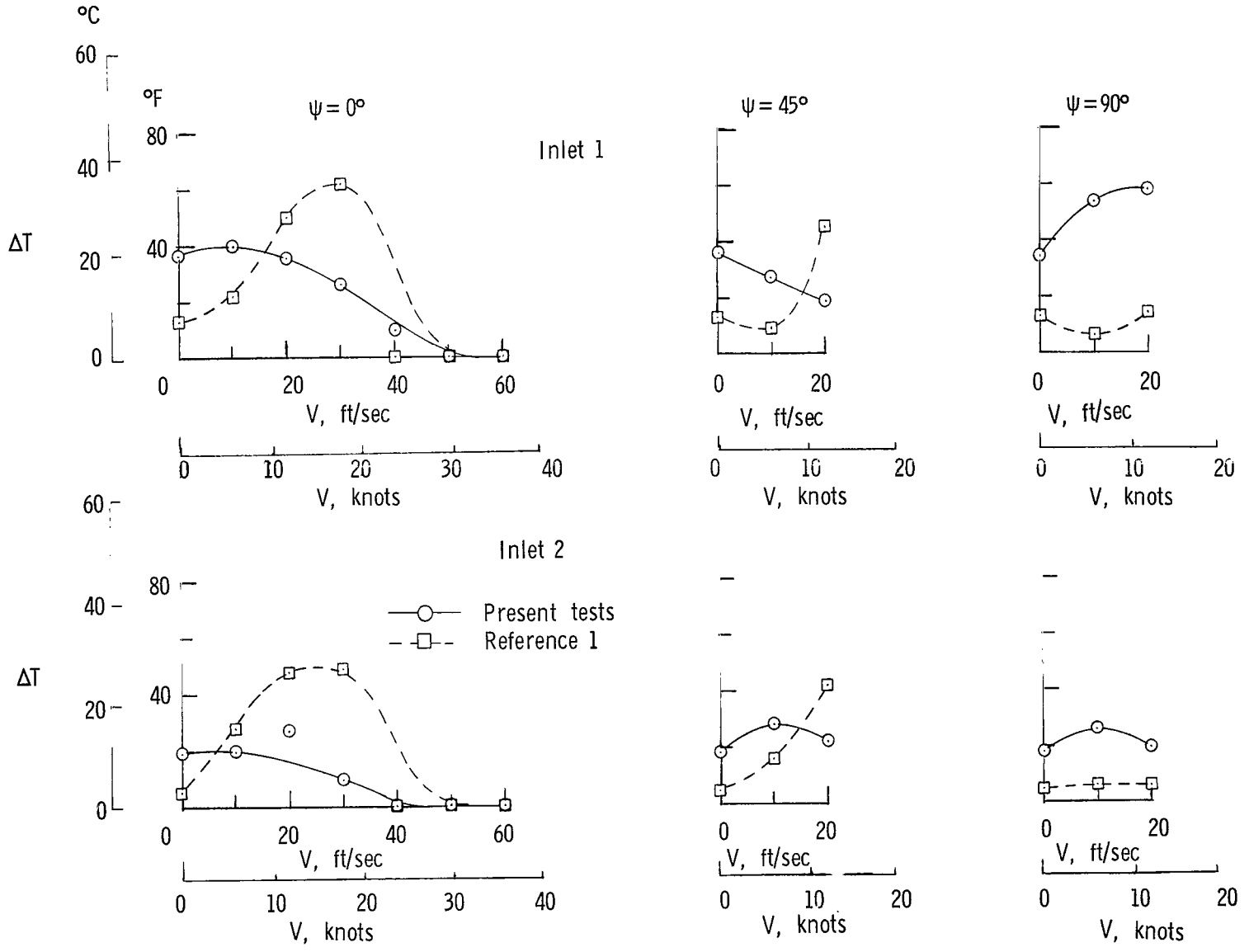

Figure 18.- Comparison of previous and present data on the variation of average inlet-air temperature rise with windspeed for the in-line nozzle arrangement with side inlets. High wing; $S_W/S_J = 43$; $h/D_e = 1.7$.

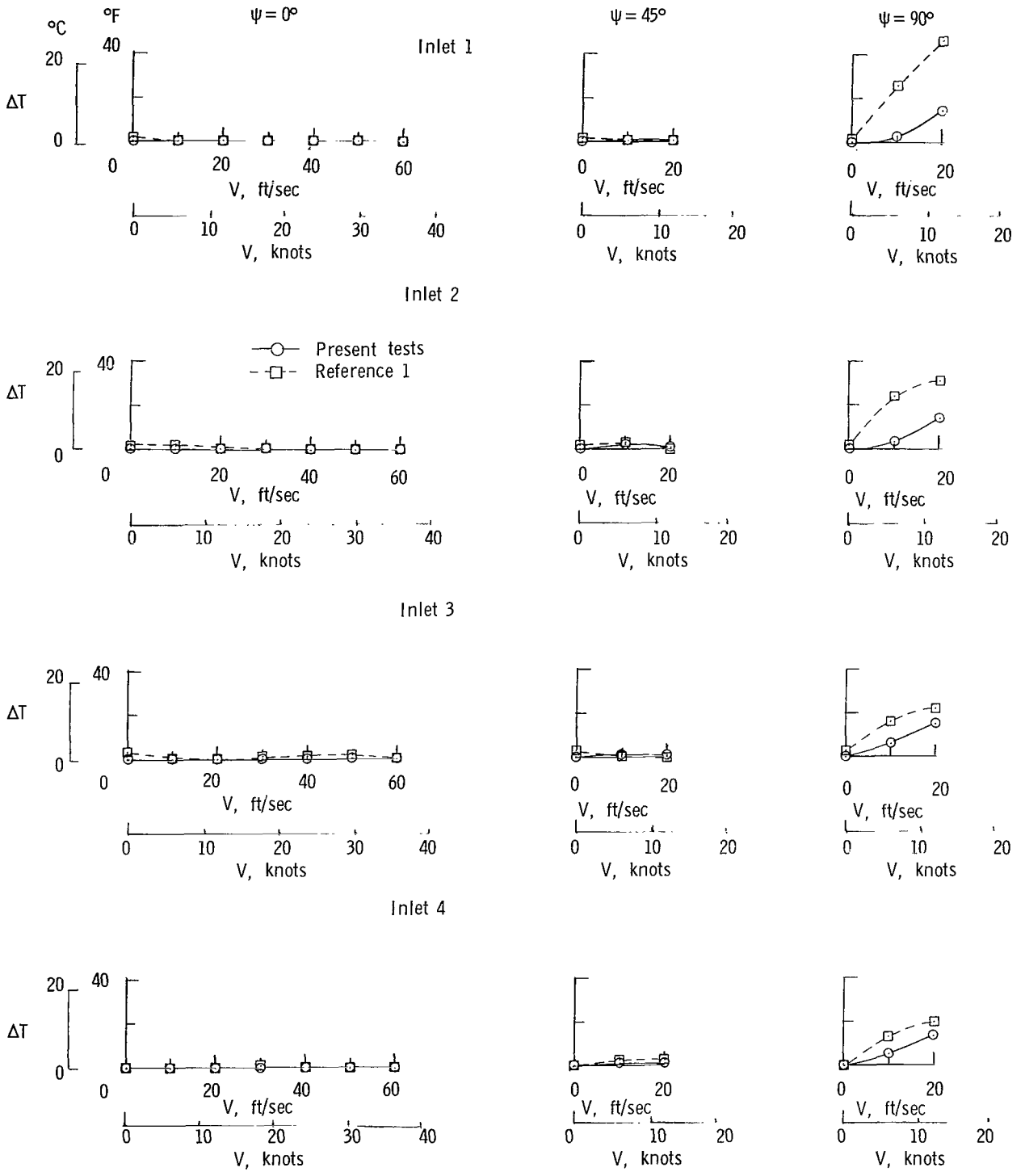

Figure 19.- Comparison of previous and present data on the variation of average inlet-air temperature rise with windspeed for the in-line nozzle arrangement with top inlets. High wing; S_W/S_J = 43; h/D_e = 3.00.

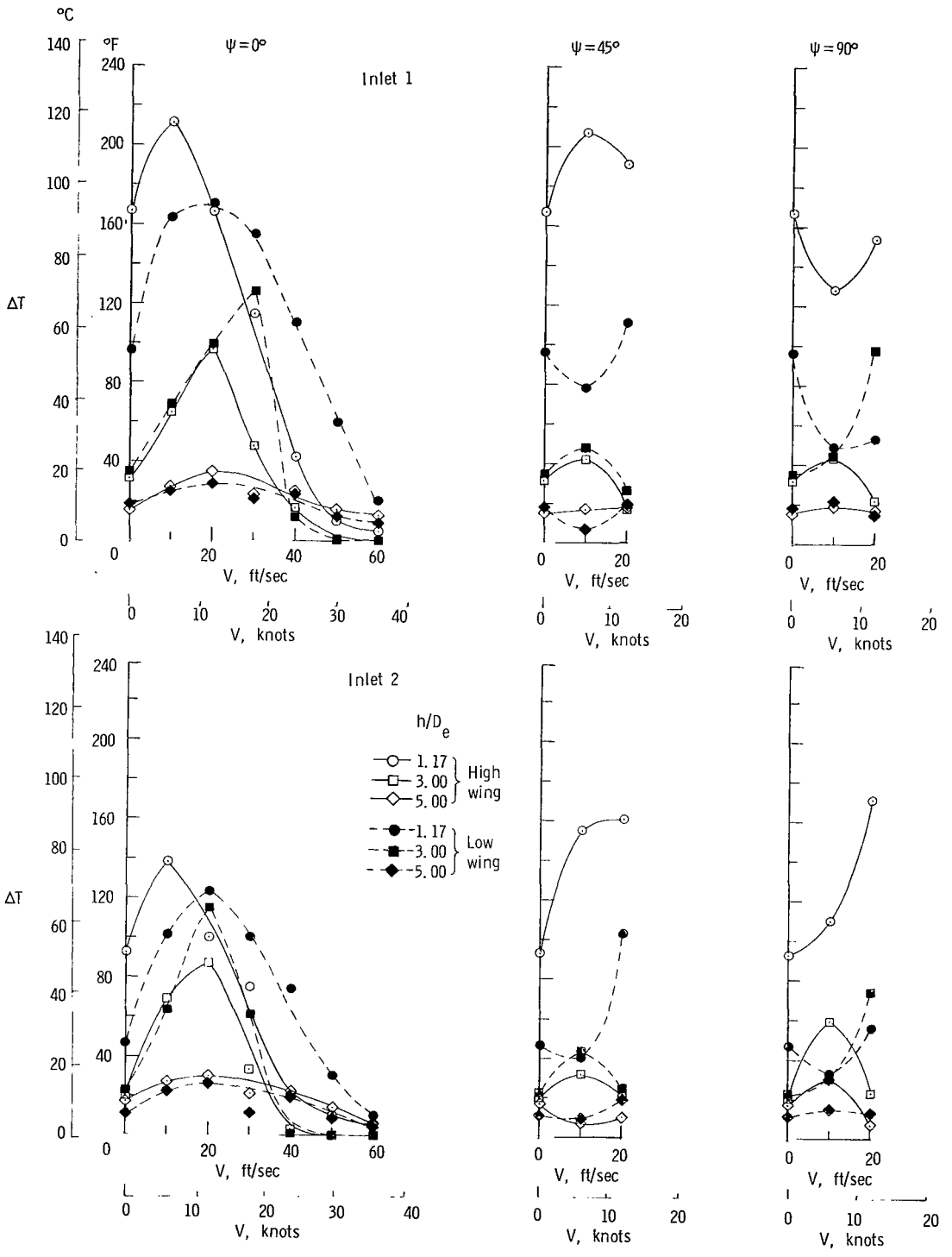

Figure 20.- Data from reference 1 on the effect of wing location on the variation of average inlet-air temperature rise with windspeed for the rectangular nozzle arrangement with side inlets. $S_W/S_J = 43$.

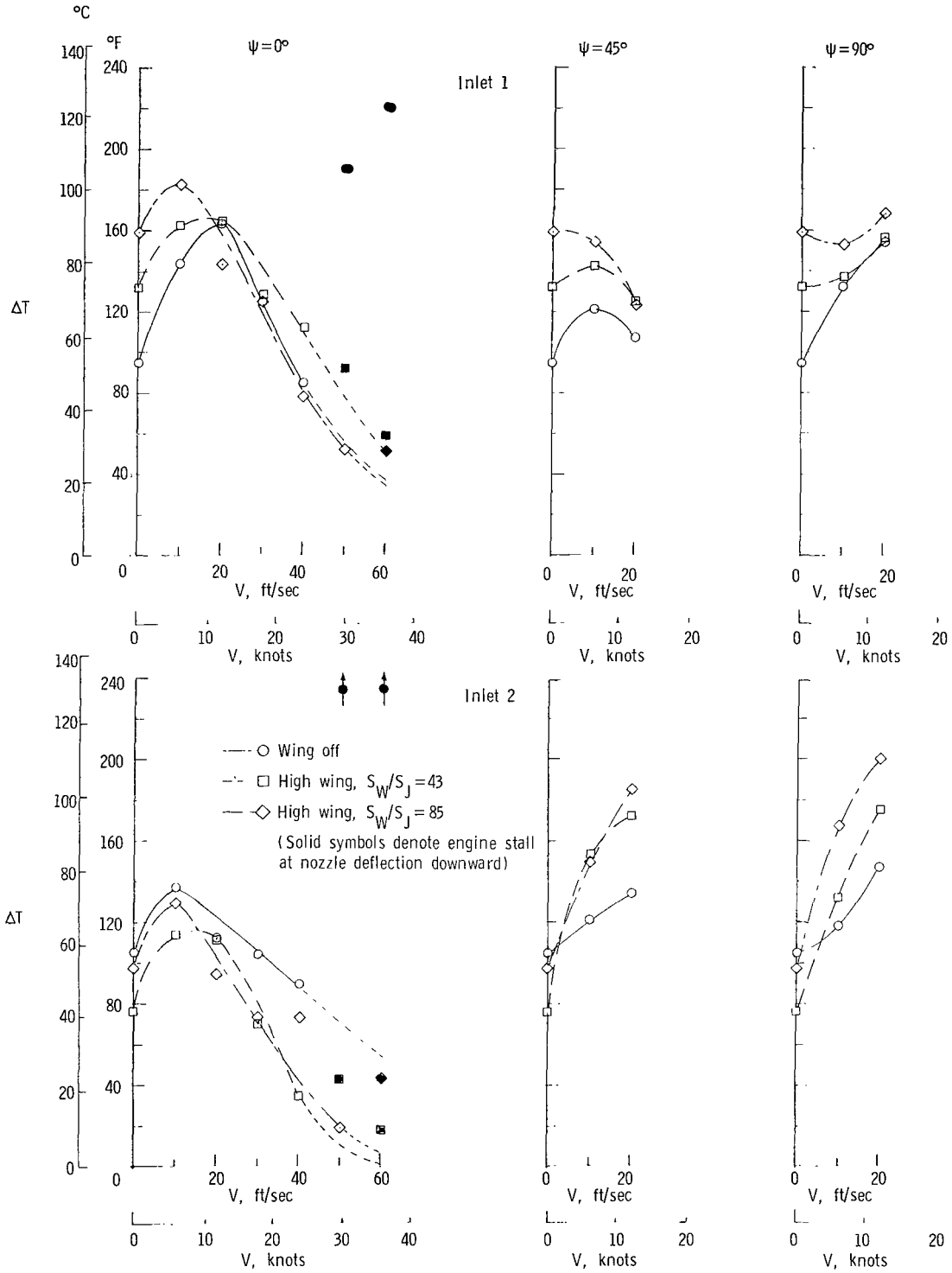

Figure 21.- Effect of wing size on the variation of average inlet-air temperature rise with windspeed for the rectangular nozzle arrangement with side inlets. h/D_e = 1.17.

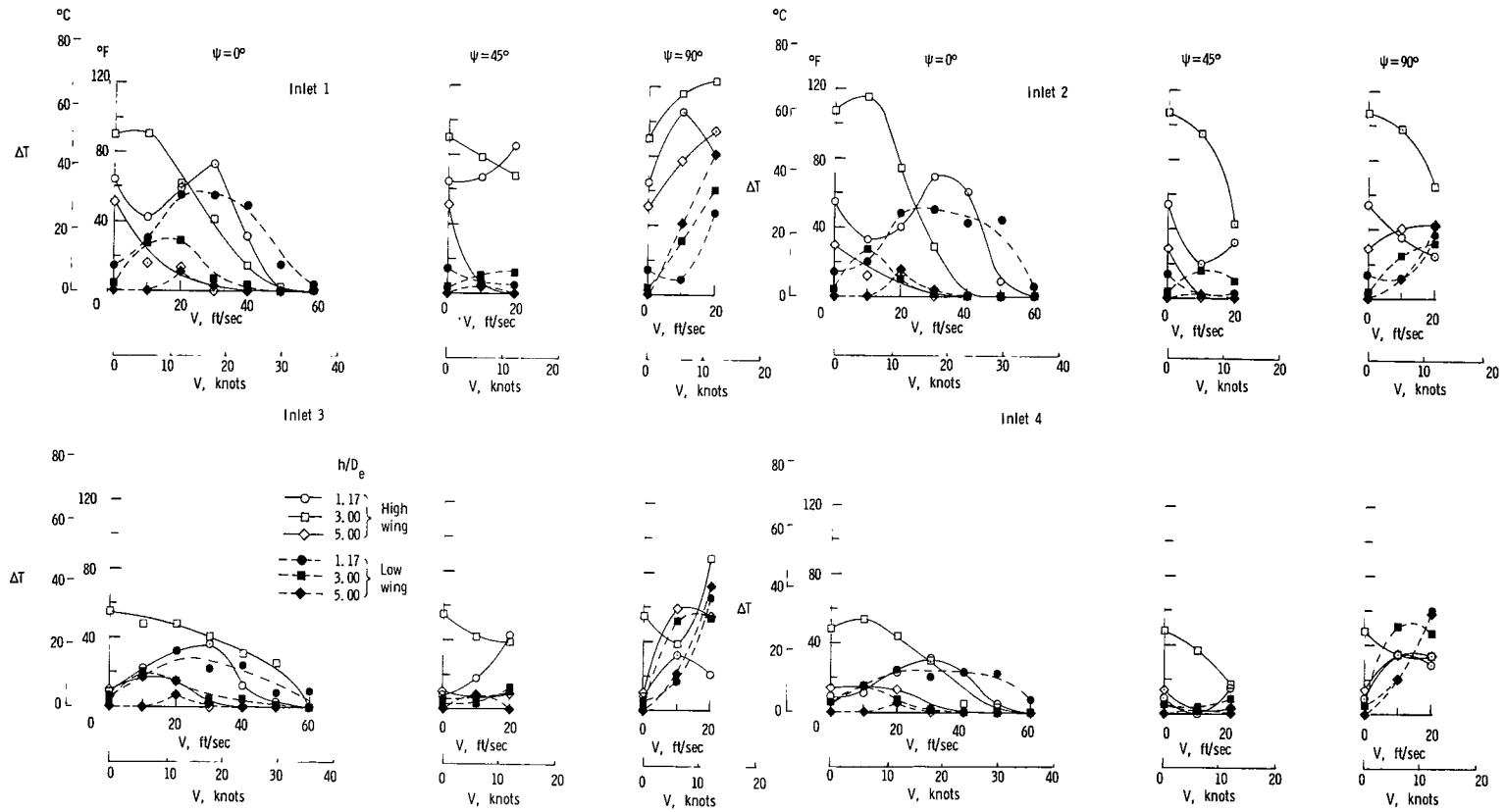

Figure 22.- Data from reference 1 on the effect of wing location on the variation of average inlet-air temperature rise with windspeed for the rectangular nozzle arrangement with top inlets. $S_W/S_J = 43$.

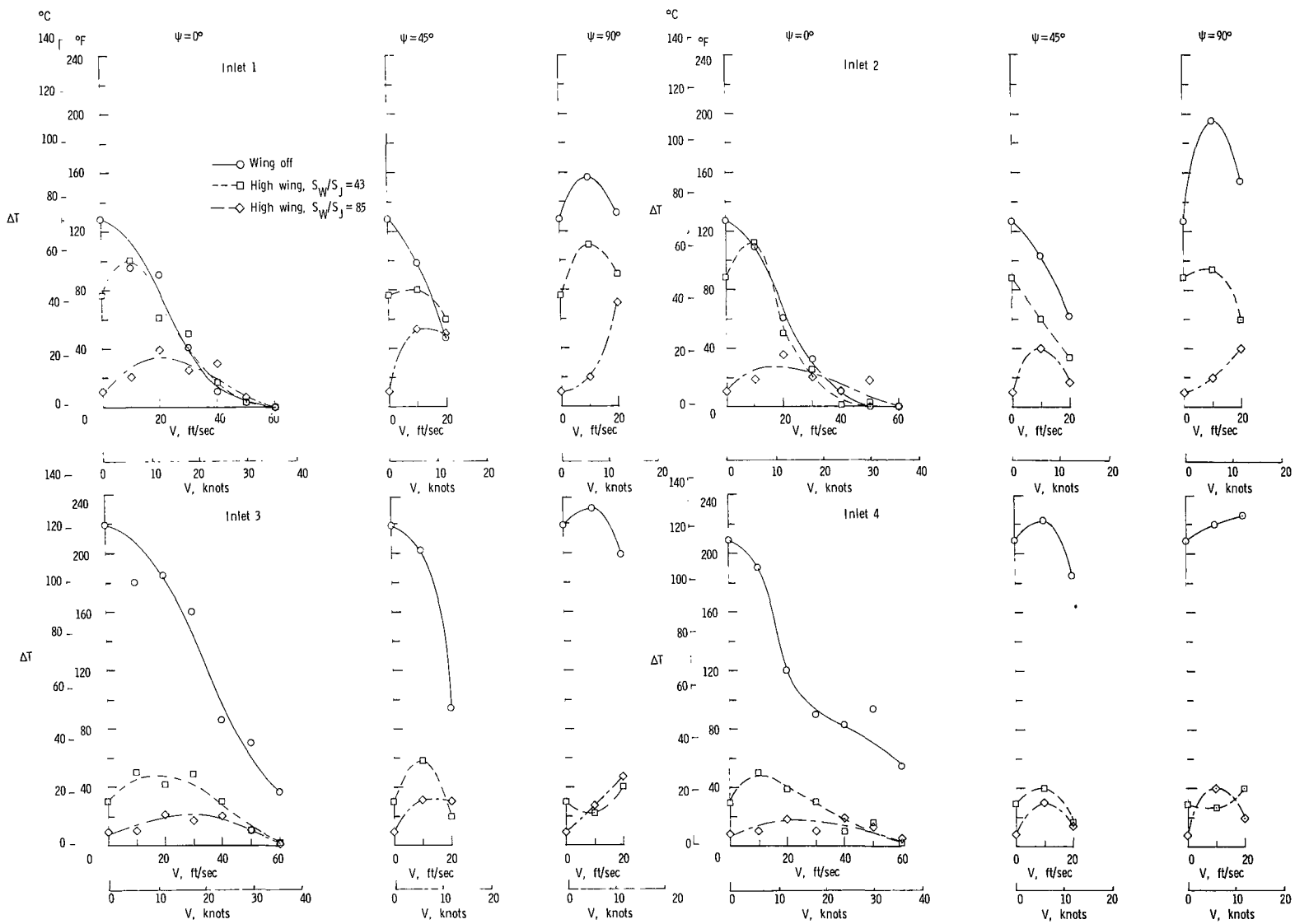

Figure 23.- Effect of wing size on the variation of average inlet-air temperature rise with windspeed for the rectangular nozzle arrangement with top inlets. $h/D_e = 3.00$.

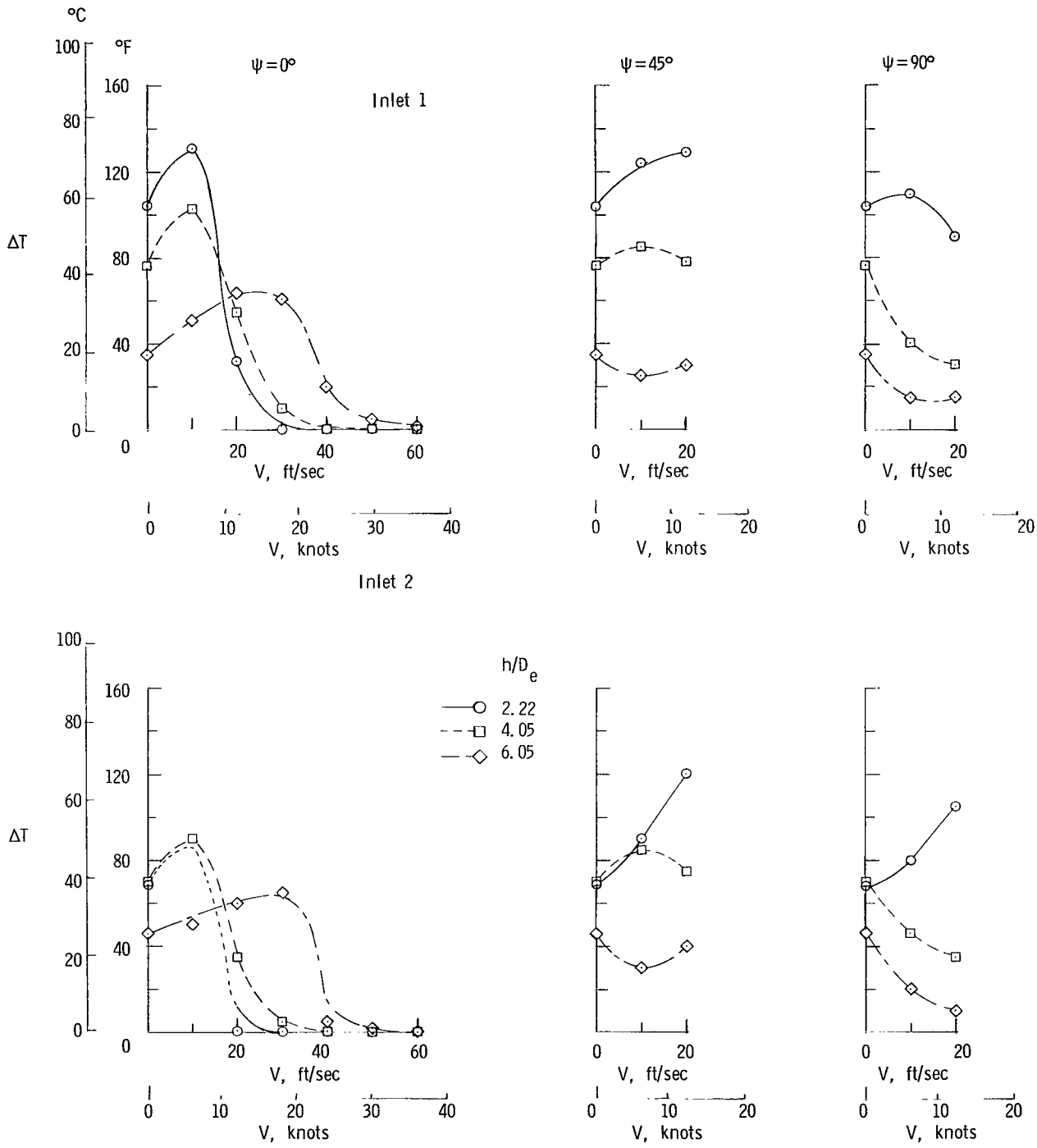

Figure 24.- Effect of nozzle height on the variation of average inlet-air temperature rise with windspeed for the side nozzle arrangement with side inlets. High wing; S_W/S_J = 43.

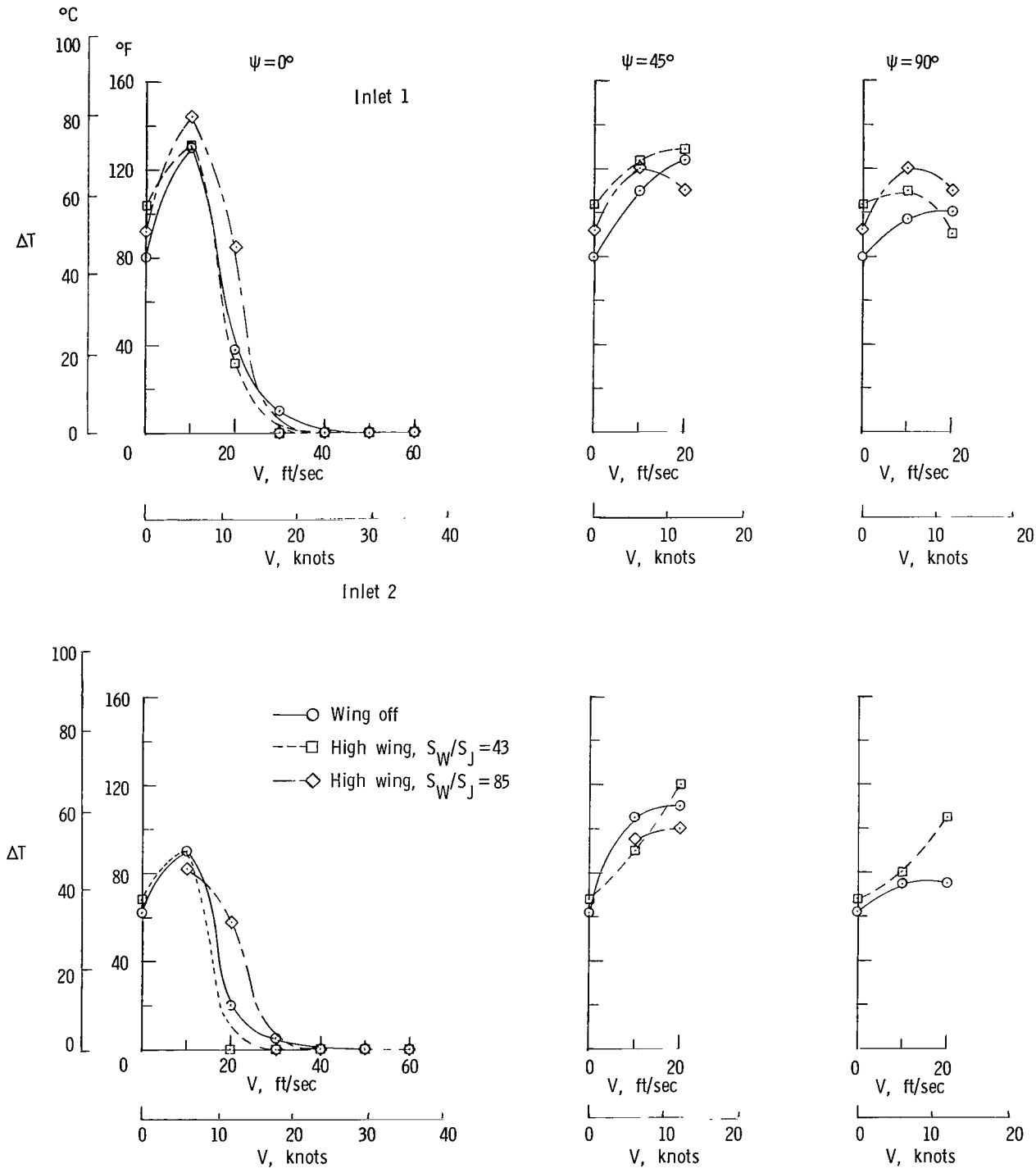

Figure 25.- Effect of wing size on the variation of average inlet-air temperature rise with windspeed for the side nozzle arrangement with side inlets. h/D_e = 2.22.

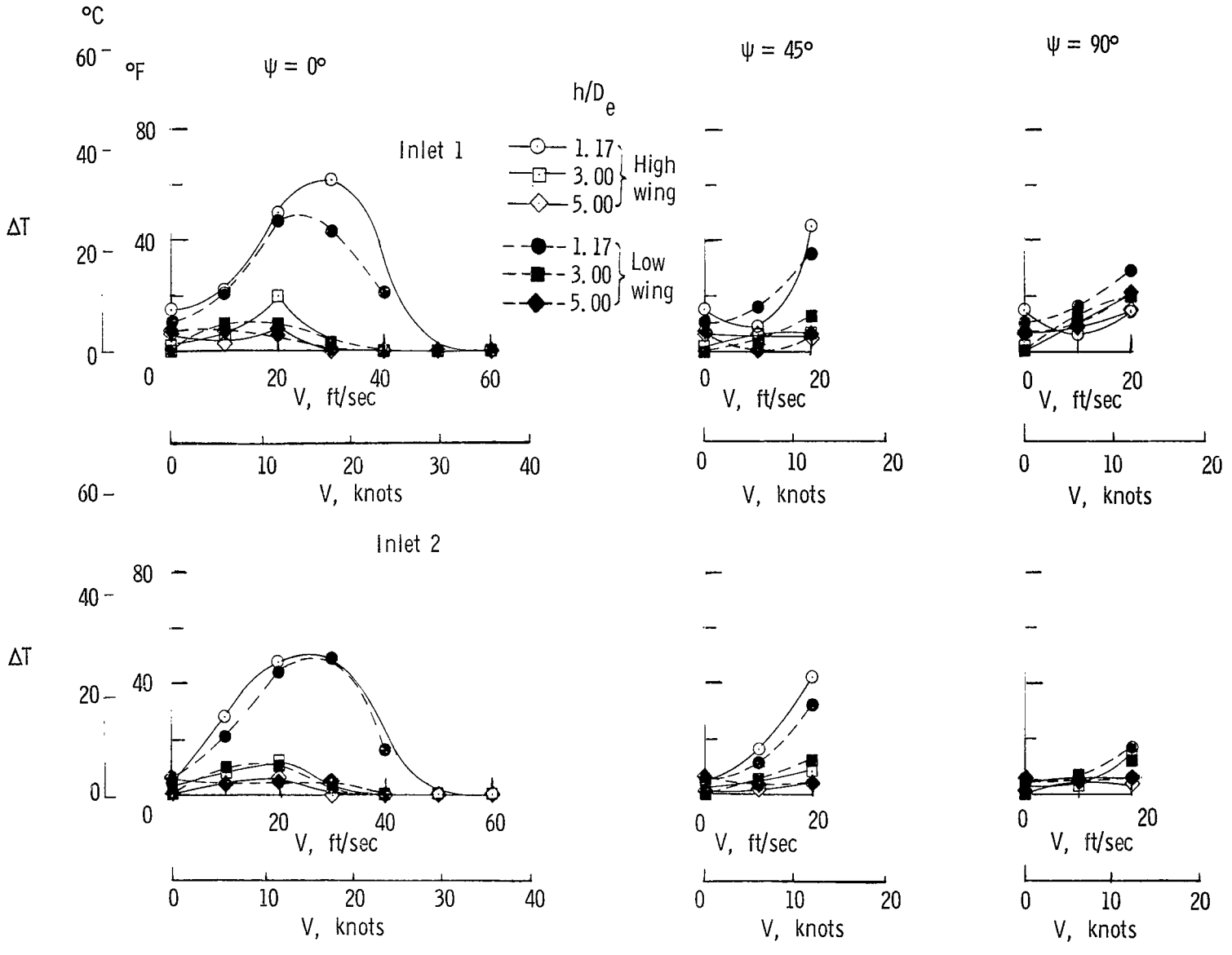

Figure 26.- Data from reference 1 on the effect of wing location on the variation of average inlet-air temperature rise with windspeed for the in-line nozzle arrangement with side inlets. $S_W/S_J = 43$.

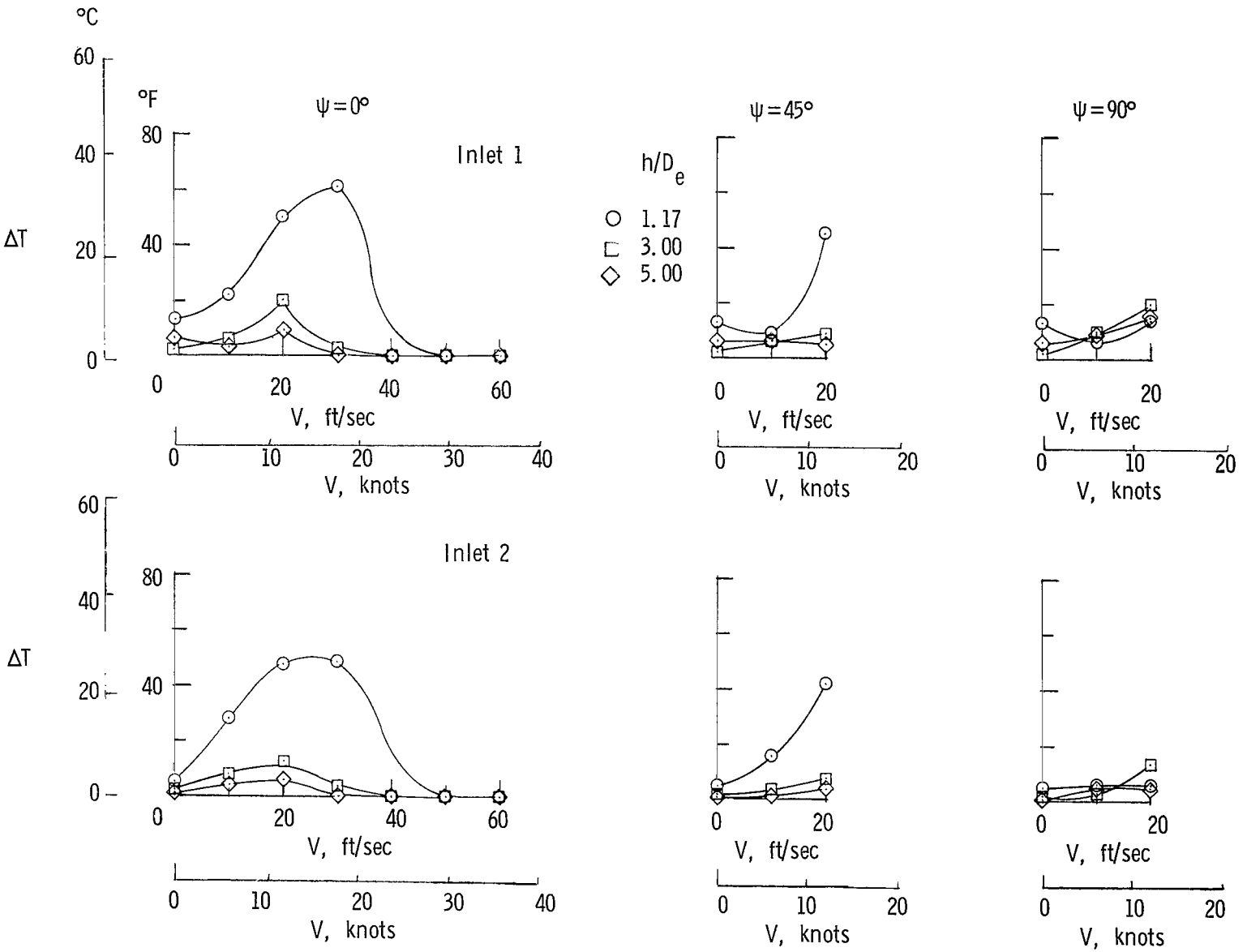

Figure 27.- Data from reference 1 on the effect of nozzle height on the variation of average inlet-air temperature rise with windspeed for the in-line nozzle arrangement with side inlets. High wing; S_W/S_J = 43.

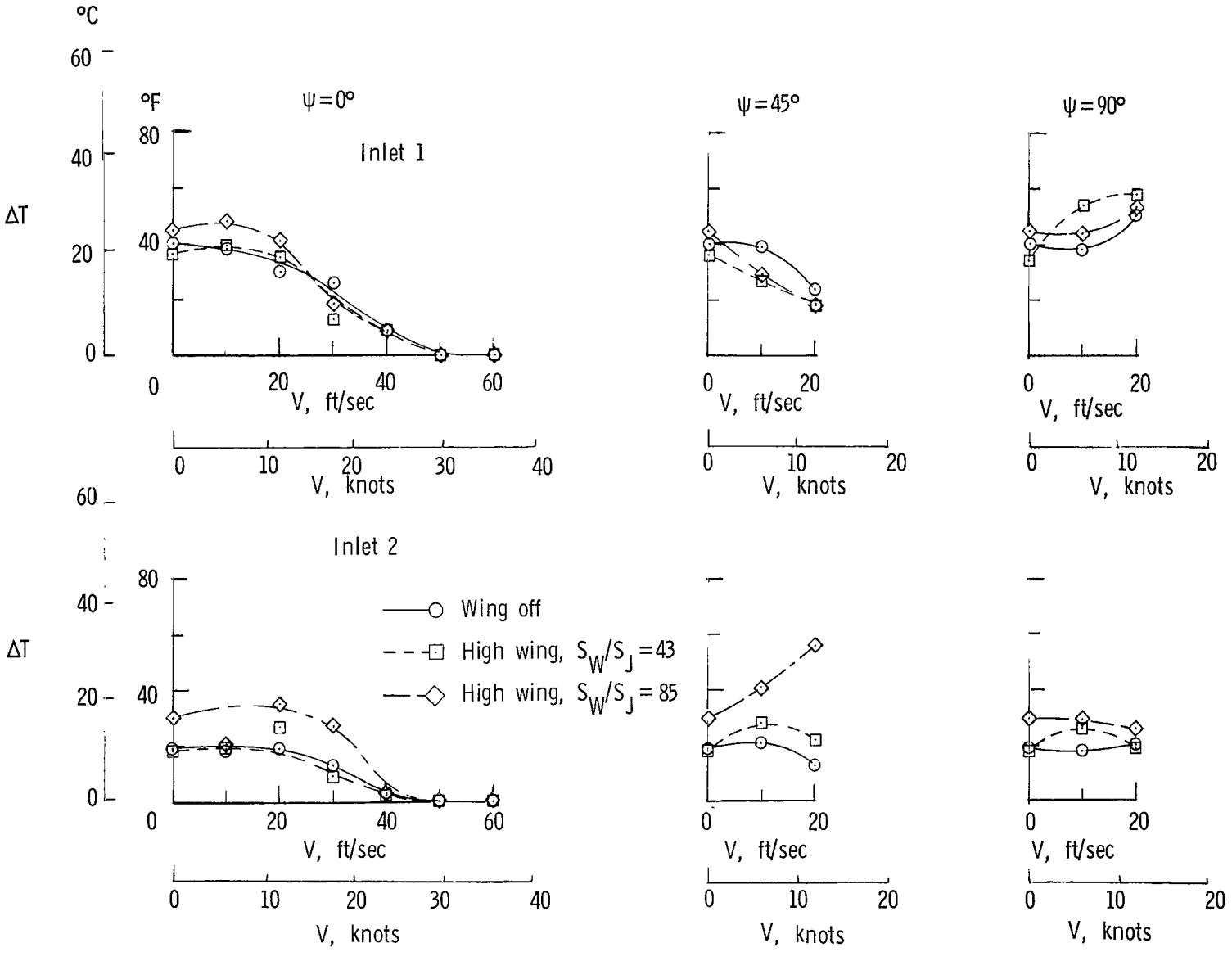

Figure 28.- Effect of wing size on the variation of average inlet-air temperature rise with windspeed for the in-line nozzle arrangement with side inlets. $h/D_e = 1.17$.

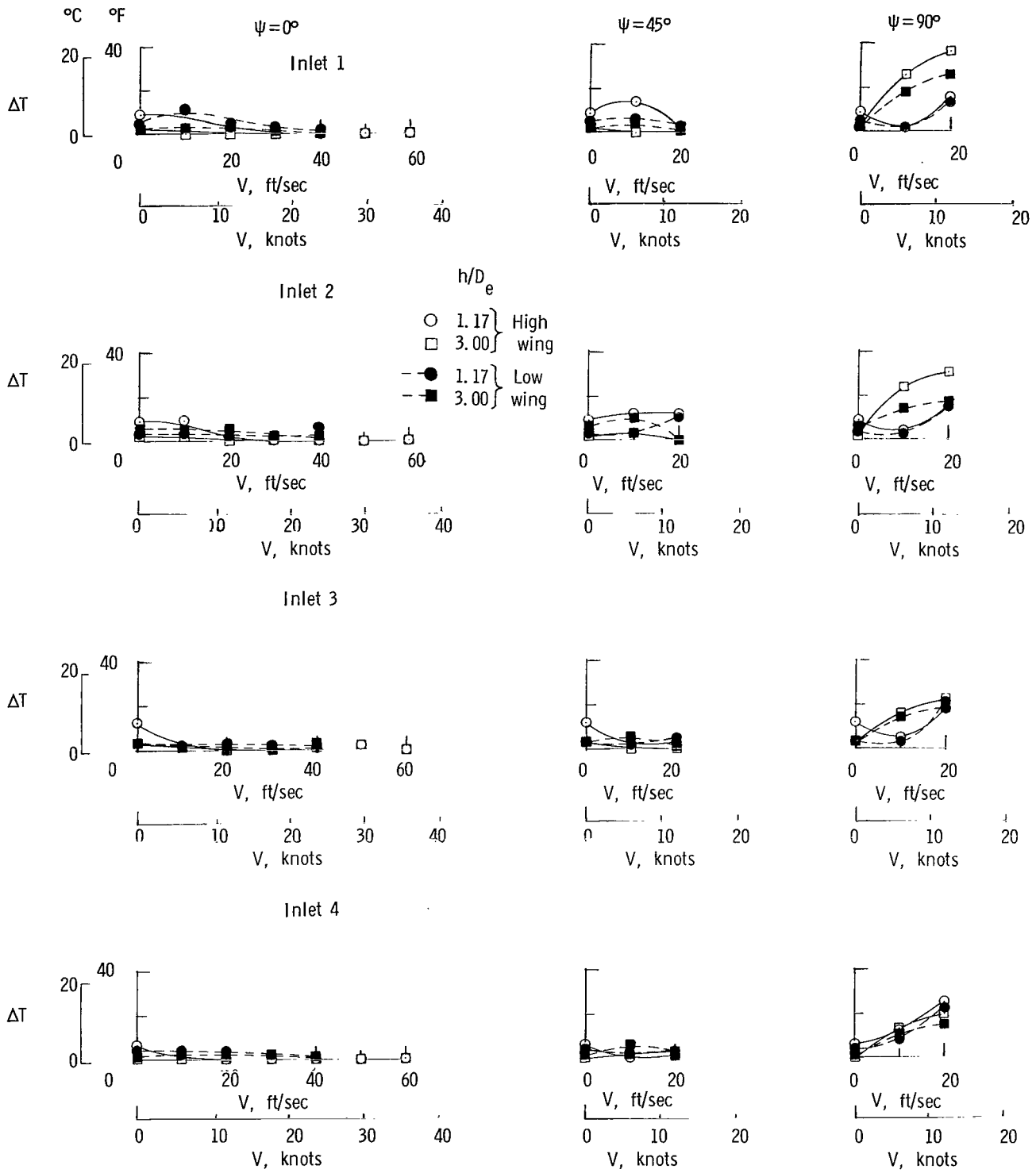

Figure 29.- Data from reference 1 on the effect of wing location on the variation of average inlet-air temperature rise with windspeed for the in-line nozzle arrangement with top inlets. $S_W/S_J = 43$.

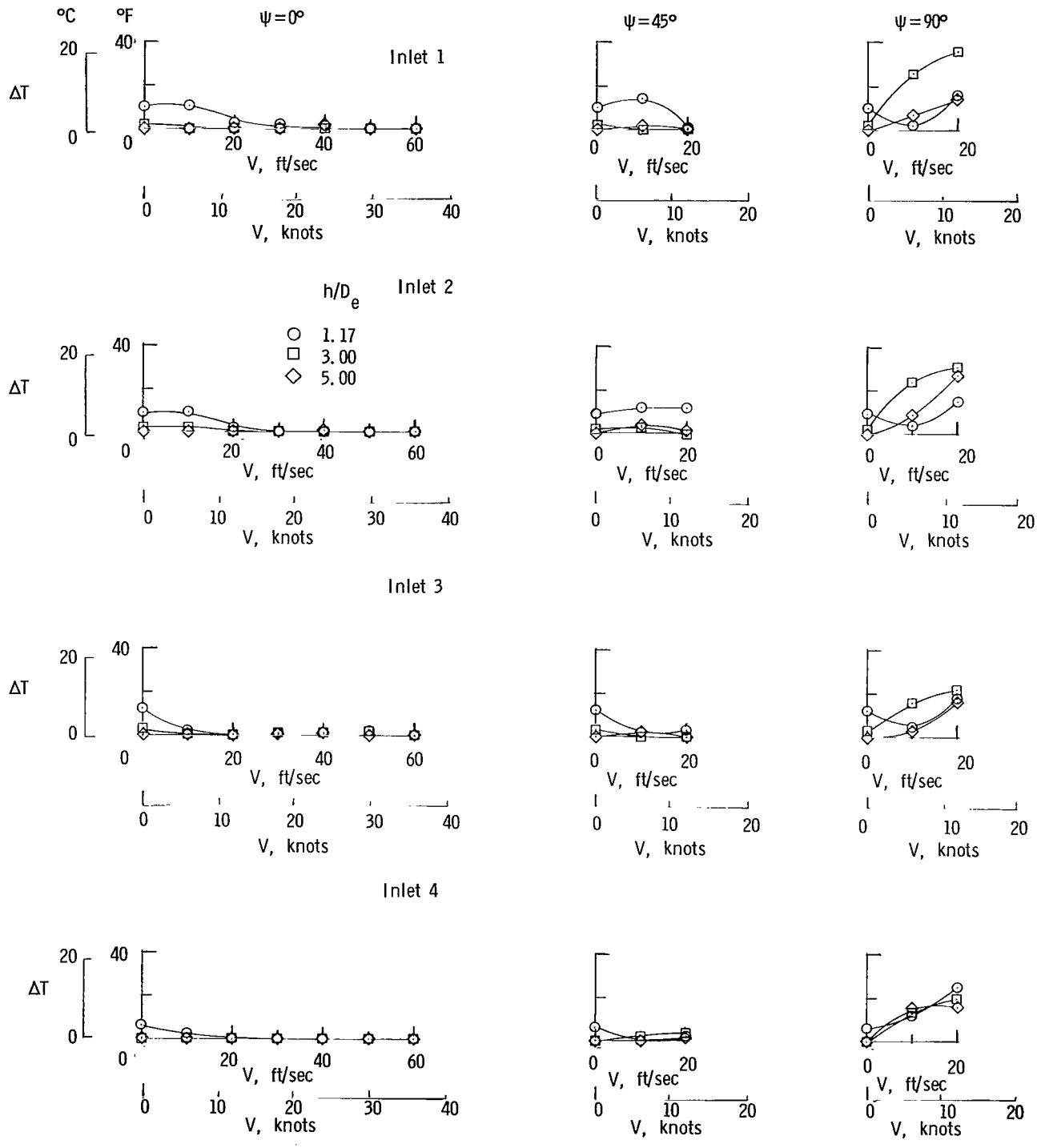

Figure 30.- Data from reference 1 on the effect of nozzle height on the variation of average inlet-air temperature rise with windspeed for the in-line nozzle arrangement with top inlets. High wing; $S_W/S_J = 43$.

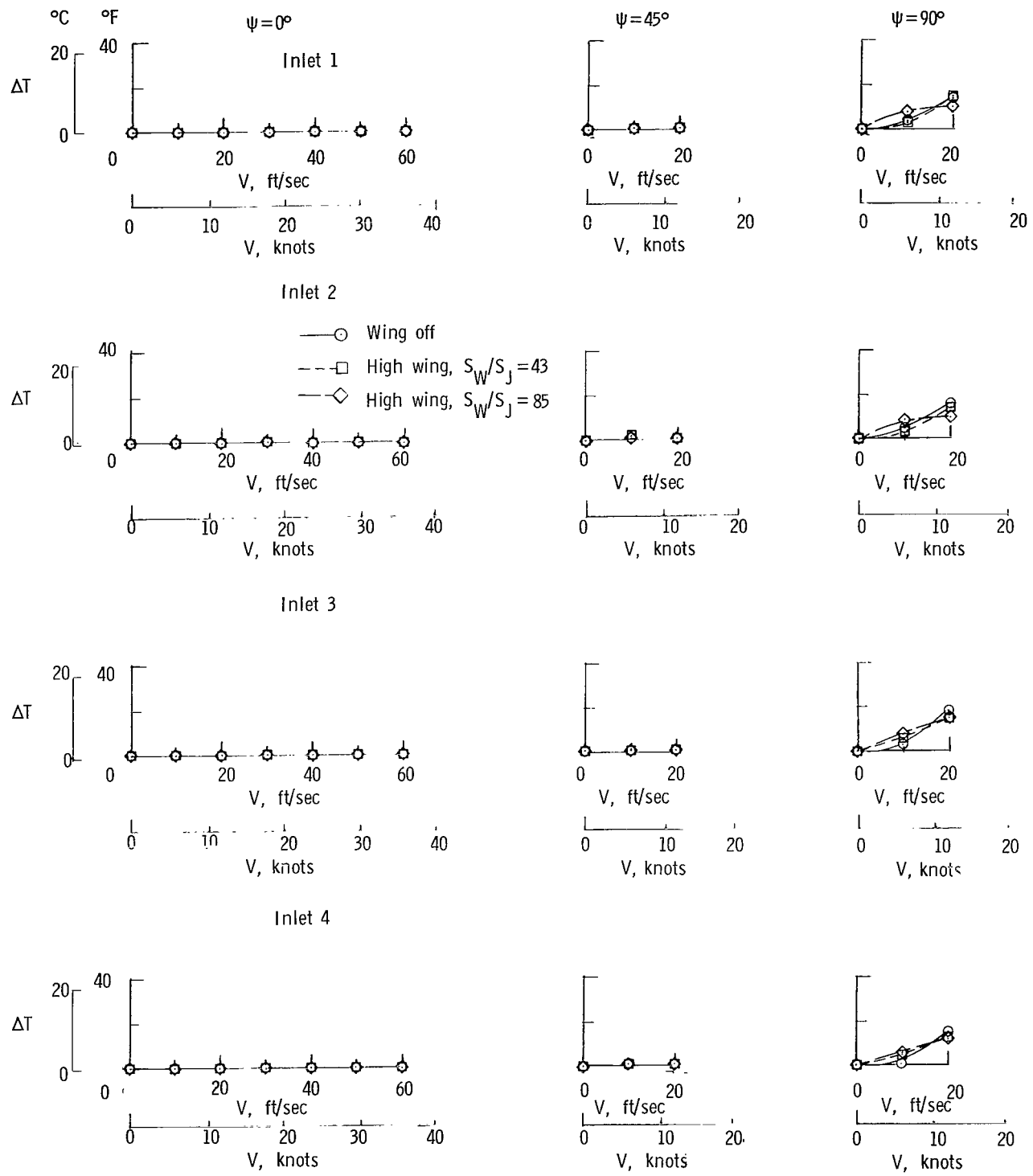

Figure 31.- Effect of wing size on the variation of average inlet-air temperature rise with windspeed for the in-line nozzle arrangement with top inlets. $h/D_e = 3.00$.

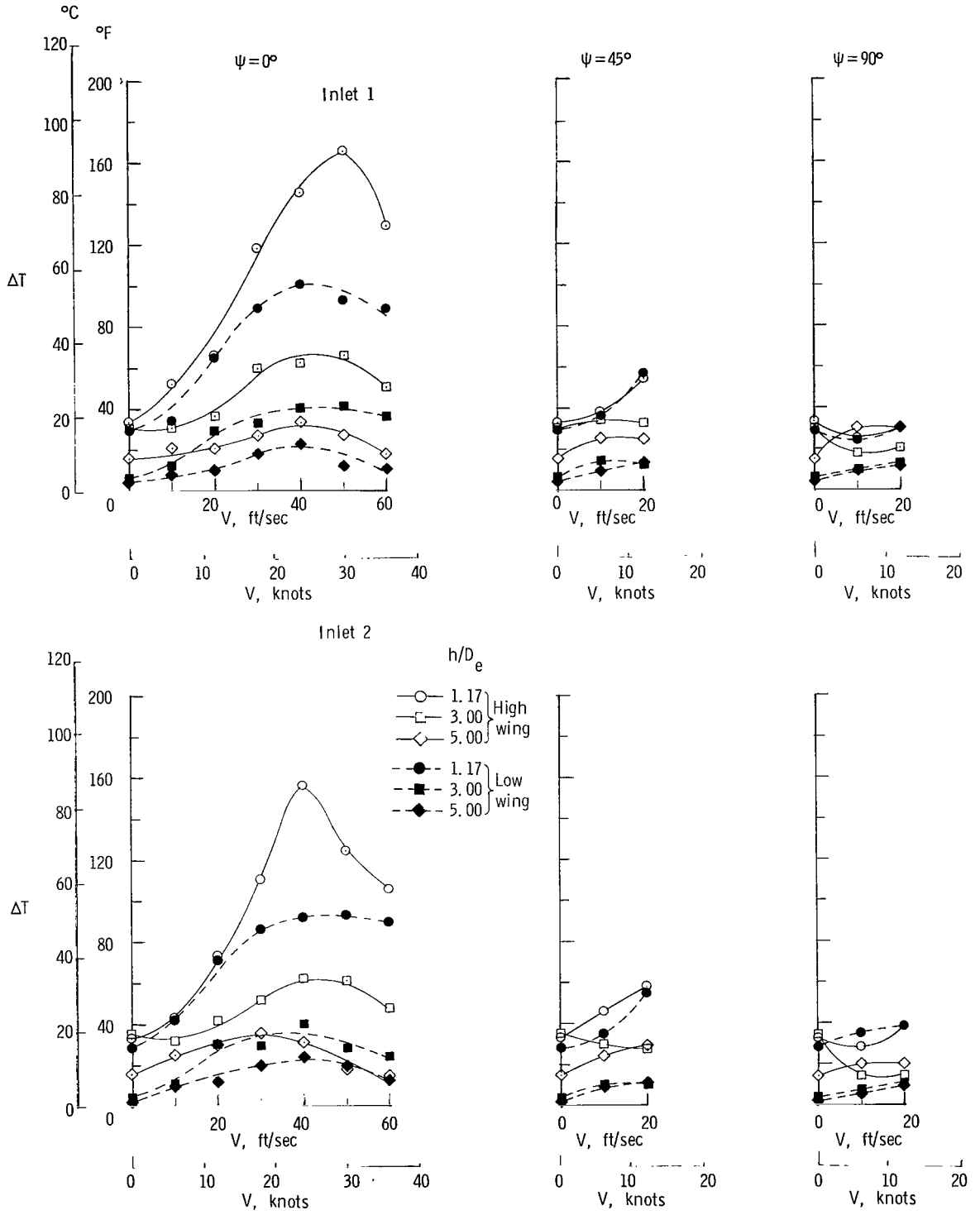

Figure 32.- Effect of wing location on the variation of average inlet-air temperature rise with windspeed for the single-nozzle arrangement with side inlets. S_W/S_J = 43.

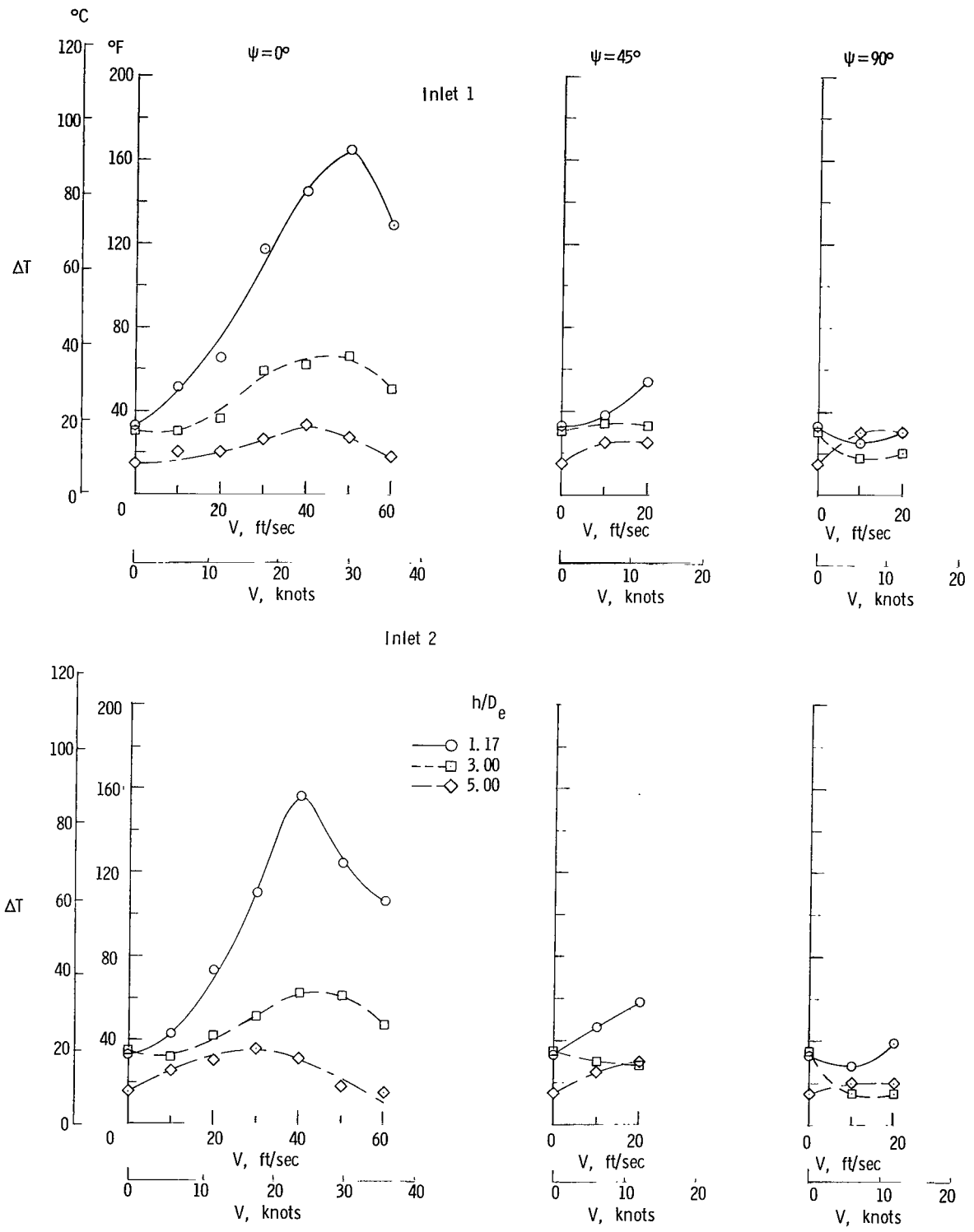

Figure 33.- Effect of nozzle height on the variation of average inlet-air temperature rise with windspeed for the single-nozzle arrangement with side inlets. High wing; S_W/S_J = 43.

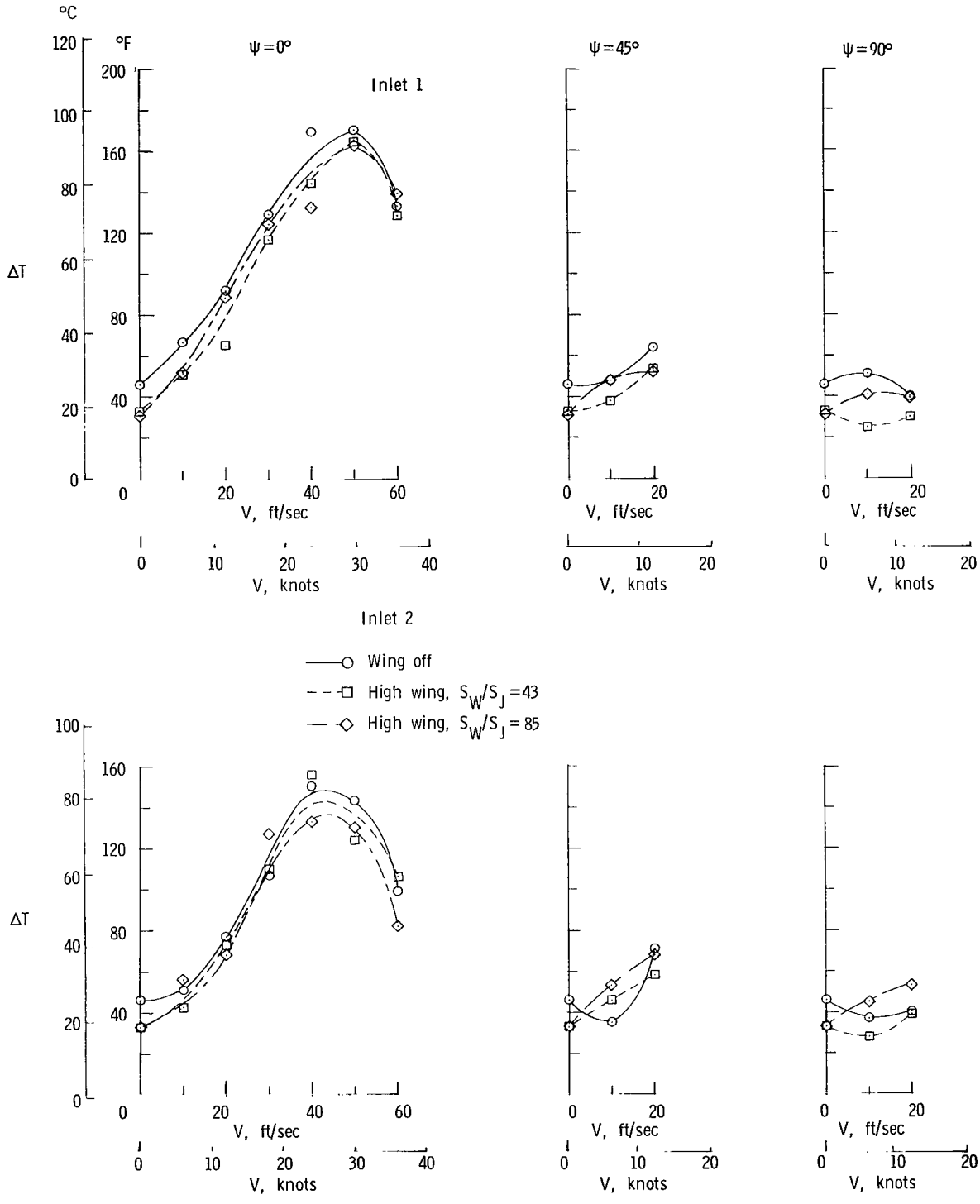

Figure 34.- Effect of wing size on the variation of average inlet-air temperature rise with windspeed for the single-nozzle arrangement with side inlets. h/D_e = 1.17.

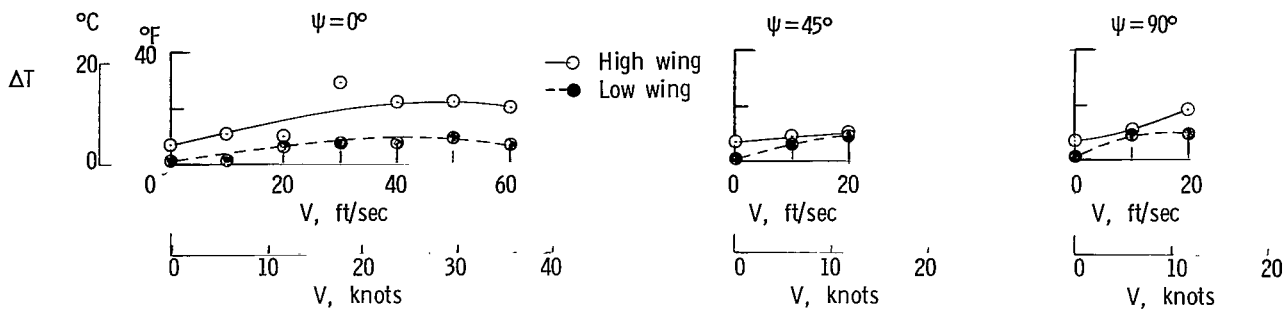

Figure 35.- Effect of wing location on the variation of average inlet-air temperature rise with windspeed for the single-nozzle arrangement with top inlet. S_W/S_J = 43.

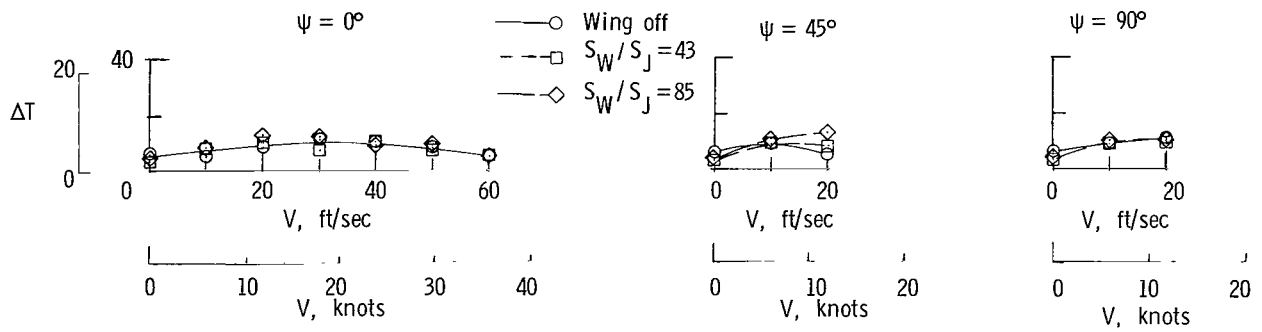

Figure 36.- Effect of wing size on the variation of average inlet-air temperature rise with windspeed for the single-nozzle arrangement with top inlet. h/D_e = 3.00.

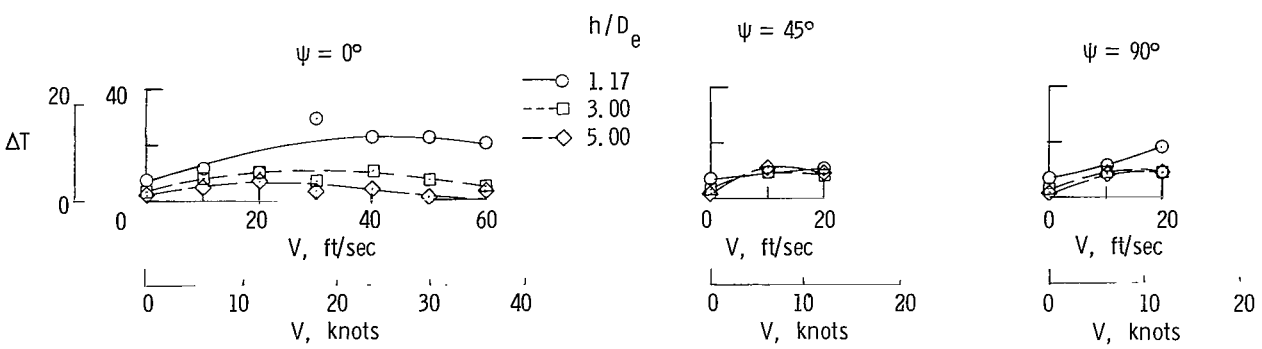

Figure 37.- Effect of nozzle height on the variation of average inlet-air temperature rise for the single-nozzle arrangement with top inlet. High wing; S_W/S_J = 43.

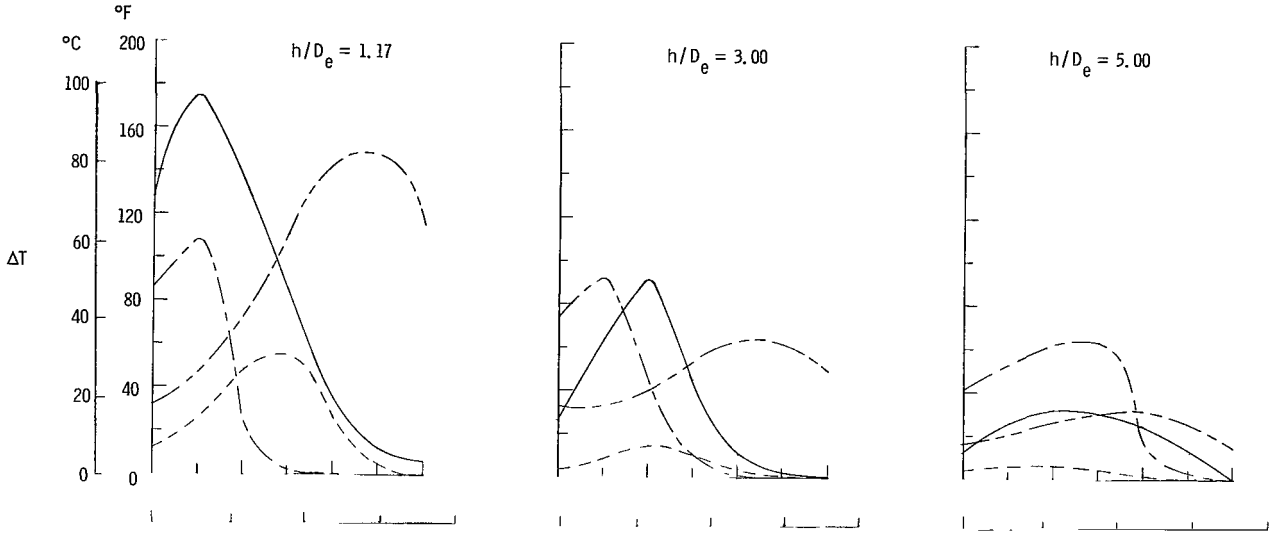

(a) Side inlets.

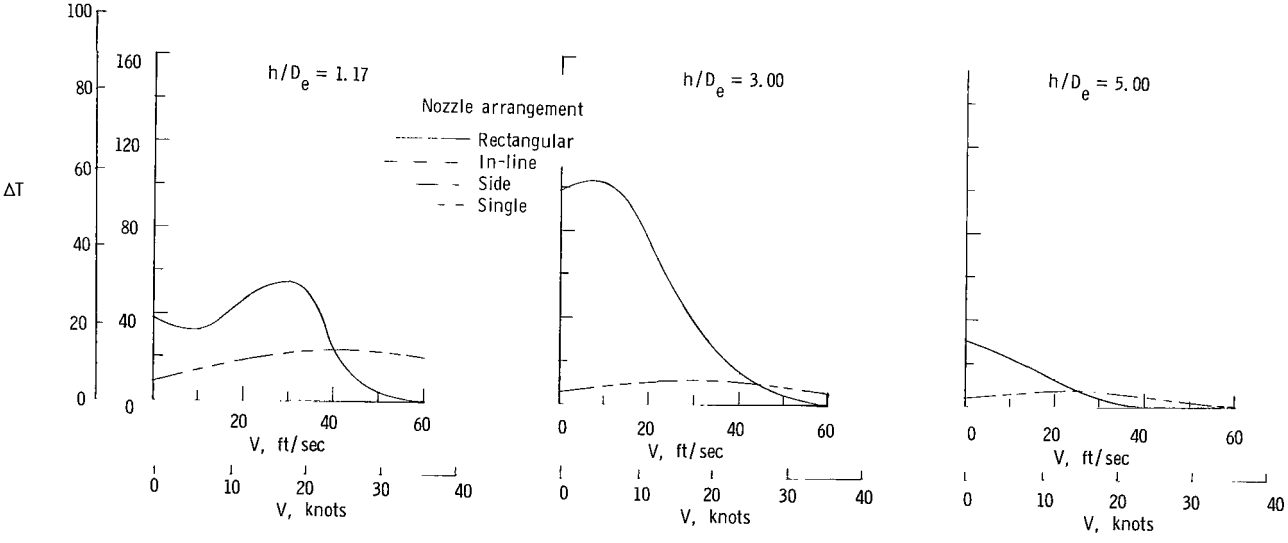

(b) Top inlets (average of two forward inlets). No ingestion for in-line nozzle arrangement; side nozzle arrangement not tested.

Figure 38.- Effect of nozzle height and windspeed on the hot-gas ingestion characteristics of the various test configurations. $\psi = 0^{o}$; $S_W/S_J = 43$. (Data for rectangular and in-line nozzle arrangements are from ref. 1.)

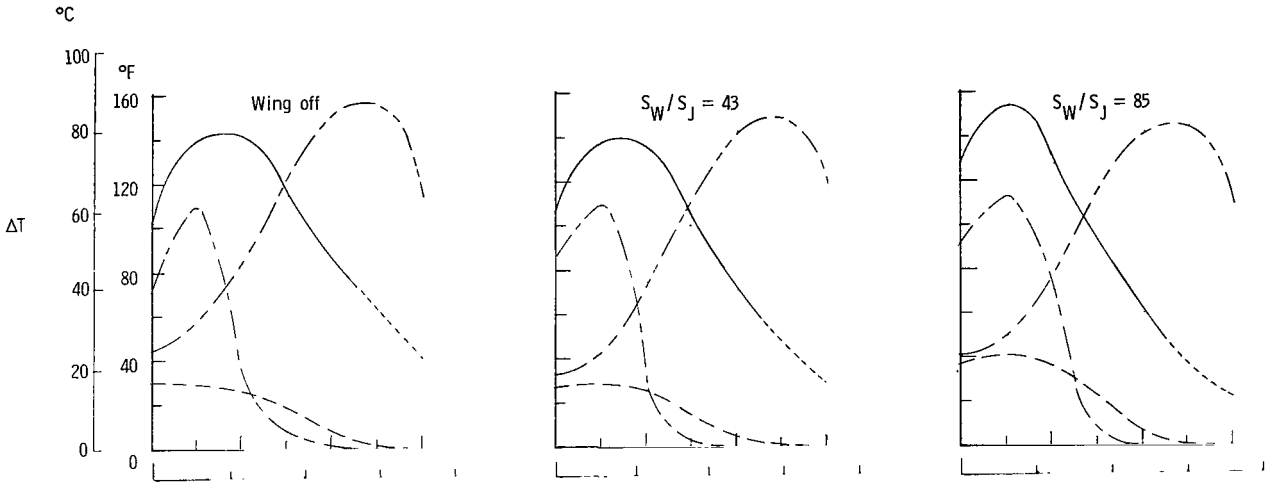

(a) Side inlets. h/D_e = 1.17.

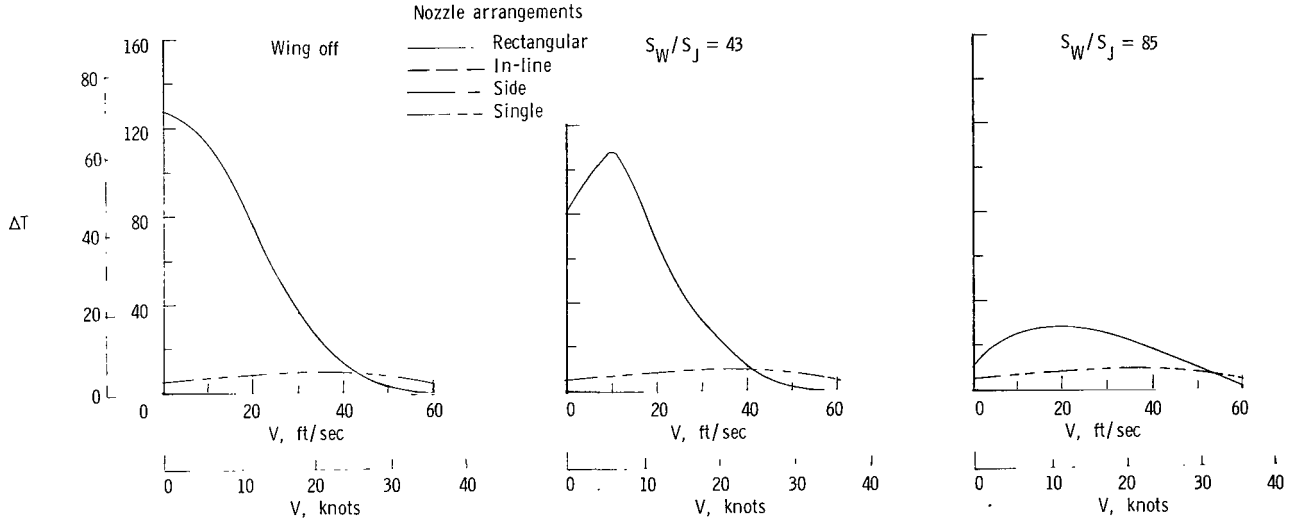

(b) Top inlets (average of two forward inlets). h/D_e = 3.00; no ingestion for in-line nozzle arrangement; side nozzle arrangement not tested.

Figure 39.- Effect of wing size and windspeed on hot-gas ingestion characteristics of the various test configurations. $\psi = 0^0$.

NASA-Langley, 1969 — 1 L-6805

NATIONAL AERONAUTICS AND SPACE ADMINISTRATION
WASHINGTON, D.C. 20546
OFFICIAL BUSINESS

FIRST CLASS MAIL

POSTAGE AND FEES PAID
NATIONAL AERONAUTICS AND
SPACE ADMINISTRATION

"The aeronautical and space activities of the United States shall be conducted so as to contribute . . . to the expansion of human knowledge of phenomena in the atmosphere and space. The Administration shall provide for the widest practicable and appropriate dissemination of information concerning its activities and the results thereof."

—NATIONAL AERONAUTICS AND SPACE ACT OF 1958

NASA SCIENTIFIC AND TECHNICAL PUBLICATIONS

TECHNICAL REPORTS: Scientific and technical information considered important, complete, and a lasting contribution to existing knowledge.

TECHNICAL NOTES: Information less broad in scope but nevertheless of importance as a contribution to existing knowledge.

TECHNICAL MEMORANDUMS: Information receiving limited distribution because of preliminary data, security classification, or other reasons.

CONTRACTOR REPORTS: Scientific and technical information generated under a NASA contract or grant and considered an important contribution to existing knowledge.

TECHNICAL TRANSLATIONS: Information published in a foreign language considered to merit NASA distribution in English.

SPECIAL PUBLICATIONS: Information derived from or of value to NASA activities. Publications include conference proceedings, monographs, data compilations, handbooks, sourcebooks, and special bibliographies.

TECHNOLOGY UTILIZATION PUBLICATIONS: Information on technology used by NASA that may be of particular interest in commercial and other non-aerospace applications. Publications include Tech Briefs, Technology Utilization Reports and Technology Surveys.

Details on the availability of these publications may be obtained from:

SCIENTIFIC AND TECHNICAL INFORMATION DIVISION

NATIONAL AERONAUTICS AND SPACE ADMINISTRATION

Washington, D.C. 20546